Atmospheric Chemistry of Hydrofluorocarbons and Hydrochlorofluorocarbons

Sehested, Jens

Publication date:
1995

Document Version
Publisher's PDF, also known as Version of record

RISØ

Risø-R-804(EN)

Atmospheric Chemistry of Hydrofluorocarbons and Hydrochlorofluorocarbons

Jens Sehested

Risø National Laboratory, Roskilde, Denmark
March 1995

Atmospheric Chemistry of Hydrofluorocarbons and Hydrochlorofluorocarbons

Risø-R-804(EN)

Jens Sehested

Risø National Laboratory, Roskilde, Denmark
March 1995

Abstract

The atmospheric chemistry of halogenated compounds is important since these compounds are produced in hundred thousand of tonnes both antropogenically and naturally. This work has concentrated on the atmospheric chemistry of HFCs and HCFCs.

Using pulse radiolysis coupled with a time resolved UV absorption detection system, reaction rates for a series of reactions of HFCs and HCFCs were investigated:

$$F + RH \rightarrow R + HF$$
$$R + O_2 + M \rightarrow RO_2 + M$$
$$RO_2 + NO \rightarrow \text{products}$$
$$RO_2 + NO_2 + M \rightarrow RO_2NO_2 + M$$

together with UV absorption spectra of the halogenated alkyl (R) and halogenated alkyl peroxy radicals (RO_2). Kinetics and UV spectra of FO_2 and SF_5O_2 were also studied because of their potential interference with the HFC and HCFC investigations.

A FTIR spectrometer coupled to a 140 l reaction chamber at Ford Motor Company was used to study the reaction products. Photolysis of molecular chlorine or fluorine were used to initiate the reactions. A relative rate study of the reactions of F atoms with a series of HFCs and HCFCs was performed. The products following the self reactions of RO_2 radicals for RO_2 = $CF_3CF_2O_2$, $CF_2HCF_2O_2$, $CF_3CH_2O_2$, CFH_2CFHO_2, CF_3O_2, and $CF_3C(O)O_2$ were investigated. The results show that the self reaction of halogenated peroxy radicals give the alkoxy radical, RO, as product. The atmospheric fate of these radicals were C-C bond cleavage for CF_3CF_2O, CHF_2CF_2O, CFH_2CHFO, and $CF_3C(O)O$; while CF_3CH_2O radicals react with O_2:

$$CF_3CH_2O + O_2 \rightarrow CF_3CHO + HO_2$$

In addition, the reaction between CFH_2O_2 and HO_2 was shown to give 29±7% CH_2FCOOH and 71±11% HCOF as the carbon containing products.

The atmospheric fate of the alkoxy radical CF_3O was also addressed in this work because of its potential for ozone depletion. A rate constant was determined for the reaction of CF_3O with NO of $(5.2\pm2.7)\times10^{-11}$ cm^3 $molecule^{-1}$ s^{-1} together with an upper limit for the rate constant of the reaction of CF_3O with ozone of 10^{-13} cm^3 $molecule^{-1}$ s^{-1}. In addition, the CF_3O radical was shown to be intermediate in the atmospheric degradation

of HFC-134a (CF_3CFH_2), which is the industrially most important HFC. CF_3O radicals were shown to react with HFC-134a and CH_4 by hydrogen abstraction to give CF_3OH and a halogenated alkyl radical. Experiments suggest that the CF_3O radical also reacts with H_2O with a rate constant in the range $(0.2\text{-}40)\times10^{-17}$ cm^3 molecule^{-1} s^{-1} to give CF_3OH and OH. The results lead to the conclusion that CF_3O_x chemistry poses no threat to the stratospheric ozone layer.

The atmospheric chemistry of two other groups of radicals, FCO_x, x=1,2,3 and FO_x, x=0,1,2, produced in the atmospheric degradation of HFCs and HCFCs was also studied. The UV absorption spectra of FCO_x radicals, self reaction, and the reaction with NO and ozone were studied. The reaction rates were $k(FC(O)+NO)=(1.0\pm0.2)\times10^{-11}$ cm^3 molecule^{-1} s^{-1}, $k(FC(O)O_2+NO)=(2.5\pm0.8)\times10^{-11}$ cm^3 molecule^{-1} s^{-1}, $k(FC(O)O+NO)=(1.3\pm0.7)\times10^{-10}$ cm^3 molecule^{-1} s^{-1}, and $k(FC(O)O+O_3)<6\times10^{-14}$ cm^3 molecule^{-1} s^{-1}. The results from this work show that FCO_x radicals have no implications for the stratospheric ozone layer. The last atmospheric HFC degradation product investigated as part of this work were FO_x radicals, x=0,1,2. The reactions of FO_2 with NO, NO_2, CH_4, CO, and O_3 and the reaction of FO with O_3 were studied. The determined rate constants were $k(FO_2+NO)=(1.47\pm0.08)\times10^{-12}$ cm^3 molecule^{-1} s^{-1}, $k(FO_2+NO_2)=(1.05\pm0.15)\times10^{-13}$ cm^3 molecule^{-1} s^{-1}, $k(FO_2+CO)<5.1\times10^{-16}$ cm^3 molecule^{-1} s^{-1}, $k(FO_2+CH_4)<4.1\times10^{-15}$ cm^3 molecule^{-1} s^{-1}, $k(FO_2+O_3)<3.4\times10^{-16}$ cm^3 molecule^{-1} s^{-1}, and $k(FO+O_3)<1.2\times10^{-12}$ cm^3 molecule^{-1} s^{-1}. The results from this work together with data available in the literature indicate that FO_x chemistry does not threat the stratospheric ozone layer.

This Ph.D. Thesis was defended Oktober 28. 1994 at the University of Copenhagen.

ISBN 87-550-2065-8
ISSN 0106-2840

Grafisk Service Risø 1995

Danish Summary

Forståelsen af halogenerede forbindelsers atmosfærekemi er vigtig, da disse forbindelser bliver produceret i store mængder både antropogent og naturligt. Denne afhandling handler om atmosfærekemien af HFCer og HCFCer.

Puls radiolyse med tidsopløst UV absorptions spektroskopi er blevet brugt til at undersøge reaktioner for en serie af HFCer og HCFCer. Følgende reaktioner er blevet undersøgt:

$$F + RH \rightarrow R + HF$$
$$R + O_2 + M \rightarrow RO_2 + M$$
$$RO_2 + NO \rightarrow \text{produkter}$$
$$RO_2 + NO_2 + M \rightarrow RO_2NO_2 + M$$

sammen med UV spektrene af R og RO_2 radikalerne. Kinetik og UV spektrene for FO_2 of SF_5O_2 radikalerne er også undersøgt på grund af deres potentielle indflydelse på studiet af HFCerne og HCFCerne.

Et 140 liter reaktionskammer med FTIR detektion på Ford Motor Company blev brugt til at studere produkterne af selvreaktionen af halogenerede peroxy radikaler, RO_2. Fotolyse of Cl_2 eller F_2 er blevet brugt til at initiere reaktionerne. En relativ metode blev brugt til at bestemme hastighedskonstanter for reaktionen mellem F atomer og en serie af HFCer of HCFCer. Selv-reaktionen af de undersøgte peroxy radikaler giver kun alkoxy radikaler, RO. I atmosfæren går disse radikaler i stykker ved brydning af en C-C binding for CF_3CF_2O, CHF_2CF_2O, CFH_2CHFO og $CF_3C(O)O$ mens CF_3CH_2O vil reagere med O_2.

$$CF_3CH_2O + O_2 \rightarrow CF_3CHO + HO_2$$

Desuden blev fordelingen of kulstof produkter af reaktionen mellem HO_2 og CFH_2O_2 bestemt til 29±7% CH_2FOOH og 71±11% HCOF.

Det er blevet vist at CF_3O radikalet er et produkt af nedbrydningen i atmosfæren af HFC-134a (CF_3CFH_2), den industrielt vigtigste HFC. Atmosfærekemien af alkoxy radikalet CF_3O er undersøgt som en del af dette arbejde. Hastighedskonstanten for reaktionen mellem CF_3O og NO, $(5.2\pm2.7)\times10^{-11}$ cm^3 $molekyle^{-1}$ s^{-1} og en øvre grænse for hastighedskonstanten for reaktionen mellem CF_3O radikalet og ozon på 10^{-13} cm^3 $molecule^{-1}$ s^{-1} er blevet bestemt. Det er også vist, at CF_3O radikalet reagerer med HFC-

134a og CH_4, ved hydrogen abstraktion og giver CF_3OH samt et halogeneret alkyl radikal. Experimenterne indikerer, at CF_3O radikalet også reagerer med H_2O med en hastigheds-konstant på $(0.2\text{-}40)\times10^{-17}$ cm^3 molekyle^{-1} s^{-1} og giver CF_3OH og OH som produkter. Disse forsøg viser, at CF_3O_x kemi i atmosfæren ikke har nogen nævneværdig indvirkning på det stratosfæriske ozonlag.

Atmosfærekemien af to andre grupper af radikaler, FCO_x, x=1,2,3 og FO_x, x=0,1,2, som dannes under den atmosfæriske nedbrydning af HFCer of HCFCer, er blevet studeret. UV spektrene af FCO_x radikalerne, selv-reaktionerne for disse radikaler samt reaktionerne med NO og ozon er blevet undersøgt. Hastighedskonstanterne er $k(FC(O)+NO)=(1.0\pm0.2)\times10^{-12}$ cm^3 molekyle^{-1} s^{-1}, $k(FC(O)O_2+NO)=(2.5\pm0.8)\times10^{-11}$ cm^3 molekyle^{-1} s^{-1}, $k(FC(O)O+NO)=(1.3\pm0.7)\times10^{-10}$ cm^3 molekyle^{-1} s^{-1}, og $k(FC(O)O+O_3)<6\times10^{-14}$ cm^3 molekyle^{-1} s^{-1}. Resultaterne fra dette arbejde viser, at FCO_x radikaler ikke nedbryder det stratosfæriske ozon lag.

Det sidste produkt af atmosfærisk nedbrydning af HFC of HCFC, som er blevet studeret, er FO_x, x=0,1,2. Reaktionerne af FO_2 med NO, NO_2, CH_4, CO og O_3 samt reaktionen mellem FO og O_3 er blevet undersøgt. De fundne hastighedskonstanter er $k(FO_2+NO)=(1.47\pm0.08)\times10^{-12}$ cm^3 molekyle^{-1} s^{-1}, $k(FO_2+NO_2)=(1.05\pm0.15)\times10^{-13}$ cm^3 molekyle^{-1} s^{-1}, $k(FO_2+CO)<5.1\times10^{-16}$ cm^3 molekyle^{-1} s^{-1}, $k(FO_2+CH_4)<4.1\times10^{-15}$ cm^3 molekyle^{-1} s^{-1}, $k(FO_2+O_3)<3.4\times10^{-16}$ cm^3 molekyle^{-1} s^{-1} and $k(FO+O_3)<1.2\times10^{-12}$ cm^3 molekyle^{-1} s^{-1}. Resultaterne fra dette arbejde sammen med resultater fra litteraturen viser, at FO_x kemi kun har ubetydelig indflydelse på det stratosfæriske ozonlag.

Table of Contents

Preface

The work for this Ph. D. thesis was done at the Section of Chemical Reactivity at Risø National Laboratory during the period 1. October 1991 to 1. February 1992 and 1. September 1992 to 1. October 1994 with Dr. Ole John Nielsen (Risø) and Dr. Fleming Nicolaisen (Inst. of Chem. University of Copenhagen) as supervisors. From 1. February 1992 to 1. September 1992 I worked together with Dr. Timothy J. Wallington, Ford Research Laboratory, Michigan, US. The work is supported by the Danish Research Academy and Risø National Laboratory.

I wish to thank my supervisors for valuable help through out the three years as a Ph. D. student. Especially, I wish to thank Dr. Ole John Nielsen who has been a great inspiration during my work. Special thanks also to Dr. Timothy J. Wallington who taught me a lot in the 7 months I stayed at his laboratory. I would also like to thank Thomas Ellermann, Trine Møgelberg, and Jesper Platz whom I worked with at Risø. Finally, I would like to thank all the staff at the Chemical Reactivity Section and Ford Research Laboratory for support throughout my work.

I have tried to make this thesis as brief as possible since most of the material presented here has already been published in international journals. To reduce the size of this thesis I have presented the results, apart from the pulse radiolysis and product studies of halogenated peroxy radicals, as extended abstracts of the published papers. The articles, where only abstracts are presented, are given in full length in the Appendix. Published work is referred to by a number in the Appendix whether it is given in full length or not. The thesis reports the results of work done before april 1994.

I have only used a few acronyms, namely CFC (chlorofluorocarbon), HFC (hydrofluorocarbon), HCFC (hydrochlorofluorocarbon), ODP (ozone depletion potential), GWP (greenhouse warming potential), HGWP (halocarbon greenhouse warming potential), and VOC (volatile organic compounds).

A few minor corrections have been included in this edition compared to the thesis which was defended on October 28. 1994.

1 Atmospheric Chemistry of HFCs and HCFCs

1.1 Introduction

CFCs (freons) were developed in 1930 by General Motors Research Laboratories in the search for non-toxic non-flammable refrigerants. CFCs have also been used as aerosol propellants and as blowing agents for plastic foam production. In 1974 Molina and Rowland [1] proposed that chlorine atoms, formed by photolysis of CFCs, cause catalytic ozone destruction in the stratosphere. The ozone hole discovered in 1985 [2] over Antarctica has prompted the phase out of production of CFCs by the end of 1995. Freon substitutes are therefore sought. HFCs (hydrofluorocarbons) and HCFC (hydrochlorofluorocarbons) are prominent classes of CFC replacement compounds. For example HFC-134a (CF_3CFH_2) is used as a refrigerant and in automotive air condition systems as an alternative to CFC-12 (CCl_2F_2) and HCFC-22 ($CClF_2H$). HCFC-141b ($CFCl_2CH_3$) may be used as substitute for CFC-11 ($CFCl_3$) in foam blowing units.

The choice of using HFCs and HCFCs instead of CFCs is motivated by a number of factors. HFCs and HCFCs contain one or more C-H bond. Hence, HFCs and HCFCs are susceptible to attack by OH radicals in the troposphere (lower atmosphere). HFCs do not contain Cl atoms and so do not have any ozone depletion potential associated with the well established chlorine catalytic cycle. In this work it is been shown that no other catalytic cycles involving radicals formed from HFCs in the atmosphere destroy stratospheric ozone. HCFCs do contain Cl atoms, however, the delivery of the Cl atoms is inefficient since most of the HCFC is scavenged by OH in the troposphere.

HFCs and HCFCs are volatile compounds which will upon release migrate into the atmosphere. When introducing these new compounds, their environmental impact needs to be evaluated. Questions like; 1) What is the impact on the ozone layer of releasing huge amounts of these compounds ?; 2) What is the effect on the global radiation budget ?; 3) What are the products of the atmospheric degradation of these compounds ?. To address these questions, the detailed degradation mechanisms and the rate constants for important reactions of these compounds need to be investigated. 4 years ago little was known about the atmospheric fate of these compounds. The importance of this issue has prompted a huge research effort the last 4 years and has also been an inspiration in the present work.

In this chapter, results presented in the articles published from this work and relevant literature dealing with HFC-23 (CF_3H), HFC-125 (CF_3CF_2H), HFC-134 (CF_2HCF_2H), HFC-143a (CF_3CH_3), HFC-152 (CH_2FCH_2F), and HCFC-124 (CF_3CFClH)

are used to determined the atmospheric fate and products of the atmospheric degradation of these compounds. In addition the atmospheric chemistry of important atmospheric oxidation products of the HFCs and the HCFCs are discussed.

1.2 Reaction of OH with HFCs and HCFCs

It is expected that HFCs and HCFCs will be produced in hundred thousands of tones annually by year 2000. These compounds will eventually be released to the atmosphere. In the atmosphere the main degradation pathway (>90%) of HFCs and HCFCs is reaction with the OH radical.

$$OH + RH \rightarrow R + H_2O \qquad (1)$$

Other degradation pathways should be mentioned including photolysis, reaction with Cl atoms and $O(^1D)$ atoms in the stratosphere. However, these pathways are of minor importance. A significant kinetic data base exists on the reaction of OH with HFCs and HCFCs [3,4,5]. From the reaction rate of HFCs and HCFCs with OH it is possible to establish the atmospheric lifetimes of the HFCs and HCFCs. Lifetimes are in the range 2-411 years and are listed in Table IV in chapter 1.5 [6,7]. These life times are important parameters in the calculation of ODP, GWP and HGWP as discussed later.

1.3 Reactions of Peroxy Radicals

Reaction with OH initiates the degradation of the HFC or HCFC. A generalized HFC or HCFC degradation scheme is shown in Figure 1. Order of magnitude estimates for the lifetimes of the different species are shown in parentheses. X and Y may be H, Cl, or F atoms. Halogenated alkyl radicals will, after being formed from reaction of OH with the HFC or HCFC, react within a few μs with O_2 to form a peroxy radical.

$$R + O_2 + M \rightarrow RO_2 + M \qquad (2)$$

Because oxygen is so abundant in the atmosphere and the rate constant for reaction (2) generally is of the order of 10^{-12} cm^3 $molecule^{-1}$ s^{-1}, reaction (2) will be the sole fate of halogenated alkyl radicals in the atmosphere.

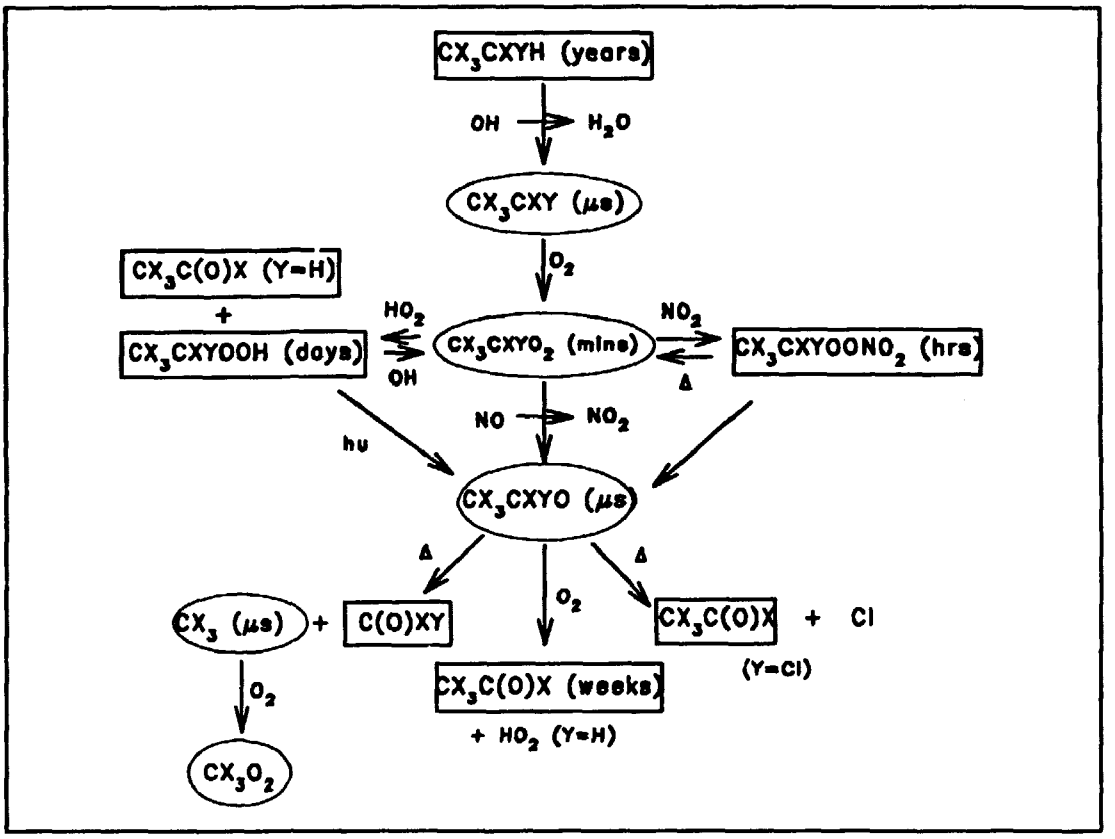

Figure 1. *Generalized scheme for the atmospheric oxidation of HFCs or HCFCs of type CX_3CXYH (X, Y = H, Cl, F). Transient radical intermediates are enclosed in ellipses. Products and less transitory species are given in boxes.*

Once the halogenated alkyl peroxy radical has been formed it has four possible reaction pathways in the atmosphere of which three are shown in Figure 1, namely reaction with NO, NO_2, and HO_2. A fourth reaction pathway is reaction with another peroxy radical, $R'O_2$. To asses the relative importance of these reactions, the rates of reaction and the atmospheric concentrations of NO, NO_2, HO_2, $R'O_2$ need to be determined. In the following we will use average atmospheric concentrations of NO, NO_2, and HO_2 from ref. [3] of 1.5, 2.5, and 10×10^8 molecules cm^{-3}, respectively. The rates, the products, and the importance of these reactions are discussed in the following paragraphs.

The importance of the fourth reaction pathway, reaction of RO_2 with other peroxy radicals, can not be evaluated at the moment, since only very few rate constants for the cross reactions between different peroxy radicals are known [8,9]. Since CH_3O_2 is the most abundant peroxy radical besides HO_2, the reactions of interest are mainly reactions of CH_3O_2 with other peroxy radicals. An estimate of the average atmospheric concentration of CH_3O_2 is 2.5×10^8 molecules cm^{-3} [3]. This is a factor of 4 less than the estimated HO_2 concentration. Hence, the reaction rates need to be of 4 times faster then the HO_2 rate

constants to be of comparable importance. The reaction of CH_3O_2 radical with other peroxy radicals is an important area of future research.

1.3.1 Reaction of RO_2 with NO

The reaction of peroxy radicals with NO have been studied extensively [8,9,Appendix 7.11.7 pp205, 7.11.12 pp205, 7.11.22 pp205, 7.6 pp158, 7.9 pp188]. The peroxy radicals derived from the HFCs and HCFCs react fast with NO, k=0.8-2x10^{-11} cm^3 $molecule^{-1}$ s^{-1}. Using an average atmospheric concentration of NO of 2.5x10^8 molecules cm^{-3}, atmospheric lifetimes for the reactions of halogenated peroxy radicals with NO of 4-8 min were derived.

The reaction of halogenated alkyl peroxy radicals with NO may proceed through two reaction pathways:

$$RO_2 + NO\ (+ M) \rightarrow RO + NO_2 \qquad (3a)$$

$$\rightarrow RONO_2\ (+ M) \qquad (3b)$$

At 1000 mbar of SF_6, the yields of NO_2 upon reaction of RO_2 radicals with NO is (100±10)% (HFC-23), >100% (CF_3CF_2H), >100% (CHF_2CF_2H), >100% (CF_3CH_3), and (73±13)% (HFC-143a). These results show that the reaction RO_2 with NO for halogenated peroxy radicals mainly proceed through reaction (3a). The low yield of NO_2 in the reaction of $CF_3CH_2O_2$ with NO, is discussed in chapter 4 and it is concluded that this reaction could give exclusively NO_2 and CF_3CH_2O. From the above results it can be concluded that formation of alkyl nitrate is not a major reaction channel of reaction (3). Alkyl nitrates are expected to photolyze in the atmosphere. The products and quantum yields of photolysis have not been extensively studied. However, the lack of structure in the absorption spectra suggests that the quantum yield for decomposition via RO-NO_2 bond cleavage is close to unity [4,10]. Thus, it is unlikely that halogenated nitrates has significant life times in the atmosphere (of the order of days). It is therefore expected that the final product of the reaction of halogenated peroxy radicals with NO in the atmosphere is the alkoxy radical, RO, and NO_2.

1.3.2 Reaction of RO_2 with NO_2

The reaction rate of the reaction of halogenated peroxy radicals with NO_2 are all similar and pressure dependent as described in the review by Lightfoot et al. [9]. k_{oo}, the

rate constant at infinite total pressure, is in the range (4.5-8.9)x10^{-12} cm^3 $molecule^{-1}$ s^{-1} while k_o, the rate constant at zero total pressure, is dependent on the size of the alkyl part of the peroxy radical. At one bar total pressure the reaction of RO_2 and NO_2 are close to the high pressure limit. As part of this work, the rate constants for the reaction of $CF_3CH_2O_2$ and CF_3CFClO_2 with NO_2 at 1 bar SF_6 were determined (see section 4.5). Rate constants are all consistent with the previous determinations of k_{oo} for the reaction of halogenated peroxy radicals with NO_2. Using an atmospheric concentration of 2.5x10^8 molecules cm^{-3} the lifetime of halogenated alkyl peroxy radicals with respect to reaction with NO_2 are 7-15 min.

The product of the reaction between RO_2 and NO_2 is a peroxy nitrate, RO_2NO_2. Alkyl peroxy nitrates are thermally unstable and decompose to regenerate RO_2 radicals and NO_2 [9]. Another possible loss reaction of peroxy nitrates in the atmosphere is photolysis. For α-halogenated peroxy radicals like $CF_2ClO_2NO_2$, $CFCl_2O_2NO_2$, and $CCl_3O_2NO_2$ the lifetime range from 5-20 sec at 298 K to 0.1 to 1 year in the upper troposphere [11]. Comparable lifetimes are expected to be found for other α-halogenated peroxy radicals, however, lifetimes for $CF_2ClCH_2O_2NO_2$, and $CFCl_2CH_2O_2NO_2$ are significantly less, approximately 2 days in the upper troposphere [12]. Recent measurements by Møgelberg et al.[13] give an upper limit for the life time of the decomposition of $CF_3CFHO_2NO_2$ at 296 K of 80 s.

The photolysis of peroxy radicals have not been studied extensively. However, results from studies of the UV spectra of $CH_3O_2NO_2$, $CFCl_2O_2NO_2$, and $CCl_3O_2NO_2$ [14,15,16] indicate, that the lifetimes of peroxynitrates in the lower troposphere of approximately 5 days. These results suggests that significant transportation of halo alkyl peroxynitrates to the stratosphere will not occur except possibly at high latitudes during winter nighttime conditions.

1.3.3 Reaction of RO_2 with HO_2

Peroxy radicals are known to react with HO_2 radicals in the atmosphere. At present both the products and the rates of the reactions of halogenated peroxy radicals with HO_2 are uncertain. Two product channels are known:

$$RO_2 + HO_2 \rightarrow ROOH + O_2 \quad (4a)$$

$$\rightarrow R'CXO + H_2O + O_2 \quad (4b)$$

The hydroperoxide (ROOH) and the carbonyl compound (RXO) are possible products of reaction (4) if the peroxy radicals contain an α-H atom (e.g. CH_2FO_2). If no α-H atom is

available, only the hydroperoxide channel is possible. The only product study of the reaction of a halogenated peroxy radical with $^{\bullet}IO_2$ is between CH_2FO_2 and HO_2 giving (71±11)% HCOF and (29±8)% CH_2FOOH [Appendix 7.11.13 pp205]. However, a recent study of the reaction of CF_3CFHO_2 with HO_2 reports an upper limit for aldehyde formation from this reaction of 5% [17]. The products of the reaction of HO_2 radicals with the peroxy radicals is therefore uncertain when an α-H atom is present in the peroxy radical. The reaction of the peroxy radicals from HFC-23, HFC-125, HFC-134, and HCFC-124 with HO_2 are expected to give 100% hydroperoxide.

The rate of reaction (4) has to be estimated from the two available studies of reactions of halogenated peroxy radicals with HO_2. The reactions of CF_3CFHO_2 and $CF_2ClCH_2O_2$ with HO_2 proceed with rates of $(4.1\pm2.2)\times10^{-12}$ cm^3 $molecule^{-1}$ s^{-1} and $(6.9\pm2.6)\times10^{-12}$ cm^3 $molecule^{-1}$ s^{-1} [18], comparable with rates of the reaction of CH_3O_2 and $C_2H_5O_2$ with HO_2. However, the rate of the reaction between $CF_3CCl_2O_2$ and HO_2 is $(1.9\pm0.3)\times10^{-12}$ cm^3 $molecule^{-1}$ s^{-1} [19] and an upper limit have been determined for the reaction of CF_3O_2 and HO_2 of 2×10^{-12} cm^3 $molecule^{-1}$ s^{-1} [18]. Recently, the rate constant for the reaction of CH_2ClO_2 with HO_2 have been determined to 4.9×10^{-12} cm^3 $molecule^{-1}$ s^{-1} [20]. The best estimate of the reaction rate of halogenated peroxy radicals with HO_2 seems therefore $(2\text{-}7)\times10^{-12}$ cm^3 $molecule^{-1}$ s^{-1}. Using an HO_2 concentration of 10^9 molecules cm^{-3} we can estimate the life time of a halogenated peroxy radical with HO_2 to 2-8 min.

As discussed by Atkinson et al. [3,4] hydroperoxides are expected to return to the peroxy or alkoxy radical pool due to either photolysis or reaction with OH. In addition wet and probably dry deposition are expected to be efficient. The life time of the hydroperoxides are therefore expected to be of the order of days. The fate of the carbonyl compounds are discussed in a later paragraph.

1.3.4 Atmospheric Fate of Peroxy and Alkoxy Radicals

As seen from the reaction scheme in Figure 1 the atmospheric chemistry of halogenated peroxy radicals is complex. However, from the life times of the reaction of RO_2 with NO_2, NO, and HO_2 it can be concluded that the reaction of RO_2 with NO and HO_2 is expected to be a major fate of RO_2 in the atmosphere. As discussed previously, the reaction between RO_2 radicals and NO will give the alkoxy radical as the product either direct or indirect by photolysis of the alkylnitrate, $RONO_2$. Peroxy nitrates, RO_2NO_2, are expected to undergo thermal decomposition or photolysis sufficiently rapid that the reaction of RO_2 with NO_2 will only be a temporary reservoir for RO_2 radicals. Hydroperoxides also tend to regenerate either the alkoxy radical, RO, through photolysis,

or RO_2 by reaction with OH. Thereby hydroperoxides also serves only as a reservoir species. However, wet and dry deposition may be fast and thereby taking a fraction of the ROOH molecules out of the RO_2 and RO pool.

The carbonyl compound may be formed by the reaction of HO_2 radicals and halogenated peroxy radicals containing an α-H atom. The importance of this reaction channel and its dependence on the structure of the halogenated peroxy radical is not known at present. This is an important area of future research.

Table I: Primary atmospheric products of alkoxy radicals.

Alkoxy radical	Products
CF_3CH_2O	CF_3CHO and HO_2
CH_2FCHFO	CH_2F and HCOF
CF_3O	discussed in 1.4.2
CF_3CF_2O	CF_3 and CF_2O
CHF_2CF_2O	CHF_2 and CF_2O
CF_3CFClO	CF_3COF and Cl
CH_2FO	HCOF and HO_2
CHF_2O	CF_2O and HO_2
CF_3CFHO	30% CF_3COF and HO_2 70% CF_3 and HCOF

Product studies of a series of halogenated hydrocarbons have led to a good understanding of the fate of halogenated alkoxy radicals. The alkoxy radicals studied as a part of this work have three main reaction pathways in the atmosphere: (i) reaction with O_2 to form an aldehyde and HO_2 (ii) C-C bond cleavage (iii) elimination of a Cl atom:

$$RCXHO + O_2 \rightarrow RCXO + HO_2 \quad (5)$$

$$RCXYO + M \rightarrow R + CXYO + M \quad (6)$$

$$RCXClO + M \rightarrow RCXO + Cl + M \quad (7)$$

In addition three other reaction pathways exist: (i) HCl elimination, (ii) H intramolecular transfer, and (iii) H atom elimination. These last three reaction pathways will not be further discussed here because they are unimportant for the present work.

Among the six HCFCs and HFCs investigated here, there are examples of all three major reaction channels. The atmospheric products of nine alkoxy radicals are listed in Table I. It is seen from Table I that only one product channel is active for all halogenated alkoxy radicals in the table apart from the CF_3CFHO radical. The fate of three alkoxy radicals that are not directly studied in this work is included in Table I: CH_2FO, CF_2HO, and CF_3CFHO. The two first radicals are included because the alkyl radicals from which they are formed, are produced in the degradation of the HFCs or HCFCs studied here. The alkoxy radical formed from the degradation of HFC-134a, CF_3CFHO, is listed for three reasons: (i) A product study of this compounds have been investigated to study the reactions of the CF_3O radical. Results are discussed in Chapter 6.2.2. (ii) HFC-134a is the industrially most important compound. (iii) CF_3CFHO is the only alkoxy radical which has more then one important degradation pathway. The atmospheric reactions of the CF_3O radical are discussed in later.

1.4 HFC and HCFC Degradation Products

Carbonyl compounds can be formed from the atmospheric degradation of HFCs and HCFCs in four different ways (see Figure 1): (i) From the reaction of HO_2 and RO_2. (ii) From the reaction of halogenated alkoxy radicals with O_2. (iii) From the decomposition of an alkoxy radicals to give a carbonyl compound and a chlorine atom. (iv) From the decomposition of an alkoxy radicals to give an alkyl radical and a carbonyl compound.

The alkoxy radical CF_3O is also formed in the atmospheric degradation of HFCs and HCFCs containing CF_3-groups. The atmospheric chemistry of the CF_3O radical is discussed in a special paragraph in the following.

The atmospheric chemistry of products formed from the atmospheric degradation of the carbonyl compounds and/or from the CF_3O radical, namely CF_3CO_x, FCO_x, and FO_x radicals are also discussed in the following.

1.4.1 Halogenated Carbonyl Compounds

As seen from Table I, four different carbonyl compounds are formed in the degradation of the HFCs and HCFCs studied in this work: CF_3COF from CF_3CFH_2 and

CF_3CFClH, CF_3CHO from CF_3CH_3, CF_2O from CHF_2CHF_2 and CF_3CF_2H, and HCOF from CH_2FCH_2F and CF_3CFH_2.

The tropospheric chemistry of CF_3COF, CF_2O, and HCOF is believed to be dominated by incorporation into water droplets leading to the formation of $CF_3C(O)OH$ (τ<5-10 days), HF and CO_2 (τ<5-10 days), and HF and HCOOH (τ=150-1500 days), respectively [Appendix 7.11.19 pp205]. The lifetime of HCOF with respect to reaction with OH is >11 years [21]. The aldehyde compound, CF_3CHO, may be incorporated into water droplets, react with OH, or photolyze in the troposphere. The lifetime for incorporation into water droplets and photolysis lifetime for CF_3CHO is unknown. However, by analogy with other halogenated aldehydes and the chloro aldehydes the hydrolysis and photolysis lifetimes are likely to be of the order of 5-10 days [Appendix 7.11.19 pp205,22]. The lifetime of CF_3CHO with respect to reaction with OH is 24 days [22]. Recently, a preliminary study suggested a yield of 56% of CF_3H from the photolysis of CF_3CHO [23]. This have serious ramifications for the GWP (greenhouse warming potential) of HFC-143a (CF_3CH_3) since the lifetime of CF_3H is an order of magnitude larger than for the parent compound CF_3CH_3. This needs to be investigated further.

In the stratosphere wet deposition is not efficient, so photolysis of HCOF, and possibly CF_2O and CF_3COF, is possible. This leads to the formation of some interesting radicals, for example FCO_x, and CF_3CO_x. The reaction of OH radicals with CF_3CHO also gives rise to CF_3CO_x radicals both in the stratosphere and the troposphere. The fluorine atoms formed by photolysis of for example CF_2O and CF_3COF will produce FO_2 radicals by reaction with O_2.

It have been suggested that HFCs and HCFCs could have an impact on the stratospheric ozone layer through CF_3CO_x [24], CF_3O_x [25], FCO_x [26], and FO_x [27] catalytic cycles destroying ozone. The atmospheric chemistry of CF_3CO_x, CF_3O_x, FCO_x, and FO_x are discussed in following sections.

1.4.2 Atmospheric Chemistry of $CF_3C(O)OH$

$CF_3C(O)OH$ is known to be produced from the hydrolysis of CF_3COF, CF_3CHO, and possibly $CF_3CFHOOH$. In addition, a fraction of the reaction of $CF_3C(O)O_2$ with HO_2 may give $CF_3C(O)OH$. The only channel for $CF_3C(O)OH$ in atmosphere is reaction with OH. The rate constant for this reaction has recently been determined to $1.2\text{-}1.7\times10^{-13}$ $cm^3molecule^{-1}s^{-1}$ [28,29]. It was estimated that this reactions consume approximately 10% of the $CF_3C(O)OH$ formed in the atmosphere. There are no known sinks for $CF_3C(O)OH$ in rain droplets and ground water. The concentrations of $CF_3C(O)OH$ in rainwater will be low. For example, HFC-134a (CF_3CFH_2) is a replacement for CFC-12

(CF_2Cl_2). In 1986 the global production of CFC-12 was $4x10^8$ kg. If HFC-134a replaces CFC-12 on an equal mass basis and all the HFC-134a is released without recovery, the emission to the atmosphere would be $4.0x10^8$ kg or $3.9x10^9$ mol/year. At steady state, assuming each CF_3CFH_2 is converted into $CF_3C(O)OH$, $3.9x10^9$ mol of $CF_3C(O)OH$ would be formed and incorporated into water droplets annually. The global annual rainfall is $4.9x10^{17}$ L [30]. Thus, rainwater might be expected to contain $8x10^{-9}$ M (0.15 ppb). This concentration is not expected to have any impact on the human health [3,31]. There are also no published data which suggest that 0.15 ppb $CF_3C(O)OH$ in rainwater should have any impact on plant systems. Further research is needed to establish the environmental fate and impact of $CF_3C(O)OH$.

1.4.3 Atmospheric Chemistry of Acyl Peroxy Radicals

The fate of $CF_3C(O)O_2$ radicals in the atmosphere has been studied in this work [Appendix 7.9 pp189 and 7.10 pp198]. The results are described in section 6.1.

As discussed above, CF_3CO radicals may be formed by photolysis of CF_3COF in the stratosphere. In addition, photolysis of CF_3CHO may form CF_3CO and the reaction of OH with CF_3CHO will produce CF_3CO radicals in both the stratosphere and the troposphere. In the atmosphere, the CF_3CO radical can either add O_2 or decompose to CF_3 and CO:

$$CF_3CO + M \rightarrow CF_3 + CO \quad (8)$$

$$CF_3CO + O_2 + M \rightarrow CF_3C(O)O_2 + M \quad (9)$$

It have been shown that the sole fate of CF_3CO radicals in the atmosphere is reaction with O_2 to form $CF_3C(O)O_2$ [Appendix 7.9 pp189]. The reactions of $CF_3C(O)O_2$ with NO and NO_2 have been investigated and the rate constants determined to be $(1.03\pm0.29)x10^{-11}$ cm^3 $molecule^{-1}$ s^{-1} and $(6.6\pm1.3)x10^{-12}$ cm^3 $molecule^{-1}$ s^{-1} (see section 6.1). With these reaction rates and atmospheric concentrations of $2.5x10^8$ molecules cm^{-3} for both NO and NO_2, I arrive at atmospheric lifetimes for the $CF_3C(O)O_2$ radical with respect to reaction with NO and NO_2 of 6 min and 10 min, respectively. The atmospheric fate of the alkoxy radical, $CF_3C(O)O$, produced by the reaction of $CF_3C(O)O_2$ with NO has been shown to be decomposition to CF_3 and CO_2. The peroxynitrate formed by the reaction of $CF_3C(O)O_2$ and NO_2 is very stable towards thermal decomposition with decomposition life times of a few days at the earths surface to thousands of years in the upper troposphere [32,Appendix 7.10 pp198]. The lifetime of $CF_3C(O)O_2NO_2$ is expected to be limited by photolysis and transport to the lower troposphere. The UV spectrum of $CF_3C(O)O_2NO_2$ is not known but by analogy to the peroxy acetyl nitrate the life time will be of the order of

1 month [33]. Some transportation could therefore take place over the tropospause. However, $CF_3C(O)O_x$ radicals will not harm the stratospheric ozone layer since the radicals involved in a possible ozone destroying cycle, $CF_3C(O)O$ (τ=0.015-20 ms) and CF_3CO (τ=μs) will decompose in the atmosphere [Appendix 7.9 pp189].

The reaction of $CF_3C(O)O_2$ with HO_2 is likely to be of some importance in the atmosphere. Neither the products nor the rate constant are known for this reaction. However, by analogy with the reaction of the acetyl peroxy radical with HO_2 it is expected that both $CF_3C(O)OH$ and $CF_3C(O)OOH$ will be products of this reaction. The most likely fate of these products is rain out and reaction with OH.

1.4.4 Atmospheric Chemistry of CF_3O Radicals

CF_3H (HFC-23), CF_3CF_2H (HFC-125), CF_3CFH_2 (HFC-134a) and probably also other HFCs containing CF_3-groups will, upon release to the atmosphere, form CF_3O_x radicals. It have been suggested that CF_3O_x radicals destroy ozone by a chain process, reaction (10) and (11) [25]:

$$CF_3O_2 + O_3 \rightarrow CF_3O + 2O_2 \quad (10)$$

$$CF_3O + O_3 \rightarrow CF_3O_2 + O_2 \quad (11)$$

$$O_3 + O_3 \rightarrow 3O_2$$

k_{10} and k_{11} together with the rate constants for loss reactions of CF_3O are essential in the model calculations of the ozone depletion efficiency of CF_3O_x radicals in the stratosphere. Model calculations are beyond the scope of this work but, in the following I will give an overview of the reactions involved and an estimate of the possible ozone destruction due to the CF_3O_x radicals.

The rate constants known for CF_3O_x reactions of stratospheric interest are listed in Table II. The key reactions in the possible cyclic destruction of stratospheric ozone in the CF_3O_x cycle are the chain initiation step: the formation of CF_3O_x from HFCs containing CF_3 groups, the chain propagation steps: the reaction of CF_3O_x radicals with ozone, and the only known termination processes: the reactions of CF_3O radicals with NO and CH_4. In addition holding process like the CF_3O_2 reaction with NO_2 producing the reservoir species $CF_3O_2NO_2$ and processes leading to a net ozone null destruction cycle like the reaction of CF_3O_2 with NO followed by NO_2 photolysis are also important.

The products of the reaction of CF_3O_x radicals with ozone are not known but they could produce the species shown in Table II. The product distribution of the reaction of CF_3O radicals with NO is very important since formation of FNO and CF_2O from this

reaction is one of the main chain termination reactions known at the moment. The products of the reaction of CF_3O and NO have been determined at room temperature. At stratospheric temperatures the product could be CF_3ONO. This species could photolyze to reform CF_3O_x radicals and thereby not terminate the chain process. The products of this reaction at low temperatures should be one of the major targets for future investigations.

Table II. Summary of CF_3O_x reactions.

Reaction	Rate constant (295 K) ($cm^3molecule^{-1}s^{-1}$)	
$CF_3O_2 + O_3 \rightarrow (CF_3O + 2O_2)$	$<10^{-14}$	[Appendix 7.7 pp165]
	$<3x10^{-15}$	[34]
$CF_3O_2 + NO_2 + M \rightarrow CF_3O_2NO_2 + M$	$3.8x10^{-12}$ [b]	[9]
$CF_3O_2NO_2 + M \rightarrow CF_3O_2 + NO_2 + M$	$1.5x10^{-10}$ [c]	[9]
$CF_3O_2 + NO \rightarrow CF_3O + NO_2$	$2.3x10^{-11}$ [a]	[9]
$CF_3O + O_3 \rightarrow CF_3O_2 + O_2$	$<3x10^{-13}$	This work
	$1x10^{-12}$	[25]
	$<6x10^{-14}$	[35]
	$<5x10^{-14}$	[36]
	$<4x10^{-14}$	[34]
	$<2x10^{-15}$	[37]
	$2.5x10^{-14}$	[38]
$CF_3O + NO \rightarrow CF_2O + FNO$	$5.2x10^{-11}$	[34,Appendix 7.6 pp151,38,39,40]
$CF_3O + NO_2 (+ M) \rightarrow (CF_3ONO_2 + M)$	$9x10^{-12}$	[39,41]
$CF_3O + CO \rightarrow$ products	$4.4x10^{-14}$	[39]
$CF_3O + CH_4 \rightarrow CF_3OH + CH_3$	$2.2x10^{-14}$	[40,42,43,44]

[a] T=220 K, [b] T=220 K, P=10mbar, [c] Unit: s^{-1}, T=220K

Other potential loss processes for CF_3O_x radicals in the stratosphere include the reaction of CF_3O with NO_2 and hydrocarbons. The product of the reaction of CF_3O and NO_2 at room temperature is CF_3ONO_2. This product is likely to photolyze in the

stratosphere to reproduce CF_3O radicals and NO_2. The reaction of CF_3O radicals with methane, is also important in the stratosphere. The reaction is known to give CF_3OH and alkyl radicals. CF_3OH will presumably be stable in the stratosphere, since a lower

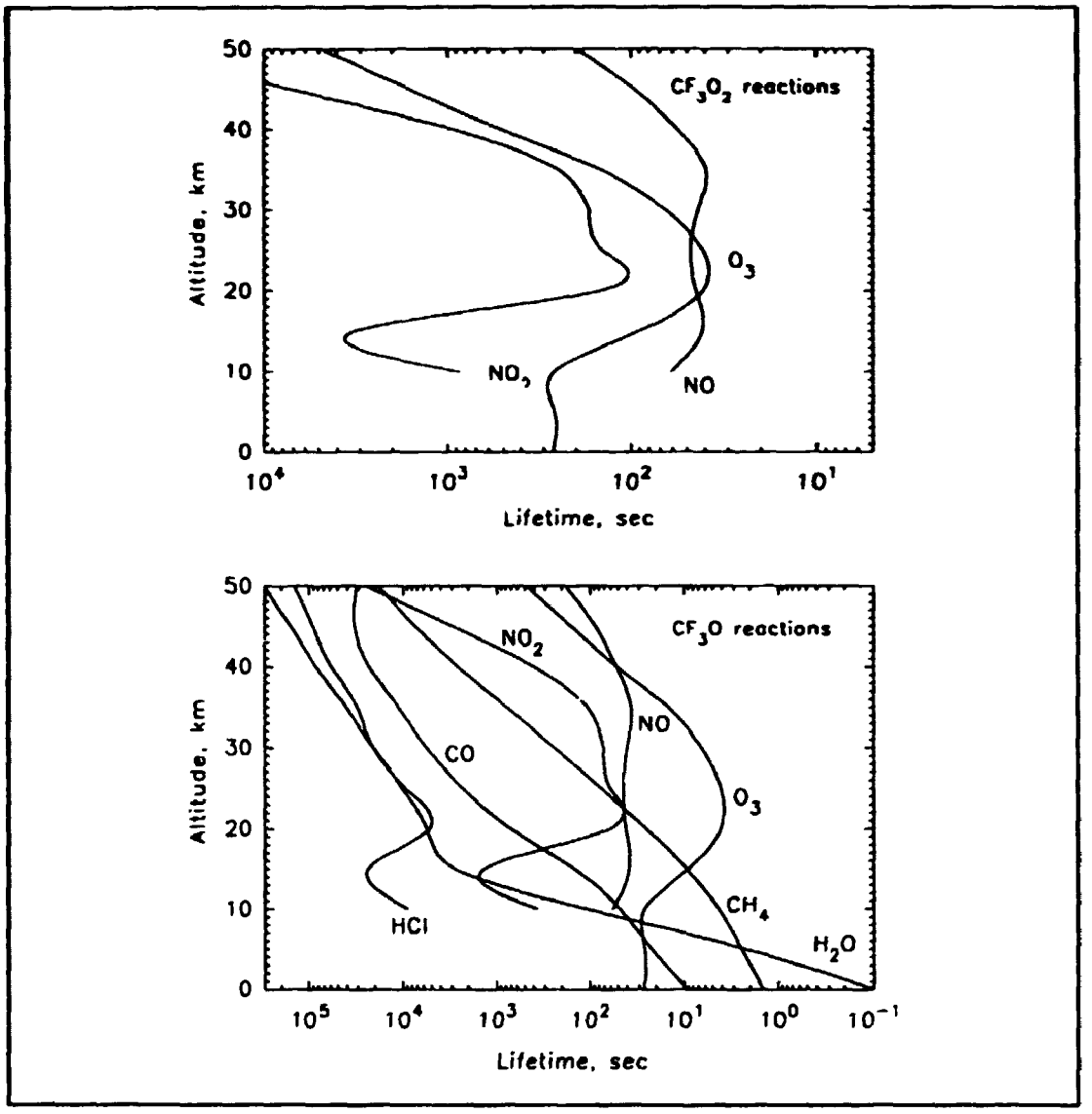

Figure 2. *Relative importance of CF_3O_2 and CF_3O reactions in the stratosphere as a function of altitude. Noon concentrations are taken from Brasseur and Solomon [45].*

limit for the thermal decomposition of lifetime of 5 hours have been established at room temperature [Appendix 7.5 pp151]. By analogy with CH_3OH, it is unlikely that CF_3OH will photolyze in the stratosphere and attack from OH is insignificant due to the strong OH-bonding in CF_3OH [Appendix 7.4 pp134]. Heterogeneous decomposition of CF_3OH on

particles in the stratosphere will presumably give CF_2O and HF as products. Hydrolysis will not be important in the stratosphere due to the low water content of the stratosphere.

In Figure 2 the lifetimes of CF_3O_x radicals towards reaction with trace gas species is displayed as a function of altitude. The trace gas concentrations at noon are taken from Brasseur and Solomon [45]. For CF_3O_x radicals reaction with ozone, upper limits of $k_{10}<10^{-14}$ $cm^3molecule^{-1}s^{-1}$ and $k_{11}<5x10^{-14}$ $cm^3molecule^{-1}s^{-1}$ have been used. It can be seen from the figure that with the upper limits for k_{10} and k_{11} established, the reactions of CF_3O_x radicals with ozone may still be the main reaction channels for these radicals in the stratosphere. However, the chain length of the cyclic of CF_3O_x radicals will be no more than ten.

It is interesting to consider the model work by Ko et al. [46,47] in the light of the upper limits of k_{10} and k_{11}. By model calculations and using $k_{10}=3x10^{-15}$ cm^3 $molecule^{-1}$ s^{-1}, $k_{11}=2x10^{-11}$ cm^3 $molecule^{-1}$ s^{-1}, and assuming the rate constant and the products of the reaction of CF_3O radicals and NO at 298 K is also valid at 220 K, Ko and Sze [46] calculate an ODP for HFC-134a of 0.02. It seems reasonable to assume that the ODP of HFC-134a is approximately proportional to k_{11} since chain length of the ozone depleting circle is approximately proportional to k_{11}. Then, by comparing the upper limit for k_{11} determined in this work with the model work of Ko and Sze [46], I arrive with an upper limit for the ODP of HFC-134a of $3x10^{-4}$. This would be 3-4 orders of magnitude less than the ODPs of CFCs and 2 orders of magnitude less than ODPs of hydrochlorofluorocarbons (HCFCs).

Recently, a model study of the impact of CF_3O_x radicals on the stratospheric ozone layer have shown that the ODP of HFCs due to CF_3O_x reactions are of the order of 10^{-4}-10^{-5} [34].

1.4.5 Atmospheric Chemistry of FCO_x Radicals

The FCO radical is formed by photolysis of HCOF (z>20 km) and CF_2O (z>30 km) in the atmosphere. Within a few μs, the FCO radical will add O_2 to give $FC(O)O_2$ radicals. These radicals react rapidly with NO to give FC(O)O and NO_2. The reaction rate of $FC(O)O_2$ with NO_2 is comparable to that of other peroxy radicals with NO_2 [8,9]. The stability of $FC(O)O_2NO_2$ is close to that of $CF_3C(O)O_2NO_2$ [48]. The rate and the products of the reaction of $FC(O)O_2$ with HO_2 are not known.

In the atmosphere, $FC(O)O_2$ radicals are expected to be converted largely into FC(O)O radicals. It has been suggested that $FC(O)O_2$ and FC(O)O radicals could form a catalytic cycle destroying ozone in the stratosphere [26]. However, the experimental results show that FC(O)O react very fast with NO, $k=(1.3\pm0.7)x10^{-10}$ cm^3 $molecule^{-1}$ s^{-1}, to form

FNO and CO_2. In addition, an upper limit for the reaction of FC(O)O radicals with ozone of $6x10^{-14}$ cm^3 $molecule^{-1}$ s^{-1} have been determined [Appendix 7.3 pp125]. The reaction of FC(O)O radicals with NO and possibly photolysis, break any possible ozone destroying process and the very low reaction rate for FC(O)O radicals with ozone make any ozone depletion due to FCO_x radicals negligible. If we compare the reactions of FCO_x with NO and ozone with the reactions of CF_3O with NO and ozone, it can readily be seen that the effect of FCO_x on the ozone layer is negligible.

1.4.6 Atmospheric Chemistry of FO_x Radicals

The FO_2 radical is in equilibrium with F atoms and O_2 in the atmosphere:

$$F + O_2 + M \rightleftharpoons FO_2 + M \qquad (12,-12)$$

The known FO_x reactions of importance in the atmosphere are displayed in Table III. Apart from the unimolecular decomposition of the FO_2 radical, all known activation energies are small. The rate constants at 295 K and 220 K are within a factor of two. For the sake of simplicity I have therefore only considered the temperature dependence of the decomposition of the FO_2 radicals in the following. While the temperature dependence of the rate constants of the first five reactions in Table III are not known, it is expected that the rates of these reactions will slow down at lower temperatures because of the significant energy involved in abstraction of F atoms from the FO_2 radical.

To evaluate the relative importance of the reactions of the F, FO, and FO_2 radicals in the atmosphere, knowledge of the atmospheric concentrations of the reactants are necessary. I have used the values of [NO], [NO_2], [CO], [O_3], [O], [M] and the temperature as function of altitude from Brasseur and Solomon [45]. These are noon and mid latitude values. The following reactions in Table III directly, or indirectly, destroy odd oxygen (O atoms or O_3 molecules):

$$F + O_3 \rightarrow FO + O_2 \qquad (13)$$
$$FO + O_3 \rightarrow FO_2 + O_2 \qquad (14)$$
$$FO + O \rightarrow F + O_2 \qquad (15)$$
$$FO + ClO \rightarrow F + Cl + O_2 \qquad (16)$$
$$FO_2 + O_3 \rightarrow FO + 2O_2 \qquad (17)$$
$$FO_2 + O \rightarrow FO + O_2 \qquad (18)$$

Table III. FO_x reactions.

Reaction	Rate constant (295K) $cm^3molecule^{-1}s^{-1}$	
$FO_2 + NO \rightarrow FNO + O_2$	$(1.5\pm0.1)\times10^{-12}$	This work
$FO_2 + O_3 \rightarrow FO + 2O_2$	$<3.4\times10^{-16}$	This work
$FO_2 + NO_2 \rightarrow$ products	$(1.05\pm0.10)\times10^{-13}$	This work
$FO_2 + CO \rightarrow$ products	$<5.1\times10^{-16}$	This work
$FO_2 + CH_4 \rightarrow$ products	$<4.1\times10^{-15}$	This work
$FO_2 + M \rightarrow F + O_2 + M$	$3.75\times10^{-8}[M]\exp(-6711/T)$ ¤	[49,50]
$FO_2 + O \rightarrow FO + O_2$	5.0×10^{-11} *	[5]
$FO + NO \rightarrow NO_2 + F$	2.6×10^{-11}	[5]
$FO + O \rightarrow F + O_2$	2.7×10^{-11}	[51]
$FO + O_3 \rightarrow$ Products	$<2\times10^{-16}$	[51]
$FO + O_3 \rightarrow$ Products	$<1.2\times10^{-12}$	This work
$FO + ClO \rightarrow F + Cl + O_2$	5×10^{-11}	#
$F + CH_4 \rightarrow CH_3 + HF$	$(6.8\pm1.4)\times10^{-11}$	[Appendix 7.11.3 pp205]
$F + H_2O \rightarrow OH + HF$	1.4×10^{-11}	[5]
$F + O_3 \rightarrow FO + O_2$	1.0×10^{-11}	[Appendix 7.11.9 pp205,36]
$F + O_2 + M \rightarrow FO_2 + M$	$4.4\times10^{-33}[M]$	[50]

* Uncertain, no experimental data [5]

¤ Calculated from $k_{-12}=k_{12}/K_d$. k_{12} is taken from [50] and K_d from [49].

Rate and products found by analogy with other halogen oxides self-reactions

There are two reactions which remove the F atoms efficiently from the FO_x catalytic cycle:

$$F + CH_4 \rightarrow HF + CH_3 \quad (19)$$

$$F + H_2O \rightarrow HF + OH \quad (20)$$

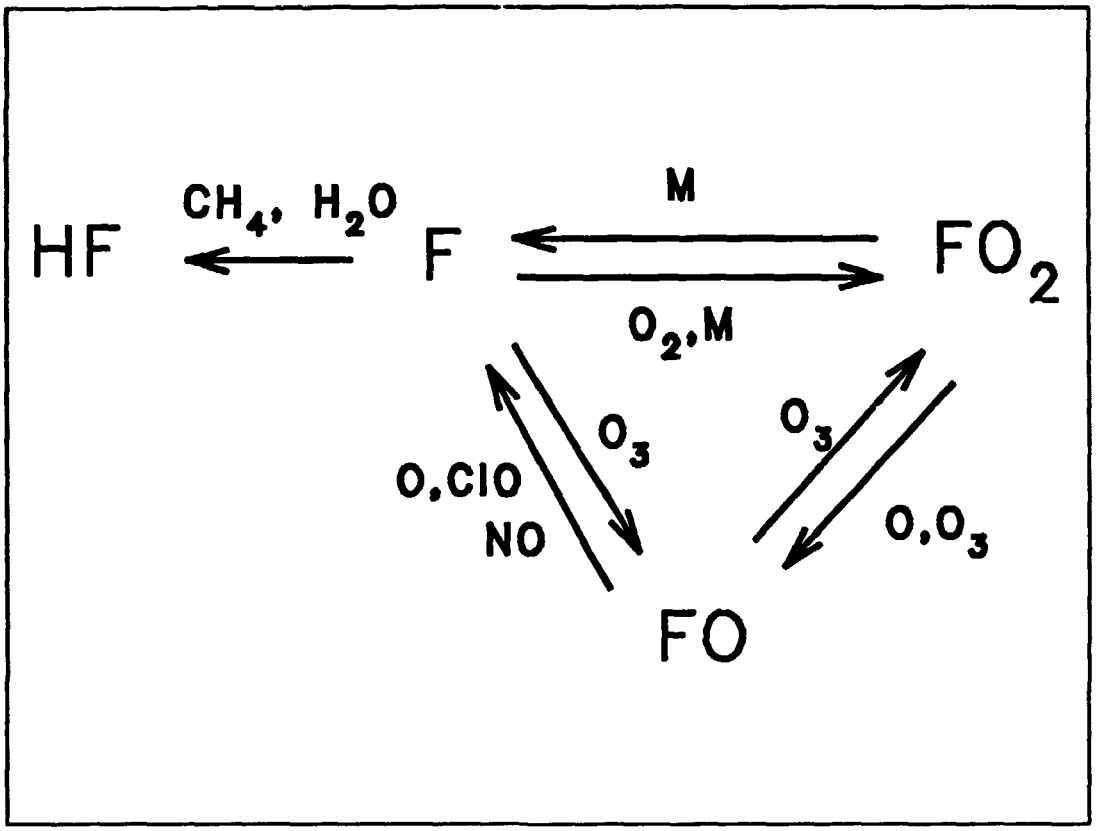

Figure 3. *Reaction scheme of the kinetic model used in the calculation of the effect of the FO_x radicals on the stratospheric ozone layer.*

HF is very unreactive in the stratosphere apart from reaction with $O(^1D)$ it is inert. Therefore HF is transported to the troposphere where it is incorporated into rain droplets and rained out.

In the following an upper limit for the number of ozone molecules destroyed by one F atom formed in the atmosphere is established. The mechanism applied to evaluate this is shown in Figure 3. The main reaction of F atoms in the atmosphere is reaction with O_2 to form FO_2. F atoms are then reformed by unimolecular decomposition of FO_2. FO radicals may be formed from the reaction of FO_2 radicals with O atoms and O_3 molecules and by the reaction of F atoms with ozone. FO radicals reform F atoms or FO_2 radicals by reaction with NO, O atoms, ClO, or O_3. F atoms are removed from the cycle by reaction with CH_4 and H_2O.

The number of times FO_2 radicals are reformed through the equilibrium (12,-12) before its removal by reaction with H_2O or CH_4 is:

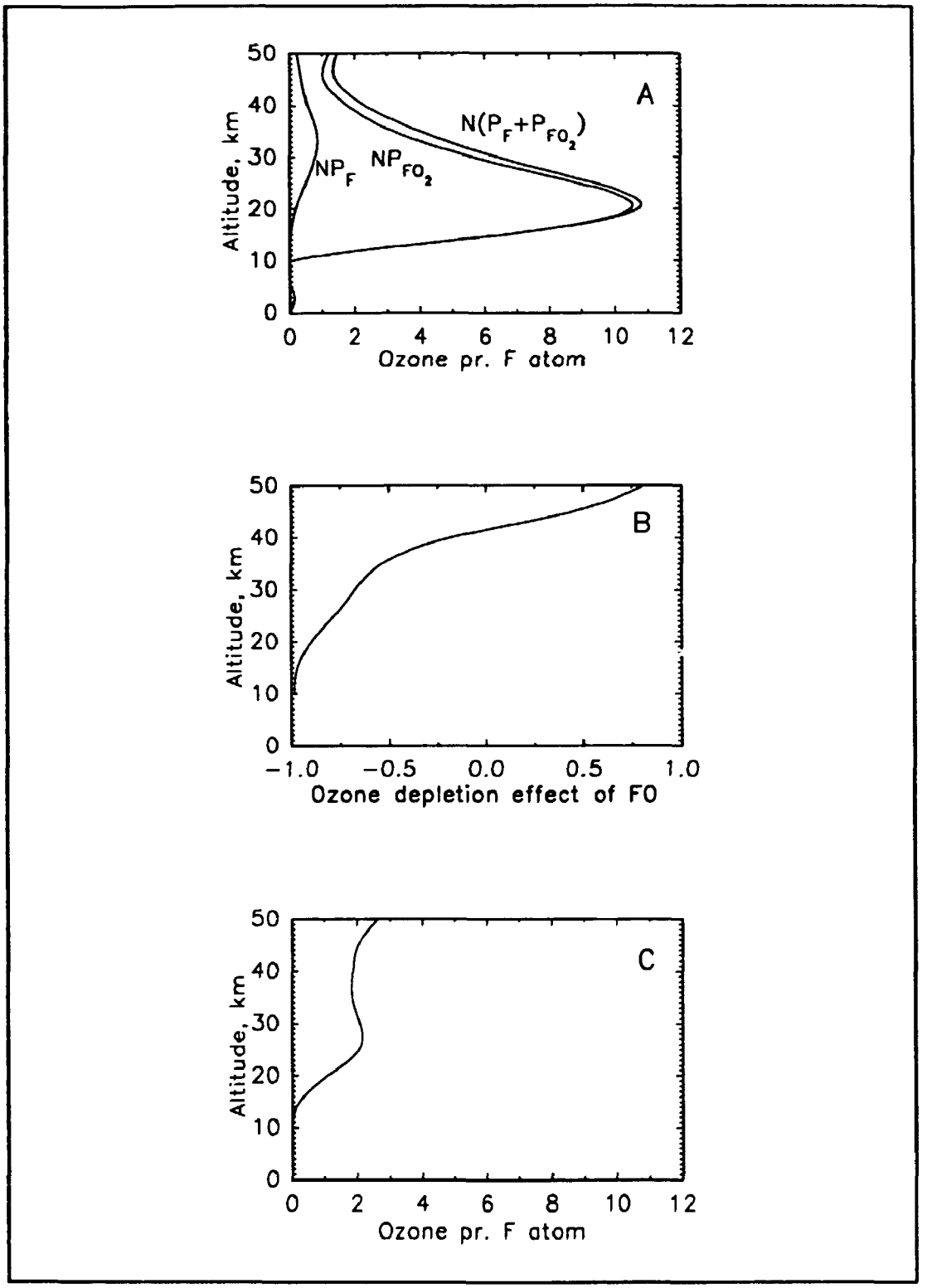

Figure 4. *Plot of the number of ozone molecules formed or destroyed by F atoms released to the stratosphere: simple model (A) and advanced model (C). Effect of a FO radical on the ozone layer before it forms FO_2 or F atoms (B). See text for details.*

$$N = k_{12}[O_2]/(k_{19}[CH_4]+k_{20}[H_2O])$$

The probability that F or FO_2 destroys an ozone molecule either as O_3 or O, before decomposition or reaction with O_2, is, respectively:

F: $$P_F=k_{13}[O_3]/k_{12}[O_2]$$

FO_2: $$P_{FO2}=(k_{17}[O_3]+k_{18}[O])/k_{-12}[O_2]$$

Under the assumption that FO radicals neither destroy nor form ozone before it forms FO_2 radicals or F atoms, we can derive an upper limit for the number of ozone molecules destroyed by one F atom released to the stratosphere. The upper limit is the product of the probability that a FO_2 radical or a F atom will destroy an ozone molecule before it is removed by decomposition or reaction with O_2, P_{FO2} and P_F, and the number of times F and FO_2 are reformed before F reacts with CH_4 or H_2O, $N(P_F+P_{FO2})$. NP_F, NP_{FO2}, and $N(P_F+P_{FO2})$ are plotted in Figure 4A at different altitudes. As seen from Figure 12A the maximum number of ozone molecules destroyed per F atom formed in the stratosphere from this simple model is 11 at 20 km altitude.

Now we will make our model a little more sophisticated. We will consider the FO reactions and include a reaction which has an analog in ClO chemistry.

$$FO + ClO \rightarrow F + Cl + O_2 \qquad (16)$$

This reaction could be fast by analogy with the self reaction of the FO radical, $(1.5^{+3}_{-1})\times10^{-11}$ cm^3 $molecule^{-1}$ s^{-1} [5]. In the following, $k_{16}=5\times10^{-11}$ $cm^3molecule^{-1}s^{-1}$ was used as a worst case assumption. The maximum ozone destruction potential of a FO radical before it is converted into FO_2 or F atoms is determined by reaction with ClO, O atoms, O_2, and NO_2. FO destroys one ozone molecule before it forms F or FO_2 if it reacts with ClO, O_3, or O atoms. If it reacts with NO it actually reforms an ozone molecule because the product, NO_2, photolyses to give NO and an O atom. The effect of FO radicals on the stratospheric ozone layer may be calculated from:

$$(k_{FO+NO}[NO]-k_{16}[ClO]-k_{14}[O_3]-k_{15}[O])/(k_{FO+NO}[NO]+k_{16}[ClO]+k_{14}[O_3]+k_{15}[O])$$

The values determined by this equation at different altitudes are plotted as a function of the altitude in Figure 4B. -1 means that an ozone molecule is formed, by reaction with NO, before FO is converted into F atoms or FO_2 radicals and +1 means that one ozone molecule is destroyed before FO is converted into FO_2 or F.

The real ozone destroying effect of the FO_x cycle may now be calculated as $N(P_F+P_{FO2})(1+FOeffect)$ because every time a FO radical is produced an ozone molecule is lost and the effects of reforming F or FO_2 from FO may be calculated from the equation above. As seen from Figure 4C, the effect of the FO_x cycle is small. About 2 ozone molecules are destroyed per F atom released to the stratosphere. This number should be compared 10^4-10^5 for Cl atoms. The effect of F atoms on the stratospheric ozone layer is negligible.

The method used to calculate the upper limit for the number of ozone molecules destroyed per F atom released to the stratosphere, is not exact. However, it gives a good estimate of the possible ozone depleting effect of FO_x radicals and shows that with the currently known FO_x reactions, the FO_x cycles do not pose a threat to the stratospheric ozone layer. The reactions of FO_2 with HO_2 and the temperature dependence of the reactions with NO_x need to be investigated because they have an impact on the stratospheric chemistry of FO_x radicals. Also the decomposition rate of FO_2 need to be confirmed.

1.5 ODP and GWP for HFCs and HCFCs

1.5.1 ODP for HFCs and HCFCs

In the discussion of the effects of halocarbons on stratospheric ozone the concept of "ozone depletion potential" ODP is useful because it is a measure for the relative effect of a species on the stratospheric ozone layer. The ODP is defined as the ratio of the calculated ozone column change per mass of a given compound released to the column for the same mass of CFC-11. In ODP it is assumed that no long lived products are formed which could transport chlorine to the stratosphere.

This definition describes the cumulative effect of the release and an estimate of the maximum calculated effect. One should note, however, that the time horizon is important. Let us compare a constant release of a CFC with a life time of 100 years with a constant release of a HCFC with a lifetime of 5 years. A steady state concentration of the HCFC in the atmosphere will be reached in about 20 years. The worst calculated effect on the ozone layer of a release of that particular HCFC with that particular rate will be reached in 20 years. For the atmospheric CFC concentration to reach its steady state level takes 400 years. A constant release of CFCs in 400 years is unrealistic while a 20 years release of HCFCs is possible because the international agreements now put a time limit on HCFC production to year 2030. These considerations should be taken into account when the decision on which compounds to use for air condition systems, as refrigerants, and for foam blowing the next 40 years.

Even though the ODP definition has limitations as discussed above, it is still interesting to compare the overall ozone depletion effect expressed by the ODP number. The ODPs for common HCFC and CFC-11 and CFC-12 are displayed in Table IV. It is seen from the table that the ODP for HCFCs are generally a factor of 10-100 less than those of CFC-11 and CFC-12. HFCs do not contain chlorine and therefore have no ODP associated with the well established chlorine destruction cycle. As discussed above, none of the radical degradation products of HFCs: $CF_3C(O)O_x$, CF_3O_x, FCO_x, and FO_x destroy ozone to any significant amount. Hence, HFCs are "ozone neutral".

1.5.2 HGWP of HFCs and HCFCs

Table IV: Chemical rate data, lifetimes, ODPs and HGWP for HFCs and HCFCs.

Compound	lifetime[a]	ODP[b]	HGWP[c]
HFC-125 (CF_3CF_2H)	26	0	0.58
HFC-134a (CF_3CF_2H)	14	0	0.27
HFC-143a (CF_3CH_3)	40	0	0.74
HFC-134 (CF_2HCF_2H)	11	0	[d]
HFC-23 (CF_3H)	411	0	[d]
HCFC-152a (CF_2CHCH_3)	1.6	0	0.030
HCFC-124 (CF_3CFClH)	6.0	0.018	0.096
HCFC-22 (CHF_2Cl)	14	0.047	0.36
HCFC-123 (CF_3CCl_2H)	1.5	0.016	0.019
HCFC-141b ($CFCl_2CH_3$)	7.1	0.085	0.092
HCFC-142b (CF_2ClCH_3)	17.8	0.053	0.36
CFC-11 ($CFCl_3$)	60	1.0[e]	1.0[e]
CFC-12 (CF_2Cl_2)	105	0.93	3.1

a: Average of values given by Derwent et al., page 124 [3].

b: Average of values given in Table 4 of Fisher et al. [6].

c: Average of values given in Table 5 of Fisher et al. [7].

d: No values available

e: By definition.

f: The global warming potential of CFC-11 is approximately 1300 times greater than that of CO_2 [52].

HGWP (Halocarbon global warming potential) is defined as the ratio of the steady state calculated warming for the fixed mass release of the gas relative to that calculated for the release of the same mass of CFC-11. The HGWP may also be found by integrating the total radiative forcing from releasing a certain amount of a HCFC compared with releasing the same amount of CFC-11.

The HGWP derived from these two definitions does not give any information about the time dependence of the radiative forcing of the earth. The time dependence of the radiative forcing of the climate is discussed later.

A couple of assumptions are made above. For example is it assumed that the oxidation products are short lived compared to the parent halocarbon, so that once a halocarbon molecule has reacted with OH there is no further contribution to radiative forcing. As discussed later this may not be the case for HFC-143a (CF_3CH_3).

To evaluate the radiative forcing GWP is often used. HGWP and GWP is equivalent apart from the reference compound: GWP use CO_2 while HGWP use CFC-11. The green house warming of CFC-11 is about 1300 times bigger then CO_2 [52].

As seen from Table IV, HGWPs of are generally lower for HCFCs and HFCs then for CFCs by a factor of 1.5 to 30, so use of HCFCs and HFCs instead of CFCs will substantially lower the radiative forcing. For example the HGWP of CFC-12 is ten times greater than the HGWP of its substitute, HFC-134a. It can be concluded from Table IV, that the HGWPs scale approximately linearly with atmospheric lifetime. This is because CFCs, HCFCs, and HFCs have similar molecular structures. Hence, the strengths and positions of their infrared absorptions are similar. The impact of these species is then largely determined by their atmospheric concentrations and hence lifetimes.

However, when comparing HGWPs for different compounds, one should also consider the time dependence of radiative forcing and the indirect effect on radiative forcing due to destruction of stratospheric ozone due to CFCs. The time dependent effect is discussed in ref. [4]. The radiative forcing are considered after releasing CO_2 and the compound of interest at time zero with integrating times of 20, 50, 100, 200, and 500 years. If we compare the time dependent GWP of HFC-134a with that of CFC-12 (Which is the time dependent radiative forcing of HFC-134a relative to CFC-12) it is 1/2, 1/4, and 1/6 using integration time of 20, 50, and 100 years, respectively. This means that the effect of release of HFC-134a compared to CFC-12 is bigger at short time scales than the values expressed by the HGWP.

Another uncertainty in the calculations of HGWPs of CFCs and HCFCs is their effect on the ozone layer. CFCs and HCFCs are known to destroy ozone in the stratosphere. A loss in ozone could lead to lower temperature in the lower stratosphere.

This effect is an negative radiation forcing of the climate. Although the magnitude is uncertain it may lead to a zero net radiative forcing for CFCs [4].

In the calculation an assumption was made that the products formed upon the reaction of OH with the parent compound is short lived compared with the life time of the parent compound. This might not be the case for HFC-143a, since the photolysis of a major atmospheric HFC-143a product, CF_3CHO, may lead to production of CF_3H and CO [23]. The lifetime of CF_3H is an order of magnitude greater than that of HFC-143a. The product distribution of photolysis of HFC-143a therefore need to be determined.

The numbers in Table IV is a way of putting the cumulative effect of different compounds on a relative scale. This relative placement on the scale is relatively precise (with the exceptions noted above), however, the effects on the global and regional temperatures of releasing these compounds is very uncertain. The effect dependents strongly on the feed backs, for example increasing water content in the air due to higher temperature and the effect of clouds and the loss of ozone discussed above. It is generally agreed that the earth is heated due to CO_2, H_2O, CH_4, N_2O and other trace gasses. It is also common knowledge that the concentrations of CO_2, CH_4, N_2O, and other compounds which have an effect of the radiative forcing of the earth is increasing. Ice core measurements indicate that the CO_2 and CH_4 content in the atmosphere correlate with the temperature. However, it is not known whether a higher temperature is a reason or the effect of increased CO_2 and CH_4. Global average temperature measurements indicate that the global average temperature have increased by approximately 0.8 °C during the last 110 years [4]. However, it has not been shown, that the increasing content of green house gases in the atmosphere is responsible for this temperature increase. This is due to the poorly understood mechanisms governing the radiative budget of the atmosphere. This is therefore an important subject of future research.

2 Experimental Techniques

2.1 Pulse Radiolysis UV Absorption Spectroscopy

2.1.1 Equipment

The experimental setup is shown in Figure 5. The setup consists of an electron accelerator to initiate the reactions, a one liter stainless steel cell where the reactions take place, a vacuum system for gas handling, and an UV absorption detection system.

The reactions are initiated by a Febetron 705B field emission accelerator which deliver a 30 ns pulse of 2 MeV electrons into the stainless steel reactions cell. The main part of the radiation goes through the cell, however, the small fraction of the radiation which is absorbed in the bath gas is capable of forming up to $3x10^{15}$ molecule cm^{-3} F atoms in the case where SF_6 is used as bath gas. The dose delivered in the cell may be varied by insertion of attenuators between the accelerator and the cell. The attenuators are stainless steel sheets with holes over the area of the electron beam. The dose of the accelerator is determined by the size of the holes [53]. In this work the dose delivered in the cell will be given relative to that at full dose.

The gas handling system consists of a MKS Baratron 170 absolute membrane manometer with a resolution of 10^{-2} mbar, a Balzers TPG 306 manometer with a resolution of 10^{-4} mbar, five inlets to the cell and a pump, capable of pumping the pressure in the cell down to 10^{-4}-10^{-3} mbar. The temperature in the reaction cell were measured by a platinum resistance thermometer located in the center of the reaction cell.

The detection light is delivered by a pulsed 150 W Xenon arc lamp. This lamp allow detection down to 220 nm and may be used in both the UV and the VIS wavelength region. A feed back system controls the light intensity during the pulse and ensures the stability of the lamp during the pulse. The lamp may be pulsed up to 10 ms. The analyzing light enters the reaction cell through a quartz window and is reflected in the cell by a internal White type mirror system. The optical pathlengths of the analyzing light in the reaction cell used for this work are 40, 80, and 120 cm depending on whether the analyzing light is reflected 3, 7, or 11 times on the internal mirrors before exiting the reaction cell. The light from the Xenon lamp was then focused on the entrance slit of the monochromator. Two monochromators were used for the present work: A Hilger and Watts and a McPherson grating monochromator. Both have focal lengths of 1 m and 1200 lines/mm grating, which give an optical resolutions of 0.8 nm/mm slit. The performance of

the McPherson monochromator is better than the Hilger and Watts monochromator. Especially in UV below 250 nm the McPherson has a better discrimination against scattered light. The wavelength offset of the monochromators was determined by measuring the Hg lines in a pen ray mercury lamp.

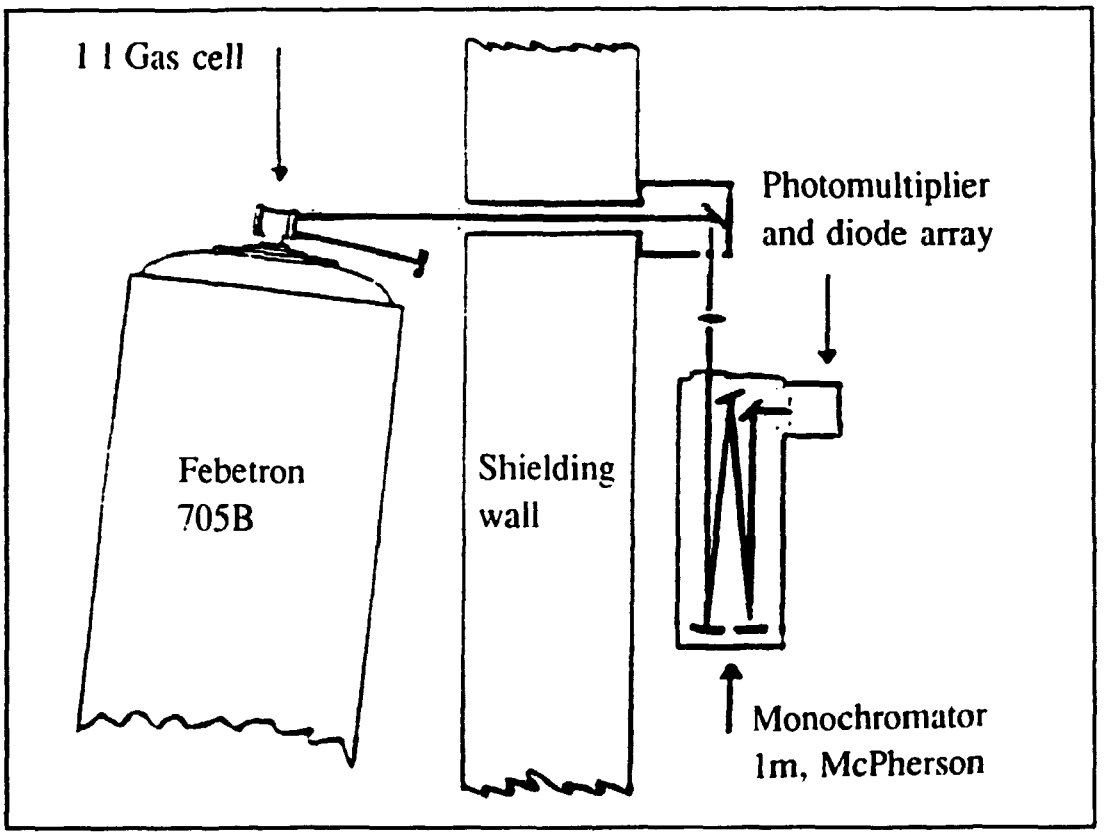

Figure 5. *Pulse radiolysis setup.*

The light is detected by a Hamamatsu R928 photomultiplier. A Biomation 8100 waveform digitizer record the transmittance as a function of time. A measurement consists of 2000 points. The time resolution is 10 ns and the resolution of the transmittance is 1/256.

Scattered light may be a problem at low wavelength ≤230 nm. As discussed in [54], scattered light will be light from the visible wavelength region, since the intensity of the Xenon lamp in the VIS wavelength region is much higher than in the UV wavelength region. Most radicals do not absorb in the visible wavelength region so the scattered light will not be absorbed by the radicals in the cell like the light with the right wavelength. A correction therefore have to be made if one have significant scattered light.

The correction is simple, only the intensity of the scattered light have to be subtracted from the intensity in Lambert-Beers law:

$$Abs(t)=\log(I_o-I_{scattered}/I(t)-I_{scattered})$$

where Abs(t) is the time dependent absorbance, I_o is the average light intensity before the electron pulse, $I_{scattered}$ is the light intensity of the scattered light, and I(t) in the time dependent light intensity.

The absorbance used in the computer is base 10 while the σ values used for absorption cross sections are base e. Lambert-Beers law therefore have to be slightly modified to connect these two quantities:

$$A\ln 10=2.303A=\sigma lc$$

This correction have to be done when ever the absorbance values are connected to absorption cross sections.

2.1.2 First and Second Order Fit Applied to the Data

The data handling and storage is done by a PDP-11 computer using a program constructed by K.B. Hansen. With the program it is possible to perform nonlinear first and second order fit to the data. An example of a first order rise fit is seen in Figure 6. For the first order fit the following expression was used:

$$A(t)=-b\exp(-kt)+c$$

where A(t) is the absorption as a function of dose, c-b is the absorbance at time zero and c is the absorption at $t=\infty$. In this fit the parameters b, c, and k are fitted simultaneously. This expression is equal to the expression for an exponential rise:

$$A(t)=b(1-\exp(-kt))+(c-b)$$

Formation of absorbing products in a first order decay reaction is not changing the obtained rate constant since a combination of first order decays or/and first order formations with the same rate constant will give the right rate constant in the fit. The validity of the fit can be inspected visually both by showing the fit to the transient and by the deviation of the transient from the fit as seen in Figure 6.

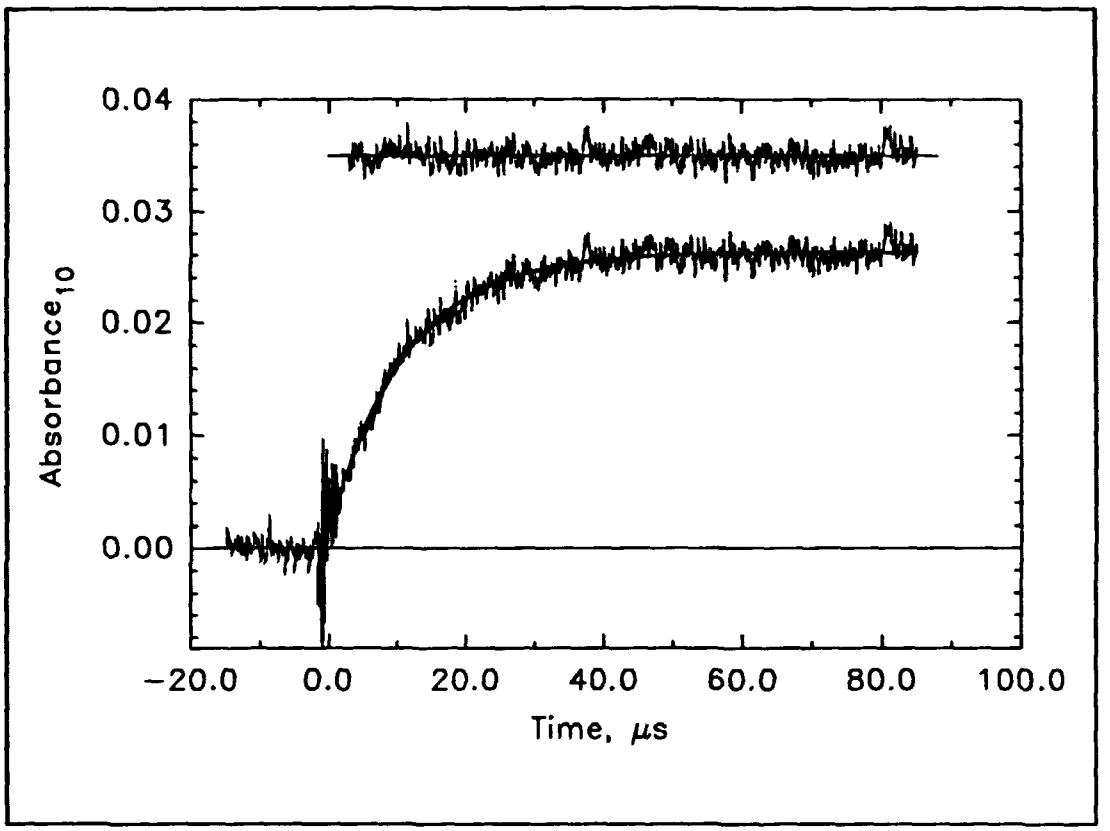

Figure 6. *Transient absorbance (path-length 120 cm) following pulse radiolysis of 0.31 mbar NO, 50 mbar CF_3CH_3, 20 mbar O_2, and 930 mbar SF_6. The solid line is a first order fit to the experimental data.*

Second order fits were used in this work to fit decays of transient absorption due to the self reactions of an absorbing radical. An example is seen in Figure 7. Second order kinetics were fitted using a non linear fit of the parameters A_o, A_{inf}, and k' in the following expression:

$$A(t)=(A_o-A_{inf})/(1+2k'(A_o-A_{inf})t)+A_{inf}$$

where A(t), A_o, and A_{inf} is the absorbance as a function of the time, at time zero, and at infinite time. k' is the second order rate constant. The validity of the fit can be inspected visually both by showing the fit to the transient and by the deviation of the transient from the fit (see Figure 7).

The self reaction rate constants were derived from the fitted data by plotting $1/t_{1/2}$ against maximum transient absorption, A_{max}. $t_{1/2}$ is determined by the computer from the fitted values of A_o, A_{inf}, and k' and A_{max}. If other radicals contribute to A_{max} a correction

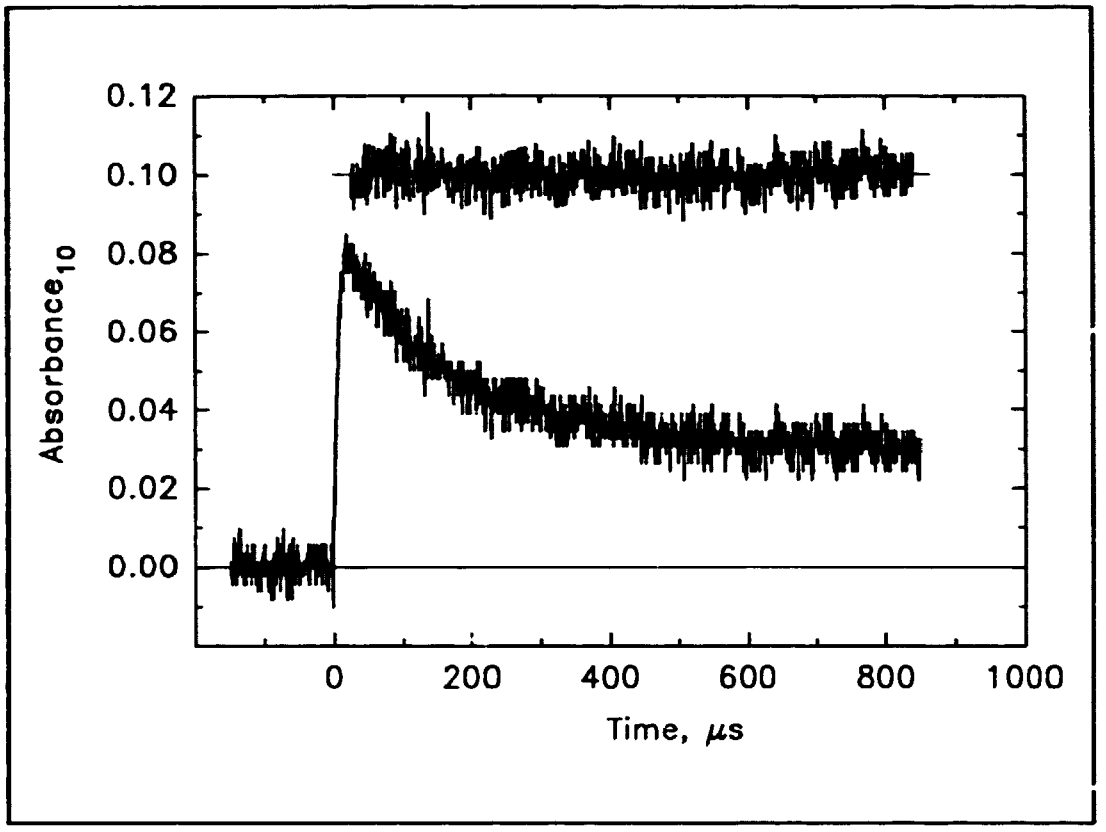

Figure 7. *Absorption at 230 nm following the pulse radiolysis of a mixture of 50 mbar CF_3H, 2 mbar O_2, and 948 mbar of SF_6. A pathlength of 80 cm and a dose of 0.319 were applied.*

have to be made so only the maximum absorbance due to the radicals that undergo self reaction are included in the plot. The slope of a $1/t_{1/2}$ vs A_{max} plot may be used to determine the second order rate constant. From second order kinetics it can be derived:

$$1/t_{1/2}=2kc$$

where $t_{1/2}$ is the half life, k is the rate constant, and c is the concentration of the radical that undergo self reaction. Using Lambert-Beers law we get:

$$1/t_{1/2}=2kc=2k\{2.303A_{max}/(l\sigma)\}=A_{max}\{2k2.303/(l\sigma)\}$$

σ is the absorption cross section of the radical and l is the path-length of the analyzing light in the reaction cell. It is seen from this equation that the slope of the $1/t_{1/2}$ vs A_{max} plot equals $2k2.303/(l\sigma)$. A value of k may then be derived. The uncertainty is then done

by normal error propagation of 2 standard deviations of both σ and the slope of the $1/t_{1/2}$ vs A_{max} plot.

2.1.3 Radiolysis of SF_6

Generally, the rate constants for the ionic and intra molecular processes following radiolysis are very fast, and take place on a nanosecond time scale [55]. The radical reactions, however, are on microsecond and millisecond time scale [55]. Thus, the different type of reactions are divided into different time regimes. In this work, changes on the micro and millisecond time scale are recorded so only radical reactions have been studied.

Radiolysis of SF_6 have been used extensively throughout this work as a convenient source of F atoms. A potential problem in this system is formation of reactive SF_x radicals. Of the SF_x species, SF_2, SF_4, and SF_6 are stable species.

The initial reactions in the radiolysis of SF_6 have been described by Markert [54]. SF_4 and SF_5 are expected to be major products in the radiolysis of SF_6 mixtures since SF_6 is an excellent electron scavenger and the products of the formed SF_6^- ion is expected to be SF_4 and SF_5 [54]. However, no firm conclusion was derived about the possible formation of SF_x radicals. In this work the overall yield of SF_5 radicals of the initial ion reactions was studied.

It is not easy to detect any of the SF_x radicals. The SF_5 radical only absorbs weakly in the UV at wavelength above 220 nm (see section 3.2, $\sigma(SF_5)<55\times10^{-20}$ cm^2 molecule^{-1} at 220 nm) [Appendix 7.8 pp174]. The absorption in the UV of the SF_4 molecule is also negligible. However, as shown later, SF_5O_2 has an absorption spectrum in the UV wavelength region. From the absorption of SF_5O_2 it is possible to estimate of the number of SF_5 radicals formed.

To estimate the possible contribution from SF_5 radicals I have radiolysed three reaction mixtures using a variety of doses. Mixture no. 1 consist of 20 mbar SF_4, 40 mbar O_2, and 940 mbar SF_6, mixture no. 2 of 18 mbar of H_2O, 40 mbar O_2, and 940 mbar of SF_6 and mixture no. 3 of 18 mbar H_2O and 982 mbar SF_6. In Figure 8 the maximum transient absorption at 230 nm following radiolysis of the three reaction mixtures is plotted as function of the dose. The straight lines are found from linear regressions of the low dose data. The high dose data fall below the linear extrapolation of the low dose data. This is due to radical radical reactions. Therefore the high dose data are excluded from the regression analysis.

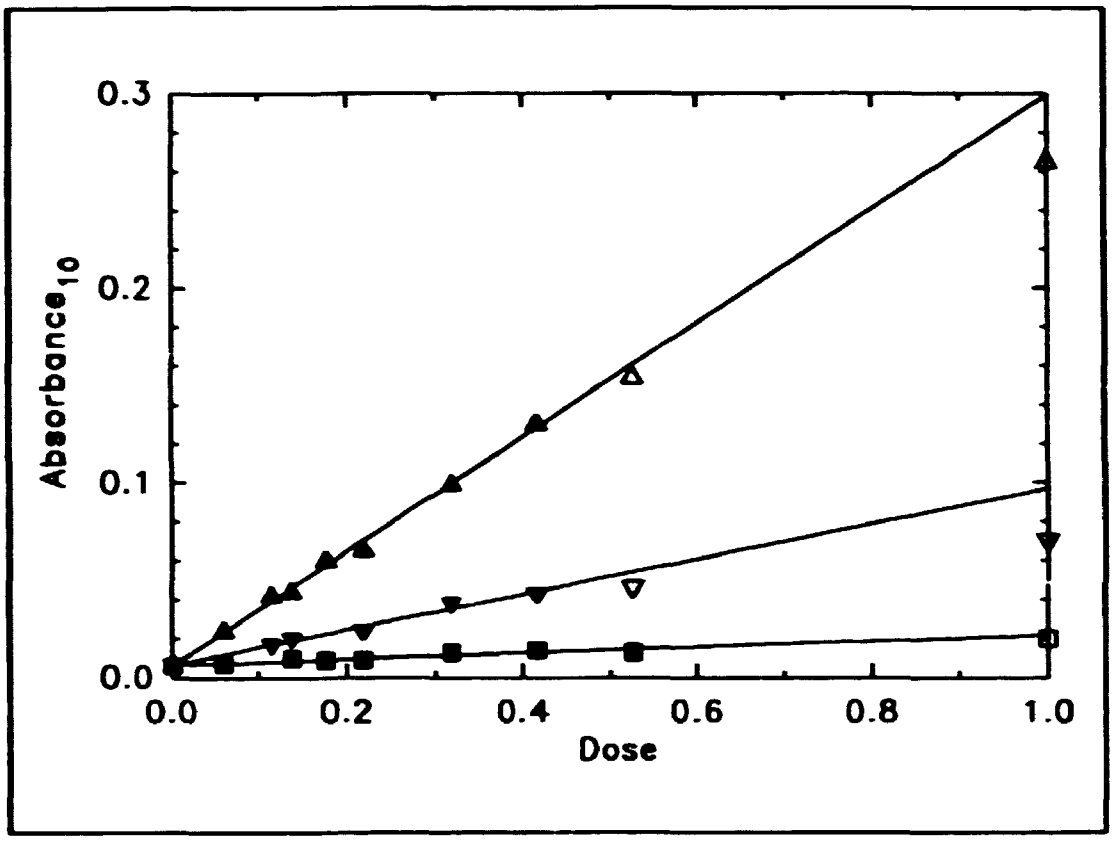

Figure 8. *Maximum transient absorption at 230 nm (pathlength 80 cm) as function of dose following pulse radiolysis of 20 mbar SF_4, 40 mbar O_2, and 940 mbar SF_6 (triangles up); 18 mbar H_2O, 40 mbar O_2, and 942 mbar SF_6 (triangles down); 18 mbar H_2O and 982 mbar SF_6 (squares).*

In reaction mixture no. 1, SF_5O_2 are formed by the following reactions:

$$SF_6 + 2MeV\ e^- \rightarrow F + Products \quad (21)$$

$$F + SF_4 + M \rightarrow SF_5 + M \quad (22)$$

$$SF_5 + O_2 + M \rightarrow SF_5O_2 + M \quad (23)$$

SF_5O_2 radicals are known to absorb at 230 nm with an absorption cross section of $(3.70\pm0.92)\times10^{-18}$ cm^2 $molecule^{-1}$ [Appendix 7.8 pp174]. The data in Figure 8 is consistent with the previous determination.

In reaction mixture no. 2, OH radicals and possibly SF_5O_2 radicals are formed by the following reactions:

$$SF_6 + 2MeV\ e^- \rightarrow F + SF_5 + other\ products \quad (21)$$

$$F + H_2O \rightarrow HF + OH \quad (20)$$

$$SF_5 + O_2 + M \rightarrow SF_5O_2 + M \quad (23)$$

The small transient absorption observed, see Figure 8, may be due to SF_5O_2 radicals formed by the reaction of SF_5 radicals from the radiolysis processes and O_2 present in the cell. In reaction mixture no. 3, OH radicals are formed by reaction (20).

The slope of the three straight lines in Figure 8 were determined by linear regression to 0.293±0.016 (triangles up), 0.051±0.012 (triangles down), and 0.015±0.005 (squares). The slopes obtained from experiments with reaction mixtures containing O_2 had to be corrected for the small yield of FO_2 formed in the cell by the reaction between F atoms and O_2:

$$F + O_2 + M \rightarrow FO_2 + M \quad (12)$$

From $\sigma_{FO2}(230nm)=508\times10^{-20}$ cm^2 molecule^{-1} [Appendix 7.1 pp117], $k_{22}=(1.3\pm0.3)\times10^{-11}$ cm^3 molecule^{-1} s^{-1} [Appendix 7.8 pp174], $k_{20}=1.4\times10^{-11}$ cm^3 molecule^{-1} s^{-1} [5], $k_{12}=(1.9\pm0.3)\times10^{-13}$ cm^3 molecule^{-1} s^{-1} [Appendix 7.1 pp117], and an initial F atom yield of 3×10^{-15} molecules cm^{-3} I get the corrected slopes to be 0.278±0.016 and 0.036±0.012. To obtain the absorption due to SF_5O_2, the absorbance from experiments without O_2, reaction mixture no. 3, had to be subtracted from experiment no. 2. The absorbance due to SF_5O_2 is then 0.020±0.010. By dividing this number with 0.278±0.016, an upper limit of (7±4)% of SF_5O_2 radicals and thereby SF_5 radicals was derived. Since the absorption could be due to something else this serves only as an upper limit for the production of SF_5 radicals from the pulsed radiolysis. For example the formation of O_3 by direct radiolysis of O_2 might explain up to 3% of the 7%. In addition, the formation of H atoms from either direct radiolysis of H_2O quenching of "hot" SF_6 molecules by H_2O may also absorb since H atoms will be converted quickly to HO_2 radicals which is known to absorb at 230 nm. Considering the noise level and the general difficulties of measuring gas kinetics, less than (7±4)% SF_5 radicals in the gas mixture is not alarming. However, one should be conscious about the potential problems arising from this.

It should also be mentioned that radiolysis of SF_6 has been used to measured many rate constants and absorption spectra, which agree well with the values obtained using other techniques. If a substantial amount of SF_x radicals were formed by radiolysis of SF_6 it would have been detected.

To determine UV absorption cross sections and second order rate constants it is necessary to know the concentration of the radicals in the cell. Therefore the initial F atom concentration in the cell need to be determined and we need to choose the experimental

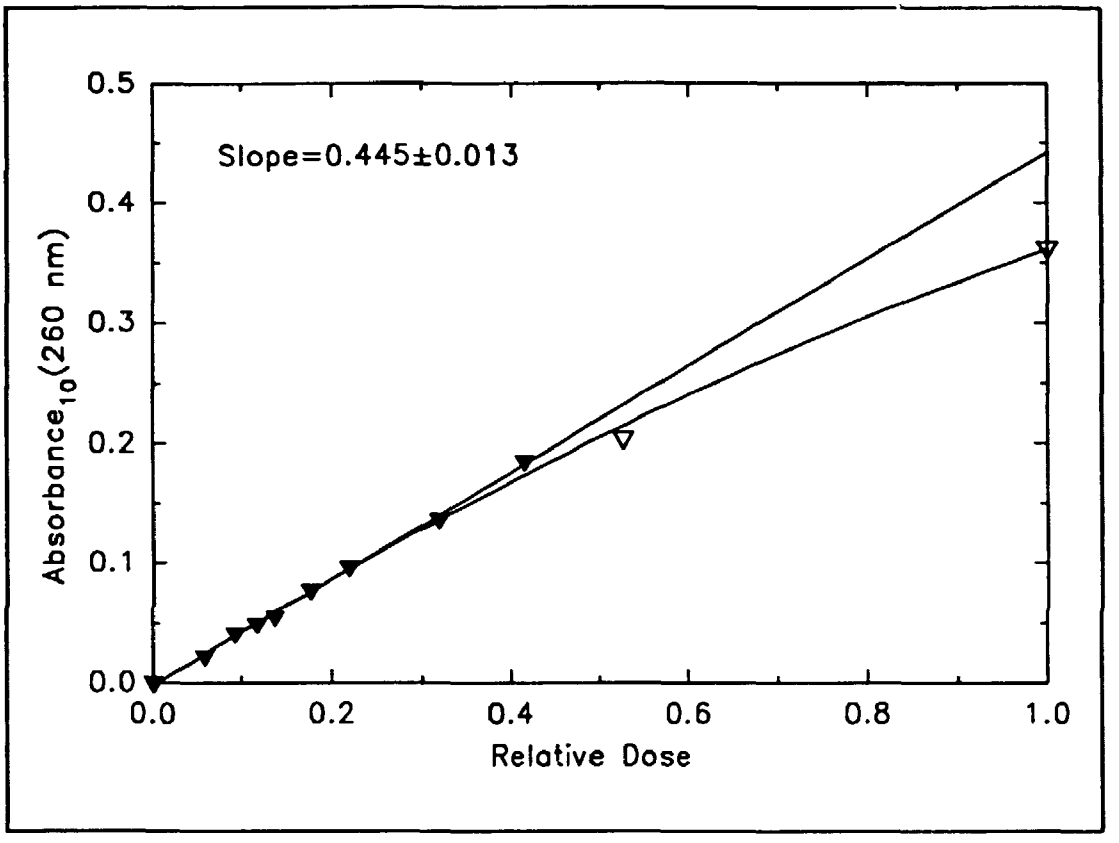

Figure 9. *Transient absorptions at 260 nm (pathlength 120 cm) following radiolysis of 10 mbar CH_4, 40 mbar O_2, and 950 mbar SF_6. The straight line is a linear least squares fit of the low dose data.*

conditions so that the F atoms are converted stoichiometrically into the desired radical. Several methods have been used to determine the initial F atom concentration in the cell: (i) The absorption of CH_3O_2 at 230, 240, and 260 nm. (ii) The absorption of CH_3 at 216.4 nm. (iii) The absorption of FNO at 310.5 nm [56]. All three methods give within the error level the same F atoms concentration. The absorption of a species, CH_3O_2, CH_3, or FNO is determined under conditions of complete conversion of F atoms into the species and the obtained absorbance is compared with a literature absorption cross section. In the case of FNO the absorption cross section of FNO was determined by forming FNO from known concentrations of F_2 and NO [56]. In this section I will discuss how to determine $[F]_0$ by the absorption of CH_3O_2 at 260 nm.

CH_3O_2 radicals is formed by radiolysis of a mixture of 10 mbar CH_4, 40 mbar O_2, and 950 mbar SF_6 by the following reactions:

$$SF_6 + 2MeV\ e^- \rightarrow F + Products \quad (21)$$

$$F + CH_4 \rightarrow CH_3 + HF \quad (19)$$

$$CH_3 + O_2 + M \rightarrow CH_3O_2 + M \quad (24)$$

In the following I neglect the small part of the F atoms, approximately 1%, which react with the O_2 to give FO_2 radicals.

The maximum transient absorbance at 260 nm, which is due to CH_3O_2, is plotted as a function of the relative radiolysis dose in Figure 9. The dose is given relative to full dose. The absorbance at higher doses falls below a linear extrapolation of the low dose data. This is due to unwanted radical radical reactions such as:

$$F + CH_3 + M \rightarrow CH_3F + M \quad (25)$$
$$F + CH_3O_2 \rightarrow \text{products} \quad (26)$$
$$CH_3 + CH_3 + M \rightarrow CH_3CH_3 + M \quad (27)$$
$$CH_3 + CH_3O_2 \rightarrow \text{products} \quad (28)$$

Instead of correcting for these reactions I chose to work under conditions where the influence of reactions (25-28) is negligible compared with the experimental uncertainty. This is accomplished by using only the data up to doses where the absorbance is still proportional with the dose. It is evident from Figure 9 that this is the case for doses up to 41.6% of full dose. By linear regression, the low dose data in Figure 9 are then used to determine the slope of the straight line in the figure to (0.445±0.013). This is the absorbance at full dose if no secondary radical radical chemistry were important. From the slope, (0.445±0.015), the absorption cross section of CH_3O_2 at 260 nm, $(3.18\pm0.32)\times10^{-18}$ cm^2 $molecule^{-1}$ [8], we derive a F atom yield at full dose and 1000 mbar of SF_6 of $(2.83\pm0.30)\times10^{15}$ atoms cm^{-3}. The uncertainty is two standard deviations and are found by conventional error propagation of the error on $\sigma_{260nm}(CH_3O_2)$ and the slope on the straight line in Figure 9. This method of reporting errors is used throughout this work.

The reported F atom yield has measured to be $(3.4\text{-}2.8)\times10^{15}$ atoms cm^{-3} in papers published in connection with this work. This change could be explained by the wear of the capacitors in the Febetron accelerator in the three year of this Ph.D. study.

2.1.4 Uncertainties

Two potential problems in using pulse radiolysis for kinetic measurements are wall reactions and the inhomogeneous radical distribution in the cell. These two potential complications are discussed in the following.

The possible contribution to the observed kinetics due to surface reactions are very limited due to the short reaction times. The reaction times used in this work were less than 10 ms. The diffusion coefficient, D, in N_2 at 295 K at a pressure of 1 atmosphere is about

0.1 $cm^2 s^{-1}$ [57]. In SF_6 the diffusion must be expected to be approximately 5 times less due to the bigger mass and volume of the SF_6 molecule (D=0.02 $cm^2 s^{-1}$). The root mean square distance travelled by diffusing particles are [57]:

$$x=(2Dt)^{1/2}$$

Using D=0.02 $cm^2 s^{-1}$ and t=10 ms, I arrive with a root mean square distance of approximately 0.1 mm. If 1/6 of the radicals in the cell go towards the walls and windows in the cell it must be expected that on average, only radicals which are less than 0.02 mm from the walls will hit it. This is clearly negligible compared to the total length of 10 cm between the mirrors. However, this calculation does not take convection into account. It is not possible to evaluate the convection in the cell hence its influence can not be calculated. However, the reaction times applied by pulse radiolysis is substantial lower than for many other experimental setups, where no experimental error due to wall reactions have been reported.

When the electron beam enters the cell it has a diameter of about 5 cm. It spreads in the cell because of repulsion between the electrons. The distribution of dose in the cell is therefore inhomogeneous. The dose distribution along an axis connecting the center of the mirrors is most important since the analytical light follow largely the straight line between the center of the mirrors. In the following I will therefore only discuss the radiation distribution between the mirrors. The radiation doubles going from a mirror to the center of the cell [53]. It should be noted that only second order kinetics is influenced by an inhomogeneous radiation distribution in the cell. Absorption cross sections and first order kinetics are not influenced by the radiation distribution.

Two publications have recently discussed the radical distribution in the reaction cell [53,58]. Ellermann [53] use the radiation distribution measured in the Risø cell while Fagerström et al. [58] use the radiation distribution in the cell in Linköping, Sverige. The distribution in the Linköping cell is slightly more inhomogeneous than that in the Risø cell.

Ellermann used a box model, where he followed the kinetics in each of his ten boxes and make a summation over the boxes to calculate the observed decay:

$$C_{obs}(t)=1/10\sum C(i,0)/(1+2kC(i,0)t)$$

where i is the box number and is summarized from 1 to 10, k is the second order rate constant, C(i,0) is the radical concentration in box i at time 0 and $C_{obs}(t)$ is the observed concentration at time t.

Fagerstrøm et al. [58] fitted the radiation distribution with a second order polynomium and thereafter found an analytical expression for the observed decay:

$$C_{obs}(t)=1/(2kt)(1-I/(2x_o))$$
$$I=1/(ab)^{1/2}\ln\{(a+x_o(ab)^{1/2})/(a-x_o(ab)^{1/2})\}$$
$$a=1+2Akt \text{ and } b=2Bkt$$

where x_o is the distance from the center of the cell to the mirrors, 5 cm, and k and C_{obs} are explained above. A and B are the parameters describing the radical distribution between the mirrors through the formula:

$$C(x)=A-Bx^2$$

where x is the distance from the center of the cell and C(x) is the radical concentration x cm from the center of the cell.

Both Ellermann [53] and Fagerstrom et al. [58] find that the observed second order decay is indistinguisble from a pure second order decay. Ellerman find that the radiation distribution rise the observed second order rate by 12 % as compared to the true rate constant. However, Fagerstrom find that the change in the second order rate constant is only between 1 and 3% because of the radiation distribution. They find that the change is most pronounced for in first half life (3%) while the following half lives are only perturbated by 1-2%.

As a part of this work I have recalculated the observed decay rate using both the method of Ellermann [53] and Fagerstrom et al. [58] observed decays from both techniques are fitted with a second order expression and this rate constant called the observed rate constant are compared with the true rate constant. Generally, the observed rate constants are 1-2% higher than the true rate constants using the both Ellermanns and Fagerstrom et al.s methods [53,58]. The two methods give the same result within 0.3%. If only the first half life is observed up to 4% difference between the observed and the true rate constant have been calculated. If the decay rate constants are determined from transients that at least contain 2 half lives, the observed rate constant is within 2 % from the true rate constant which in most cases is small as compared to other uncertainties.

2.2 Long Pathlength Fourier Transform Infrared Spectroscopy

2.2.1 Equipment and Data Handling

The experimental setup for the product studies consists of a 140 l pyrex chemical reactor surrounded by 22 blacklamps for initiation of the reactions and a Mateson Sirius-100 FTIR spectrometer for detection. The setup is shown schematically in Figure 10.

The FTIR spectrometer was operated at an optical resolution of 0.25 cm^{-1}. Usually, 32 spectra were coadded to increase the S/N, but for special purposes 16, 64, or 128 coadded spectra was used either to increase the acquisition speed or the S/N ratio of the spectra. Approximately 1.5 min was used to acquire and transform 32 coadded interferograms.

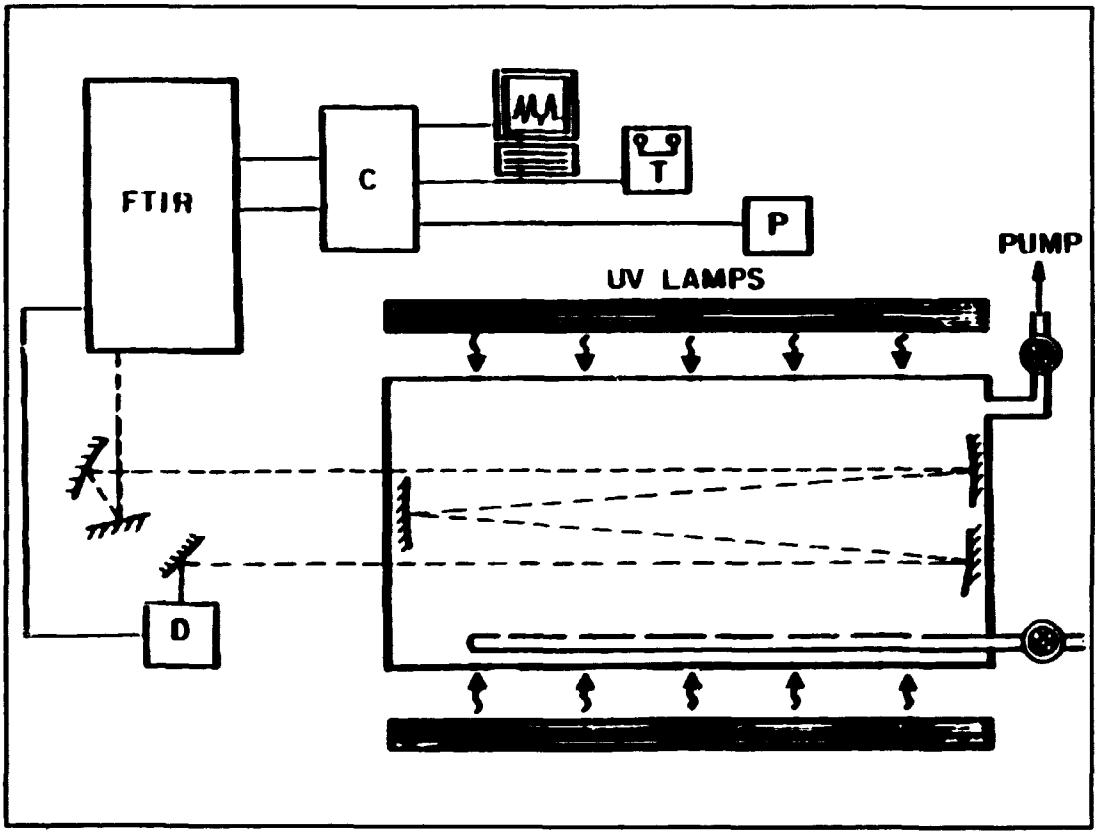

Figure 10. *FTIR setup.*

A conventional globar source supplied the detection light and a MCT Infrared Associates Model#0465-0008-0 detector was used as a detector for the infrared light. The data handling were done by a Masscomp 5500 mini computer where subtraction and

addition of spectra could be carried out. A reference library consisting of approximately 300 calibrated spectra aided the analysis of the experimental data. All spectra were recorded at the same resolution, 0.25 cm^{-1}, at a temperature of 296±2 K, and a total pressure of 700 Torr. From the Masscomp 5500 mini computer the data could be moved to a personal computer and stored on a magnetic band. Data handling on the PC were carried out using a program made by M. D. Hurley.

An example of how the data are handled the are shown in Figure 11. The figure show the spectra before irradiation (A) and after 25 min of irradiation (B) of a mixture of 102 mbar CF_3H, 0.26 mbar F_2, 200 mbar O_2, and 590 mbar N_2. Subtraction of features due to CF_3H, HC(O)F, and CF_2O from Figure 11B gives Figure 11C. Figure 11D is the reference spectrum of CF_3OOOCF_3. The feature at 1030 cm^{-1} is attributed to SiF_4.

The reaction chamber is a cylinder with a length of 2 m and a diameter of 30 cm made of pyrex and with metal plates at each end. On these metal plates a White type gold coated mirror system is mounted. The detection IR beam enters the reaction cell through a KBr window and is multipassed in the cell by the mirror system and escapes the cell through another KBr window. An optical pathlength of 28 m were usually applied. The optical pathlength were determined by flushing known volumes of CH_4 into the cell, measuring the absorbance, and then compare it with a reference spectrum.

22 GTE F40BLB fluorescent blacklamps surrounded the reaction chamber. The lamps had emission maximum at 350 nm, well suited for using molecular chlorine and fluorine as reaction initiators in the chamber. The pyrex walls of the reaction chamber ensures that no light with a wavelength of less than 300 nm enters the reaction chamber.

Gases were allowed into the reaction cell through a pyrex pipe in the bottom of the reaction cell. A pyrex gas handling system with teflon taps was used.

The pressure was measured by a Baratron Type 122A absolute membrane manometer with an resolution of 0.001 Torr. All pressures are measured in Torr and this unit have been used in all publications (but one) reporting the results of from the FTIR setup. Torr will therefore also be used as the pressure unit when results from the FTIR are reported in the following (1 Torr=1.32 mbar=1000 mTorr=1/760 atm).

The partial pressures of the gases were determined by allowing the gases into pyrex bulbs of known volumes and thereafter flushing the gas into the cell by the diluent gas. 700 Torr of oxygen, nitrogen, or synthetic air were used.

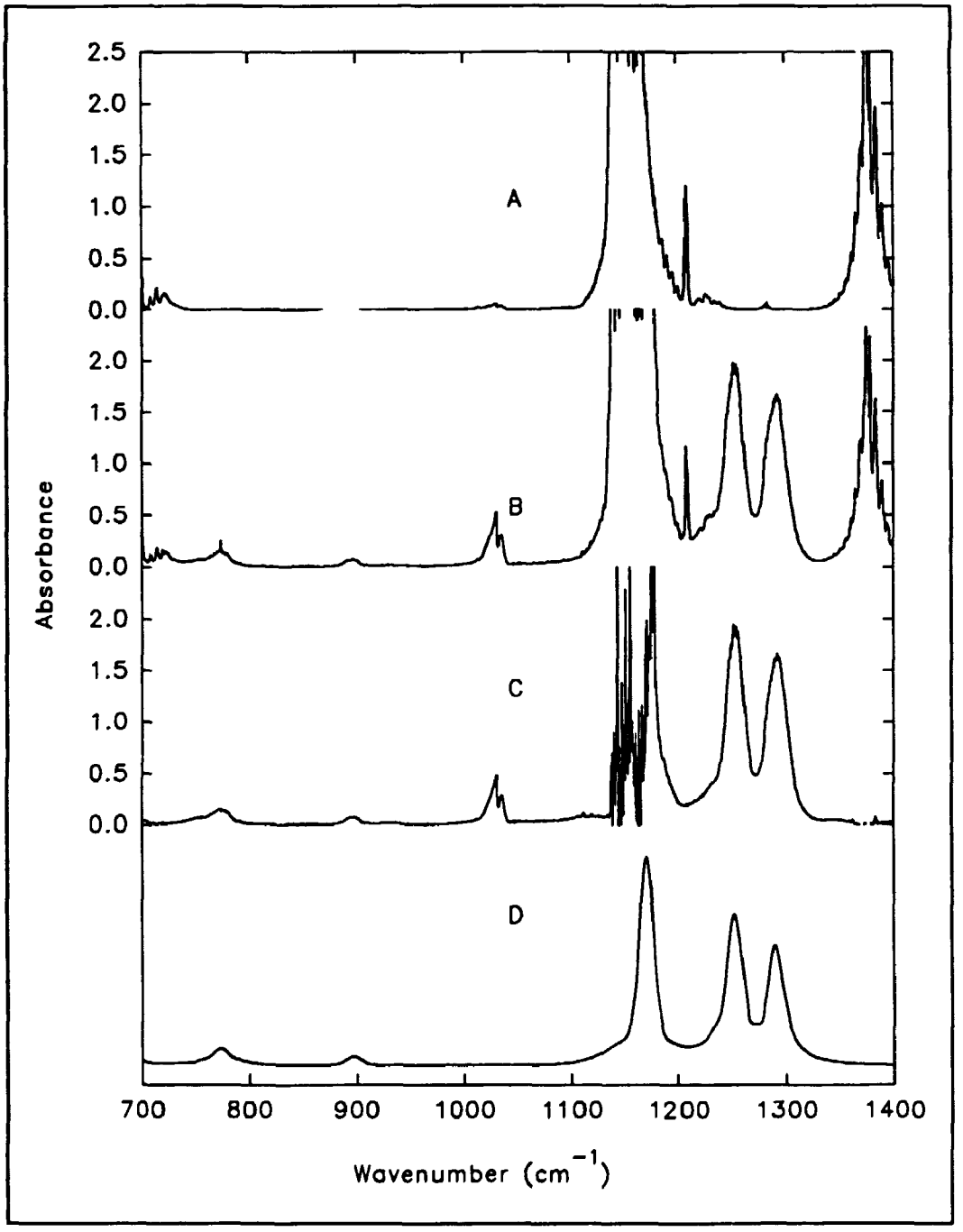

Figure 11. *Infrared spectra acquired before (A) and after (B) 25 min irradiation of a mixture of 0.102 mbar of CF_3H, 0.26 mbar of F_2, 200 mbar of O_2, and 590 mbar N_2. Subtraction of features attributable to CF_3H, $HC(O)F$, and CF_2O from Figure 11B gives Figure 11C. Figure 11D is a reference of CF_3OOOCF_3. The feature at 1030 cm^{-1} in Figure 11C is attributed to SiF_4.*

2.2.2 Uncertainties: Resolution and Quantitative Determination

The quantitative analysis of species in the smog chamber depend on the intensity of the FTIR bands of the species to be linear with the concentration of the species in the cell. For FTIR spectrometers, the principal factor leading to deviations of Lambert Beers law is the effect of insufficient resolution [59].

The effect of measuring a spectrum at a resolution that is too low is best discussed in terms of the *resolution parameter* ρ, where ρ is the ratio of the nominal resolution of the spectrometer to the *full width at half height* of the absorption band. The apparent peak absorbance, $A_{apparent}$, varies as a function of ρ and the "true" peak absorbance, A_{true} [59]. For $A_{true}<0.5$ and $\rho<0.5$ the effect of the spectrometer resolution on the spectrum is negligible. For higher values of ρ, $A_{apparent}$ falls below A_{true}. However, if only peaks with $A_{true}<0.7$ is used, the absorbance versus concentration plot is linear, hence the FTIR spectrum may still be used for quantitative purposes. For peaks with higher absorptions or greater values of ρ the absorption versus concentration plots are not linear hence quantification is only possible if the unknown concentration and the reference concentration is very close. It should be mentioned that for broad bands ($\rho<0.1$), linear plots of $A_{apparent}$ against sample concentration can be obtained to absorbances as great as 3.5 [59].

The resolution used for this work was 0.25 cm^{-1}. This is not enough to resolve spectra of for example HCl, HCOF, CF_2O etc. One therefore have to be careful when using the FTIR features of these species for quantification. In this work I generally used absorptions from these species well below 0.7. Reasonable quantification should therefore be possible using FTIR spectroscopy.

3 Basic Studies: FO_2 and SF_5 in Pulse Radiolysis

3.1 The FO_2 Radical

The formation of small amounts of FO_2 radicals is inevitable when alkyl peroxy radicals are studied by pulse radiolysis of SF_6. F atoms are used to initiate the reactions and oxygen have to be present in the reaction cell to react with the alkyl radical and form peroxy radicals. FO_2 radicals are then formed by the following reaction:

$$F + O_2 + M \rightarrow FO_2 + M \qquad (12)$$

This reaction competes with the reaction of F atoms with the studied hydro or hydrohalo carbon:

$$F + RH \rightarrow HF + R \qquad (29)$$

To determine the amount of FO_2 radicals formed in the system and correct the UV absorption for FO_2, the UV absorption spectrum and k_{12} need to be known. The article published on this subject is given in Appendix 7.1 pp117.

FO_2 is formed by pulse radiolysis of mixtures of SF_6 and O_2. The UV absorption is broad and has the same shape as alkyl peroxy radical spectra. The absorption cross section of FO_2 radicals at 230 nm is $(5.08\pm0.70)\times10^{-18}$ cm^2 $molecule^{-1}$ [Appendix 7.1 pp117]. The formation kinetics were studied at 230 nm and the rate constant for the formation of FO_2 at 295 K and 1000 mbar SF_6 were $k_{12}=(1.9\pm0.3)\times10^{-13}$ cm^3 $molecule^{-1}$ s^{-1}.

The reaction between F and O_2 in reversible, however, the work above was done under conditions where $[FO_2]_{eq}>>[F]_{eq}$.

3.2 The SF_5 Radical

Because of the potential formation of SF_5 radicals in the pulse radiolysis of SF_6 and due to the current interest on sulfur oxygen adducts, the absorption spectra and kinetics of SF_5 and SF_5O_2 radicals was studied. The article published on this subject is found in Appendix 7.8 pp174.

SF_5 radicals were formed by the reaction of F atoms with SF_4:

$$F + SF_4 + M \rightarrow SF_5 + M \qquad (22)$$

The rate constant for this reaction were measured relative to the reaction rates of (12) and (30) by detection of FO_2 at 230 nm and FNO at 310.5 nm:

$$F + O_2 + M \rightarrow FO_2 + M \quad (12)$$

$$F + NO + M \rightarrow FNO + M \quad (30)$$

Both relative measurements gave $(1.3\pm0.3)\times10^{-11}$ cm^3 $molecule^{-1}$ s^{-1} for the reaction of F atoms with SF_4.

The SF_5 radical absorbs only weakly in the UV. The absorption cross section at 220 nm is 55×10^{-20} cm^2 $molecule^{-1}$.

SF_5O_2 radicals are formed by addition of O_2:

$$SF_5 + O_2 + M \rightleftharpoons SF_5O_2 + M \quad (23)$$

This reaction was shown to be reversible with $k_{23}=(8\pm2)\times10^{-13}$ cm^3 $molecule^{-1}$ s^{-1}, $k_{-23}=(1.0\pm0.5)\times10^{5}$ s^{-1}, and $K_{eq}=(8.0\pm4.5)\times10^{-18}$ cm^3 $molecule^{-1}$. From these values a SF_5-O_2 bond strength of (13.7±2.0) kcal mol^{-1} was derived by assuming that the entropy change associated with reaction (23) is similar to the entropy change in reactions of alkyl radicals with O_2.

The UV absorption spectrum of SF_5O_2 is broad and similar to the UV spectra of the alkyl peroxy radicals. The absorption cross section at 230 nm was found to be $(3.7\pm0.9)\times10^{-18}$ cm^2 $molecule^{-1}$. The rate constant of the reaction of SF_5O_2 with NO was determined to $(1.1\pm0.3)\times10^{-11}$ cm^3 $molecule^{-1}$ s^{-1} by monitoring the kinetics of NO_2 formation at 400 nm.

4 Kinetic Studies of Halogenated Peroxy Radicals

Pulse radiolysis coupled to time resolved UV absorption spectroscopy was used to study the kinetic behavior of the radicals involved in the atmospheric chemistry of HFCs and HCFCs. The data have been published previously [Appendix 7.11 pp205].

4.1 The Reactions of F Atoms with HFCs and HCFCs

Four methods have been used to determine the rate constants for the reaction of F atoms with HFCs and HCFCs: (i) Direct observation of the formation of the halo alkyl radical (ii) Measurements relative to the reaction of F atoms with O_2 (iii) Measurements relative to the reaction of F atoms with NO (iv) Relative rate measurements using FTIR. Method (iv) is discussed in the next chapter while methods (i)-(iii) are discussed below.

4.1.1 Formation of the Halo Alkyl Radical

The direct determination of the rate constant for the reaction of F atoms with halocarbons can only be used under certain conditions: (i) The R radical absorb UV or VIS light (ii) Radical-radical such as reactions (31-32) have to be much slower than the formation of the R radicals. The secondary chemistry include the self reaction of the alkyl radical and the reaction of F atoms with the alkyl radical:

$$F + R + M \rightarrow RF + M \quad (31)$$

$$R + R + M \rightarrow R_2 + M \quad (32)$$

These reactions are most important for low initial halocarbon concentrations, $[RH]_0$.

Under conditions where reaction (31) and (32) are negligible, a first order fit to the rise of the absorbance due to the R radical will give the pseudo first order rate constant for the reaction of F atoms with RH. This have been done in the case of the reaction of F atoms with CF_3CFClH and CF_3CCl_2H. As an example, the obtained first order rates are plotted as a function of $[CF_3CFClH]_0$ in Figure 12. The slope of the straight line is determined by linear regression analysis to $k=(7.1\pm0.9)\times10^{-13}$ cm^3 molecule^{-1} s^{-1}. This rate constant is also determined by a relative rate method to $(9.4\pm1.8)\times10^{-13}$ cm^3 molecule^{-1} s^{-1} (see later). I therefore choose to report $(8\pm2)\times10^{-13}$ cm^3 molecule^{-1} s^{-1}. The determination of the rate constant for the reaction of F atoms with CF_3CCl_2H is similar to the determination of $k_{F+CF3CFClH}$ above. The obtained value is $(1.2\pm0.4)\times10^{-12}$ cm^3 molecule^{-1} s^{-1}.

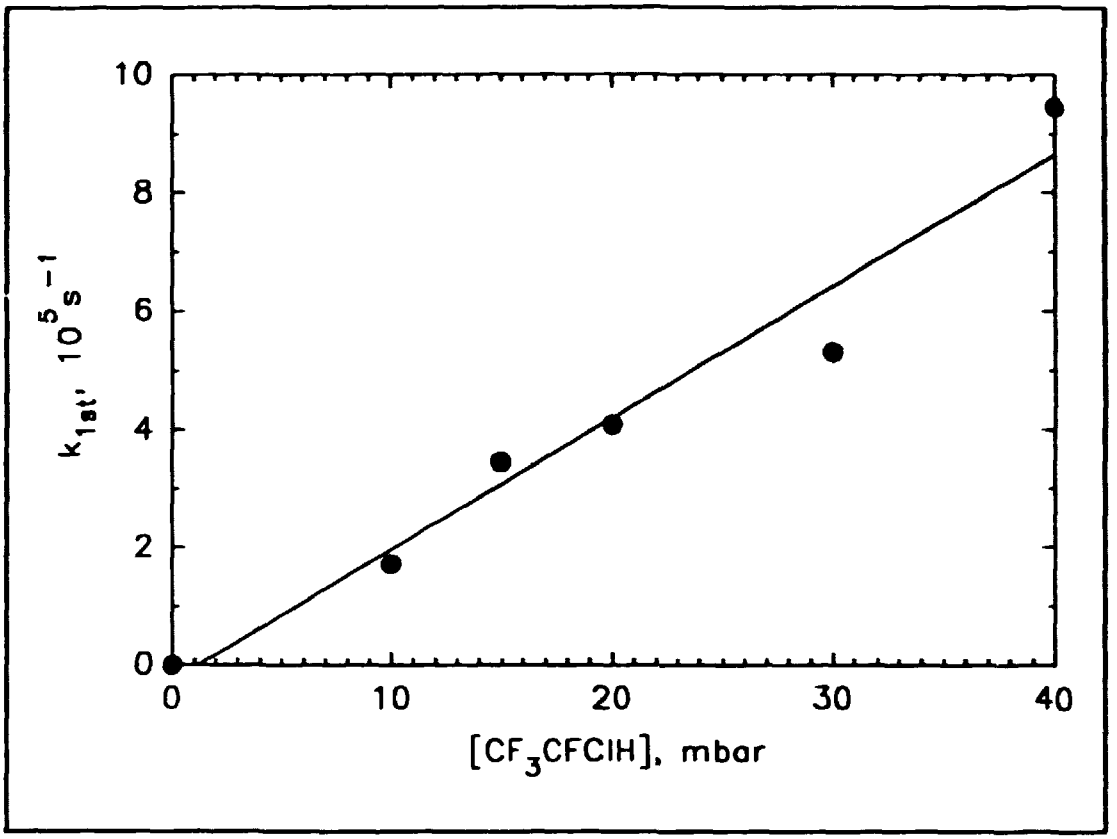

Figure 12. *First order formation rate constants of the CF_3CFCl radical recorded at 220 nm plotted as a function of $[CF_3CFClH]_0$. The solid line is determined by linear regression of the data.*

4.1.2 FO_2 Relative Method

Three rate constants have been measured in this work using the FO_2 relative method, namely the rate constants for the reaction of F atoms with CF_3H, CF_3CF_2H, and CF_3CH_3. To measure the rate constant for the reaction of F atoms with the CF_3H, CF_3CF_2H, and CF_3CH_3, experiments were performed in which the maximum in the transient absorption at 230, 230, and 250 nm, respectively, was measured following the pulse radiolysis of $SF_6/RH/O_2$ mixtures. In these experiments, the radiolysis dose and the SF_6 concentration were held constant. Figure 13 shows the observed variation of the maximum absorption as a function of the concentration ratio $[RH]/[O_2]$. As seen from Figure 13, the initial absorption at low $[CF_3CF_2H]/[O_2]$ and $[CHF_3]/[O_2]$ was large. As the ratios, $[RH]/[O_2]$, were increased, the initial absorption maximum decreased until a ratio of 14.2 and 25 was reached. Further increase in the concentration ratios $[RH]/[O_2]$ had no discernable effect on the initial absorption maximum.

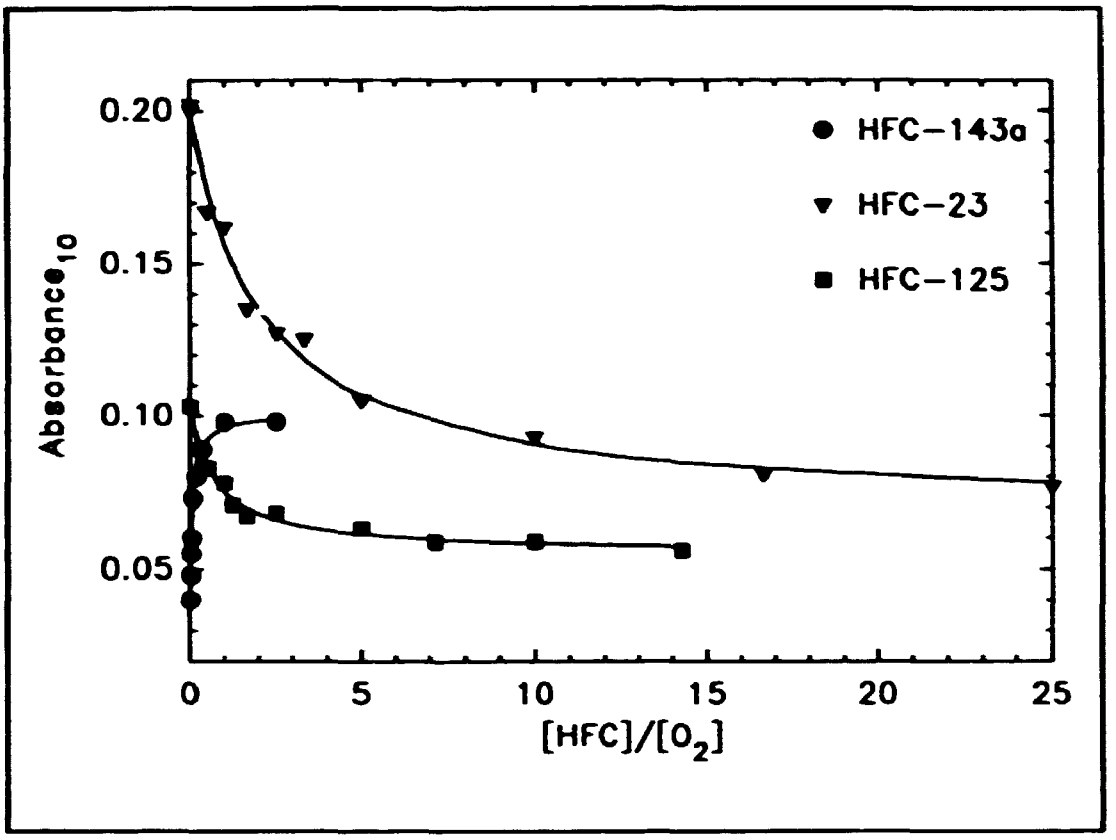

Figure 13. *Maximum transient absorption at 230 nm (HFC-23 (CF_3H) and HFC-125 (CF_3CF_2H)) and 250 nm (HFC-143a (CF_3CH_3)) as function of the concentration ratio [HFC]/[O_2]. The solid line are a fit to the experimental data.*

This behavior is rationalized in terms of the competition between RH and O_2 for the available F atoms. With low RH concentrations, an appreciable amount of FO_2 is formed; hence, a large initial absorption is seen. As the RH concentration is increased, RO_2 radicals are formed at the expense of FO_2, and the initial maximum absorption decreases. In the CF_3CH_3 system the arguments above are also valid, the only difference is that the absorbance change is observed at 250 nm instead of the 230 nm used for CF_3H and CF_3CF_2H. At 250 nm the absorbance of the RO_2 radical is larger than the absorbance of the FO_2 radical. Therefore the absorbance as a function of [RH]/[O_2] is inverted in the CF_3CH_3 system compared to the CF_3CF_2H and CF_3H systems.

The solid lines in Figure 13 represent fits of the following expression to the data:

$$A_{max}=\{A_{FO2} + A_{RO2}(k_{29}/k_{12})[RH]/[O_2]\}/\{1 + (k_{29}/k_{12})[RH]/[O_2]\}$$

where A_{max} is the observed maximum absorbance, A_{FO2} is the maximum absorbance expected if FO_2 is the sole absorbing species, and A_{RO2} is the maximum absorbance

expected if RO_2 (CF_3O_2, $CF_3CF_2O_2$, or $CF_3CH_2O_2$) is the sole absorbing species. Parameters A_{FO2}, A_{RO2} and k_{29}/k_{12} were simultaneously varied and gave the best fit with A_{FO2}=0.20±0.009, A_{CF3O2}=0.063±0.008, and k_{29}/k_{12}=0.49±0.12, A_{FO2}=0.055±0.003, $A_{CF3CF2O2}$=0.103±0.004, and k_{29}/k_{12}=1.37±0.42, and A_{FO2}=0.046±0.003, $A_{CF3CH2O2}$=0.100±0.003, and k_{29}/k_{12}=13.67±3.17. Errors are 2σ. Using our previous value of $k_{12}=(1.9\pm0.3)\times10^{-13}$ $cm^3molecule^{-1}s^{-1}$ at 1000 mbar total pressure [Appendix 7.1 pp117] then leads to $k_{29}=(0.9\pm0.3)\times10^{-13}$ $cm^3molecule^{-1}s^{-1}$, $k_{29}=(2.6\pm0.9)\times10^{-13}$ $cm^3molecule^{-1}s^{-1}$, and $k_{29}=(2.6\pm0.7)\times10^{-12}$ $cm^3molecule^{-1}s^{-1}$ for RH=CF_3H, CF_3CF_2H, and CF_3CH_3, respectively. These data are compared with data from the literature in section 5.1. It should be noted that values for k_{29} for RH = CF_3H and CF_3CF_2H are changed slightly, -8% and -33% respectively, compared to the previous published values. This is due to a new and more reliable value for k_{12}.

4.1.3 FNO Relative Method

The rate constant for the reaction of F atoms with CF_3CFClH was measured relative to the rate constant for the reaction of F atoms with NO:

$$F + CF_3CFClH \rightarrow HF + CF_3CFCl \quad (33)$$

$$F + NO + M \rightarrow FNO + M \quad (30)$$

The amount of FNO formed upon radiolysis of mixtures of $CF_3CFClH/NO/SF_6$ depends upon the rate constant ratio k_{33}/k_{30} and the concentration ratio [CF_3CFClH]/[NO]. k_{30} has been determined previously in our laboratory to $(5.1\pm0.7)\times10^{-12}$ $cm^3molecule^{-1}s^{-1}$ and FNO is known to absorb at 310.5 nm [Appendix 7.3 pp134 and 7.8 pp174]. To determine k_{33}, experiments were performed in which the maximum of the transient absorption at 310.5 nm was measured following the pulse radiolysis of $SF_6/CF_3CFClH/NO$ mixtures. In these experiments, the radiolysis dose and the SF_6 concentration were held fixed at a dose of 0.527 and [SF_6] = 950 mbar ($[F]_0=1.48\times10^{15}$ molecules cm^{-3}) and the concentrations of CF_3CFClH and NO were varied over the ranges 0-100 and 1-10 mbar, respectively.

Figure 14 shows the observed variation of the maximum absorption at 310.5 nm as a function of the concentration ratio [CF_3CFClH]/[NO]. At low [CF_3CFClH]/[NO] ratios the initial absorption was large. As the concentration ratio was increased, the initial absorption maximum decreased until a ratio of [CF_3CFClH]/[NO]=100 was reached. Further increase in the [CF_3CFClH]/[NO] ratio had no discernable effect on the initial absorption maximum. This behavior is rationalized in terms of the competition between

CF_3CFClH and NO for the available F atoms. At low CF_3CFClH concentrations, an appreciable amount of FNO is formed; hence, a large initial absorption is seen. As the CF_3CFClH concentration is increased, an increasing fraction of the F atoms reacts with CF_3CFClH on the expense of NO, and the initial maximum absorption decreases. The CF_3CFCl radicals formed may react with NO to produce $CF_3CFClNO$:

$$CF_3CFCl + NO + M \rightarrow CF_3CFClNO + M \qquad (34)$$

The formation of $CF_3CFClNO$ may explain the residual absorbance for large ratios of $[CF_3CFClH]/[NO]$.

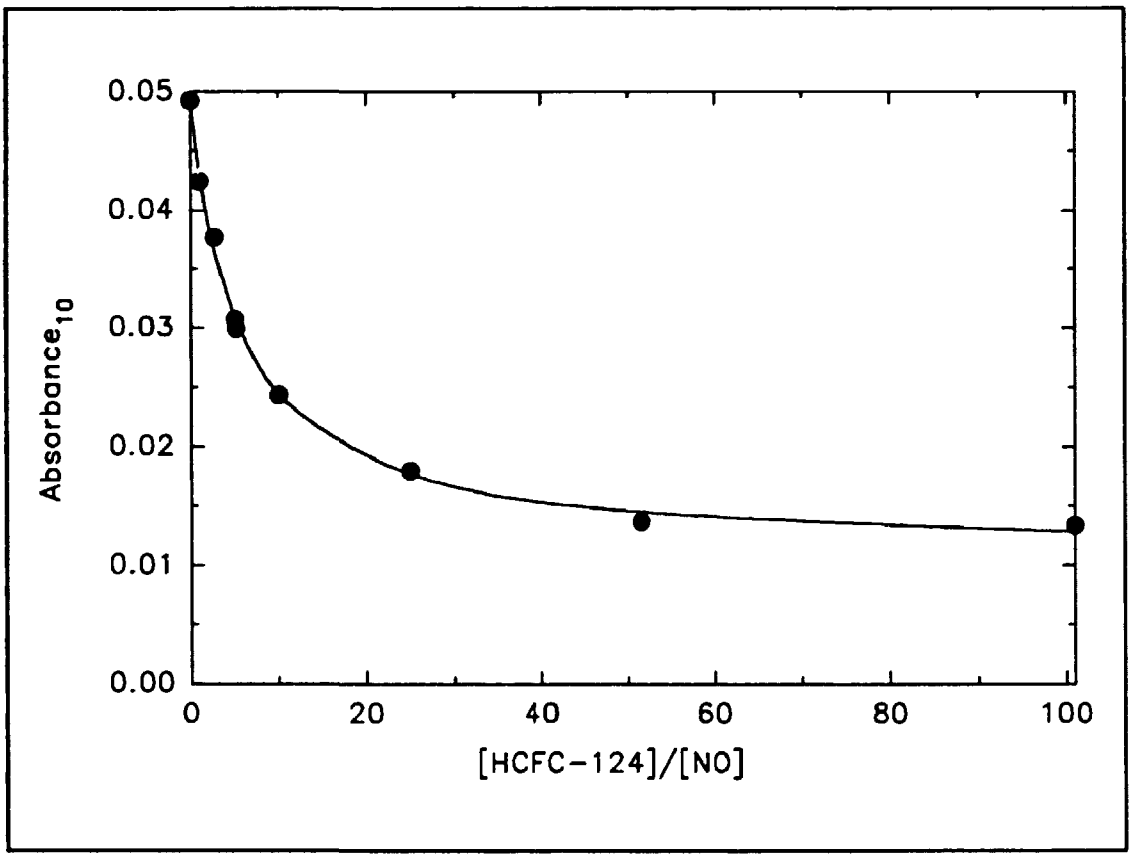

Figure 14. *Maximum transient absorption measured at 310.5 nm following pulse radiolysis of 1-10 mbar NO, 0-100 mbar CF_3CFClH, and 950 mbar SF_6. The solid line is a fit to the data. See text.*

The solid line in Figure 14 represents a three parameter fit of the following expression to the data:

$$A_{max}=\{A_{FNO} + (A_{CF3CFClNO}(k_{33}/k_{30})[CF_3CFClH]/[NO])\}/(1 + (k_{33}/k_{30})[CF_3CFClH]/[NO])$$

where A_{max} is the observed maximum absorbance, A_{FNO} is the maximum absorbance expected if only FNO is produced, and $A_{CF3CFClNO}$ is the maximum absorbance expected if all F atoms react with CF_3CFClH. The best fit was obtained for $k_{33}/k_{30}=0.185\pm0.023$, $A_{FNO}=0.049\pm0.001$, and $A_{CF3CFClNO}=0.011\pm0.001$. Using our previous value of $k_{30}=(5.1\pm0.7)\times10^{-12}$ $cm^3molecule^{-1}s^{-1}$ at 1000 mbar total pressure [Appendix 7.3 pp134 and 7.8 pp174], k_{33} is found to be $(9.4\pm1.8)\times10^{-13}$ $cm^3molecule^{-1}s^{-1}$. This number is consistent with the direct determination of k_{33}, $(7.1\pm0.9)\times10^{-13}$ $cm^3molecule^{-1}s^{-1}$. When the experimental difficulties in monitoring CF_3CFCl and the limited dynamic range (absorbance=0.05-0.013) of the plot in Figure 14 is taken into account the agreement between the relative and the absolute measurement is acceptable. I choose to quote the average of the two k_{33} values and uncertainties covering the extremes of the two determinations, $(8\pm2)\times10^{-13}$ cm^3 $molecule^{-1}$ s^{-1}. No value for k_{33} exists in the literature for comparison.

4.2 UV Spectra of Halogenated Peroxy Radicals

The UV absorption spectra of CF_3O_2, $CF_3CF_2O_2$, CF_3CFClO_2, $CF_3CH_2O_2$, CH_2FCHFO_2, and $CHF_2CF_2O_2$ are reported as part of this work. To quantify the UV absorption spectrum of these RO_2 radicals, their concentration needs to be determined. The yields of the RO_2 radicals can only be obtained if F atoms are converted stoichiometrically into RO_2 radicals. To obtain this we must avoid secondary radical-radical reactions such as the following reactions:

$$R + F + M \rightarrow \text{products} \quad (31)$$

$$R + R + M \rightarrow R_2 + M \quad (32)$$

$$RO_2 + R \rightarrow \text{products} \quad (35)$$

$$RO_2 + F \rightarrow \text{products} \quad (36)$$

$$RO_2 + RO_2 \rightarrow \text{products} \quad (37)$$

In addition the reaction of F atoms with O_2 needs to be minimized:

$$F + O_2 + M \rightarrow FO_2 + M \quad (12)$$

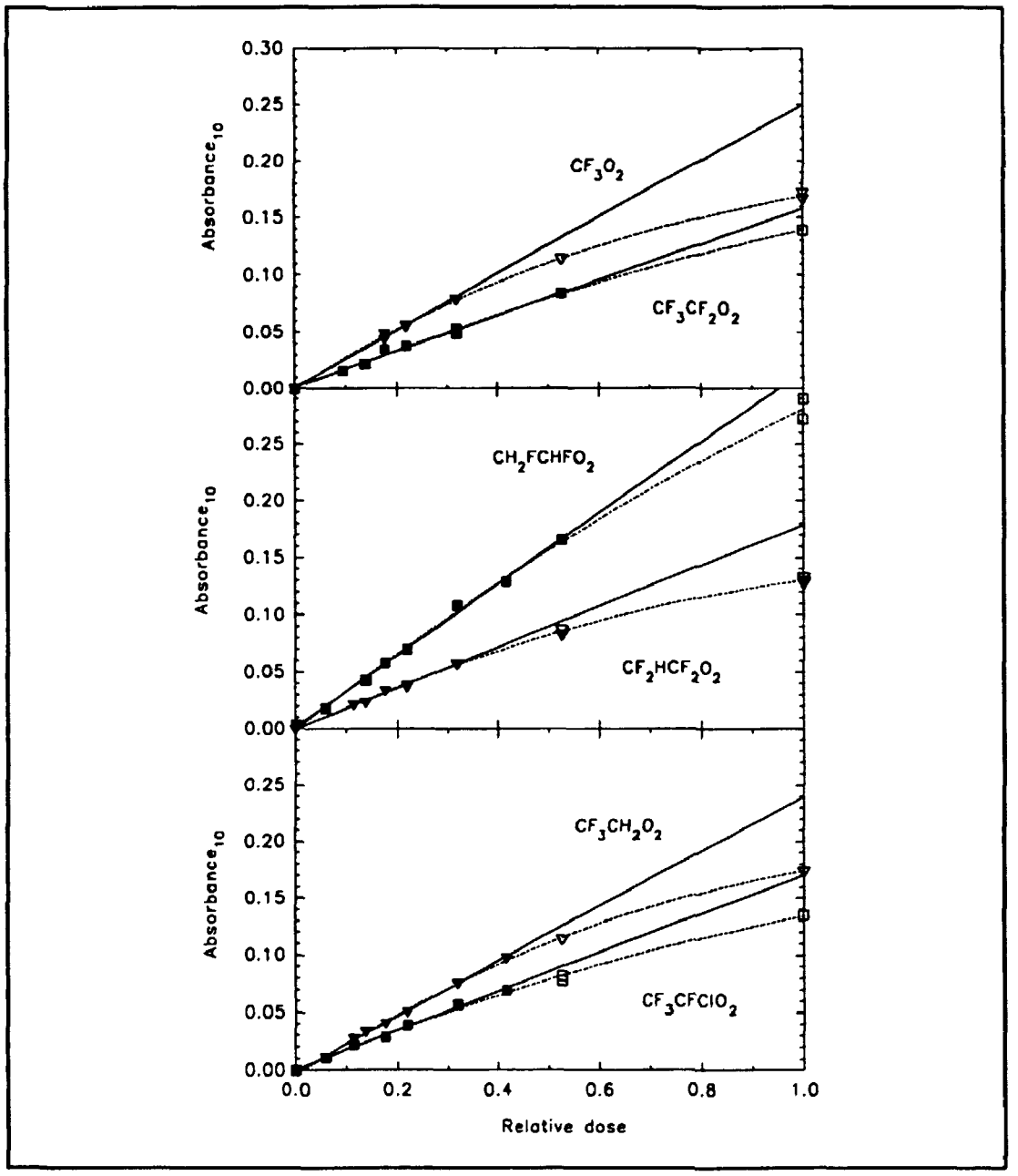

Figure 15. *Maximum transient absorption following the formation of CF_3O_2 (at 230 nm), $CF_3CF_2O_2$ (at 230 nm), CH_2FCHFO_2 (at 240 nm), $CF_2HCF_2O_2$ (at 230 nm), $CF_3CH_2O_2$ (at 250 nm), and CF_3CFClO_2 (at 230 nm). The solid lines are fit to the low dose data.*

To minimize the amount of F atoms consumed by reaction (12) the oxygen concentration needs to be low. However, a low oxygen concentration will increase the importance of reactions (31,32,35). Clearly a compromise needs to be met. Initial O_2 concentrations of 2-40 mbar were chosen. The amount of FO_2 formed under these experimental conditions was calculated from k_{12} and the rate constants for the reactions of F atoms with the HFC or

HCFC studied. Since the FO_2 spectrum is known [Appendix 7.1 pp117] it is possible to correct for the absorbance due to this radical.

There are no literature data concerning the kinetics of reactions (31,32,35,36,37), hence we cannot calculate their importance. To check for these unwanted radical-radical reactions the maximum transient absorption as a function of the relative dose were measured upon radiolysis of mixtures of O_2, RH, and SF_6. The radiolysis dose was varied over an order of magnitude. Figure 15 shows the observed maximum of the transient absorption as a function of the dose. As seen from Figure 15, the absorption increase linearly with the radiolysis dose up to doses of 0.416 (CF_3CFClO_2), 0.527 ($CF_3CF_2O_2$), 0.319 (CF_3O_2), 0.416 ($CF_3CH_2O_2$), 0.319 ($CHF_2CF_2O_2$) and 0.527 (CH_2FCHFO_2). At higher doses the data fall below that expected from a linear extrapolation of the low dose results. This is due to incomplete conversion of F atoms into RO_2 radicals caused by secondary radical-radical reactions at high initial F atom concentrations.

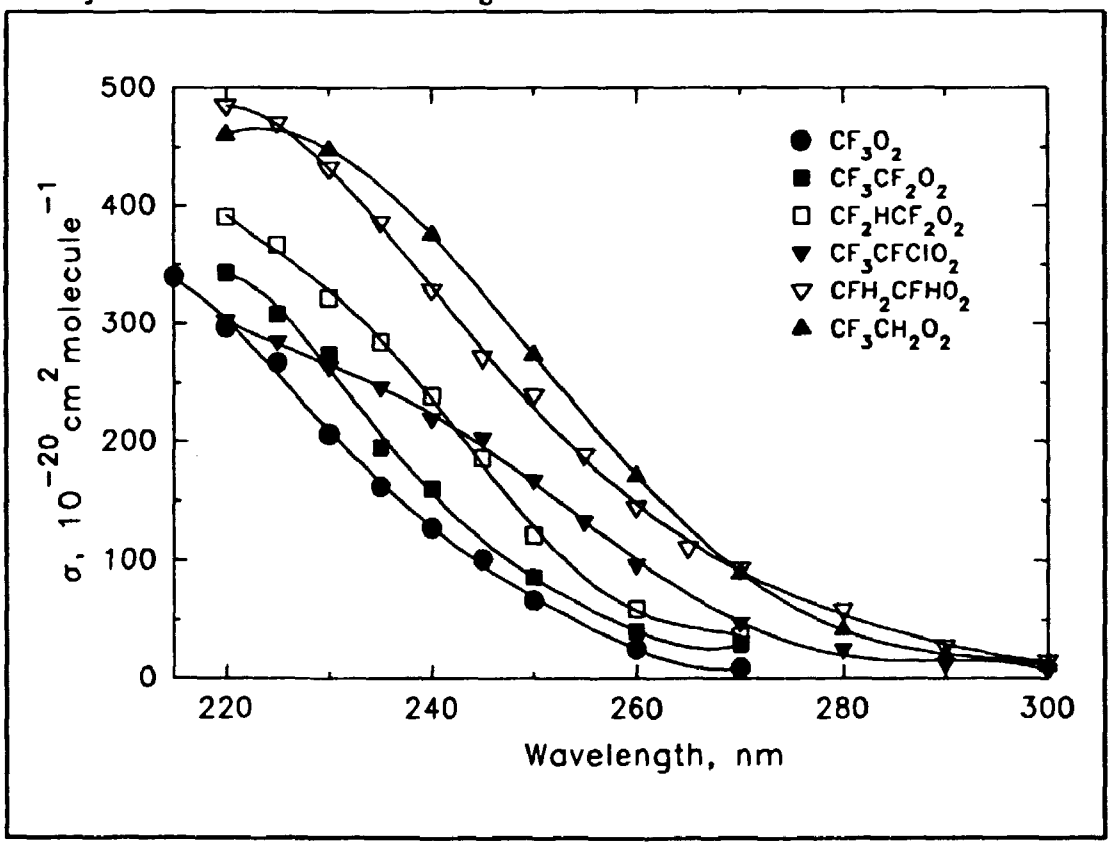

Figure 16. *UV absorption spectra of the six peroxy radicals investigated as part of this work.*

The solid lines drawn through the data in Figure 15 are linear least squares fit of the low dose data. The slopes are 0.170±0.009 (CF_3CFClO_2), 0.156±0.012 ($CF_3CF_2O_2$), 0.255±0.009 (CF_3O_2), 0.2415±0.0082 ($CF_3CH_2O_2$), 0.179±0.008 ($CHF_2CF_2O_2$) and

0.312±0.014 (CH_2FCHFO_2). From these value and three additional pieces of information, (i) the F atom yield (ii) the conversion of F atoms into RO_2 and FO_2 calculated from k_{12} and the rate constants listed in Table X, and (iii) the absorption cross section for FO_2 [Appendix 7.1 pp117], $\sigma(CF_3CF_2O_2)$ at 230 nm = (2.74±0.46)x10^{-18} cm^2 $molecule^{-1}$, $\sigma(CF_3O_2)$ at 230 nm = (2.06±0.50)x10^{-18} cm^2 $molecule^{-1}$, $\sigma(CF_3CFClO_2)$ at 250 nm = (1.67±0.09)x10^{-18} cm^2 $molecule^{-1}$, $\sigma(CF_3CH_2O_2)$ at 250 nm = (2.73±0.30)x10^{-18} cm^2 $molecule^{-1}$, $\sigma(CHF_2CF_2O_2)$ at 230 nm = (3.2±0.5)x10^{-18} cm^2 $molecule^{-1}$, and $\sigma(CH_2FCFHO_2)$ at 240 nm = (3.28±0.40)x10^{-18} cm^2 $molecule^{-1}$ are calculated. The quoted error are combined uncertainties of the linear least squares fits of all the data in Figure 15 and the uncertainty in our absolute calibration of the fluorine atom yield.

To map out the spectra, experiments were performed to measure the transient absorption between 220 nm and 300 nm following the pulsed irradiation of $SF_6/RH/O_2$ mixtures. The transient absorptions were corrected for FO_2 and then scaled to the absorption cross sections determined above to obtain absolute absorption cross sections. Absorption cross sections for the six RO_2 radicals are shown in Figure 16. All the spectra are similar in shape. The observed trend in Figure 16 is consistent with the literature spectra of halogenated alkyl peroxy radicals where substitution of electron withdrawing groups on the carbon bearing the -O-O• group leads to a spectral shift to the blue [9]. From the available UV spectra of alkyl peroxy radicals it can be seen that a F atoms on the α carbon seems to increase the absorption cross section of the maximum while chlorine atoms give a broader and less intense absorbance [19,20].

4.3 The Kinetics of the Self Reaction of Halogenated Peroxy Radicals

As a part of this work the self reactions of $CF_3CF_2O_2$, $CF_2HCF_2O_2$, $CF_3CH_2O_2$, CF_3O_2, and CF_3CFClO_2 have been studied. The self reactions of $CF_3CF_2O_2$, $CF_2HCF_2O_2$, $CF_3CH_2O_2$, and CF_3O_2 have been studied by fitting a second order expression to the decay of the absorbance due to the peroxy radical.

An example of a decay of a peroxy radical and a second order fit is seen in Figure 7. The reciprocal of the half life obtained from the second order fit is plotted as a function of the absorbance of the peroxy radical. The slope of this plot equals 2k2.303/(lσ) as discussed in section 2.1.2. From the optical pathlength l, the absorption cross section σ, and the slope of the $1/t_{½}$ vs Amax plot the observed second order rate constant can then be calculated. The observed rates are (3.6±0.9)x10^{-12} cm^3 $molecule^{-1}$ s^{-1} for CF_3O_2, (2.1±0.4)x10^{-12} cm^3 $molecule^{-1}$ s^{-1} for $CF_3CF_2O_2$, (2.7±0.6)x10^{-12} cm^3 $molecule^{-1}$ s^{-1} for $CF_2HCF_2O_2$, and (8.4±1.1)x10^{-12} cm^3 $molecule^{-1}$ s^{-1} for $CF_3CH_2O_2$.

The observed rate constants above are not "true" rate constants because of the potential influence of secondary chemistry. Product studies described in the Chapter 5 show that the self reactions of the CF_3O_2, $CF_3CF_2O_2$, $CHF_2CF_2O_2$, and $CF_3CH_2O_2$ radicals form alkoxy radicals:

$$RO_2 + RO_2 \rightarrow RO + RO + O_2 \qquad (37)$$

The alkoxy radicals proceed via C-C bond cleavage (CF_3CF_2O, CF_2HCF_2O, and CH_2FCHFO), react with O_2 and give an aldehyde and HO_2 (CF_3CH_2O), or eject an Cl atom (CF_3CFClO). Since the rate constants for these and the subsequent reactions are unknown, I can not correct the decays for secondary chemistry. However, in the case of the self reaction of CF_3O_2 the product study give enough information to do a correction for the secondary chemistry (see later). In addition the self reaction rate constant of CF_3CFClO_2 was derived by an initial rate method.

The product study of the self reaction of the CF_3O_2 radical showed that the end product is 50±3% CF_3OOOCF_3. As discussed later, this yield result implies that the alkoxy radical, CF_3O, is formed from the self reaction and that these alkoxy radicals react with CF_3O_2 radicals. This reaction rate is greater than 2.5×10^{-11} cm^3 $molecule^{-1}$ s^{-1} under the assumption that $k_{39}\approx k_{40}$ [section 5.2.1]:

$$CF_3O_2 + CF_3O + M \rightarrow CF_3OOOCF_3 + M \qquad (39)$$
$$CF_3O + CF_3O + M \rightarrow CF_3OOCF_3 + M \qquad (40)$$

In the pulse radiolysis system the reaction of CF_3O with CF_3O_2 is much faster than the self reaction of CF_3O_2. Simulations show [section 5.2.1] that the resulting decays are indistinguishable from pure second order kinetics and that the rate constants determined from the decay is essentially a factor of two larger than the "true" rate constant. The observed rate constant of $(3.6\pm0.9)\times10^{-12}$ cm^3 $molecule^{-1}$ s^{-1} should be divided by 2 to correct for the reaction of CF_3O radicals with CF_3O_2. The "true" rate constant is then $(1.8\pm0.4)\times10^{-12}$ cm^3 $molecule^{-1}$ s^{-1}. This rate constant agree with the self reaction rate constant of $(1.8\pm0.4)\times10^{-12}$ cm^3 $molecule^{-1}$ s^{-1} determined by Maricq and Szente [60].

The decay of the absorption transient at 250 nm following pulse radiolysis of mixtures of 50 mbar CF_3CFClH, 10 mbar O_2, and 940 mbar SF_6 is mainly due to the self reaction of the CF_3CFClO_2 radical:

$$CF_3CFClO_2 + CF_3CFClO_2 \rightarrow CF_3CFClO + CF_3CFClO + O_2 \qquad (41a)$$
$$\rightarrow CF_3CFClO_2CFClCF_3 + O_2 \qquad (41b)$$

The apparent decay of the CF_3CFClO_2 radicals may be influenced by reactions of the products of reaction (41). For example:

$$CF_3CFClO + M \rightarrow CF_3CFO + Cl + M \quad (42)$$
$$CF_3CFClO_2 + CF_3CFClO \rightarrow \text{products} \quad (43)$$
$$Cl + CF_3CFClO_2 \rightarrow ClO + CF_3CFClO \quad (44)$$
$$Cl + CF_3CFClH \rightarrow CF_3CFCl + HCl \quad (33)$$
$$CF_3CFCl + O_2 + M \rightarrow CF_3CFClO_2 + M \quad (45)$$

Reaction (42) is expected to be fast ($t_{½}$<few μs) [Appendix 7.11.18 pp205], Hence chlorine atoms are expected to be produced in the system within a few μs after the formation of the CF_3CFClO radicals. Therefore reaction (44) and (33) and the subsequent reactions of ClO radicals are believed to be the major secondary reactions in the system. Too little is known about these reactions to derive the rate constant of reaction (41) by simulations of the observed decay of the absorption at 250 nm following the pulse radiolysis of $CF_3CFClH/O_2/SF_6$ mixtures. Hence, I have used an initial rate method to determine k_{41}. The slope of the decay (the initial rate or k_{init}) after all CF_3CFClO_2 radicals have been formed, is a measurement of the initial decay rate of the CF_3CFClO_2 radical and hence will not be influenced by secondary chemistry. Since the products CF_3CFClO and CF_3CFO are not expected to absorb significantly at 250 nm, the initial rate, k_{init},may be expressed as follows:

$$k_{init} = (2x2.303/l)(k_{41}/\sigma_{CF3CFClO2}(250nm))xA_0^2$$

Where l is the optical path length and A_0 is the transient absorbance.

The initial rate of two full dose, a half dose, and 0.416 dose experiments were determined by a linear regression analysis of the absorption data in a short time interval. A_0 was determined as the average value of the transient absorptions in the time interval. The results are shown in Table V. Time intervals were started 10 μs, or later, after the electron pulse to avoid any possible interference from the formation kinetics of the CF_3CFClO_2 radicals. Two checks were made for secondary chemistry. Firstly, the slope was measured in three successive time intervals of 20 μs for the full dose experiments. As seen in Table V the values of k_{41} calculated from the data in the first two time intervals were essentially the same, while the value of k_{41} calculated from the third time interval was significantly lower than the first two measurements. This might be due to the formation of CF_3CFClO_2 by reaction (33) and (45). We choose to use only the first 50 μs

of the transients to determine k_{41}. Secondly, k_{44} may increase the apparent decay rate of the absorption at 250 nm if it is fast. As a check of this I estimated the ClO concentration (from reaction (44)) in the first 50 μs after the electron pulse by the absorption at 277.5 nm. The ClO radical has a sharp absorption feature at 277.5 nm [5]. The maximum transient absorption at 277.5 nm in the first 50 μs after pulse radiolysis of $CF_3CFClH/O_2/SF_6$ mixtures was less than 0.008 using a spectral resolution of 0.2 nm, full dose, and a 40 cm pathlength. From the absorption cross section of ClO at 277.5 nm, $5.8x10^{-18}$ cm^2 $molecule^{-1}$, I estimate an upper limit of the ClO formation of $8x10^{13}$ molecule cm^{-3}. This is <10% of the loss of CF_3CFClO_2 which is approximately $1.0x10^{15}$ molecule cm^{-3}.

The average of the data in Table V, not including results from the time interval 50-70 μs data, gives $(2.6\pm0.5)x10^{-12}$ cm^3 $molecule^{-1}$ s^{-1}. This result also includes the uncertainty in $\sigma_{CF_3CFClO_2}$.

Table V: Initial rate of the decay of CF_3CFClO_2 radical:

Dose	Time μs	Absorbance base 10	Init. Rate s^{-1}	k_3 10^{-12} $cm^3molecule^{-1}s^{-1}$
1.0	10-30	0.1147	-1206	2.66
	30-50	0.0943	-804	2.62
	50-70	0.0840	-224	0.92
1.0	10-30	0.1203	-1235	2.48
	30-50	0.1005	-845	2.42
	50-70	0.0889	-491	1.80
0.527	10-50	0.0685	-470	2.91
0.416	10-50	0.0593	-334	2.75

4.4 The Reaction of Halogenated Peroxy Radicals with NO

The reaction between a peroxy radical, RO_2, and NO can proceed through two channels:

$$RO_2 + NO \rightarrow RO + NO_2 \quad (3a)$$
$$RO_2 + NO + M \rightarrow RONO_2 + M \quad (3b)$$

In this work k_3 are determined by the first order formation rate of NO_2 formation at 400 nm and 450 nm following pulse radiolysis of mixtures of NO, RH, O_2, and SF_6. Hence, it is the overall rate constant which is determined. An example of an experimental transient is displayed in Figure 6 in chapter 2. The transient absorbance at 400 nm following radiolysis of mixtures of RH/SF6, NO/SF_6, and RH/O_2/SF_6 mixtures as well as pure SF_6 are zero. Since the relative intensities at 400 nm and 450 nm correspond to those reported in the literature for NO_2 [5] it seems reasonable to conclude that NO_2 is responsible for the transient absorption at 400 nm and 450 nm. The experimental transients were fitted beginning from 2-4 μs to the maximum of the transient absorption with a first order rise expression. The reason for not fitting from time zero is that the formation of CF_3CFClO_2 radicals have to be complete before reaction (3) can be first order.

The first order rate constants obtained from fitting the experimental absorbance transients were plotted as functions of [NO]. In Figure 17 the first order rates for the formation of NO_2 for 16 different species are plotted as a function of [NO]. The filled circles are the experimental points while the triangles are corrected for secondary chemistry (see below).

Before a value for k_3 can be extracted from the observed kinetics of the NO_2 formation the impact of potential secondary reactions needs to be considered. Four possible complications need to be considered: (i) The reaction of RO_2 radicals with NO_2. (ii) The reaction of RO radicals with NO_2. (iii) The formation rate of the RO_2 radical. (iv) The decomposition of the RO radical. Peroxy radicals, RO_2, are known to react with NO_2 to form peroxy nitrates [9,8]. Hence, following the formation of NO_2 from reaction (3), there is a competition between reactions (3) and (46) for the available RO_2 radicals:

$$RO_2 + NO \rightarrow \text{products} \quad (3)$$
$$RO_2 + NO_2 + M \rightarrow RO_2NO_2 + M \quad (46)$$

Similarly, alkoxy radicals produced in reaction (3) also react with both NO and NO_2:

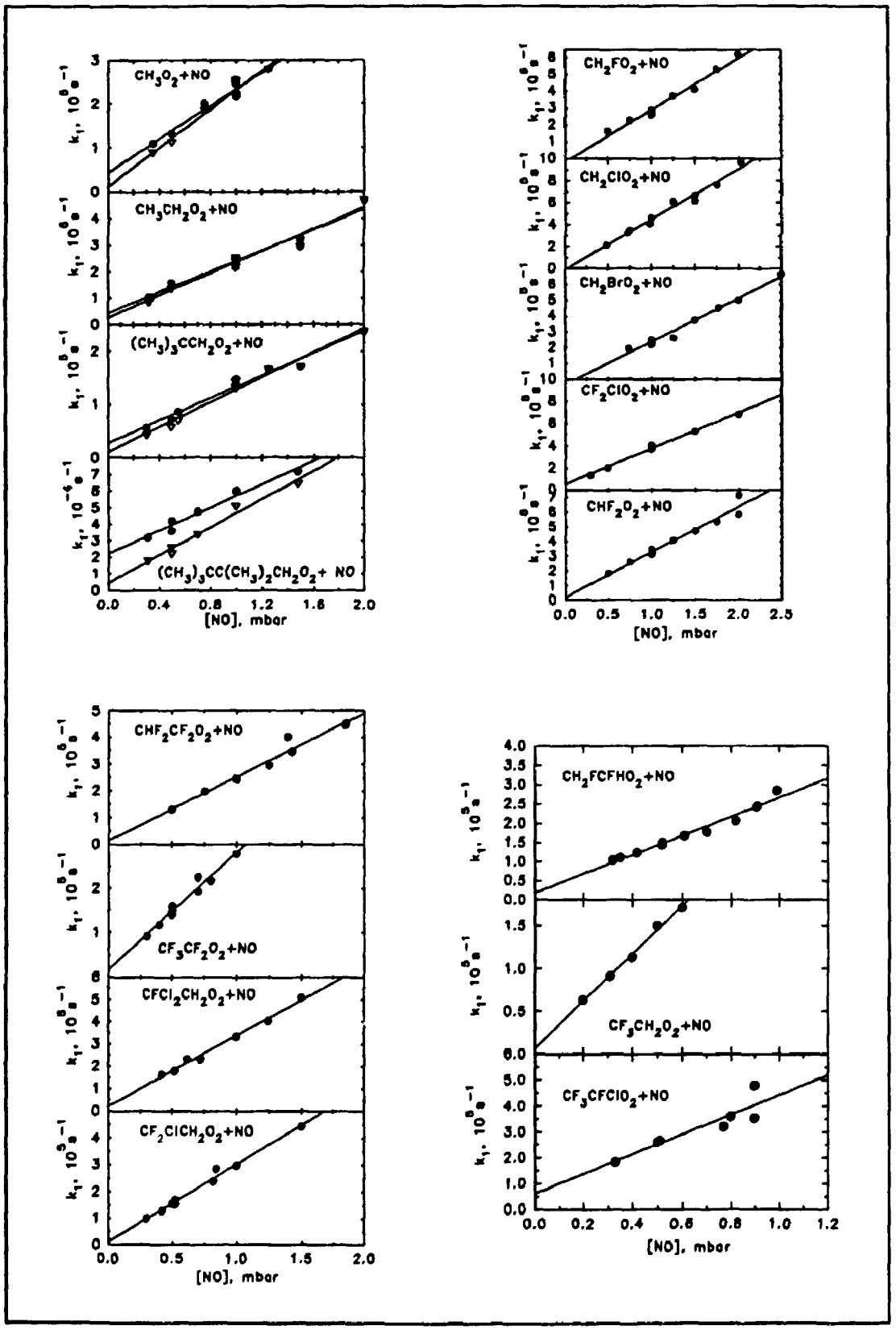

Figure 17. *Plot of k^{1st} versus [NO] for various peroxy radicals. Closed circles are raw data and the open triangles are corrected data. See text.*

$$RO + NO + M \rightarrow RONO + M \quad (47)$$

$$RO + NO_2 + M \rightarrow RONO_2 \quad (48)$$

Reactions (46) and (48) remove NO_2 from the system with an efficiency which increases at long reaction times and thereby at low NO concentrations. The removal decreases the time taken for the NO_2 concentration to reach a maximum. Hence, reaction (46) and (48) lead to an increase in the apparent pseudo first order rate constant for the NO_2 formation. This effect is most pronounced under low $[NO]_0$ concentrations leading to positive intercepts in plots of k^{1st} versus [NO]. In Figure 17, plots of k^{1st} versus [NO] for alkyl peroxy radicals, halogenated methyl peroxy radical, and halogenated ethyl peroxy radicals are presented. Positive intercepts were observed for all the alkyl peroxy radicals studied here. Interestingly, similar plots for the halogenated peroxy radicals have intercepts which are zero, within the experimental uncertainty. To assess the impact of reactions (46), (47) and (48) and, hence, to compute corrections for such, detailed modelling of the experimental data presented in Figure 17 was performed using the Chemsimul chemical kinetic modelling program [61] with a mechanism consisting of the reactions in Table VI.

Table VI. Reaction mechanism for the formation of NO_2.

Reaction	Rate constant (295 K) ($cm^3molecule^{-1}s^{-1}$)	
$F + RH \rightarrow HF + R$	varied	
$F + NO + M \rightarrow FNO + M$	$5.1x10^{-12}$	[Appendix 7.3 and 7.8]
$F + O_2 + M \rightarrow FO_2 + M$	$1.9x10^{-13}$	[Appendix 7.1]
$R + NO + M \rightarrow RNO + M$	$1.0x10^{-11}$	see text
$R + O_2 + M \rightarrow RO_2 + M$	$(1\text{-}5)x10^{-12}$	see text
$RO_2 + NO \rightarrow RO + NO_2$	$6.0x10^{-12}$	see text
$RO_2 + NO_2 + M \rightarrow RO_2NO_2 + M$	$6.0x10^{-12}$	see text
$RO + NO + M \rightarrow RONO + M$	$2.0x10^{-11}$	see text
$RO + NO_2 + M \rightarrow RONO_2 + M$	$1.5x10^{-11}$	see text
$RO_2 + RO_2 \rightarrow RO + RO + O_2$	$0\text{-}8x10^{-12}$	see text

First, the interference of reaction (46) and (48) are addressed. Values for k_3 were taken from the present work. Values of k_{46} were taken from the literature where available [8,9]. In the absence of recommended literature data, k_{46}=6.0x10^{-12} cm^{3}molecule^{-1}s^{-1} was used, as a typical value for this reaction [8,9]. There is little literature data available concerning the kinetics of reaction (47) and (48). We assume here that all alkoxy radicals display the same kinetics as methoxy radicals in their reaction toward NO and NO_2, k_{47}=2.0x10^{-11} cm^3 molecule^{-1} s^{-1} and k_{48}=1.5x10^{-11} cm^3 molecule^{-1} s^{-1} [62]. The rate constants for the reactions between alkyl radicals and O_2 and NO are assumed to be (1-5)x10^{-12} cm^3 molecule^{-1} s^{-1} and 10^{-11} cm^3 molecule^{-1} s^{-1}, respectively. A rate constant of (2-5)x10^{-12} cm^3 molecule^{-1} s^{-1} for the reaction of alkyl and haloalkyl radicals is estimated from the NIST chemical database. For the reaction of the alkyl radical with NO, was used a rate constant for the reaction of CH_3 with NO from Wallington et al. [63]. The simulated NO_2 results were converted into a plot of absorption versus time, and a first order rise was fitted to the simulated transient. In all cases, the simulated data were closely fit by first order kinetics.

For RO_2 radicals with k_3>k_{46} (i.e. the halogenated alkyl peroxy radicals), the pseudo first order rate constants derived from the simulated data were in close agreement (within 1% for $[NO]_0 \geq 1$ mbar and within 10% for $[NO]_0$=0.3 mbar) with those expected. As seen from Figure 17, there is no experimental evidence that measured values of k^{1st} for the halogenated peroxy radicals using lower NO concentrations are systematically larger than expected based upon a linear extrapolation of the data using higher NO concentrations. However, it is worth noting that a 10% effect would probably be masked by the experimental scatter and go undetected. As a further check for reactions (46) and (48) the maximum change in absorption at 400 nm, attributable to NO_2, was measured as a function of $[NO]_0$. If reactions (46) and (48) are significant, the NO_2 yield should decrease with decreasing $[NO]_0$. No such trend was observed for the halogenated peroxy radicals. No corrections to the experimental data concerning the haloperoxy radicals are required.

For the alkyl peroxy radicals with $k_3 \leq k_{46}$ the pseudo first order rate constants derived from the model were larger than those expected. This discrepancy increased as $[NO]_0$ and k_3/k_{46} decrease, and was most pronounced for $(CH_3)_3CC(CH_3)_2CH_2O_2$ radicals. Further evidence for secondary chemistry comes from the observation that the yields of NO_2 in experiments involving $(CH_3)_3CCH_2O_2$ and $(CH_3)_3CC(CH_3)_2CH_2O_2$ radicals decreased substantially at low $[NO]_0$. No discernable decrease in the NO_2 yield in experiments using low $[NO]_0$ was observed in experiments involving either CH_3O_2 or $C_2H_5O_2$ radicals. Corrections were computed to account for reactions (46), (47) and (48).

Corrected and uncorrected data are shown in Figure 17. As seen from Figure 17, linear least squares analysis of the corrected data produces a line which, within the experimental uncertainties, passes through the origin. In view of the corrections applied to the data for CH_3O_2, $C_2H_5O_2$, $(CH_3)_3CCH_2O_2$, and $(CH_3)_3CC(CH_3)_2CH_2O_2$ radicals, I choose to add an additional 10% and 20% uncertainty range to the measured rate constants of the reactions of CH_3O_2 and $C_2H_5O_2$ radicals, and $(CH_3)_3CCH_2O_2$ and $(CH_3)_3CC(CH_3)_2CH_2O_2$ radicals with NO, respectively. Values cited in Table VII reflect only the precision.

So far I have not considered the influence of the formation rate of RO_2 on the k_{1st} obtained from the fit of the NO_2 transient. In the simulations above I have chosen the rise time of the RO_2 radical to be much faster than the rise time of NO_2. When the rise time of RO_2 is getting close to the NO_2 rise time the k_{1st} obtained from the fit of the absorption transient falls below the real value. This effect is of cause most pronounced for high NO concentrations. Two experimental situations will be discussed here: The rate constant for the rise of RO_2 is 1.23×10^6 s^{-1} ($k_2=5\times10^{-12}$ cm^3molecule^{-1} s^{-1}, 10 mbar O_2, and $k_{2a}[RH]>>k_2[O_2]$) and the rise of NO_2 is 0, 4, 6, and 8×10^5 s^{-1} ($k_3=1.5\times10^{-11}$ cm^3 molecule^{-1} s^{-1} and [NO]=1.1-2.2 mbar). The values of k_{1st} fall <0.5%, 3%, 4%, and 6% below the "true" value. Hence, as long as the first order formation of NO_2 is less than half of the formation rate of RO_2, the results should be good to within 5%.

Another possible complication is the self reaction of the RO_2 radical. This complication is most important at low [NO] concentrations. With $k_3=6\times10^{-12}$ cm^3 molecule^{-1} s^{-1}, [NO]=0.3 mbar, and $k(RO_2+RO_2)=0,3,5,8\times10^{-12}$ cm^3 molecule^{-1} s^{-1} the obtained first order rate constant falls 6.3, 8.2, 9.4, and 11.1% above the "true" value. Again this is with in the noise level of the experiments.

The last complication of the measurements which will be discussed here is the decomposition of the alkoxy radical. The alkoxy radical may react with O_2 to give a carbonyl compound and HO_2, or decompose either via C-C bond cleavage or ejection of a Cl atom. The rate constant for the reaction of alkoxy radicals with O_2 are generally less than 10^{-14} cm^3 molecule^{-1} s^{-1} [64]. Since the rate constant for the reaction of RO with NO is three orders of magnitude greater than the rate constant for this reaction, The reaction of RO with NO will dominate in these cases and the formation of HO_2 will therefore be small.

The alkoxy radical may also decompose via C-C bond cleavage. The rate constant for this reaction is generally fast, $k<5\times10^4$ s^{-1} [See discussion in Appendix 7.11.18 pp205]. The alkyl radical formed by the C-C bond cleavage will be converted fast ($t_{1/2}<15$ μs) into alkyl peroxy radicals. These peroxy radicals react with NO to form NO_2. Therefore this complication is detected by the NO_2 yield exceeds 100% in terms of the F atom yield.

Table VII. Summary of rate constants for RO_2+NO -> products reactions

Species	Technique[a)]	$10^{12}k_3$[b,c)]	Reference
CH_3O_2	FP-UV	3.0±0.2	[65]
	FP-UV	7.1±1.4	[15]
	DF-MS	6.5±2.0	[66]
	FP-UV	7.7±0.9	[67]
	DF-MS	8.6±2.0	[68]
	LP-LIF	7.8±1.2	[69]
	LP-LA	7.0±1.5	[70]
	PR-UV	8.8±1.4	This work
$C_2H_5O_2$	FP-UV	2.7±0.2	[71]
	DF-MS	8.9±3.0	[72]
	PR-UV	8.5±1.2	This work
i-$C_3H_7O_2$	FP-UV	3.5±0.2	[73]
	DF-MS	5.0±1.2	[74]
t-$C_4H_9O_2$	DF-MS	4.0±1.1	[74]
$(CH_3)_3CCH_2O_2$	PR-UV	4.7±0.4	This work
$(CH_3)_3C(CH_3)_2CH_2O_2$	PR-UV	1.8±0.2	This work
CF_3CHFO_2	PR-UV	12.8±3.6	[75]
CFH_2CHFO_2	PR-UV	>8.7	This Work
$CF_3CH_2O_2$	PR-UV	5.6±1.1	This Work
CF_3CFClO_2	PR-UV	1.5±0.6	This Work
$CHF_2CF_2O_2$	PR-UV	>9.7±1.3	This work
$CF_3CF_2O_2$	PR-UV	>10.7±1.5	This work
$CFCl_2CH_2O_2$	PR-UV	12.8±1.1	This work
$CF_2ClCH_2O_2$	PR-UV	11.8±1.0	This work
CH_2FO_2	PR-UV	12.5±1.3	This work
CH_2ClO_2	PR-UV	18.7±2.0	This work
CH_2BrO_2	PR-UV	10.7±1.1	This work
CHF_2O_2	PR-UV	12.6±1.6	This work
CF_3O_2	DF-MS	17.8±3.6	[76]
	LP-MS	14.5±2.0	[77]
	PR-UV	16.9±2.6	This work
CF_2ClO_2	LP-MS	16±3	[77]
	PR-UV	13.1±1.2	This work
$CFCl_2O_2$	LP-MS	16.0±2.0	[78]
	LP-MS	14.5±2.0	[77]
CCl_3O_2	DF-MS	18.6±2.8	[79]
	LP-MS	17.0±2.0	[77]

a) FP-UV, Flash Photolysis - UV Absorption; DF-MS, Discharge Flow - Mass Spectrometry; LP-LIF, Laser Photolysis - Laser Induced Fluorescence; LP-LA, Laser Photolysis - Laser Absorption; PR-UV, Pulse Radiolysis - UV Absorption; LP-MS, Laser Photolysis - Mass Spectrometry

b) in units of $cm^3molecule^{-1}s^{-1}$

c) errors quoted for results from this work are $\pm 2\sigma$ and represent precision only.

In these cases only an upper limit for the rate constants for k_3 can be obtained. Secondary peroxy radicals are always formed after a primary peroxy radicals have reacted with NO. Therefore only the resulting NO_2 formation due to the secondary RO_2 radical will always be slower than the NO_2 formation due to the primary peroxy radical. Hence, the resulting first order rate constant derived from a first order fit to the experimental data will always be slower than the "true" rate constant.

Finally, as in the case of CF_3CFClO, an alkoxy radical may decompose via ejection of an Cl atom. The rate constant of the reaction of chlorine atoms with NO_2 is $4x10^{-11}$ cm^3 $molecule^{-1}$ s^{-1}. Since a dose of 0.416 was used for the experiments with CF_3CFClO, the first order formation rate for the reaction of Cl atoms with NO_2 is $<2.5x10^4$ s^{-1} ($t_{1/2}$>28μs). This rate constant is 13% or less than the observed rate constants for the NO_2 rise. The complication is therefore small however not unimportant in the discussed case.

The absolute accuracy of the rate constants depends on the precision of reactant concentrations and possible unidentified systematic errors. The overall accuracy of the measured rate constants is estimated to be of the order ±25%.

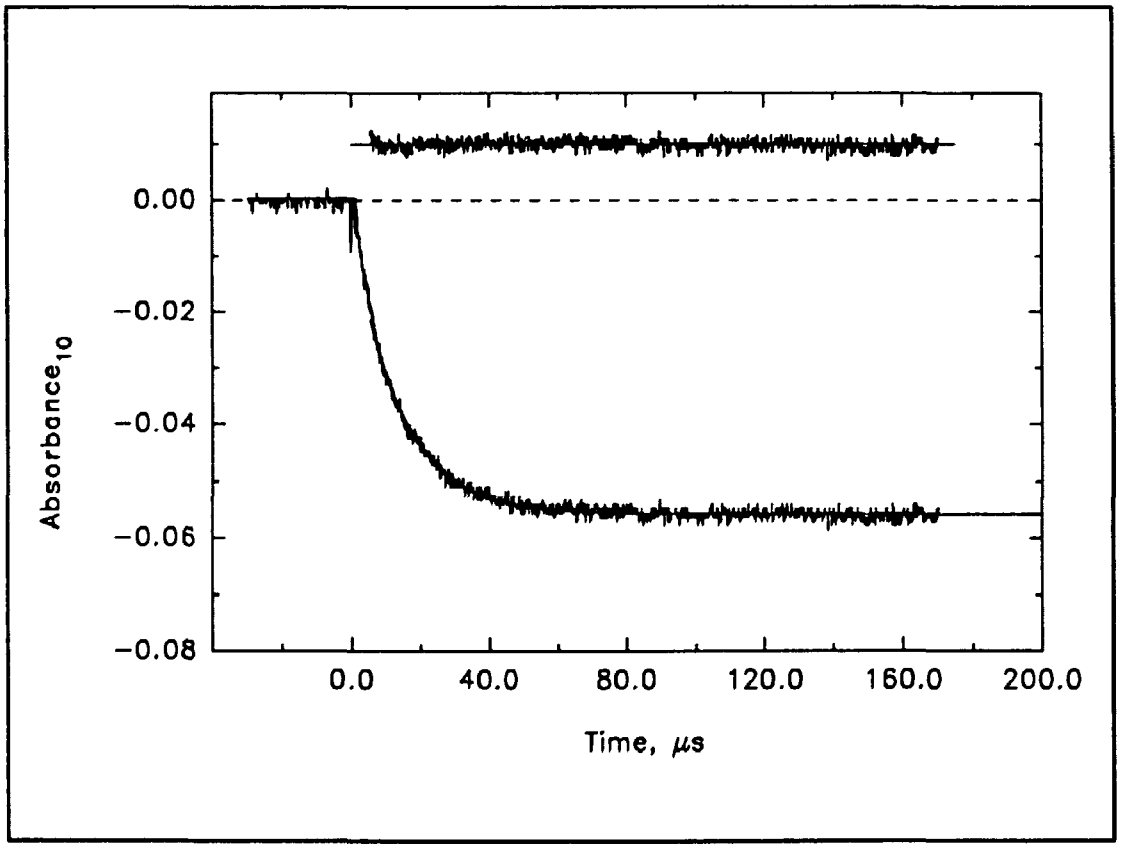

Figure 18. *Transient absorption at 400 nm following radiolysis of 0.5 mbar NO_2, 10 mbar O_2, 50 mbar CF_3CFClH, and 940 mbar SF_6. The solid line is a fit to the data. The upper part of the figure show the residual from the fit.*

4.5 The Reaction of Halogenated Peroxy Radicals with NO_2

The reactions of CF_3CFClO_2 and $CF_3CH_2O_2$ with NO_2 have been studied as part of this work. The reaction rates have been determined by the rate of disappearance of NO_2 at 400 nm. In Figure 18, the absorption transient observed at 400 nm following pulse radiolysis of 0.5 mbar NO_2, 50 mbar CF_3CFClO_2, 10 mbar of O_2, and 940 mbar of SF_6 is shown. The decay rate of the absorption increases with $[NO_2]$. NO_2 is known to absorb at 400 nm. It seems reasonable to explain the transient in Figure 18 by a loss in NO_2.

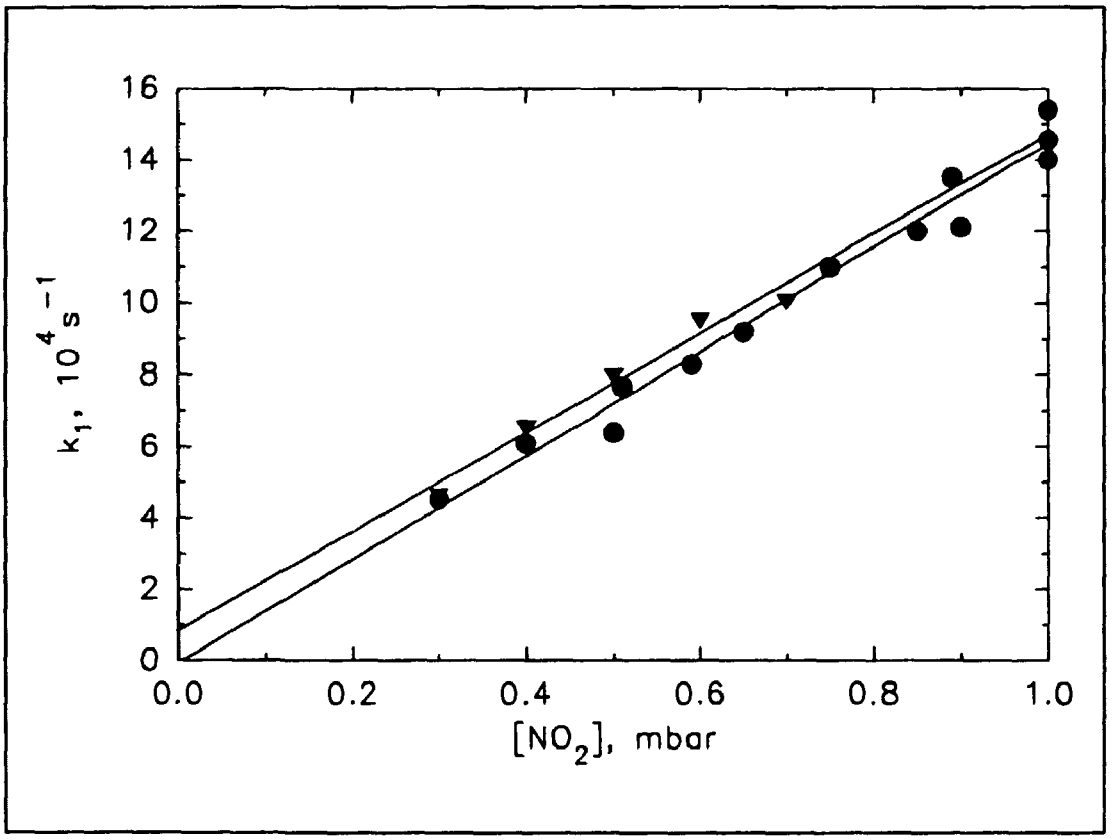

Figure 19. *First order decay rate constants obtained by fitting the NO_2 decay observed at 400 nm following radiolysis of mixtures of NO_2, O_2, SF_6, and CF_3CFClH (filled circles) or CF_3CH_3 (triangles).*

Three reactions could be responsible for the loss of NO_2:

$$F + NO_2 + M \rightarrow FNO_2/FONO + M \quad (49)$$

$$R + NO_2 + M \rightarrow \text{products} \quad (50)$$

$$RO_2 + NO_2 + M \rightarrow RO_2NO_2 + M \quad (46)$$

The first two reactions have been avoided by using only the kinetics from 4 μs to derive the rate constant of reaction (46). The formation of CF_3CFClO_2 and $CF_3CH_2O_2$ is 94% completed at 4 μs after the electron pulse. This makes the influence from reaction (49) and (50) negligible. In Figure 19, first order rate constants obtained by fitting a first order decay expression to the NO_2 decays are plotted as a function of $[NO_2]$. A linear regression analysis of the data in Figure 19 gives rate constants of the reactions of CF_3CFClO_2 and $CF_3CH_2O_2$ with NO_2 of $(5.9\pm0.5)\times10^{-12}$ $cm^3molecule^{-1}s^{-1}$ and $(5.6\pm1.1)\times10^{-12}$ $cm^3molecule^{-1}s^{-1}$, respectively. References [8,9] have reviewed the known rate constants of peroxy radicals with NO_2 and found that the rates are pressure dependent and that $k_\infty=6\text{-}8\times10^{-12}$ cm^3 $molecule^{-1}$ s^{-1} for halogenated peroxy radicals. It is expected that the RO_2+NO_2 rate constants are close to the high pressure limit at 1 bar SF_6. Hence the derived values of $(5.9\pm0.5)\times10^{-12}$ $cm^3molecule^{-1}s^{-1}$ and $(5.6\pm1.1)\times10^{-12}$ $cm^3molecule^{-1}$ s^{-1} are close to the rate constants of the reactions of other halogenated peroxy radicals with NO_2.

5 Product Studies of Halogenated Compounds

5.1 FTIR Relative Rate Method

The relative rate technique was used to determine the reactivity of fluorine atoms towards CH_3F, CH_3Cl, CH_3Br, CF_2H_2, CF_3H, CF_3CH_2F (HFC-134a), $CFCl_2CH_3$ (HCFC-141b), CF_2ClCH_3 (HCFC-142b), CHF_2CH_3 (HFC-152a), and CF_3CF_2H (HFC-125) relative to methane. In addition, the rate constant for the reaction of F atoms with CFH_2CFH_2 and CF_3CH_3 were determined relative to those of the reactions of F atoms with CH_4, CH_3F, CH_2F_2, and CF_3CFH_2, respectivly.

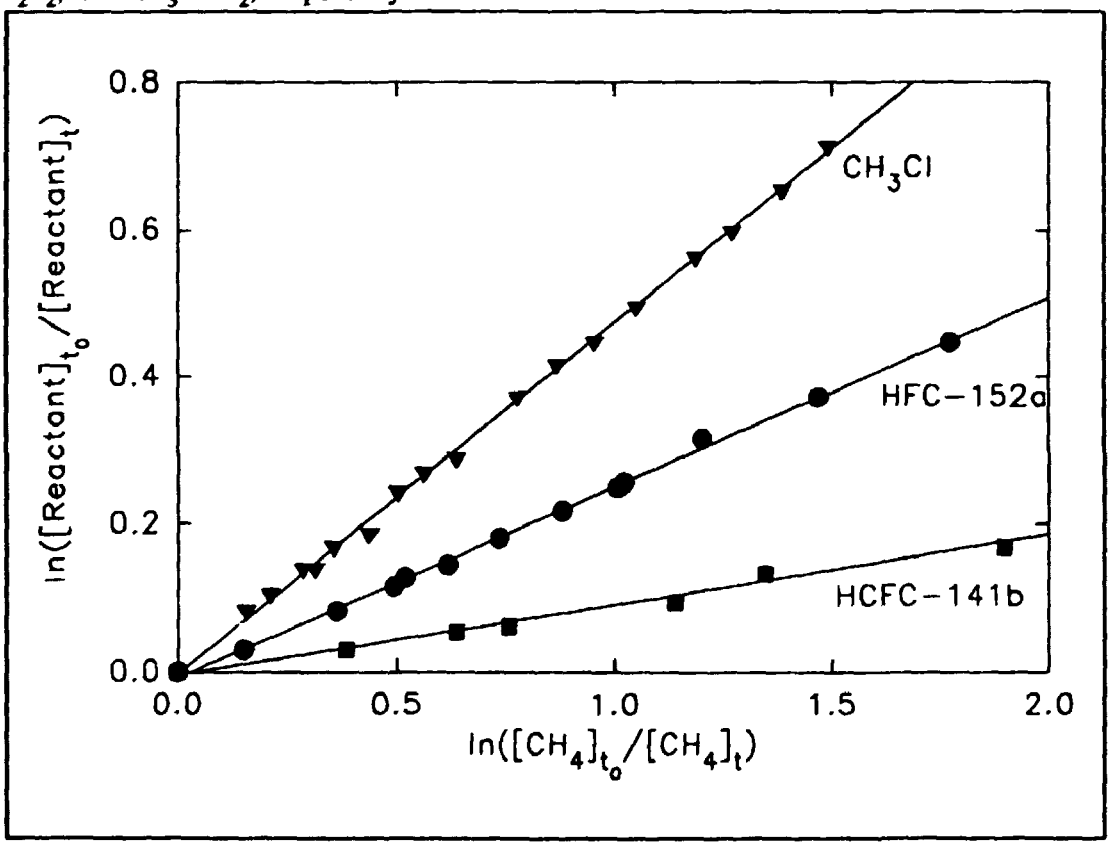

Figure 20. *Plot of $ln([Reactant]_{t0}/[Reactant]_t)$ versus $ln([CH_4]_{t0}/[CH_4]_t)$ for CH_3Cl, HFC-152b, and HCFC-142b. Solid lines are first order fits to the data.*

Photolysis of molecular fluorine were used to generate fluorine atoms. Reaction mixtures consisting of the reactant and reference organics and fluorine (5% in He) diluted in

nitrogen were admitted to the reaction chamber. In the presence of atomic fluorine the reactant and reference decay via reactions (51) and (52):

$$F + \text{reactant organic} \rightarrow \text{products} \quad (51)$$

$$F + \text{reference organic} \rightarrow \text{products} \quad (52)$$

Provided that the reactant and reference are lost solely by reactions (51) and (52) and that neither is reformed in any process, it can be shown that

$$\ln\left\{\frac{[reactant\ organic]_t}{[reactant\ organic]_{t_0}}\right\} = \frac{k_{51}}{k_{52}} \ln\left\{\frac{[reference\ organic]_t}{[reference\ organic]_{t_0}}\right\}$$

where [reactant organic]$_{t_0}$ and [reference organic]$_{t_0}$, and [reactant organic]$_t$, [reference organic]$_t$ are the concentrations of the reactant and reference organics at times t_0 and t respectively, and k_{51} and k_{52} are the rate constants of reactions (51) and (52).

With one exception, all experiments were performed in the presence of 700 Torr total pressure of ultra pure Nitrogen diluent. In the study of the relative reactivity of HFC-125 versus HFC-134a ultra pure synthetic air was used as bath gas. All experiments were conducted in 295±2 K.

Figure 20 shows typical plots of ln([reactant]$_{t_0}$/[reactant]$_t$) versus ln([reference]$_{t_0}$/[reference]$_t$) for selected experiments. These plots are linear going through the origin suggesting the absence of complications due to secondary chemistry. For each reactant organic studied, at least two separate gas mixtures with different initial conditions of the organics were prepared and irradiated to assess the experimental reproducibility and to check for unwanted secondary reactions; in all cases indistinguishable results were obtained from successive experiments. Rate constant ratios, k_{51}/k_{52}, obtained from linear least squares analysis of the data shown in Figure 20, and analogous plots, are given in Table VIII, (quoted errors represent 2σ).

For the determination of k(F+HFC-125)/k(F+HFC-134a) we must consider the formation of HFC-125 from the reaction of HFC-134a by following reactions:

$$F + CF_3CFH_2(\text{HFC-134a}) \rightarrow CF_3CFH + HF \quad (53)$$

$$CF_3CFH + F_2 \rightarrow CF_3CF_2H(\text{HFC-125}) + F \quad (54)$$

Table VIII: Rate constant ratios, k_{51}/k_{52}, measured during the present work.

Reactant	Reference				
	CH_4	CD_4	CH_2F_2	CF_3CF_2H	CF_3H
CD_4	(0.69±0.02)[b]				
CH_3F		(0.79±0.03)			
CH_3Cl	(0.48±0.02)	(0.72±0.03)	(7.7±0.4)		
CH_3Br	(0.44±0.03)				
CF_3CF_2H (HFC-125)					(2.6±0.1)
HFC-134a			(0.30±0.02)	(3.1±0.5)[c]	(8.7±0.8)
HFC-134					(6.9±0.4)
HFC-152a	(0.25±0.02)				
HCFC-142b	(0.057±0.006)			(10.9±1.0)	

a: Quoted errors are 2σ.

b: Taken from Wallington and Hurley [80].

c: measured with air as bath gas

Table IX: Reactivities relative to methane.

Reactant	k(F+Reactant)/k(F+CH_4)
CH_4	1
CD_4	0.69±0.02
CH_3F	0.54±0.03
CH_3Cl	0.48±0.02
CH_3Br	0.44±0.03
HFC-152a	0.25±0.01
CF_2H_2	0.063±0.004
HCFC-142b	0.057±0.006
HFC-134a	0.019±0.002
HFC-134	0.014±0.002
HFC-125	0.0052±0.0007
CF_3H	0.0020±0.0003

In these experiments, air was used as the diluent gas. The 160 Torr partial pressure of oxygen in 700 torr of air provides an efficient scavenging mechanism for CF_3CFH radicals, thereby precluding any significant formation of HFC-125 via reaction (54).

In Table VIII a large body of relative rate data for the reaction of F atoms with halogenated organics is presented. To place these data on an absolute scale we need to choose one or more reference whose reactivity towards F atoms has been established using absolute techniques. In the present work our choices are CH_4, CH_3Cl, CH_3Br, HFC-141b or CO. Of these possible references, CH_4 has been studied the most extensively. Thus, at the present time, CH_4 is the most appropriate choice of reference compound. With CH_4 defined as the primary reference I need to relate the reactivity of each of the compounds studied to methane. The method used to achieve this is as follows. First, where CH_4 has been used directly as a reference in our relative rate experiments I used our directly measured ratios. For compounds which were not measured directly against methane I have multiplied those rate constant ratios which involved the smallest number of steps to relate the reactivity of the compound to that of methane. To relate the reactivity of HFC-134a to that of methane there are two different paths, both involve three steps. I choose the path with the lowest associated statistical uncertainty (via CH_3Cl and CF_2H_2).

Table X: Rate constants (F+X) from the present work together with the previous literature data.

Reactant	k(295±2)	Reference
CH_3F	$(2.7\pm0.2)\times10^{-11}$	Manocha et al.[81]
	$(3.7\pm0.8)\times10^{-11}$	This work
CH_3Cl	$(3.1\pm0.9)\times10^{-11}$	Clyne et al.[91]
	$(2.4\pm0.5)\times10^{-11}$	Wickramaaratchi et al.[82]
	$(3.3\pm0.7)\times10^{-11}$	This work
CH_3Br	$(6.1\pm0.7)\times10^{-11}$	Iyer and Rowland [83]
	$(4.5\pm0.9)\times10^{-11}$	Nielsen et al.[84]
	$(3.0\pm0.7)\times10^{-11}$	This work
HFC-152a	$(1.7\pm0.4)\times10^{-11}$	This work
CF_2H_2	$(4.0\pm1.6)\times10^{-12}$	Manocha et al.[81]
	$(5.7\pm0.3)\times10^{-12}$	Clyne et al.[85]
	$(1.0\pm0.4)\times10^{-11}$	Nielsen et al.[86]
	$(4.3\pm0.9)\times10^{-12}$	This work
HCFC-142b	$(3.9\pm0.9)\times10^{-12}$	This work(pulse radiolysis)
HCFC-123	$(1.3\pm0.7)\times10^{-12}$	This work
HFC-134a	$(2.1\pm0.7)\times10^{-12}$	Wallington et al.[75]
	$(1.4\pm0.1)\times10^{-12}$	This work[a]
	$(1.3\pm0.3)\times10^{-12}$	This work
HFC-134	$(1.0\pm0.3)\times10^{-12}$	This work
CO	$(1.2\pm0.6)\times10^{-12}$	Baulch et al.[87][b]
	$(5.0\pm1.0)\times10^{-13}$	This work[a]
HCFC-124	$(8\pm2)\times10^{-13}$	This work
HFC-125	$(2.6\pm0.7)\times10^{-13}$	This work(pulse radiolysis)
	$(3.5\pm0.9)\times10^{-13}$	This work
CF_3H	$(1.2\pm0.2)\times10^{-13}$	Maricq and Szente[88]
	$(0.9\pm0.3)\times10^{-13}$	This work(pulse radiolysis)
	$(1.4\pm0.4)\times10^{-13}$	This work
HFC-143a	$(2.0\pm0.5)\times10^{-12}$	This work
HFC-152	$(3.8\pm1.1)\times10^{-11}$	This work

a: Laser flash photolysis (see [Appendix 7.11.3 pp205])

b: Helium diluent.

The reactivities relative to methane towards F atoms of the compounds studied in this work apart from CH_2FCH_2F and CF_3CH_3 are given in Table IX. Quoted errors in Table VIII and IX are 2σ from statistical analyses of our data. Errors in Table IX are either taken directly from Table VIII, or if the reactivity was calculated from two or more measured relative rates, the errors are calculated using conventional error propagation analysis.

As seen from Table VIII, for the majority of compounds investigated, two or more relative rates were measured in the present work. In all cases the measured rate constant ratios are consistent. For example, the reactivity of HFC-125 can be found relative to that of methane using either, (i) HCFC-142b, (ii) HFC-134a, CF_2H_2, and CH_3Cl or (iii) CF_3H, HCFC-134a, CF_2H_2, and CH_3Cl as intermediate steps. These data sets allow us to establish $k(F+HFC\text{-}125)/k(F+CH_4)$ = 0.0052±0.0007, 0.0061±0.0010, and 0.0057±0.0008 respectively. It is gratifying to note that these values are consistent.

To place our relative rate data in Table IX on a absolute scale we need to adapt a value for the rate constant of reaction (19).

$$F + CH_4 \rightarrow CH_3 + HF \qquad (19)$$

There have been six determinations of k_{19}; 7.9 [89], 7.15 [90], 6.0±6.0 [91], 5.7±0.3 [92], 6.64 [93], and 6.6±0.6 [94] (in units of 10^{-11} cm^3 $molecule^{-1}$ s^{-1}). With the exception of the result from reference 91 there is no obvious reason to prefer any of these studies. Thus, I have chosen to place our relative rate data on an absolute basis by using an average of the above studies (reference 91 excluded) of $k_{19} = (6.8\pm1.4)\times10^{-11}$ cm^3 $molecule^{-1}$ s^{-1}. The absolute rate constants are given in Table X. The combined uncertainty of k_{19} and the uncertainty quoted in Table IX is given in Table X. In addition to the results mentioned in Table VIII and IX, the rate constants for the reactions of F atoms with CH_2FCH_2F and CF_3CH_3 are listed in Table X. These two rates have been studied relative to those CH_4 and CH_3F, and CH_2F_2 and CF_3CFH_2, respectively. The two rate constants were put on an absolute scale using the rate constants in Table X for the reactions of F atoms with CH_4, CH_3F, CH_2F_2, and CF_3CFH_2. The derived values for the reactions of F atoms with CH_2FCH_2F and CF_3CH_3 are shown in Table X.

In Table X the obtained rate constants are compared with previous studies. Within the uncertainties, our measured rate constants are generally consistent with the literature values where they exist. There is one exception; CH_3Br. Our measured reactivity of CH_3Br is 33% less than a previous determination by Nielsen et al. [84] and 51% less than

the rate constant obtained by Iyer and Rowland [83]. The reason for the discrepancy is unknown.

5.2 Product Studies using FTIR

To provide insight into the mechanism of the self reaction of haloalkyl peroxy radicals RO_2, and the fate of the subsequent formed alkoxy radical, product studies were performed. The photolysis of mixtures of molecular chlorine or fluorine in the presence of RH/O_2 mixtures were used to generate the RO_2 radicals:

$$Cl_2(F_2) + h\nu \rightarrow 2Cl(2F) \quad (55)$$
$$RH + Cl(F) \rightarrow R + HCl(HF) \quad (29)$$
$$R + O_2 + M \rightarrow RO_2 + M \quad (2)$$
$$RO_2 + RO_2 \rightarrow 2RO + O_2/\text{products} \quad (37)$$
$$RO + M/O_2 \rightarrow \text{products} \quad (56)$$

The products of reaction (37) and (56) were studied as a function of the loss of RH for CF_3H, CF_3CF_2H, CF_2HCF_2H, CF_3CH_3, and CH_2FCH_2F. In addition the products of the reaction of CFH_2O_2 with HO_2 were studied.

The self reactions of the halo alkyl peroxy radicals proceed through three reaction channels:

$$RO_2 + RO_2 \rightarrow 2RO + O_2 \quad (37a)$$
$$RO_2 + RO_2 \rightarrow ROOR + O_2 \quad (37b)$$
$$RCHXO_2 + RCHXO_2 \rightarrow RCXO + RCXHOH + O_2 \quad (37c)$$

Generally, reaction channel (b) is only a minor channel [8,9]. The five HFCs studied as a part of this work give 100% alkoxy radical yield within the experimental uncertainty as discussed below.

The alkoxy radicals formed by reaction (37a) have three different reactions pathways: (i) reaction with O_2 to give an aldehyde and a HO_2 radical. This demands that the peroxy radical have an α-H atom. (ii) decomposition via C-C bond cleavage (the alkoxy radical cannot be a methoxy derivate) (iii) ejection of Cl atom; this demands that the alkoxy have an α-Cl atom. As discussed in chapter 1, alkoxy radicals have a few other reactions pathways. These reaction pathways will not be discussed further here.

The product studies of the five different HFC are discussed individually below. Pressures are measured in Torr and are therefore given in this unit below (760 Torr=760,000 mTorr=1013 mbar).

The product yields referred to below are of two kinds: (i) the molar yields of the carbon bearing products in terms of molar loss of the parent compound. (ii) the total carbon balance where the number of carbon atoms in the product are taken into account.

5.2.1 CF_3O_2

To study the products of the CF_3O_2 self reaction and the fate of the alkoxy radical CF_3O, irradiation of mixtures of CF_3H, F_2, and O_2 in N_2 up to 700 Torr were used. The yield of CF_3OOOCF_3 expressed as moles of CF_3OOOCF_3 produced per mole of CF_3H consumed were shown to be 50±3%. Variation of $[O_2]$ between 1 and 150 Torr had no discernable effect on the yield of CF_3OOOCF_3. In terms of carbon balance, the observed CF_3OOOCF_3 accounts for 100±6% of the loss of CF_3H. In addition to CF_3OOOCF_3, small amounts of FC(O)F, HC(O)F, and SiF_4 products were observed following the irradiation of $CF_3H/O_2/F_2$ mixtures. The yields of FC(O)F and HC(O)F were 5-10% of the observed loss of CF_3H.

Following the subtraction of feature attributable to the trioxide there were no residual IR features that could be assigned to the peroxide CF_3OOCF_3, by comparison with the literature spectrum of Arvía and Aymonino [95] we estimate an upper limit of 10% for the yield (in molar terms) of CF_3OOCF_3.

In view of the low reactivity of F atoms towards CF_3H care must be taken to assure that the products observed are from the self reaction of CF_3O_2 radicals and not from other reactions. To test for such complications, experiments were performed in which mixtures of F_2 were irradiated in air (without added CF_3H). Following the irradiation of F_2/air mixtures three products were observed; FC(O)F, HC(O)F and SiF_4. For a given irradiation time, the yields of FC(O)F and SiF_4 were indistinguishable from those measured in the presence of CF_3H. Hence, these products are formed by reactions in our chamber that do not originate from the formation of CF_3O_2 radicals. Silicon tetrafluoride is presumably formed as a result of HF or F atom attack on the Pyrex cell. Likely secondary reactions responsible for the formation of FC(O)F include reaction of F atoms with trace impurities in the diluent, or heterogeneous reactions of F atoms with organic compounds on the chamber walls.

The formation of HC(O)F following irradiation of F_2 mixtures in air was approximately a factor of 4 less than that observed when CF_3H was present in the

chamber. The most probable explanation for this HC(O)F product observed upon irradiation of $CF_3H/F_2/O_2$ mixtures is existence of small amounts of reactive impurities in the CF_3H sample. Infrared analysis of the CF_3H sample revealed no detectable impurities (<1%), nevertheless, in light of the low reactivity of F atoms towards CF_3H the presence of trace impurities may explain all or part of the observed HC(O)F yield.

The self reaction of CF_3O_2 radicals can proceed via two possible channels;

$$CF_3O_2 + CF_3O_2 \rightarrow CF_3O + CF_3O + O_2 \quad (57a)$$

$$CF_3O_2 + CF_3O_2 \rightarrow CF_3OOCF_3 + O_2 \quad (57b)$$

The absence of any IR product features attributable to the peroxide CF_3OOCF_3 shows that (57b) is not an important reaction channel. The absence of the peroxide together with essentially 100% yield (in terms of carbon) of the trioxide, shows that the self reaction of CF_3O radicals (reaction (40)) does not compete effectively with reaction (39) for CF_3O radicals:

$$CF_3O + CF_3O_2 + M \rightarrow CF_3OOOCF_3 + M \quad (39)$$

$$CF_3O + CF_3O + M \rightarrow CF_3OOCF_3 + M \quad (40)$$

The fact that the CF_3OOOCF_3 product accounts for essentially all the CF_3O_2 radicals formed in the FTIR reactor has interesting ramifications for the kinetic data obtained in the study of the self reaction of the CF_3O_2 radical using the pulse radiolysis system. Each CF_3O radical that reacts via reaction (39) consumes a CF_3O_2 radical. In the kinetic experiments the decay of CF_3O_2 is used to derive the rate constant for reaction (57). Hence, the observed rate constant for reaction (57) must be an overestimate of the true rate constant. To examine this possibility, the chemistry was modeled using the Acuchem program [96using a chemical mechanism consisting of reactions (57), (2), (29), (40) and (39), using; literature rate data (in units of cm^3 $molecule^{-1}$ sec^{-1}) $k_{29}=1.2\times10^{-13}$ (Table X); $k_2=8.5\times10^{-12}$, [5]; $k_{57a}=1.8\times10^{-12}$, [assumed to be $k_{obs}/2$]; $k_{40}=1.4\times10^{-11}$ [average of values from references 97 and 98]. To the best of my knowledge there is no available kinetic data for reaction (39). It seems reasonable to assume that the kinetics of reactions (40) and (39) are similar. Initially, we used $k_{40}=k_{39}=1.4\times10^{-11}$ cm^3 $molecule^{-1}$ s^{-1}. Use of the above data predicts yields, in terms of carbon, of 84% and 16% for CF_3OOOCF_3 and CF_3OOCF_3 respectively; inconsistent with our experimental observations.

There is considerable uncertainty in k_{40}, the value used initially is the average of the values derived by Kennedy and Levy [97] ($k_{40}=6.6\times10^{-12}$ cm^3 $molecule^{-1}$ s^{-1}) and Batt

and Walsh [98] (k_{40}=2.1x10^{-11} cm^3 molecule^{-1} s^{-1}). Assuming that k_{40} and k_{39} are equal, our measured upper limit of 10% for the peroxide yield requires that k_{40}>2.5x10^{-11} cm^3 molecule^{-1} sec^{-1}. Hence our measured product yields are more consistent with the kinetic data of Batt and Walsh.

The chemical mechanism described above, (with k_{40}=k_{39}=2.5x10^{-11} cm^{3}molecule^{-1} s^{-1}) can be used to relate the rate constant for reaction (57) measured in the pulse radiolysis experiments, k_{57obs}, to the "true" bimolecular rate constant. Simulations of the decay of CF_3O_2 radicals for the experimental conditions in the pulse radiolysis experiments were performed using a simple mechanism consisting of reaction (57) with, and without, reactions (40) and (39). The CF_3O_2 decay profiles were then fit to a second order decay to return values of k_{57} and k_{57obs}. The simulated CF_3O_2 decays were well fit by second order kinetics. Inclusion of reactions (40) and (39) with k_{40}=k_{39}=2.5x10^{-11} cm^{3}molecule^{-1}s^{-1} leads to k_{57obs} values 80% larger than k_{57}. As discussed above, the upper limit for the CF_3OOCF_3 yield measured in the present work places a lower limit of 2.5x10^{-11} cm^{3}molecule^{-1}s^{-1} for k_{39}. Use of an increased rate constant for reaction (39) increases the ratio k_{57obs}/k_{57}. I chose to apply a correction factor of 1/2 to our measured value of k_{57obs} to derive k_{57}=(1.8±0.4)x10^{-12} molecule^{-1} s^{-1}.

5.2.2 $CF_3CF_2O_2$

To provide insight into the mechanism of the self reaction of $CF_3CF_2O_2$ radicals and the fate of the alkoxy radical CF_3CF_2O, a product study was performed. The photolysis of molecular chlorine in CF_3CF_2H/Cl_2/air mixtures was used to generate $CF_3CF_2O_2$ radicals.

$$Cl_2 + h\nu \rightarrow 2Cl \quad (55)$$

$$CF_3CF_2H + Cl \rightarrow CF_3CF_2 + HCl \quad (58)$$

$$CF_3CF_2 \cdot O_2 + M \rightarrow CF_3CF_2O_2 + M \quad (59)$$

$$CF_3CF_2O_2 + CF_3CF_2O_2 \rightarrow \text{products} \quad (60)$$

Four experiments were performed. The experimental conditions and results are given in Table XI. All experiments were performed at 700 Torr total pressure of air diluent at 295K.

The observed yields of COF_2, $CF_3O_3CF_3$ and $CF_3O_3C_2F_5$ following successive irradiations of a mixture of 101 mTorr of CF_3CF_2H and 897 mTorr of Cl_2 in 700 Torr of air (experiment #2) are given in Table XI. The molar yields of COF_2, $CF_3O_3CF_3$ and $CF_3O_3C_2F_5$ were independent of HFC-125 consumption over the range 3-73%. Linear

least squares analysis of the yields of COF_2, $CF_3O_3CF_3$ and $CF_3O_3C_2F_5$ as a function of the loss of CF_3CF_2H are linear and gives the following molar yields; COF_2, 86±4%; $CF_3O_3CF_3$, 16±2%; and $CF_3O_3C_2F_5$, 13±2%. Errors are 2 standard deviations. The peroxide $CF_3O_2CF_3$ was tentatively identified as a product in this system. Identification and quantification of $CF_3O_2CF_3$ is complicated by the presence of overlapping absorption features due to $CF_3O_3C_2F_5$, nevertheless, based upon the feature at 1285 cm^{-1}, an estimate of 15±5% for the yield of $CF_3O_2CF_3$ can be made. Within the experimental uncertainty, the observed yields of COF_2, $CF_3O_3CF_3$ and $CF_3O_3C_2F_5$, together with our estimate for the yield of $CF_3O_2CF_3$, account for 100% of the HFC-125 loss.

For experiment #1 a mixture of 11.8 mTorr of HFC-125 with 891 mTorr of Cl_2 was irradiated. The COF_2 yield in this experiment was 100%. A significant amount of $CF_3O_3CF_3$ was formed (20%) together with a trace amount of $CF_3O_3C_2F_5$ (5%). As in experiment #2, $CF_3O_2CF_3$ was tentatively observed by virtue of its absorption at 1285 cm^{-1} with a yield estimated as approximately 10±5%.

For experiment #3 a mixture of 567 mTorr of HFC-125 and 576 mTorr of Cl_2 in air was used. This mixture was irradiated for 10 minutes and then an additional 10 minutes with the results listed in Table XI. Four products were observed; COF_2, $CF_3O_3CF_3$, $CF_3O_3C_2F_5$, and CF_3OH. CF_3OH was identified by virtue of its absorption feature at 3664 cm^{-1} and quantified using $\sigma_{3664\ cm-1}(CF_3OH) = 9.0 \times 10^{-19}$ cm^2 $molecule^{-1}$ [Appendix 7.5 pp151]. The spectral region 1150-1300 cm^{-1} was optically black thereby precluding any estimation of the $CF_3O_2CF_3$ yield in this experiment. However, it is worth noting that the combined yields of COF_2, $CF_3O_3CF_3$, $CF_3O_3C_2F_5$, and CF_3OH, account for 91 and 94% of the loss of HFC-125 in the two irradiations. Hence, the yield of $CF_3O_2CF_3$ in experiment #3 was <9% and <6% in the two irradiations.

Immediately following the second 10 minutes irradiation, the reaction mixture from experiment #3 was allowed to stand in the dark for 5 minutes. On standing in the dark the CF_3OH disappeared (less than 0.4 mTorr remained) and an equivalent amount of COF_2 was formed. On standing for an additional 30 minutes there was no further change in the IR spectra. The loss of CF_3OH is ascribed to heterogeneous decomposition on the reaction chamber walls.

For experiment #4, a mixture comprising of 938 mTorr of HFC-125 and 747 mTorr of Cl_2 was prepared in the chamber and irradiated for 10 minutes. Results are given in Table XI. As in experiment #3, four products were observed; COF_2, $CF_3O_3CF_3$, $CF_3O_3C_2F_5$, and CF_3OH. The combined yield of these species accounts for 102% of the HFC-125 loss.

Table XI: Observed product yields[a,b] following the irradiation of CF_3CF_2H/Cl_2 mixtures in 700 Torr of air.

Expt.	$[HFC\text{-}125]_o$	$[Cl_2]_o$	t_{UV}(min)	Δ[HFC-125]	Δ[COF_2]	Δ[$CF_3O_3CF_3$]	Δ[$CF_3O_3C_2F_5$]	Δ[CF_3OH]
1	11.8	891	5	1.4	1.4 (100%)	0.27 (19%)	0.07 (5%)	n.d.
			10	2.48	2.49 (100%)	0.51 (20%)	0.14 (6%)	n.d.
2	101	897	2	3.0	2.6	0.4	0.4	n.d.
			7	11.1	8.6	1.6	1.4	n.d.
			14	20.2	15.9	3.39	2.9	n.d.
			20	28.3	22.0	4.84	3.9	n.d.
			30	40.4	33.9	6.8	0.5	n.d.
			40	50.5	44.6	9.2	8.0	n.d.
			50	60.1	50.8	10.2	8.2	n.d.
			60	67.7	57.2	10.6	8.9	n.d.
			70	73.8	63.3	11.1	9.3	n.d.
					(84±6%)	(16±2%)	(13±2%)	
3	567	576	10	56.7	41.9	8.7	14.3	0.8
					(74%)[b]	(15%)	(25%)	(1.4%)
			20	102	83.6	14.5	26.6	0.8
					(81%)	(14%)	(26%)	(0.8%)
4	938	747	10	75.0	47.5	12.1	25.0	2.4
					(63%)	(16%)	(34%)	(3.2%)

a: observed concentrations in units of mTorr, no corrections of any kind applied to data.

b: values in parentheses are molar yields.

n.d.: not detected, i.e. below 0.4 mTorr.

The self reaction of $CF_3CF_2O_2$ radicals can proceed via two channels:

$$CF_3CF_2O_2 + CF_3CF_2O_2 \rightarrow CF_3CF_2O + CF_3CF_2O + O_2 \quad (60a)$$
$$\rightarrow CF_3CF_2O_2CF_2CF_3 + O_2 \quad (60b)$$

The observation of 100% yield of COF_2 in experiment #1 together with the fact that in experiment #4 100% of the loss of HFC-125 can be accounted for as products other than the peroxide formed in reaction (60b), shows that (60b) is not a significant channel of reaction (60).

CF_3CF_2O radicals formed in reaction (60a) are expected to either decompose or, possibly, react with CF_3O_2 radicals to form the mixed trioxide $CF_3O_3C_2F_5$.

$$CF_3CF_2O + M \rightarrow CF_3 + COF_2 + M \quad (61)$$
$$CF_3CF_2O + CF_3O_2 + M \rightarrow CF_3O_3C_2F_5 + M \quad (62)$$

The relative importance of reactions (61) and (62) depends upon the lifetime of CF_3CF_2O radicals. The lifetime of CF_3CF_2O must be less than 15 μs due to the more than 100% NO_2 yield observed following the reaction of $CF_3CF_2O_2$ with NO (see previous chapter) and considering the substantial yields of COF_2 observed in the present work it seems reasonable to conclude that decomposition (reaction (61)) will be the sole loss of CF_3CF_2O radicals in the chamber. Decomposition gives COF_2 and a CF_3 radical which rapidly adds O_2 to give CF_3O_2. The self reaction of CF_3O_2 radicals is known to produce CF_3O radicals [Appendix 7.11.1 pp205]. It seems likely that CF_3O_2 radicals also react with $CF_3CF_2O_2$ radicals to give alkoxy radical products.

$$CF_3 + O_2 + M \rightarrow CF_3O_2 + M \quad (63)$$
$$CF_3O_2 + CF_3O_2 \rightarrow CF_3O + CF_3O + O_2 \quad (57)$$
$$CF_3O_2 + CF_3CF_2O_2 \rightarrow CF_3O + CF_3CF_2O + O_2 \quad (64)$$

The observation of $CF_3O_3CF_3$, $CF_3O_3C_2F_5$, CF_3OH and $CF_3O_2CF_3$ products show that CF_3O radicals in the chamber have four possible fates: (i) reaction with CF_3O_2 radicals to give $CF_3O_3CF_3$, (ii) reaction with $C_2F_5O_2$ radicals to give $CF_3O_3C_2F_5$, (iii) self reaction to give $CF_3O_2CF_3$, and (iv) reaction with a hydrogen containing species to give CF_3OH. Hydrogen containing species in the chamber include HFC-125, HCl, impurities in the reaction mixtures, or compounds on the chamber walls. From Table XI it can be seen that the yield of CF_3OH following a 10 minute irradiation in experiment #4 was

approximately a factor of 2 larger than after the same period of irradiation in experiment #3. The most significant difference between these experiments is the use of a larger amount of HFC-125 in experiment #4 which suggests that reaction of CF_3O radicals with either HFC-125, or impurities present in the HFC-125 sample, is responsible for the CF_3OH formation. The sample of HFC-125 was supplied at a stated purity >98% and there were no impurities observable in our infrared spectra. In light of the relatively slow reaction of Cl atoms with HFC-125 it seems likely that any reactive impurity present in the HFC-125 sample would be preferentially removed by Cl atom attack. Hence, it seems likely that the 3.2% yield of CF_3OH observed in experiment #4 is attributable largely, or solely, to reaction of CF_3O radicals with HFC-125:

$$CF_3O + CF_3CF_2H \rightarrow CF_3OH + CF_3CF_2 \qquad (65)$$

During the course of this study I became aware of two other experimental investigations of the Cl atom initiated oxidation of HFC-125 in air. Edney and Driscoll [99] and Tuazon and Atkinson [100] used initial concentrations of HFC-125 of 3-4 mTorr and after irradiation for 30-83 minutes observed a molar yield of COF_2 of essentially 100%. This result is in good agreement with our work. Tuazon and Atkinson also identified the trioxide $CF_3O_3CF_3$ as a product in their experiments. Edney and Driscoll report a product with IR features at 1166, 1265 and 1287 cm^{-1} which they suggest may be the peroxide $CF_3O_2CF_3$. It is interesting to note that in the spectra presented by both Edney and Driscoll and Tuazon and Atkinson there are small unassigned product features which appear at approximately 1080 cm^{-1}. These features may indicate the presence of a small yield of the mixed trioxide $CF_3O_3C_2F_5$, as observed in the present work.

5.2.3 $CF_2HCF_2O_2$

The photolysis of molecular chlorine in CHF_2CHF_2/Cl_2/air mixtures was used to generate $CHF_2CF_2O_2$ radicals. Two sets of experiments were performed to study the products resulting from reaction the self reaction of the $CF_2HCF_2O_2$ radical using either low (21-44 mTorr) or high (8-9 Torr) initial concentrations of HFC-134. Both sets of experiments were performed at 700 Torr total pressure of air diluent at 295 K.

Following the irradiation of mixtures with low initial CHF_2CHF_2 concentrations only one carbon-containing product was observed; COF_2. The molar yield of COF_2 in

terms of loss of CHF_2CHF_2 is (197±3)%. The observed COF_2 product then accounts for (98±2)% of the carbon. I estimate that there may be up to 5% systematic uncertainty in the calibration of our COF_2 and HFC-134 reference spectra. Hence, we choose to add an additional 10% range to the uncertainty associated with our carbon balance, thus COF_2 accounts for (98±12)% of the products following the self reaction of $CF_2HCF_2O_2$ radicals. The fact that COF_2 accounts for all of the loss of HFC-134 does not prove that other products were not formed in our system. The relatively low reactivity of Cl atoms towards CHF_2CHF_2 raises the possibility of significant secondary chemistry which could remove primary products. For example, the hydroperoxide CHF_2CF_2OOH might be formed in the chamber but may react rapidly with Cl atoms to regenerate $CHF_2CF_2O_2$ radicals and so escape detection.

$$CHF_2CF_2O_2 + HO_2 \rightarrow CHF_2CF_2OOH + O_2 \quad (66)$$

$$CHF_2CF_2OOH + Cl \rightarrow CHF_2CF_2O_2 + HCl \quad (67)$$

To minimize the importance of such secondary reactions, for a given absolute product yield, I need to maximize the initial HFC-134 concentration used. There is a compromise however, as increased HFC-134 concentration leads to decreased IR signal. In the present work I chose to use mixtures of CHF_2CHF_2/Cl_2/air with $[CHF_2CHF_2]_o$ = 8-9 Torr. In these experiments the conversions of HFC-134 were small (0.02-0.2%) and could not be determined precisely. The yields of HCl and CF_2O were determined in these experiments. $\Delta COF_2/\Delta HCl$ were derived to 2.10±0.17. Errors are 2 standard deviations. I estimate that there may be up to 5% systematic uncertainty in the calibration of the COF_2 and HCl reference spectra. Hence, I choose to add an additional 10% uncertainty range to our measurement of $\Delta COF_2/\Delta HCl$ = 2.1±0.4. Because of the possible presence of reactive impurities in the HFC-134 sample and the possible reaction of Cl atoms with reaction products the yield of HCl represents an upper limit of the loss of HFC-134. Our measured product ratio $\Delta[COF_2]/\Delta[HCl]$ = 2.1±0.4 provides us with two pieces of information: (i) a lower limit for the molar yield of COF_2 of 170%, (ii) an upper limit of 15% for the fraction of HFC-134 which is oxidized to products other than COF_2.

The agreement between the COF_2 yields measured in experiments using low and high initial HFC-134 concentrations suggests that secondary reactions of Cl atoms with products are not a significant complicating factor in the present experiments. For every two molecules of COF_2 product observed at least one molecule of HFC-134 is consumed, $\Delta[\text{HFC-134}] \geq (\Delta[COF_2]/2)$. Our measured product ratio $\Delta[COF_2]/\Delta[HCl]$ = (2.1±0.4) then gives an upper limit of $\Delta[HCl]/\Delta[\text{HFC-134}] \leq 1.18$. Thus, secondary reactions of Cl

atoms such as reaction (15) are, at most, an 18% effect. Hence, we derive an upper limit of 18% for the combined yield of hydroperoxides and alcohols such as CHF_2CF_2OOH, CHF_2OOH, CHF_2CF_2OH, and/or CHF_2OH formed in our system but consumed in secondary reactions with Cl atoms and so not detected.

The self reaction of $CHF_2CF_2O_2$ radicals can proceed via two channels:

$$CHF_2CF_2O_2 + CHF_2CF_2O_2 (+ M) \rightarrow CHF_2CF_2O + CHF_2CF_2O + O_2 \quad (68a)$$
$$\rightarrow CHF_2CF_2O_2CF_2CHF_2 (+ M) \quad (68b)$$

Our observed yield, in terms of carbon, of (98±12)% COF_2 shows that the peroxide formed in channel (68b) is not a major product of reaction (68). CHF_2CF_2O radicals decompose to give COF_2 and a difluoromethyl radical, CHF_2 which rapidly adds O_2 to give CHF_2O_2.

$$CHF_2CF_2O + M \rightarrow CHF_2 + COF_2 + M \quad (69)$$
$$CHF_2 + O_2 + M \rightarrow CHF_2O_2 + M \quad (70)$$

Difluoromethyl peroxy radicals, once formed, can react with themselves or with $CHF_2CF_2O_2$ radicals. The cross reaction can proceed via two possible channels:

$$CHF_2O_2 + CHF_2CF_2O_2 \rightarrow CHF_2O + CHF_2CF_2O + O_2 \quad (71a)$$
$$CHF_2O_2 + CHF_2CF_2O_2 \rightarrow COF_2 + CHF_2CF_2OH + O_2 \quad (71b)$$

The approximately 100% yield of COF_2 and the lack of excess HCl, together show that reaction (71b) is not significant in our system.

The self reaction of CHF_2O_2 radicals is known to proceed largely, or solely, via one channel to give alkoxy radicals; CHF_2O [86]. CHF_2O radicals react with O_2 to give COF_2 and HO_2.

$$CHF_2O_2 + CHF_2O_2 \rightarrow CHF_2O + CHF_2O + O_2 \quad (72)$$
$$CHF_2O + O_2 \rightarrow COF_2 + HO_2 \quad (73)$$

A mechanism consisting of reactions (68a,69,70,71a,72,73) is consistent with our observed product yields. It is interesting to note that the observed product data can be rationalized with a chemical mechanism that does not include reaction of HO_2 radicals with either $CHF_2CF_2O_2$ or CHF_2O_2. By modelling the reactions in the system an upper

limit of the reactions of $CHF_2CF_2O_2$ with HO_2 of $2x10^{-12}$ cm^3 $molecule^{-1}$ s^{-1} have been determined. This is consistent with the rate constant of the reaction of HO_2 with $CF_3CFCl_2O_2$ ($k=(1.9\pm0.3)x10^{-12}$ cm^3 $molecule^{-1}$ s^{-1}), CHF_2O_2 ($k\leq1.5x10^{-12}$ cm^3 $molecule^{-1}$ s^{-1}), and CFH_2O_2 ($k=10^{-12}$ cm^3 $molecule^{-1}$ s^{-1}) [19,101,86]

5.2.4 $CF_3CH_2O_2$

Experiments were performed in which $F_2/CF_3CH_3/O_2$ mixtures at a total pressure of 700 Torr made up with N_2 diluent were irradiated in the FTIR-Smog Chamber system. The loss of CF_3CH_3 and the formation of products were monitored by FTIR spectroscopy.

Three sets of experiments were performed with O_2 partial pressures of 1, 5, and 147 Torr. In all cases CF_3CHO was the major product. Figure 21 shows a plot of the observed yield of CF_3CHO versus the loss of CF_3CH_3. For all of the experiments shown in Figure 21 $[CF_3CH_3]_0$ was 101-102 mTorr. As shown in Figure 21, the molar yield of CF_3CHO decreased with increasing consumption of CF_3CH_3. Such a trend is indicative of secondary reactions consuming the CF_3CHO product. This behavior is expected based on the fact that CF_3CHO reacts considerably more rapidly ($(2.3\pm0.4)x10^{-11}$ cm^3 $molecule^{-1}$ s^{-1} [Appendix 7.9 pp189]) with F atoms than does CF_3CH_3 ($(2.0\pm0.5)x10^{-12}$ cm^3 $molecule^{-1}$ s^{-1}, Appendix 7.11.22 pp205).

Acuchem chemical kinetic modelling program [Appendix 7.11.22 pp205] were used to calculate appropriate corrections for the data shown in Figure 21. Correction factors applied to the data ranged from 1.1 to 3.2. Corrected and uncorrected data are shown in Figure 21.

There are several points of interest regarding the data shown in Figure 21. First, within the experimental errors, the corrected data all lie on one straight line. The corrections applied range from 10% to a factor of 3.2. CF_3CHO is a major product of the F atom initiated oxidation of CF_3CH_3. Linear least squares analysis of the composite data set in Figure 21 gives a molar CF_3CHO yield of $(101\pm8)\%$ (the y-axis intercept is $-(0.7\pm0.8)$). There is no discernable effect of the O_2 partial pressure on the yield of CF_3CHO.

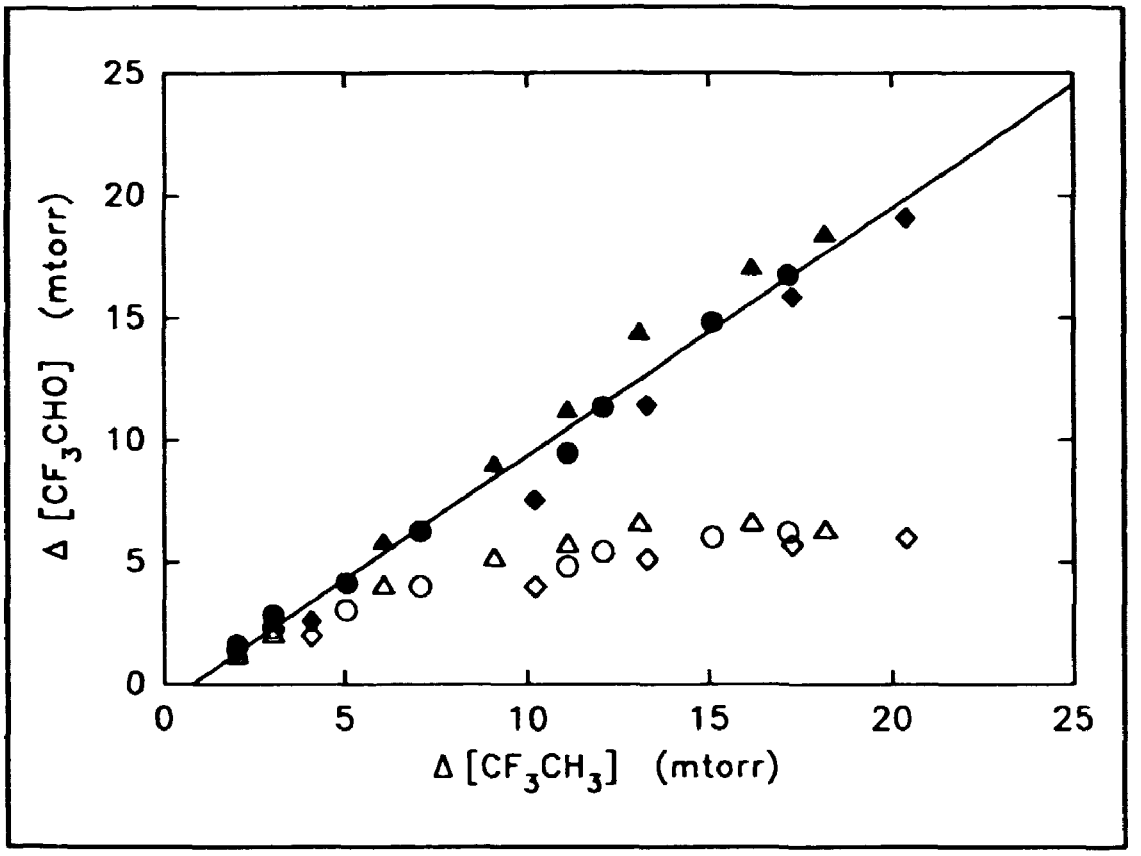

Figure 21. *The observed yield of CF_3CHO plotted as a function of the loss of CF_3CH_3 following irradiation of mixtures of 101-102 mTorr of CF_3CH_3, F_2, and 1 (diamonds), 5 (triangles), or 147 (circles) Torr O_2 at 700 Torr total pressure in N_2. Open symbols are the observed data. Filled symbols are data corrected for the reaction with CF_3CHO. See text for details.*

There are two possible sources of CF_3CHO in the present chemical system; reaction (74b) and reaction (75).

$$CF_3CH_2O_2 + CF_3CH_2O_2 \rightarrow CF_3CH_2O + CF_3CH_2O + O_2 \quad (74a)$$

$$CF_3CH_2O_2 + CF_3CH_2O_2 \rightarrow CF_3CH_2OH + CF_3CHO + O_2 \quad (74b)$$

$$CF_3CH_2O + O_2 \rightarrow CF_3CHO + HO_2 \quad (75)$$

The observation of a CF_3CHO yield which is significantly in excess of 50% suggests that reaction (75) is the major source of CF_3CHO. It is possible that channel (74b) together with reactions (76) and (77) could contribute significantly to the observed CF_3CHO yield.

$$F + CF_3CH_2OH \rightarrow CF_3CHOH + HF \quad (76)$$

$$CF_3CHOH + O_2 \rightarrow CF_3CHO + HO_2 \quad (77)$$

There was no observable CF_3CH_2OH product in experiments conducted in the presence of 147 or 5 Torr of O_2. Interestingly, CF_3CH_2OH was observed as a product in experiments using 1 Torr of O_2. At the lowest conversions of CF_3CH_3 (2%), the yield of CF_3CH_2OH was approximately 20%. With higher conversions of CF_3CH_3 the yield of CF_3CH_2OH dropped substantially. This dependence of yield on conversion of CF_3CH_3 is suggestive of loss of CF_3CH_2OH via reaction (76). To investigate this possibility a relative rate method was used to measure the rate constant ratio $k_{76}/k_{F+CH4} = (0.81\pm0.04)$. Combining this ratio with $k_{F+CH4} = 6.8\times10^{-11}$ [Appendix 7.11.3 pp205] gives $k_{76} = (5.5\pm0.3)\times10^{-11}$ cm^3 $molecule^{-1}$ s^{-1}. F atoms react approximately 30 times more rapidly with CF_3CH_2OH than with CF_3CH_3. Hence, it is not surprising that where CF_3CH_2OH is an observed product, the measured yields of this species are sensitive to the degree of conversion of CF_3CH_3 over the range used (2-20%).

The aim of the present experiments was to establish the relative importance of reactions (75) and (78) in the atmospheric chemistry of CF_3CH_2O radicals.

$$CF_3CH_2O + O_2 \rightarrow CF_3CHO + HO_2 \quad (75)$$

$$CF_3CH_2O + M \rightarrow CF_3 + HC(O)H + M \quad (78)$$

The CF_3CHO product serves as a tracer for the importance of reaction (75). However, as discussed above it is possible that CF_3CH_2OH is a significant product of reaction (74). For the experimental conditions pertaining to the data shown in Figure 21 any CF_3CH_2OH formed will rapidly react with F atoms and probably give CF_3CHO. To evaluate this potential complication, the relative importance of channels (74a) and (74b) needs to be determined. To provide such information experiments were performed in which a mixture of 1 Torr of CF_3CH_3, 0.15 Torr of F_2, in 700 Torr of air was irradiated. In experiments using 1 Torr of CF_3CH_3 the fractional loss of CF_3CH_3 was small (<1%) and was not detectable. Hence, product yields were determined relative to the observed yield of CF_3CHO. The product mixtures were analyzed for CF_3CHO and CF_3CH_2OH. While CF_3CHO was observed no CF_3CH_2OH was detected. The CF_3CH_2OH yield was less than 6% of that of CF_3CHO. The conversion of CF_3CH_3 (as measured by the observed yield of CF_3CHO) was <0.5%. With such a low conversion of CF_3CH_3 any loss of CF_3CH_2OH (or CF_3CHO) via reaction with F atoms will be of minor importance. It seems reasonable to ascribe the relative yields of CF_3CHO and CF_3CH_2OH to the relative importance of channels (74a) and (74b). Taking into account the small loss of CF_3CHO and possible loss of CF_3CH_2OH via reaction with F atoms gives a branching ratio of $k_{74b}/k_{74a} < 0.077$. In this calculation it is implicitly assumed that all CF_3CH_2O radicals formed in reaction

channel (74a) react with O_2 and do not decompose. This assumption does not impact the upper limit derived above.

As seen from Figure 21, the yield of CF_3CHO following irradiation of $CF_3CH_3/F_2/O_2/N_2$ mixtures with $[O_2]$ = 5 or 147 Torr is indistinguishable from 100%. Assuming that 100% of reaction (74) proceeds via channel (74a) and that the combined random and systematic uncertainty of the determination of the CF_3CHO yield is ±20%. Then in the presence of 5 Torr of O_2 at least 80% of the CF_3CH_2O radicals generated in the system must react with O_2 in preference to decomposition via reaction (78). Hence, at 700 Torr in N_2 diluent at (296±2K), $k_{75}/k_{78} > 2.5 \times 10^{-17}$ cm^3 $molecule^{-1}$.

Having established that reaction (74b) is of no consequence it is interesting to consider the origin of the CF_3CH_2OH product observed in the experiments in which 1 Torr of O_2 was used. It is well established that CF_3O radicals readily abstract H atoms from H containing compounds to form CF_3OH [Appendix 7.5 pp151]. The same reaction is possible for CF_3CH_2O radicals. CF_3CH_3 is the most likely H atom donor in the present experimental system.

$$CF_3CH_2O + CF_3CH_3 \rightarrow CF_3CH_2OH + CF_3CH_2 \qquad (79)$$

Reaction (79) has to compete with reaction (75) for the available CF_3CH_2O radicals. The rate of reaction (75) will be directly proportional to $[O_2]$. Hence, with $[O_2]$ = 147 and 5 Torr it is possible that reaction (75) dominates the loss of CF_3CH_2O radicals. Whereas with $[O_2]$ = 1 Torr reaction (75) is sufficiently slow that an appreciable fraction of the CF_3CH_2O radicals react via reaction (79). If this hypothesis is correct then the CF_3CH_2OH yield in the experiments employing an oxygen partial pressure of 5 Torr should be approximately 5 times less than observed in the corresponding 1 Torr experiments, i.e. 4%. Such a small CF_3CH_2OH yield is below the experimental detection limit. The experimental evidence suggests, but does not prove, that reaction (79) is the source of the CF_3CH_2OH observed in the lowest $[O_2]$ experiments. To resolve this point would take further product studies using a range of different initial [HFC-143a]/$[O_2]$ ratios and is beyond the scope of the present work.

5.2.5 CFH_2CFHO_2

To determine the atmospheric fate of the alkoxy radical CH_2FCFHO, formed in the reaction of CFH_2CFHO_2 with NO, experiments were performed in which $Cl_2/CH_2FCH_2F/NO$ mixtures in 700 Torr of air diluent were irradiated using the FTIR-

Smog Chamber system. The loss of CH_2FCH_2F and the formation of products were monitored by FTIR spectroscopy. A mixture of 44.0 mTorr of CH_2FCH_2F, 49.3 mTorr of NO, and 116 mTorr of Cl_2 were irradiated 920 s. Using our calibrated reference spectrum for HC(O)F we can quantify the HC(O)F product versus the loss of CH_2FCH_2F. Linear least squares analysis of the data gives a molar HC(O)F yield of 182±19%. Hence, HC(O)F accounts for 91±10% of the loss of CH_2FCH_2F. The observed molar yield of HCl in terms of loss of CFH_2CFH_2 was 103±19%. Within the experimental errors HC(O)F accounts for 100% of the loss of CH_2FCH_2F, there were no other IR product features that could be ascribed to CH_2FCH_2F oxidation products. Under atmospheric conditions the reaction of CFH_2CFHO_2 with NO gives CH_2FCFHO radicals and NO_2.

The expected atmospheric fate of CH_2FCFHO radicals is either decomposition or reaction with O_2. Decomposition yields HC(O)F and a CH_2F radical which will further react to produce an additional HC(O)F molecule.

$$CH_2FCFHO + M \rightarrow CH_2F + HC(O)F + M \quad (80)$$

$$CH_2FCFHO + O_2 \rightarrow CH_2FC(O)F + HO_2 \quad (81)$$

$$CH_2F + O_2 + M \rightarrow CH_2FO_2 + M \quad (82)$$

$$CH_2FO_2 + NO \rightarrow CH_2FO + NO_2 \quad (83)$$

$$CH_2FO + O_2 \rightarrow HC(O)F + HO_2 \quad (84)$$

In the present experiments HC(O)F product accounted for the entire loss of HFC-152 showing that in the presence of 700 Torr of air (147 Torr of O_2) reaction (81) does not compete effectively with reaction (80). Similar behavior has been observed for CF_3CFHO radicals (produced during the atmospheric oxidation of HFC-134a) [102]. At 700 Torr total pressure of air, 20% of CF_3CFHO radicals react with O_2 and 80% decompose via C-C bond scission [102]. The results from the present work suggest that in the case of CH_2FCFHO radicals the balance between decomposition and reaction with O_2 is tilted further towards decomposition.

5.2.6 $CFH_2O_2 + HO_2$

To provide insight into the factors which influence the mechanism of the reaction of peroxy radicals with HO_2 radicals and to elucidate the atmospheric chemistry of hydrofluorocarbons, an experimental investigation of the products of reaction (85) was performed.

$$CH_2FO_2 + HO_2 \rightarrow CH_2FOOH + O_2 \quad (85a)$$

$$CH_2FO_2 + HO_2 \rightarrow HC(O)F + O_2 + H_2O \quad (85b)$$

The chlorine atoms formed by the photolysis of molecular chlorine in the presence of H_2, CH_3F, and air forms CH_2FO_2 and HO_2 radicals via reactions (55,82,86–88).

$$Cl_2 + h\upsilon \rightarrow 2Cl \quad (55)$$
$$Cl + CH_3F \rightarrow CH_2F + HCl \quad (86)$$
$$CH_2F + O_2 + M \rightarrow CH_2FO_2 + M \quad (82)$$
$$Cl + H_2 \rightarrow H + HCl \quad (87)$$
$$H + O_2 + M \rightarrow HO_2 + M \quad (88)$$

The loss of CH_3F and the formation of products were monitored using Fourier transform infrared spectroscopy. Products were quantified by fitting reference spectra of the pure compounds to the observed product spectra using integrated absorption features. A reference spectrum for CH_2FOOH was not available. Instead, the integrated absorption over the region 780-850 cm^{-1} was compared to the corresponding feature in our calibrated CH_3OOH reference spectrum. The feature at 780-850 cm^{-1} is ascribed to an O-O stretch. A computational study was performed to explore in detail the relative IR absorption strengths of CH_2FOOH and CH_3OOH [Appendix 7.11.13 pp205]. The O-O stretching feature was calculated to be 1.33±0.20 times more intense in CH_2FOOH than in CH_3OOH. This scaling factor was used in the experimental quantification of CH_2FOOH.

Reactions (85) and (89) compete for the available CH_2FO_2 radicals.

$$CH_2FO_2 + CH_2FO_2 \rightarrow CH_2FO + CH_2FO + O_2 \quad (89a)$$
$$CH_2FO_2 + CH_2FO_2 \rightarrow CH_2FOH + HC(O)F + O_2 \quad (89b)$$

Although kinetic data are available for reaction (89) [101,103] there are no data available for reaction (85). Hence, it is not possible to calculate the excess HO_2 concentration needed to ensure that the bulk of the CH_2FO_2 radicals are scavenged by reaction with HO_2. The strategy employed in the present study was to conduct experiments with different initial $[H_2]_o/[CH_3F]_o$ concentration ratios and measure the relative yields of HC(O)F and CH_2FOOH. As the ratio $[H_2]_o/[CH_3F]_o$ increases, more HO_2 radicals are generated in the system for a given level of CH_2FO_2. Thus, in terms of the loss of CH_2FO_2 radicals, reaction (85) increases in importance and reaction (89) decreases as the ratio $[H_2]_o/[CH_3F]_o$ increases. At sufficiently high ratios of $[H_2]_o/[CH_3F]_o$, reaction (85) will dominate the loss of CH_2FO_2 radicals. Further increases

in $[H_2]_o/[CH_3F]_o$ will not change the observed yields of CH_2FOOH and HC(O)F, which then reflect the relative importance of channels (85a) and (85b).

Two major carbon containing products were observed following the UV irradiation of $CH_3F/H_2/Cl_2$ mixtures: HC(O)F and CH_2FOOH. The observed yields of CH_2FOOH and HC(O)F following successive irradiations of a reaction mixture consisting of 31.5 mTorr of CH_3F and 5.98 Torr of H_2 in 700 Torr of air were 73±6% and 29±4%. In all experiments, the yields of CH_2FOOH and HC(O)F increased linearly with the loss of CH_3F, suggesting the absence of significant secondary loss processes for these products. As described later, small corrections have been applied to the yield of CFH_2OOH to account for reaction of Cl atoms with CH_2FOOH.

Experiments were performed using a range of $[H_2]_o/[CH_3F]_o$. The observed yields of CH_2FOOH and HC(O)F are plotted versus $[H_2]_o/[CH_3F]_o$ in Figure 22. Small corrections for loss of CH_2FOOH via reaction with Cl atoms (see below) have been applied to the data shown in Figure 22. From Figure 22 it can be seen that as the concentration ratio $[H_2]_o/[CH_3F]_o$ is increased from 0 to 120, the yield of hydroperoxide increases at the expense of HC(O)F. This reflects the increased importance of reaction (85) as a loss of CH_2FO_2 radicals. For concentration ratios greater than 120, there is no observable dependence of product yields on $[H_2]_o/[CH_3F]_o$ suggesting that, under these conditions, essentially all the CH_2FO_2 radicals are consumed by reaction (85). Averaging all the product data obtained using $[H_2]_o/[CH_3F]_o$ of 120 or more, gives yields of CH_2FOOH and HC(O)F of 29±3% and 71±3%. While the estimation of potential systematic uncertainties is difficult, I estimate that they could contribute additional 6% and 10% uncertainty ranges in the yields of CH_2FOOH and HC(O)F, respectively. Using conventional propagation of error analysis to incorporate the potential systematic uncertainties leads to yields for CH_2FOOH and HC(O)F of 29±7% and 71±11%, respectively. Together, CH_2FOOH and HC(O)F, account for 100±13% of the loss of CH_3F. From our product yields of CH_2FOOH and CH_3F, the branching ratios of k_{85a}/k_{85}= 0.29±0.07 and k_{85b}/k_{85} = 0.71±0.11 can be derived.

As with all product studies, careful attention needs to be paid to the possibility of loss of products via secondary reactions in the chamber. Possible unwanted secondary processes include photolysis, heterogeneous losses, and reaction with Cl atoms. It has been established previously that HC(O)F is not photolyzed in the chamber by the blacklamps [101]. A sample of CH_2FOOH was not available so it was not possible to perform an experiment to assess the photolysis of this species in the chamber. However, by analogy to the behavior of other hydroperoxides, it is expected that photolysis of CH_2FOOH will be of negligible importance. To check for heterogeneous loss of HC(O)F

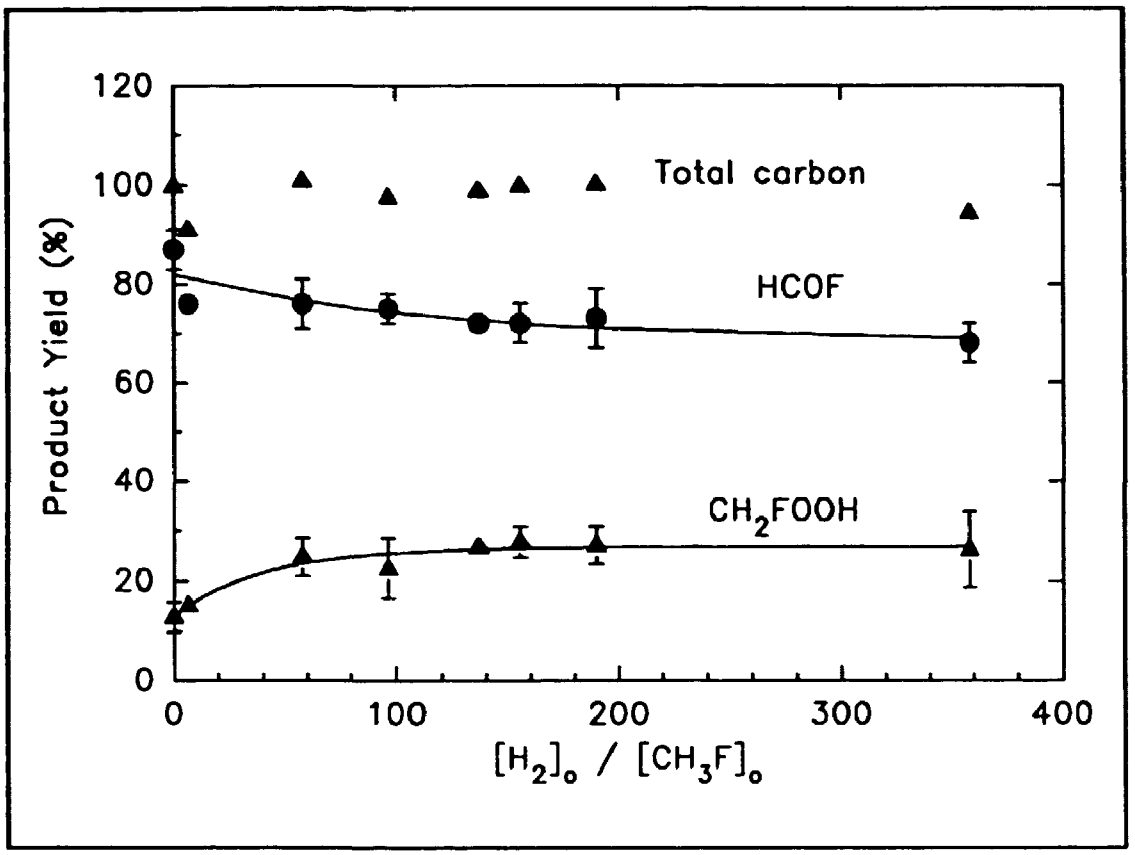

Figure 22. *Observed yields of CH_2FOOH and HCOF as a function of $[H_2]_0/[CH_3F]_0$ concentration ratio. The lines are fits to an arbitrary function to aid the visual inspection of the data trends.*

and CH_2FOOH, reaction mixtures were left to age in the chamber for 2 hours. There was no observable (<2%) loss of either species showing that heterogeneous losses are insignificant.

Cl atoms are 160 times less reactive towards HC(O)F than towards CH_3F [104]. The consumption of CH_3F used in the present work was 5-52%, so secondary reaction of HC(O)F with Cl atoms is negligible. The impact of the possible secondary reaction of Cl atoms with CH_2FOOH is examined below.

Kinetic study of the reaction of Cl atoms with CH_2FOOH and CH_2FCl

To assess the impact of possible secondary reaction of Cl atoms with CH_2FOOH requires kinetic data for reaction (90). Unfortunately such data are not available. A study of reaction (90) was performed as part of this work.

$$Cl + CH_2FOOH \rightarrow \text{products} \qquad (90)$$

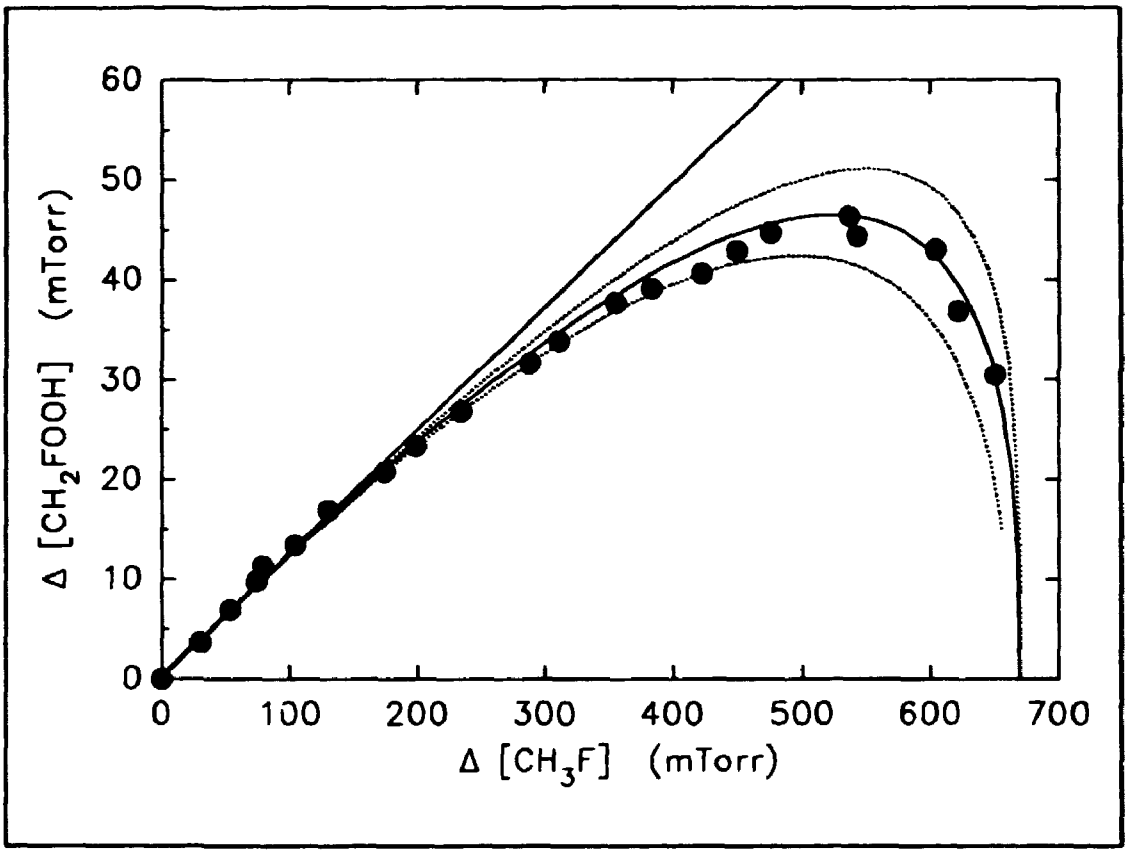

Figure 23. *Plot of the yield of CH_2FOOH following successive irradiations of mixtures of 670 mTorr of CH_3F and 1340 mTorr of Cl_2 in air. The straight line is a linear least squares fit of the data obtained for CH_3F consumptions of less than 150 mTorr. The solid and dotted curved lines are fit to the data. See text.*

To measure k_{90}, experiments were performed in which mixtures of 670 mTorr of CH_3F and 1340 mTorr of Cl_2 in 700 Torr of air were irradiated. CH_2FOOH is formed in the Cl atom initiated oxidation of CH_3F via reaction (85a). The formation of CH_2FOOH was measured as a function of the loss of CH_3F. Results are shown in Figure 23. As seen from Figure 23, initially the CH_2FOOH yield increased linearly with the consumption of CH_3F. Linear least squares analysis of the data obtained using conversions of CH_3F less than 150 mTorr gives a yield of CH_2FOOH of 13±3%. Quoted errors are 2 standard deviations. This result is consistent with a previous determination of 11±4% for the CH_2FOOH yield following the Cl initiated oxidation of CH_3F in air [101]. For consumptions of CH_3F greater than 300 mTorr, evidence for secondary loss of CH_2FOOH is apparent. For consumptions of CH_3F greater than 500 mTorr the concentration of CH_2FOOH decreased with increasing conversion of CH_3F. We attribute the decline of the

concentration of CH_2FOOH in the chamber to reaction of Cl atoms with CH_2FOOH which becomes important at high conversions of CH_3F.

The shape of the data plot in Figure 22 contains information regarding the rate constant ratio k_{90}/k_{86}. To extract a value for k_{90}/k_{86} the chemistry in the chamber was modelled using the Acuchem chemical kinetic program [96] with a mechanism consisting of reactions (90) and (86). In the mechanism it was assumed that reaction of Cl atoms with CH_3F in air generates CH_2FOOH in a yield of 13%. The effect of varying the rate constant ratio k_{90}/k_{86} on the predicted behavior of CH_2FOOH is shown in Figure 23. The experimental data is fit using k_{90}/k_{86}= 0.4±0.1. Combining this ratio with k_{86} = (3.2±0.5) x 10^{-13} [101] gives k_{90} = (1.3±0.4) x 10^{-13} cm^3 $molecule^{-1}$ s^{-1}.

There are two potential complications in our determination of k_{90} that need to be considered. First, if reaction (90) proceeds via channel (a) then CH_2FO_2 radicals will be formed and these could then react with HO_2 radicals via reaction (85a) to reform CH_2FOOH, thereby masking the true decay rate of this species.

$$Cl + CH_2FOOH \rightarrow CH_2FO_2 + HCl \qquad (90a)$$

$$Cl + CH_2FOOH \rightarrow CHFOOH + HCl \qquad (90b)$$

As shown in Figure 23, the formation of CH_2FOOH from CH_2FO_2 radicals in the chamber is relatively inefficient. The yield of CH_2FOOH measured under conditions of low consumption of CH_3F (and hence negligible loss of CH_2FOOH) is 13±3%. The potential impact of reaction (90a) was explicitly evaluated by including this reaction in the model used to derive the ratio k_{90}/k_{86} and assuming that 100% of the reaction of Cl atoms with CH_2FOOH proceeded via channel (90a). With reaction (90a) included in the mechanism the best fit value of k_{90}/k_{86} increased by 13% giving k_{90} = (1.5±0.5) x 10^{-13} cm^3 $molecule^{-1}$ s^{-1}.

The second complication arises if (90b) is the dominant reaction pathway. The CHFOOH radical formed is expected to decompose to generate OH radicals.

$$CHFOOH + M \rightarrow HC(O)F + OH + M \qquad (91)$$

Hydroxyl radicals will react with either CH_3F, CH_2FOOH, HC(O)F, or Cl_2. At ambient temperature, OH radicals react slowly with CH_3F, HC(O)F, and Cl_2; $k(OH+CH_3F)$ = 1.8 x 10^{-14} [5], $k(OH+HC(O)F) < 4 \times 10^{-15}$[21], and $k(OH+Cl_2)$ = 6.7 x 10^{-14} cm^3 $molecule^{-1}$ s^{-1} [5], respectively. The reactivity of OH radicals towards CH_2FOOH is unknown.

To shed light on the relative importance of channels (90a) and (90b), the strengths of the alkyl and peroxy hydrogen bonds have been calculated. The energy of the CH_2FO_2-H bond was determined to 93.2 kcal/mol while the H-CHFOOH bondstrength was derived to 104.4 kcal/mol [Appendix 7.11.13 pp205]. Hence, reaction (90a) is predicted to be exothermic by 10 kcal/mol while reaction (90b) is endothermic by 1.2 kcal/mol. Thus, based on thermodynamic arguments alone, channel (90a) should dominate over channel (90b).

Corrections applied to our measured CH_2FOOH product data shown in Figure 22 to account for reaction (90) were calculated assuming this reaction proceeds entirely via channel (a) and used $k_{90} = 1.5 \times 10^{-13}$ cm^3 molecule^{-1} s^{-1}. Corrections were in the range 1-16%.

6 The Reactions of CF_3CO_x, CF_3O_x, FCO_x, and FO_x

CF_3CO_x, CF_3O_x, FCO_x, and FO_x radicals are all produced in the atmospheric degradation of HFCs and HCFCs as discussed in chapter 1. Therefore studies of atmospheric relevant reactions of these four radical series were a part of this PhD work.

6.1 CF_3CO_x Reactions

Pulse radiolysis was used to study the kinetics of the reactions of the CF_3CO radical with O_2, the reactions of $CF_3C(O)O_2$ with NO and NO_2, and the decomposition rates via C-C bond cleavage of CF_3CO, and $CF_3C(O)O$ radicals. [Appendix 7.9 pp189].

CF_3CO radicals were formed upon pulse radiolysis of mixtures of CF_3CHO, O_2, in SF_6:

$$SF_6 + 2\ MeV\ e^- \rightarrow F + products \quad (21)$$

$$F + CF_3CHO \rightarrow HF + CF_3CO \quad (92)$$

By the formation rate of CF_3CO radicals observed at 230 nm, a rate constant of reaction (92) of $(2.3\pm0.4)\times10^{-11}$ cm^3 $molecule^{-1}$ s^{-1} was derived. When O_2 were added to the reaction mixture an increase in the maximum transient absorption from 220 to 300 nm were observed. This absorption is due to the formation of $CF_3C(O)O_2$ radicals via reaction (9). By observation of the rate of increase of the absorbance at 230 nm originating from $CF_3C(O)O_2$ and CF_3O_2 the rate constants for reactions (8) and (9) were determined in 1000 mbar of SF_6 to $k_8=(1.2\pm0.8)\times10^5$ s^{-1} and $k_9=(7.3\pm1.1)\times10^{-13}$ cm^3 $molecule^{-1}$ s^{-1}, respectively:

$$CF_3CO + M \rightarrow CF_3 + CO + M \quad (8)$$

$$CF_3CO + O_2 + M \rightarrow CF_3C(O)O_2 + M \quad (9)$$

$$CF_3 + O_2 + M \rightarrow CF_3O_2 + M \quad (63)$$

These values were confirmed by FTIR measurements of a chlorine initiated product study of the CF_3CHO molecule in air. By measuring the formation of CO as a function of the loss of CF_3CHO the rate constant ratio k_9/k_8 were determined to $(7.4\pm0.6)\times10^{-18}$ cm^3 $molecule^{-1}$ in 1000 mbar of N_2 in good agreement with the values of k_9 and k_8 from the pulse radiolysis experiments ($k_9/k_8=(6\pm4)\times10^{-18}$ cm^3 $molecule^{-1}$).

The UV absorption spectrum of $CF_3C(O)O_2$ was studied in the wavelength range 220-300 nm, at 230 nm the absorption cross section were $(3.78\pm0.43)\times10^{-18}$ cm^2 $molecule^{-1}$.

By monitoring the formation of NO_2 at 400 nm the rate constant for the reaction of $CF_3C(O)O_2$ with NO was determined to be greater than 9.9×10^{-12} cm^3 $molecule^{-1}$ s^{-1}. The NO_2 yield following radiolysis of $CF_3CHO/O_2/NO/SF_6$ mixtures was more than 100% in terms of the initial F atom yield. From this information a lower limit for the decomposition of $CF_3C(O)O$ radical of 6×10^4 s^{-1} was derived.

The decay rate of NO_2 detected at 400 nm following radiolysis of $CF_3CHO/O_2/NO_2/SF_6$ mixtures gave a rate constant for the reaction of $CF_3C(O)O_2$ radicals with NO_2 of $(6.3\pm1.3)\times10^{-12}$ cm^3 $molecule^{-1}$ s^{-1}.

The thermal stability of $CF_3C(O)O_2NO_2$ were studied using the FTIR technique. $CF_3C(O)O_2NO_2$ was formed by irradiation of $Cl_2/O_2/CF_3CHO/N_2/NO_2$ mixtures:

$$Cl_2 + h\nu \rightarrow 2Cl \quad (55)$$

$$CF_3CHO + Cl \rightarrow CF_3CO + HCl \quad (93)$$

$$CF_3CO + O_2 + M \rightarrow CF_3C(O)O_2 + M \quad (9)$$

$$CF_3C(O)O_2 + NO_2 + M \rightarrow CF_3C(O)O_2NO_2 + M \quad (94)$$

Thereafter NO was flushed into the chamber and from the decay of $CF_3C(O)O_2NO_2$ at different temperatures and total N_2 pressure of 100-700 Torr, the decomposition rate constant was determined to $k_{-94}=(1.9^{+7.6}_{-1.5})\times10^{16}\exp(-(14000\pm480)/T)$ s^{-1} by combining our results with the results from Zabel et al. [32].

From rate constant ratio of $k_{94}/k_{CF3C(O)O2+NO}=0.64\pm0.13$ at 1000 mbar N_2 total pressure from Zabel et al. [32] and $k_{94}=(6.3\pm1.3)\times10^{-12}$ cm^3 $molecule^{-1}$ s^{-1} a rate constant for the reaction of $CF_3C(O)O_2$ with NO of $(1.03\pm0.29)\times10^{-11}$ cm^3 $molecule^{-1}$ s^{-1} was derived. This is close with the lower limit of 9.9×10^{-12} cm^3 $molecule^{-1}$ s^{-1} obtained above.

6.2 CF_3O_x Reactions

The reactions of CF_3O_x radicals have been subject to a large research effort the last couple of years. This is due to the uncertainty of the atmospheric fate of the CF_3O radical. The reactions of the CF_3O radical with NO [Appendix 7.6 pp158], ozone [Appendix 7.7 pp165], CF_3CFH_2 [Appendix 7.5 pp151], and H_2O [Appendix 7.4 pp145] were studied.

6.2.1 Reaction of CF_3O with NO and O_3

The reactions of the CF_3O radical with NO and O_3 was studied using pulse radiolysis. The problem in studying reactions of CF_3O using this experimental setup is, that CF_3O can not be detected using the present reaction system. Therefore precursors for CF_3O, products of CF_3O reactions, or species reacting with CF_3O had to be followed to derive the kinetics of the CF_3O radical.

Mixtures of $CF_3H/O_2/NO/SF_6$ were radiolysed. The CF_3O radical was formed by the following reactions:

$$SF_6 + 2\ MeV\ e^- \rightarrow F + products \quad (21)$$

$$F + CF_3H \rightarrow CF_3 + HF \quad (95)$$

$$CF_3 + O_2 + M \rightarrow CF_3O_2 + M \quad (63)$$

$$CF_3O_2 + NO \rightarrow CF_3O + NO_2 \quad (96)$$

As described in Appendix 7.6 pp158, the formation of NO_2 is observed at 400 nm and by fitting the observed transient using a detailed chemical model and the Chemsimul program a rate constant of $k_{96}=(1.68\pm0.26)\times10^{-11}$ cm^3 molecule^{-1} s^{-1} was obtained. The chemical model can then predict the formation of the CF_3O radical precisely.

The next step is to look at the formation of the product of the reaction of the CF_3O radical with NO:

$$CF_3O + NO\ (+ M) \rightarrow CF_2O + FNO \quad (97a)$$

$$\rightarrow CF_3ONO\ (+ M) \quad (97b)$$

FNO has a sharp absorption peak at 310.5 nm with an absorption cross section of $(4.7\pm0.7)\times10^{-19}$ cm^2 molecule^{-1} [Appendix 7.3 pp134]. The observed absorption at 310.5 nm greatly supersedes the absorption at 317 nm where FNO do not absorb, indicating that FNO is indeed formed in the reaction mixture. Absorption transients observed at 310.5 nm were fitted with the chemical model by varying the rate constant for reaction (97). A value for k_{97} of $(5.2\pm2.7)\times10^{-11}$ cm^3 molecule^{-1} s^{-1} was derived. The yield of FNO was >90%.

When this value was published two other values was available in the literature, $k_{97}=(2\pm1)\times10^{-11}$ cm^3 molecule^{-1} s^{-1} [105] and $k_{97}=(2.5\pm0.4)\times10^{-11}$ cm^3 molecule^{-1} s^{-1} [39]. These values have recently been changed to $(5\text{-}6)\times10^{-11}$ cm^3 molecule^{-1} s^{-1} [34,39, 38,40]. This reaction is an important loss reaction for CF_3O radicals, especially in the stratosphere as discussed in a previous chapter.

The reaction of the CF_3O radical with O_3 is potentially an important stratospheric reaction of CF_3O. In March 1993 a value of 10^{-11}-10^{-12} cm^3 $molecule^{-1}$ s^{-1} was reported at a meeting in Dublin [25]. A rate constant of 10^{-11} cm^3 $molecule^{-1}$ s^{-1} for the reaction of CF_3O with O_3 would give an ODP of the order of 0.02 for HFC-143a [46]. Therefore a study of this rate constant was performed.

Mixtures of $CF_3H/O_2/O_3/SF_6$ were radiolysed. The CF_3O radical was formed by the following set of reactions:

$$SF_6 + 2\ MeV\ e^- \rightarrow F + products \quad (21)$$

$$F + CF_3H \rightarrow CF_3 + HF \quad (95)$$

$$CF_3 + O_2 + M \rightarrow CF_3O_2 + M \quad (63)$$

$$CF_3O_2 + CF_3O_2 \rightarrow CF_3O + CF_3O + O_2 \quad (57)$$

The product of reaction (57) is well established from the product study of the CF_3H as discussed previously. If CF_3O radicals react with O_3 in the system we can observe this as a decay of the absorption due to ozone. The absorption as a function of time at 288 nm and 272 nm was then observed following radiolysis of the $CF_3H/O_2/O_3/SF_6$ mixture. The absorbance was essentially stable. The absorption transients was modelled well by the a chemical model not including the reactions of CF_3O with O_3. When this reaction was included, the fit of the chemical model to the experimental absorption transients got worse. From modelling experimental absorption transients an upper limit for the reaction of CF_3O radicals with ozone of $<1.0\times10^{-13}$ cm^3 $molecule^{-1}$ s^{-1} was determined. This result was published "back to back" with two other determinations of upper limits of this reaction $<3\times10^{-14}$ cm^3 $molecule^{-1}$ s^{-1} [35] and $<5\times10^{-14}$ cm^3 $molecule^{-1}$ s^{-1} [36]. Recently, several values for the reaction between CF_3O and ozone. I will just mention the lowest value derived by Fockenberg et al. [37] of $<2\times10^{-15}$ cm^3 $molecule^{-1}$ s^{-1}.

6.2.2 Reaction of CF_3O with CF_3CFH_2 and H_2O

Products studies following UV irradiation of $CF_3CFH_2/Cl_2(F_2)/O_2$ mixtures with and without H_2O together with model simulations of the product yields were carried out [Appendix 7.4 pp145 and 7.5 pp151]. The stable products were HCOF, CF_3COF, $CF_3O_3CF_3$, COF_2. Two unknown products were seen to decompose in the dark. One of them were identified as the "mixed trioxide" $CF_3CFHO_3CF_3$, and the other as CF_3OH. Three pieces of evidence supported the assignment of "unknown no. two" to CF_3OH: (i) A strong absorption at 3664 cm^{-1} ($\sigma=9\times10^{-19}$ cm^2 $molecule^{-1}$) characteristic for OH stretches.

(ii) The only observed product of the decomposition of the "unknown no. two" was CF_2O. The first order rate constants for the decomposition of "unknown no. two" and the formation of CF_2O was within the uncertainty the same. This may be explained by the decomposition of CF_3OH to CF_2O and HF. HF absorbs at 3800 cm^{-1} and can not be seen by the present setup. (iii) To support the assignment of the "unknown no. two" experiments were performed in which CF_3OH were formed by photolysis of CF_3NO in the presence of methane and air. "Unknown no. two" was formed. These supports the assignment of the "unknown no. two" to CF_3OH.

The yield of CF_3OH increased with increasing initial CF_3CFH_2 concentration suggesting that CF_3OH were formed partly by the reaction of CF_3O with CF_3CFH_2. The rate constant for this reaction was derived to $(1.1\pm0.7)\times10^{-15}$ cm^3 $molecule^{-1}$ s^{-1} by model simulations of the product yields. The life time of CF_3OH in the chamber towards decomposition was up to 5 hours. Perhaps with a significant heterogeneous component.

The reaction of CF_3O with water were investigated in product studies of $H_2O/CF_3CFH_2/O_2/Cl_2$ mixtures in air. The product distribution was determined after irradiation with UV light. The yield of CF_3OH, measured by the yield of CF_2O, was shown to increase with increasing water concentration. This indicates that CF_3O may abstract a hydrogen atom from H_2O with a rate constant of $(0.2\text{-}40)\times10^{-17}$ cm^3 $molecule^{-1}$ s^{-1}. In spite of the slowness of this reaction it may still be an important fate of CF_3O radicals in the troposphere due to the relative high concentration of water.

The reaction was also studied by ab initio calculations, suggesting that the reaction was exothermic by 1.7 kcal mol^{-1} implying a surprisingly high CF_3O-H bond energy of 120±3 kcal mol^{-1}. This result does not agree with the bond energy determined by the group additivity method [106]. The bond energy determined by the bond additivity method is 108.9 kcal mol^{-1}. This is an area of future research.

6.3 FCO_x Reactions

CF_2O and HCOF molecules are known to be major products of the degradation of HFCs in the atmosphere. By photolysis of CF_2O and HCOF and the reaction of HCOF with OH, the FCO radical will be produced. Reactions of atmospheric interest of FCO and its oxides $FC(O)O_2$ and FC(O)O have been investigated in this work.

Pulse radiolysis was used to study the UV spectra and kinetics of FCO, $FC(O)O_2$, and FC(O)O radicals. The following reactions were investigated:

$$FCO + O_2 + M \rightarrow FC(O)O_2 + M \quad (98)$$

$$FCO + FCO \rightarrow \text{products} \quad (99)$$

$$FC(O)O_2 + FC(O)O_2 \rightarrow \text{products} \quad (100)$$

$$FCO + NO \rightarrow FNO + O_2 \quad (101)$$

$$FC(O)O_2 + NO \rightarrow FC(O)O + NO_2 \quad (102)$$

$$FC(O)O + NO \rightarrow FNO + CO_2 \quad (103)$$

$$FC(O)O + O_3 \rightarrow \text{products} \quad (104)$$

The self reaction of the FCO radical and the observed rate constant for the self reaction of $FC(O)O_2$ radicals have been determined by the decays of the absorptions due to FCO and $FC(O)O_2$, respectively. The rate constants were, $k_{99}=(1.1\pm0.2)\times10^{-11}$ cm^3 molecule^{-1} s^{-1} and $k_{100a+b}=(6.0\pm0.7)\times10^{-12}$ cm^3 molecule^{-1} s^{-1}, respectively. In the atmosphere FCO radicals will react with O_2. The rate constant for this reaction was determined to $(1.2\pm0.2)\times10^{-12}$ cm^3 molecule^{-1} s^{-1}. Reaction with O_2 is the sole fate of FCO radicals in the atmosphere. Rate constants for the reactions of FCO, FC(O)O, and $FC(O)O_2$ radicals with NO were determined to $(1.0\pm0.2)\times10^{-12}$ cm^3 molecule^{-1} s^{-1}, $(1.3\pm0.7)\times10^{-10}$ cm^3 molecule^{-1} s^{-1}, and $(2.5\pm0.8)\times10^{-11}$ cm^3 molecule^{-1} s^{-1}, respectively. An upper limit for the reaction of FC(O)O with ozone was derived to $k<6\times10^{-14}$ cm^3 molecule^{-1} s^{-1}. The reactions of FCO_x radicals is discussed in context of atmospheric chemistry in chapter 1.

6.4 FO_x Reactions

It have been suggested that FO_x (F, FO, and FO_2) radicals could be involved in a catalytic cycle destroying ozone in the stratosphere (see discussion in chapter 1). This study was performed, to establish whether F, FO, and FO_2 radicals have any impact on the stratospheric ozone layer.

In this study pulse radiolysis was used. However, part of the experiments were done using a newly built high pressure cell and the 10 MeV Linarc linear electron accelerator in the Chemical Reactivity Section. This setup has only been used for this work. Therefore the experimental details are not described in the experimental section of this thesis but in the FO_x article in Appendix 7.2 pp125.

In this work the following reactions were investigated:

$$FO_2 + NO \rightarrow FNO + O_2 \quad (105)$$

$$FO_2 + NO_2 \rightarrow \text{products} \quad (106)$$

$$FO_2 + CO \rightarrow \text{products} \quad (107)$$

$$FO_2 + CH_4 \rightarrow \text{products} \quad (108)$$

$$FO_2 + O_3 \rightarrow \text{products} \quad (17)$$

$$FO + O_3 \rightarrow \text{products} \quad (14)$$

Values of k_{105} and k_{106} of $(1.47\pm0.08)\times10^{-12}$ cm^3 molecule^{-1} s^{-1} and $(1.1\pm0.1)\times10^{-13}$ cm^3 molecule^{-1} s^{-1}, respectively, were determined using the pulse radiolysis setup described in the experimental section. Upper limits of reactions (14,17,107,108) together with a value of k_{108} of $(1.05\pm0.10)\times10^{-13}$ cm^3 molecule^{-1} s^{-1} were determined using the high pressure experimental setup. The upper limits were $k_{107}<5.1\times10^{-16}$ cm^3 molecule^{-1} s^{-1}, $k_{108}<4.1\times10^{-15}$ cm^3 molecule^{-1} s^{-1}, $k_{17}<3.4\times10^{-16}$ cm^3 molecule^{-1} s^{-1}, and $k_{14}<1.2\times10^{-12}$ cm^3 molecule^{-1} s^{-1}.

From the rates derived in this work and kinetic data from the literature, the impact on the stratospheric ozone layer of releasing F atoms into the stratosphere can be evaluated. This has been discussed previously in chapter 1.

7 Conclusions and Future Work

The objective of this work has been to investigate the degradation pathways, mechanisms and products of HFCs and HCFCs in the atmosphere. Much information have been collected on this subject over the last three years. The atmospheric chemistry of HFCs and HCFC is now well understood. However, both in the atmospheric chemistry of HFCs, HCFCs and VOC there exist some important unresolved problems. One of the major problem is the reaction rates and the product distribution of the reaction of RO_2 radicals reaction with HO_2 radicals. So far only very few reactions of this type have been investigated especially for reactions of HO_2 radicals with halo alkyl peroxy radicals. In addition the products of these reactions is uncertain as discussed in chapter 1. As indicated by the product studies of the reaction of HO_2 with CFH_2O_2 a significant part of the reaction proceed through formation of an aldehyde. However, a recent study of the reaction of CF_3CFHO_2 and HO_2 indicate that only the hydroperoxide is formed by this reaction. Even less is known about the reactions of peroxy radicals with CH_3O_2. The product distributions and the rates of these reactions must therefore be investigated in the future.

Another uncertain factor is the temperature dependence of the reaction rates and product distributions. Especially, the product distribution for the reaction of CF_3O radicals

with NO at low temperature. This reaction is the most important loss reaction for CF_3O radicals in the stratosphere and the products therefore need to be determined at low temperature. In addition, the temperature dependence of the reaction of FO_2 radicals with NO_x and HO_2 radicals need to be studied. The work in this thesis have almost all been done at ambient temperature. Many conclusions can be made from these results. However, the temperature dependence of many important reactions should be investigated.

It is important to know the photolysis rate of $RONO_2$, RO_2NO_2, and ROOH species formed in the atmosphere from HFCs and HCFCs. So far photolysis times have been determined by analogy with CH_3ONO_2, $CH_3O_2NO_2$, and CH_3OOH. There may be a significant difference in nitrate, peroxy nitrate, and hydroperoxide spectra for different alkyl and halo alkyl groups. Finally, the products of the photolysis of CF_3CHO need to be determined.

The reactions of CF_3COOH in the liquid fase and loss reactions for this compound need to be investigated together with the influence of CF_3COOH on plant systems.

Ab-initio calculations of many of the reactions studied in this work would be of interest. Especially, for the fate of halo alkoxy radicals would be helpful to identify the factors which influence the balance between the possible atmospheric loss processes. In addition, a better theoretical understanding of self reactions and the reactions with HO_2 and NO of peroxy radicals would be of interest.

A few methods on the experiment side could also be improved. The newly installed diode array is a big advantage in the analysis of the data. In addition, a calculation of the statistical uncertainty of the fitted data should be employed in the data analysis in the future. Finally, it would be a big advantage if the reaction chamber could be cooled down to improve the possibilities of determining activation energies.

References

1. M.J. Molina and F.S. Rowland: "*Stratospheric sink for Chlorofluoromethanes: Chlorine Atom-catalyzed Destruction of Ozone*", Nature, 249, 810, 1974

2. J.C. Farman, B.G. Gardiner, J.D. Shanklin: "*Large Losses of Total Ozone in Antarctica Reveal Seasonal ClO_x/NO_x Interaction*", Nature, 315, 207, 1985.

3. Alternative Fluorocarbon Environmental Acceptability Study, World Meteorological Organization Global Ozone Research and Monitoring Project, Report No. 20; Scientific Assessment of Stratospheric Ozone, Vol I and II; 1989.

4. Scientific Assessment of Ozone Depletion: 1991, World Meteorological Organization Global Ozone Research and Monitoring Project - Report No. 25.

5. W.B. DeMore, S.P. Sander, D.M. Golden, R.F. Hampson, M.J. Kurylo, C.J. Howard, A.R. Ravishankara, C.E. Kolb, M.J. Molina: "*Chemical Kinetics and Photochemical Data for Use in Stratospheric Modeling*", Jet Propulsion Laboratory Publication, 92-20, Pasadena, CA (1992).

6. D.A. Fisher, C.H. Hales, D.L. Filkin, M.K.W. Ko, N. Dak Sze, P.S. Connell, D.J. Wuebbles, I.S.A. Isaksen, and F. Stordal: "*Model Calculations of the Relative Effects of CFCs and Their Replacements on Stratospheric Ozone*", Nature, 344, 508, 1990.

7. D.A. Fisher, C.H. Hales, W.C. Wang, M.K.W. Ko, and N. Dak Sze: "*Model Calculations of the Relative Effects of CFCs and Their Replacements on Global Warming*" Nature, 344, 513, 1990.

8. T.J. Wallington, P. Dagaut, and M.J. Kurylo: "*Ultraviolet Absorption Cross Sections and Reaction Kinetics and Mechanisms for Peroxy Radicals in the Gas Phase*", Chem. Phys. Rev., 92, 667, 1992.

9. P.D. Lightfoot, R.A. Cox, J.N. Crowley, M. Destriau, G. Hayman, M.E. Jenkin, G.K. Moortgat, and F. Zabel: "*Organic Peroxy Radicals: Kinetics, Spectroscopy, and Tropospheric Chemistry*", Atmos. Environ., 26A, 1805, 1992.

10. J.M. Roberts: "*The Atmospheric Chemistry of Organic Nitrates*", Atmos. Environ., 24A, 243, 1990.

11. D. Koppenkastrop and F. Zabel: "*Thermal Decomposition of Chlorofluoromethyl Peroxynitrates*", Int. J. Chem. Kinet., 23, 1, 1991.

12. F. Kirchner, F. Zabel, K.H. Becker:"*Thermal Stability of $CClF_2CH_2O_2NO_2$, $CCl_2FCH_2O_2NO_2$ and $CClF_2C(O)O_2NO_2$*", STEP-HALOCSIDE/AFEAS Workshop, Dublin, May 14-16, 1991.

13. T.E. Møgelberg, O.J. Nielsen, J. Sehested, T.J. Wallington, M.D. Hurley, and W.F.S. Schneider, "*Kinetics and Mechanistic Study of the $CF_3CFHO_2+NO_2$ reaction*", Chem. Phys. Lett., 225, 375, 1994.

14. R.A. Cox and G.S. Tyndall:"*Rate Constants for Reactions of CH_3O_2 in the Gas Phase*", Chem. Phys. Lett., 65, 357, 1979.

15. S.P. Sander and R.T. Watson: "*Kinetic Studies of Reactions of CH_3O_2 with NO, NO_2, and CH_3O_2 and 298 K*", J. Phys. Chem., 84, 1664, 1980.

16. O. Morel, R. Simonaitis, and J. Heicklen: "*Ultraviolet Absorption of Spectra of HO_2NO_2, $CCl_3O_2NO_2$, $CCl_2FO_2NO_2$, and $CH_3O_2NO_2$*", Chem. Phys. Lett., 73, 38, 1980.

17. M.M. Maricq, J.J. Szente, M.D. Hurley, and T.J. Wallington, "*Atmospheric Chemsitry of HFC-134a: Kinetics and Mechanistic Study of the $CF_3CFHO_2+HO_2$ Reaction*", J. Phys. Chem., 98, 8962, 1994.

18. G. D. Hayman: "*The Kinetic and Mechanisms of Processes Involved in the Atmospheric Degradation of Hydrochlorofluorocarbons and Hydrofluorocarbons*", page 65, proceedings of the STEP-HALOCSIDE/AFEAS Workshop, University College Dublin, Ireland, March 1993.

19. G.D. Hayman, M.E. Jenkin, T.P Murrells, and C.E. Johnson: "*Tropospheric Degradation Chemistry of HFC-123 (CF_3CHCl_2): A proposed Replacement Chlorofluorocarbon*", Atmos. Environ., 28, 421, 1994.

20. V. Catoire, R. Lesclaux, P.D. Lightfoot, M.T. Rayez: "*Kinetic Study of the*

Reactions of CH_2ClO_2 with Itself and with HO_2, and Theoretical Study of the Reactions of CH_2ClO, between 251 K and 600 K", J. Phys. Chem., 98, 2889, 1994.

21. T.J. Wallington and M.D. Hurley: "*Atmospheric Chemistry of HC(O)F: Reaction with OH Radicals*", Environ. Sci. Tech., 27, 1448, 1993.

22. D.J. Scollard, J.J. Treacy, H.W. Sidebottom, C. Balastra-Garcia, G. Laverdet, G. LeBras, H. MacLeod, and S. Téton: "*Rate Constants for the Reactions of Hydroxyl Radicals and Chlorine Atoms with Halogenated Aldehydes*", J. Phys. Chem., 97, 4683, 1993.

23. H.R. Richer, J.R. Sodeau, and I. Barnes: "*The Photolysis and Chlorine-Initiated Photo-Oxidation of Trifluoroacetaldehyde*",page 182, Proceeding of the STEP-HALOCSIDE/AFEAS Workshop, University College Dublin, Ireland, March 1993.

24. J.S. Francisco: "*The Role of $CF_3C(O)O_x$ Radicals in Atmospheric Chemical Processes*", Chem. Phys. Lett., 191, 7, 1992.

25. P. Biggs, C.E. Canosa-Mas, D.E. Shallcross, R.P. Wayne, C. Kelly, H.W. Sidebottom: "*The possible Atmospheric Importance of the Reaction of CF_3O Radicals with Ozone*", page 177, proceedings of the STEP-HALOCSIDE/AFEAS Workshop, University Collage Dublin, Ireland, March 1993.

26. J.S. Francisco, A.N. Goldstein, Z. Li, Y. Zhao, and I.H. Williams: "*Theoretical Investigation of Chlorofluorocarbon Degradation Processes: Structure and Energetics of $XC(O)O_x$ Intermediates (X = F, Cl)*", J. Phys. Chem., 94, 4791, 1990.

27. J.S. Francisco: "*An ab initio Investigation of the Significance of the HOOF Intermediate in Coupling Reactions Involving FOO_x and HO_x Species*", J. Chem. Phys., 98, 2198, 1993.

28. T.E. Møgelberg, O.J. Nielsen, J. Sehested, T.J. Wallington, M.D. Hurley, and W.F. Schneider: "*Atmospheric Chemistry of CF_3COOH. Kinetics of the Reaction with OH Radicals*", Chem. Phys. Lett., 226, 171, 1994.

29. S. Carr, J.J. Treacy, H.W. Sidebottom, R.K. Connell, C.E. Canosa-Mas, R.P. Wayne, and J. Franklin: "*Kinetics and Mechanisms for the Reaction of Hydroxyl Radicals with Trifluoroacetic acid under Atmospheric Conditions*", Chem. Phys. Lett., 227, 39, 1994.

30. E. Erchel: "*World Water Balance*", Elsevier, New York, 1975.

31. J.C. Ball and T.J. Wallington: "*Formation of CF_3COOH from the Atmospheric Degradation of Hydrofluorocarbon 134a: A Human Health Concern?*", J. Air Waste Manag. Assoc., 43, 1260, 1993.

32. F. Zabel, F. Kirchner, and K.H. Becker: "*Thermal Decomposition of $CF_3C(O)O_2NO_2$, $CClF_2C(O)O_2NO_2$, and $CCl_3C(O)O_2NO_2$*", Int. J. Chem. Kinet., 26, 827, 1993.

33. G.I. Senum, Y.N. Lee, and J.S. Gaffney: "*Ultraviolet Absorption Spectrum of Peroxyacetyl Nitrate and Peroxypropionyl Nitrate*", J. Phys. Chem., 88, 1269, 1984.

34. A.R. Ravishankara, A.A. Turnipseed, N.R. Jensen, S. Barone, M. Mills, C.J. Howard, and S. Solomon: "*Do Hydrocarbons Destroy Stratospheric Ozone?*", Science, 263, 71, 1994.

35. T.J. Wallington, M.D. Hurley, and W.F. Schneider: "*Kinetic Study of the Reaction $CF_3O+O_3 \rightarrow CF_3O_2+O_2$*", Chem. Phys. Lett., 213, 442, 1993.

36. M.M. Maricq and J.J. Szente: "*Upper Limits for the Rate Constants of the Reactions $CF_3O+O_3 \rightarrow CF_3O_2+O_2$ and $CF_3O_2+O_3 \rightarrow CF_3O+2O_2$*", Chem. Phys. Lett., 213, 449, 1993.

37. C. Fockenberg, H. Saathoff, and R. Zellner: "*A Laser Photolysis/LIF Study of the Rate Constant for the Reaction $CF_3O+O_3 \rightarrow Products$*", Chem. Phys. Lett., 218, 21, 1994.

38. A.A. Turnipseed, S.B. Barone, and A.R. Ravishankara: "*Kinetics of the Reaction of CF_3O_x Radicals with NO, O_3, and O_2*", J. Phys. Chem., 98, 4594, 1994.

39. R. Zellner, private communication.

40. N.R. Jensen, D.R. Hanson, and C.J. Howard: "*Temperature dependence of the Gas Phase Reactions of CF_3O with CH_4 and NO*", J. Phys. Chem., 98, 8574, 1994.

41. J. Chen, V. Young, T. Zhu, and H. Niki: "*Long Path Fourier Transform Infrared Spectroscopic Study of the Reactions of CF_3OO and CF_3O Radicals with NO_2*", J. Chem. Phys., 97, 11696, 1993.

42. H. Saathoff and R. Zellner:"*LIF Detection of the CF_3O Radical and Kinetics of Its Reactions with CH_4 and C_2H_6*", Chem. Phys. Lett., 206,349, 1993.

43. C. Kelly, J. Treacy, H.W. Sidebottom, and O.J. Nielsen: "*Rate Constants for the Reaction of CF_3O Radicals with Hydrocarbons at 298 K*", Chem. Phys. Lett., 207, 498, 1993.

44. S.B. Barone, A.A. Turnipseed, and A.R. Ravishankara: "*Kinetics of the Reactions of the CF_3O Radical with Alkanes*", J. Phys. Chem., 98, 4602, 1994.

45. G. Brasseur and S. Solomon: "*Aeronomy of the Middle Atmosphere*", Reidel, Dordrect, 1986.

46. M. Ko and D. Sze, Private communication 1993.

47. M.K.W. Ko, N.D. Sze, J.M. Rodriguez, D.K. Weistenstein, C.W. Heisey, R.P. Wayne, P. Biggs, C.E. Canosa-Mas, H.W. Sidebottom, and J. Treacy: "*CF_3 Chemistry: Potential Implications for Stratospheric Ozone*", Geophys. Res. Lett., 21, 101, 1994.

48. T.J. Wallington, M.D. Hurley, T. Møgelbjerg, O.J. Nielsen, and J. Sehested: "*Atmospheric Chemistry of FCO_x Radicals: Kinetics and Mechanistic Study of the $FC(O)O_2+NO_2$ Reaction*", Chem. Phys. Lett. in press 1994.

49. H. Hippler, private communication 1993.

50. P. Pagsberg, E. Ratajczak, A. Sillesen, and J.T. Jodkowski: "*Spectrokinetic Studies of the Gas-phase Equilibrium $F+O_2 \rightleftharpoons FO_2$ between 295 and 359 K*", Chem. Phys. Lett., 141, 88, 1987.

51. Y.R. Bedzhanyan, E.M. Markin, and Y.M. Gershenzon: "*Experimental Study of Elementary Reactions of FO Radicals. I. Sources and Measurements of Absolute Concentrations. The Reaction $F + O_3 \rightarrow FO + O_2$*", Kinet. and Catal., 33, 591, 1992.

52. D.A. Lashof and D.A Ahuja:"*Relative Contribution of Greenhouse Gas Emissions to Global Warming*", Nature, 344, 529, 1990.

53. T. Ellermann: "*Atmospheric CCl_3 Degradation*", Risø-M-2932 1991.

54. F. Markert: "*The Atmospheric Degradation of Chlorinated Alkanes and Aromatic Compounds*", Ph.D. Thesis, Risø National Laboratory, Roskilde, Denmark, Risø, 1993.

55. C.M. Sauer Jr.: "*The use of pulse radiolysis to study transient species in the gas phase*", in J.H. Baxendalem and F. Busi: "The Study of Fast Processes and Transient Species by Electron Pulse Radiolysis", D. Reidei Publishing Company, 601-626, 1982.

56. T. Ellermann: "*FNO*", unpublished results 1992.

57. P.W. Atkins: "*Physical Chemistry*", Oxford University Press, Walton Street, Oxford OX2 6DP, Third edition, 1986.

58. K. Fagerström, A. Lund, P. Pagsberg, and A. Sillesen: "*A Computerized Pulse Radiolysis System for Gas Phase Kinetics*", Acta Chem. Scand., 47, 1057, 1993.

59. P. R. Griffiths and J. A. de Haseth: "*Fourier Transform Infrared Spectroscopy*" John Wiley & Sons.

60. M.M. Maricq and J.J. Szente: "*Flash Photolysis-Time-Resolved UV Absorption Study of the Reactions $CF_3H + F \rightarrow CF_3 + HF$ and $CF_3O_2 + CF_3O_2 \rightarrow$ Products*", J. Phys. Chem., 96, 4925, 1992.

61. O.L Rasmussen and E. Bjergbakke, Risø National Laboratory, Roskilde, Denmark, 1984, E. Bjergbakke, K. Sehested, O.L. Rasmussen, and H. Christensen, Risø-M-2430, Risø National Laboratory, Roskilde, Denmark, 1984.

62. R. Atkinson, D.L. Baulch, R. Cox, R.F. Hampson, Jr., J. Kerr, and J. Troe:"*Evaluated Kinetic and Photochemical Data for Atmospheric Chemistry*", J. Phys. Chem. Ref. Data, 18, 881, 1989.

63. T.J. Wallington, M.M. Maricq, T. Ellermann, and O.J. Nielsen, "*Novel Method for the Measurement of Gas phase Peroxy Radicals Absorption Spectrum*", J. Phys.Chem, 96, 982, 1991.

64. NIST Chemical Kinetics Database, Version 5.0

65. H. Adachi and N. Basco:"*Kinetic Spectroscopy Study of the Reaction of CH_3O_2 with NO*", Chem. Phys. Lett., 63, 490, 1979.

66. R.A. Cox and G.S. Tyndall:"*Rate Constants for the Reactions of CH_3O_2 with HO_2, NO, and NO_2 Using Molecular Modulation Spectroscopy*",J. Chem. Soc. Faraday Trans. 2 76, 153, 1980.

67. R. Simonaitis and J. Heicklen:"*Rate Coefficient for the Reaction of CH_3O_2 with NO from 218 to 365K*" J. Phys. Chem. 95, 2946, 1981.

68. I.C. Plumb, K.R. Ryan, J.R. Steven, and M.F.R. Mulcahy:"*Rate Coefficient for the Reaction of CH_3O_2 with NO*", J. Phys. Chem. 85, 3136, 1981.

69. A.R. Ravishankara, F.L. Eisele, N.M. Kreutter and P.H. Wine:"*Kinetics for the Reaction of CH_3O_2 with NO*", J. Chem. Phys. 74, 2267. 1981.

70. R. Zellner, B. Fritz, and K. Lorentz:"*Methoxy Formation in the Reaction of CH_3O_2 Radicals with NO*", J. Atmos. Chem. 4, 241, 1986..

71. H. Adachi and N. Basco: "*The Reaction of Ethyl Peroxy Radicals with NO_2*",Chem. Phys. Lett., 67, 324, 1979.

72. I.C. Plumb, K.R. Ryan, J.R. Steven, and M.F.R. Mulcahy:"*Kinetics of the Reaction of $C_2H_5O_2$ with NO at 295 K*", Int. J. Chem. Kinet. 14, 183, 1982.

73. H. Adachi and N. Basco:"*Reactions of Isopropyl Radicals with NO and NO_2*", Int. J. Chem. Kinet. 14, 1243, 1982.

74. J. Peeters, J. Vertommen, and I. Langhans:"*Rate Constants for the Reactions of CF_3O_2, i-$C_3H_7O_2$, and t-$C_4H_9O_2$ with NO*", Ber. Bunsenges. Phys. Chem., 96, 431, 1992.

75. T.J. Wallington and O.J. Nielsen:"*Pulse Radiolysis Study of CF_3CFHO_2 Radicals in the gas Phase at 298 K*", Chem. Phys. Lett., 187, 33, 1991.

76. I.C. Plumb and K.R. Ryan:"*Kinetics of the Reaction of $CF_3O_2$with NO*", Chem. Phys. Lett. 92, 236, 1982.

77. A.M. Dognon, F. Caralp, and R. Lesclaux:"*Reactions des Radicaux Chlorofluoromethyl Peroxyles avec NO: Etude Cinetique dans le Domaine de Temperature Compris entre 230 et 430 K*", J. Chim. Phys. 82, 349, 1985.

78. R. Lesclaux and F. Caralp:"*Determination of the Rate Constants for the Reactions*

of $CFCl_2O_2$ Radical with NO and NO_2 by use Photolysis and Time Resolved mass Spectrometry", Int. J. Chem. Kinet. 16, 1117, 1984.

79. K.R. Ryan and I.C. Plumb:"*Kinetics of the Reactions of CCl_3 with O and O_2 and of CCl_3O_2 with NO at 295K*", Int. J. Chem. Kinet. 16, 591, 1984.

80. T.J. Wallington and M.D. Hurley: "*FTIR Product Study of the Reaction of CD_3O_2+HO_2*", Chem. Phys. Lett., 193, 84, 1992.

81. A. S. Manocha, D. W. Setser, and M. A. Wickramaaratchi:"*Vibrational Energy Disposal in Reactions of Fluorine Atoms with Hydrides of Group III, IV, and V*", Chem. Phys. 76, 129, 1983.

82. M.A. Wickramaaratchi, D.W. Setser, H. Hildebrandt, B. Korbitzer, and H. Heydtmann:"*Evaluation of HF Product Distributions Deduced from Infrared Chemiluminescence II, F Atoms Reactions*", Chem. Phys. Lett., 94, 109, 1985.

83. R.S. Iyer and F.S. Rowland:"*Thermal F/X Atomic Substitution Reactions with Methyl halides (X=Cl, Br, I)*", J. Phys. Chem. 65, 2493, 1981.

84. O.J. Nielsen, J. Munk, G. Locke, and T.J. Wallington:"*Ultraviolet Absorption Spectra and Kinetics of the Self-Reaction of CH_2Br and CH_2BrO_2 Radicals in the Gas Phase at 298 K*", J. Phys. Chem., 95, 8714, 1991.

85. M.A.A. Clyne and A. Hodgson:"*Absolute Rate Constants for the Reactions of Fluorine Atoms with H_2, CH_2Cl_2, CH_2ClF, CH_2F_2, and $CHCl_3$*", J. Chem. Soc. Faraday Trans. 2, 81, 443, 1985.

86. O.J. Nielsen, T. Ellermann, E. Bartkiewicz, T.J. Wallington, and M.D. Hurley:"*UV Absorption Spectra, Kinetics, and Mechanisms of the Self-Reaction of CHF_2O_2 Radicals in the Gas Phase at 298 K*", Chem. Phys. Lett., 192, 82, 1992.

87. D.L. Baulch, J. Duxbury, S.J. Grant, and D.C. Montague: "*Evaluated Kinetic Data for high Temperature Reactions. Volume 4. Homogeneous Gas Phase Reactions of Halogen- and Cyanide- Containing Species*", J. Phys. Chem. Ref. Data, 10, Supplement 1, 1-1, 1981.

88. M.M. Maricq and J.J. Szente:"*Flash Photolysis-Time-Resolved UV Absorption Study of the Reactions $CF_3H + F \rightarrow CF_3 + HF$ and $CF_3O_2 + CF_3O_2 \rightarrow$ Products*", J. Phys. Chem., 96, 4925, 1992.

89. H. Wagner, J. Warnatz, and C. Zetzsch:"*On the Reaction of F Atoms with Methane*", Anales Assoc. Quin. Argentina, 59, 169, 1971.

90. K.L. Kompa and J. Wanner:"*Study of some Fluorine Atom Reactions Using a Chemical Laser Method*", Chem. Phys. lett., 12, 560, 1972.

91. M.A.A. Clyne, D.J. McKenny, and R.F. Walker:"*Reactions Kinetics of Ground State Fluorine, F(2P), Atoms. I. Measurements of Fluorine Atom Concentrations and the Rates of Reactions F + CHF_3 and F + Cl_2 Using Mass Spectrometry*", Can. J. Chem., 51, 3596, 1973.

92. D.M. Fasano and N.S. Nogar:"*Rate Determination of F + CH_4 by Real-Time Competitive Kinetics*", Chem. Phys. Lett., 92, 411, 1982.

93. P. Pagsberg, J. Munk, and A. Sillesen:"*UV-Spectrum and Kinetics of Hydroxymethyl radicals*", Chem. Phys. Lett. 146, 375, 1988.

94. U. Worsdorfer and H. Heydtmann:"*Bimolecular Reactions of Fluorine Atoms with CH_3I and CH_2I_2*", Ber. Bunsenges. Phys. Chem., 93, 1132, 1989.

95. A.J. Arvía and P.J. Aymonino:"*Infrared Absorption Spectra of Bis(monofluorocarbonyl)- and Bis(trifluoromethyl)-Peroxide*", Spectrochimica Acta, 18, 1299, 1962.

96. W. Braun, J.T. Herron, and D.K. Kahaner:"*Acuchem: A Computer Program for Modeling Complex Chemical Reaction Systems*", Int. J. Chem. Kinet., 20, 51, 1988.

97. R.C. Kennedy and J.B. Levy:"*Bistrifluoromethyl Peroxide. II. Kinetics of the Decomposition to Carbonyl Fluoride and Trifluoromethyl Hypofluoride*", J. Phys. Chem., 76, 3480, 1972.

98. L. Batt and R. Walsh:"*A Reexamination of Pyrolysis of Bistrifluoromethyl Peroxide*", Int. J. Chem. Kinet., 14, 933, 1982.

99. E.O. Edney and D.J. Driscoll: "*Chlorine Initiated Photooxidation of Hydrochlorofluorocarbons (HCFCs) and Hydrofluorocarbons (HFCs): Results for HCFC-22 ($CHClF_2$); HFC-41 (CH_3F): HCFC-124 ($CClFHCF_3$); HFC-134a (CF_3CH_2F); HCFC-142b ($CClF_2CH_3$); and HFC-152a (CHF_2CH_3)*", Int. J. Chem. Kinet., 24, 1067, 1992.

100. E.C. Tuazon and R. Atkinson: *"Tropospheric Transformation Products of a Series of Hydrofluorocarbons and Hydrochlorofluorocarbons"*, J. Atmos. Chem., 17, 179, 1993.

101. T.J. Wallington, J.C. Ball, O.J. Nielsen, and E. Bartkiewicz:*"Spectroscopic, Kinetic, and Mechanistic Study of CH_2FO_2 Radicals in the Gas Phase at 298 K"*, J. Phys. Chem., 96, 1241, 1992.

102. T.J. Wallington, M.D. Hurley, J.C. Ball, and E.W. Kaiser:*"Atmospheric Chemistry of Hydrofluorocarbon 134a: Fate of the Alkoxy Radical CF_3CFHO"*, Environ. Sci. Technol., 26, 1318, 1992.

103. P. Dagaut, T.J. Wallington, and M.J. Kurylo: *"The UV Absorption Spectra and Kinetics of the Self Reactions of CH_2ClO_2 and CH_2FO_2 Radicals in the Gas Phase"*, Int. J. Chem. Kinet., 20, 815, 1988.

104.. T.J. Wallington, M.D. Hurley, and M.M. Maricq:*"FTIR Product Study of the Self-reaction of FC(O)O Radicals"*, Chem. Phys. Lett., 205, 62, 1993.

105. T.J. Bevilaqua, D. Hanson, and C.J. Howard: *"Chemical Ionization Mass Spectroscopy Studies of the Gas Phase Reactions CF_3O_2+NO, CF_3O+NO, and CF_3O+RH"*, J. Phys. Chem., 97, 3750, 1993.

106. S. Benson: *"Comment on the Thermochemistry of the CF_3O Radical and CF_3OH"*, J. Phys. Chem., 98, 2216, 1994.

ELSEVIER

18 February 1994

Chemical Physics Letters 218 (1994) 287–294

CHEMICAL PHYSICS LETTERS

Kinetics of the reaction of F atoms with O_2 and UV spectrum of FO_2 radicals in the gas phase at 295 K

Thomas Ellermann [a], Jens Sehested [a], Ole John Nielsen [a], Palle Pagsberg [a], Timothy J. Wallington [b]

[a] *Chemical Reactivity Section, Environmental Science and Technology Department, Risø National Laboratory, DK-4000 Roskilde, Denmark*

[b] *Ford Research Laboratory, Ford Motor Company, SRL-E3083, P.O. Box 2053, Dearborn, MI 48121-2053, USA*

Received 28 June 1993; in final form 16 December 1993

Abstract

The ultraviolet absorption spectrum of FO_2 radicals and the kinetics of the reaction of F atoms with O_2 have been studied in the gas phase at 295 K using pulse radiolysis combined with kinetic UV spectroscopy. At 230 nm, $\sigma_{FO_2} = (5.08 \pm 0.70) \times 10^{-18}$ cm^2 molecule^{-1}. The kinetics of the reaction $F + O_2 + M \rightarrow FO_2 + M$ (1), were investigated over the pressure range 200–1000 mbar of SF_6 diluent. At 1 atm total pressure the pseudo-second-order rate constant for reaction (1) was determined to be $(1.9 \pm 0.3) \times 10^{-13}$ cm^3 molecule^{-1} s^{-1}.

1. Introduction

In laboratory studies of the simulated atmospheric oxidation of organic compounds, fluorine atom initiation provides a convenient surrogate for the OH radical initiated photo-oxidation that occurs in the atmosphere. Pulse radiolysis of sulphur hexafluoride, SF_6, has been used extensively in our laboratory as a source of fluorine atoms in kinetic and spectroscopic studies of a series of alkylperoxy (RO_2) radicals [1–4]. The formation of FO_2 radicals via reaction (1) is a potential complication in such studies and needs careful consideration,

$$F + O_2 + M \rightarrow FO_2 + M. \qquad (1)$$

FO_2 radicals absorb strongly in the wavelength region from 200 to 250 nm, the same range where alkylperoxy radicals absorb. The fluorine atom in FO_2 is weakly bound (F–O_2 bond strength = 13 kcal mol^{-1} [5]). In one bar of argon diluent at 295 K the rate of decomposition of FO_2 radicals into F atoms and O_2 is 450 s^{-1} [5]. Depending upon the time scale of the experimental observations, reaction (−1) may also need to be considered.

$$FO_2 + M \rightarrow F + O_2 + M \qquad (-1)$$

To avoid, or correct for, potential complications associated with the formation of FO_2 radicals requires kinetic data for the rate constants k_1 and k_{-1}, and UV absorption cross sections for FO_2. There have been several studies of the kinetics of reaction (1) using a variety of third-body diluent gases [5–9]. At 1 bar total pressure, reaction (1) is in the falloff region between second- and third-order kinetics. As expected, k_1 increases with the molecular complexity of the diluent gas. Diatomic molecules such as N_2 and F_2 are more effective third bodies than monatomics such as Ar and He [9]. Polyatomics such as SF_6 are expected to be more effective than diatomics. However, there has been no systematic study of the effi-

SSDI 0009-2614(94)00006-C

ciency of SF_6 as a third body in reaction (1).

The UV spectrum of FO_2 radicals has been the subject of several studies [5,9–11]. While there is good agreement with regard to the shape of the absorption spectrum, discrepancies exist in the reported absolute absorption cross sections. Matchuk et al. [10] and more recently Pagsberg et al. [5] were the first to study the absorption spectrum of FO_2 radicals. Each report a maximum absorption cross section at 206–210 nm of $(1.9–2.0)\times10^{-17}$ cm^2 $molecule^{-1}$. In contrast, the two most recent studies of Lyman and Holland [9] and Maricq and Szente [11] suggest a lower value of $\sigma(FO_2)_{max}=1.3\times10^{-17}$ cm^2 $molecule^{-1}$.

To resolve uncertainties associated with the UV spectrum of FO_2 radicals and to provide kinetic data for reaction of F atoms with O_2 in SF_6 diluent we have conducted a pulse radiolysis study of SF_6/O_2 mixtures. Results are reported herein.

2. Experimental

The pulse radiolysis transient UV absorption spectrometer used in this work has been described in detail previously [12–14]. Fluorine atoms were generated by the pulsed radiolysis of SF_6 in a 1 ℓ stainless-steel reaction cell using a 30 ns pulse of 2 MeV electrons from a Febetron 705B accelerator.

$$SF_6 + 2\,MeV\ e^- \rightarrow F + products\ . \qquad (2)$$

Irradiation of 1000 mbar of SF_6 using the maximum radiolysis dose resulted in the formation of an initial F atom concentration of 3.44×10^{15} cm^{-3} (calibration was achieved by monitoring the formation of CH_3O_2 radicals following radiolysis of $CH_4/O_2/SF_6$, see section 3 for further details). The irradiation dose was varied by inserting electron beam attenuators between the accelerator and the reaction cell. The reaction cell was equipped with internal mirrors to provide an optical pathlength of 40–120 cm for the UV analysis light beam. After dispersal by a 1 m Hilger and Watts grating monochromator, the analysis beam was detected by a Hamatsu R928 photomultiplier coupled with a Biomation 8100 waveform digitizer. All experiments were carried out at 295 ± 2 K. Kinetic simulations were carried out using the CHEMSIMUL and ACUCHEM computer programs [15,16].

The partial pressures of the gases were measured using an absolute electronic membrane manometer with a resolution of 10^{-3} bar. SF_6 (99.9%) was supplied from Hede-Nielsen Ltd. and ultra-high-purity O_2 was obtained from Alfax Ltd. Both reagents were used as received.

3. Results and discussion

3.1. UV absorption of FO_2 radicals

Fig. 1 shows a typical absorption transient recorded at 230 nm during the pulsed radiolysis (one third of full dose) of a mixture of 50 mbar of O_2 and 950 mbar of SF_6. Control experiments were performed in which either 50 mbar of O_2, or 950 mbar of SF_6, were irradiated; no significant transient absorption (< 0.005 absorbance units) was observed. We ascribe the absorption shown in Fig. 1 to the formation of FO_2 radicals.

Measurement of absolute absorption cross sections for FO_2 radicals requires absolute calibration of the initial F atom yield. This calibration was achieved by monitoring the transient absorption at 230 nm of methyl peroxy radicals produced by radiolysis of $SF_6/CH_4/O_2$ mixtures. Fig. 2A shows the maximum absorbance of CH_3O_2 and FO_2 radicals as a function of dose at 230 nm following the radiolysis of $SF_6/CH_4/O_2$ and SF_6/O_2 mixtures, respectively. The data for FO_2 have been shifted vertically by 0.1 units for clarity. For the generation of CH_3O_2 the initial condi-

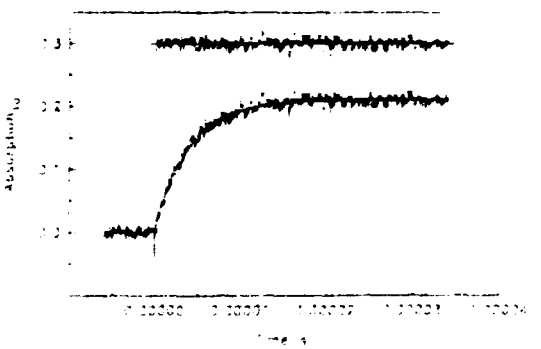

Fig. 1. Absorption at 230 nm following the pulsed radiolysis of a mixture of 50 mbar O_2 and 950 mbar of SF_6. Single pulse, one third of maximum dose and no signal averaging. The smooth line is a first-order fit with $k_{obs}=2.5\times10^5\ s^{-1}$.

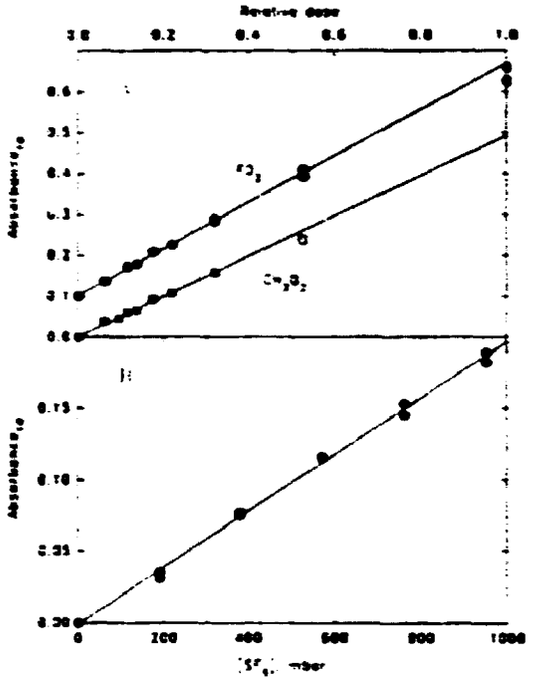

Fig. 2. (A) Maximum transient absorption of FO_2 and CH_3O_2 radicals at 230 nm following the pulsed radiolysis of 50 mbar O_2 in 950 mbar of SF_6 and 10 mbar CH_4 in 35 mbar of O_2 and 955 mbar of SF_6, respectively, as a function of radiolysis dose. The solid lines are linear regressions. The data for FO_2 (●) has been shifted vertical by 0.1 units for clarity. (B) Maximum transient absorption at 230 nm following the pulsed radiolysis of mixtures of 5% O_2 in SF_6 as a function of SF_6 concentration. The solid line is a linear regression. One third of maximum dose and an optical pathlength of 80 cm.

tions were $[SF_6]=955$ mbar, $[CH_4]=10$ mbar, and $[O_2]=35$ mbar. For the generation of FO_2 radicals the initial conditions were $[SF_6]=950$ mbar and $[O_2]=50$ mbar. As seen from Fig. 2A, in the CH_3O_2 experiments using one half of the full radiolysis dose the initial absorption was approximately 10% lower than expected based upon extrapolation of the data obtained at lower doses. Similarly, in the FO_2 experiments using full dose the initial absorption was also less than expected from the lower dose experiments.

We ascribe the curvature in the plots of CH_3O_2 and FO_2 absorbance versus radiolysis dose to secondary chemistry resulting in incomplete conversion of F atoms into CH_3O_2, or FO_2, radicals. Linear least-squares analysis of the data in Fig. 2A (half dose CH_3O_2, and full dose FO_2 experiments excepted) gives slopes of 0.566 ± 0.019 and 0.491 ± 0.027 for the FO_2 and CH_3O_2 data, respectively. Quoted errors are 2 standard deviations from the least-squares fits. Therefore, at 230 nm, $\sigma(FO_2)/\sigma(CH_3O_2)=1.15\pm0.08$ (errors are calculated using conventional error propagation analysis). Using the recommended value of $\sigma(CH_3O_2)_{230\,nm}=4.30\times10^{-18}$ cm^2 molecule^{-1} [17] gives $\sigma(FO_2)=(4.95\pm0.34)\times10^{-18}$ cm^2 molecule^{-1}. The recommended value for $\sigma(CH_3O_2)$ can be combined with the observed slope of the CH_3O_2 data in Fig. 2A to provide a calibration of the initial F atom concentration of $(3.44\pm0.19)\times10^{15}$ cm^{-3} at full radiolysis dose and 1000 mbar of SF_6. Quoted errors reflect statistical uncertainties (2 standard deviations), possible systematic errors are discussed later. Formation of FO_2 in this system under these experimental conditions is not significant.

An additional determination of $\sigma(FO_2)$ was performed by monitoring the maximum initial absorption at 230 nm following the pulse radiolysis (one third of full dose, 80 cm UV pathlength) of a mixture of 5% O_2 in SF_6 over a range of total pressure from 200–1000 mbar. Fig. 2B shows a plot of the maximum absorption observed as a function of the partial pressure of SF_6 in the mixture. No departure from linearity is evident in Fig. 2B. The lack of curvature is consistent with the data presented in Fig. 2A, where it is seen that for initial absorbances of less than 0.3 units the yield of FO_2 radicals is a linear function of the radiolysis dose (and hence initial F atom concentration). Linear least-squares analysis of the data in Fig. 2B gives a slope $=(0.198\pm0.007)\times10^{-3}$. This can be combined with the initial F atom yield of $(3.44\pm0.19)\times10^{15}$ cm^{-3} at 1000 mbar with full radiolysis dose to give $\sigma(FO_2)=(5.21\pm0.35)\times10^{-18}$ cm^2 molecule^{-1} at 230 nm. This determination is in good agreement with the value of $\sigma(FO_2)=(4.95\pm0.34)\times10^{-18}$ cm^2 molecule^{-1} determined from the data in Fig. 2A. We chose to quote the average of the two separate measurements, $(5.08\pm0.49)\times10^{-18}$ cm^2 molecule^{-1}.

Errors quoted thus far represent statistical uncertainty. We must also consider possible systematic error associated with uncertainties in $\sigma(CH_3O_2)_{230\,nm}$. In the review of Wallington et al. [17] the uncertainty in $\sigma(CH_3O_2)$ was estimated to be ±15%. Since this review the results of additional studies of

$\sigma(CH_3O_2)$ have become available [1,18]. The latest results are in close agreement (within 10% at 220–250 nm) with the recommendations of Wallington et al. [17]. At present it seems reasonable to assign an uncertainty of ±10% to $\sigma(CH_3O_2)$. Using a conventional propagation of error analysis to combine the statistical errors and possible systematic uncertainties gives $\sigma(FO_2) = (5.08 \pm 0.70) \times 10^{-18}$ cm^2 molecule^{-1}, where the quoted errors reflect the accuracy of our measurement.

To map out the absorption spectrum of the FO_2 radical, experiments were performed to measure the initial absorbance between 215 and 254 nm following the pulsed radiolysis of mixtures of SF_6 and O_2. Initial absorptions were then scaled to that at 230 nm. Using this approach absorption cross sections (in units of 10^{-18} cm^2 molecule^{-1}) of 12.6, 10.2, 7.55, 3.41, 1.80, 1.53, and 0.69 were obtained at 215, 220, 225, 235, 240, 245, and 254 nm respectively. These cross sections are plotted in Fig. 3 together with the available literature data.

The absorption cross sections measured in the present work are slightly larger than those reported by Lyman and Holland [9] and Maricq and Szente [11] and significantly lower than those reported by Pagsberg et al. [5]. Over the wavelength range 215–235 nm the results reported by Maricq and Szente [11] are 14% lower than the results from the present work while the data of Pagsberg et al. [5] is 32% higher than our present results. As discussed above, the accuracy of the absorption cross section measurements in the present work is estimated to be ± 14%.

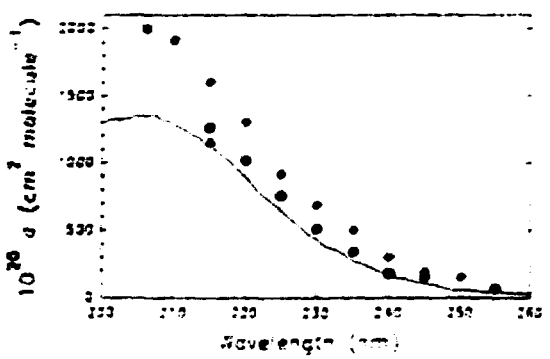

Fig. 3. Absorption cross section data for FO_2 measured in this work (circles) compared with previously reported data from Matchuk et al. [10] (■), Pagsberg et al. [5] (●), Lyman and Holland [9] (▲) and Maricq and Szente [11] (——).

Pagsberg et al. [5] have estimated the accuracy of their cross section data to be ± 10%. Maricq and Szente [11] cite an uncertainty range of ± 15%. Within the experimental uncertainties, the present work is indistinguishable from that of Lyman and Holland [9] and Maricq and Szente [11] but is distinct from that of Pagsberg et al. [5].

It is interesting to consider the origin of the ≈ 30% discrepancy between $\sigma(FO_2)$ values measured in the present work and those reported previously by Pagsberg et al. [5]. With the exception of one detail, the experimental method and techniques used are identical. The only significant difference is the chemical system used to generate F atoms. In the present work the radiolysis of an excess of SF_6 was used. In the previous work an excess of Ar was radiolyzed in the presence of a small amount of SF_6, which served to convert excited Ar atoms into F atoms.

$$Ar + 2\ MeV\ e^- \rightarrow Ar^* . \quad (3)$$

$$Ar^* + SF_6 \rightarrow Ar + SF_5 + F . \quad (4)$$

There is a possible complication with the use of reactions (3) and (4) to produce F atoms; namely the generation of SF_5 radicals. SF_5 radicals react with O_2 to give SF_5O_2 radicals (SF_5O_2 radicals are known intermediates in a variety of chemical systems, for example the decomposition of the trioxide SF_5OOOSF_5 [19]). While there have been no reports of the UV spectrum of SF_5O_2 radicals, it seems reasonable to speculate that SF_5O_2 radicals, like FO_2, will display a significant UV absorption. The formation of SF_5O_2 radicals may explain why the absorption cross sections reported previously [5] are approximately 30% higher than measured in the present work. To test this hypothesis several pieces of information are required: (i) the SF_5 yield from reaction (4), (ii) the absorption spectrum of SF_5 radicals, (iii) the rate of reaction of SF_5 radicals with O_2, and (iv) the absorption spectrum of SF_5O_2 radicals. Unfortunately, none of this information is available currently and a detailed study of SF_5/SF_5O_2 is beyond the scope of the present experiments, but will be undertaken in the future.

At this point it should be noted that Anastasi et al. [20] have studied the products following the radiolysis of SF_6. Their results are consistent with SF_6 being the major product. SF_6 does not react with O_2

and is not expected to lead to any complications in measurements of $\sigma(FO_2)$.

3.2. Kinetics of the reaction $F+O_2+SF_6 \rightarrow FO_2+SF_6$

As seen from Fig. 1, the decay of FO_2 is slow compared to its formation. The kinetics of formation and decay of FO_2 radicals can be treated separately. The solid line in Fig. 1 is a first-order fit. In all cases the observed increase in UV absorption at 215–245 nm was well fit by first-order kinetics. Fig. 4A shows a plot of the pseudo-first-order rate, k^{1st}, of the appearance of absorption at 240 nm following radiolysis (full dose) of mixtures of 950 mbar of SF_6 and 2–60 mbar of O_2 versus the oxygen concentration. Linear least-squares analysis of the data gives a pseudo-second-order rate constant of $k_1 = (1.93 \pm 0.10) \times 10^{-13}$ cm^3 molecule^{-1} s^{-1} at 950 mbar total pressure of SF_6 diluent. Quoted errors are 2 standard deviations. While the estimation of systematic errors is difficult, we believe that systematic uncertainties in the present series of measurements could add an additional 10% uncertainty to k_1. Hence, we arrive at our final value of $k_1 = (1.93 \pm 0.29) \times 10^{-13}$ cm^3 molecule^{-1} s^{-1}.

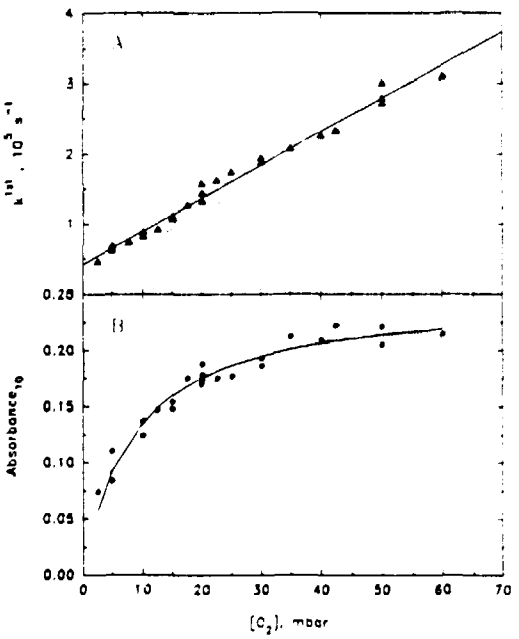

Fig. 4. (A) Plot of k^{1st} (measured at 240 nm) versus O_2 concentration for experiments using 995 mbar SF_6 and full radiolysis dose. The solid line is a linear regression. The dotted line is the behavior predicted using the chemical mechanism in Table 1, see text for details. (B) Maximum transient absorbance at 240 nm observed in the experiments used to derive the kinetic data shown in Fig. 4A. The optical pathlength was 80 cm. The solid line is a fifth-order fit to aid in visual inspection of the data trend. The dotted line is the behavior predicted using the chemical mechanism in Table 1, see text for details.

The linear least-squares fit of the data in Fig. 4A gives a significant positive intercept. We ascribe this intercept to the presence of secondary reactions which consume either F atoms, or FO_2 radicals, or both. Similar behavior has been reported previously in recent studies of the reaction of F atoms with CH_3Br [21] and CF_3CCl_2H (HCFC-123) [22]. Evidence for the importance of secondary reactions comes from the observation of a significant decrease in the maximum absorbance at low concentrations of O_2. Fig. 4B shows the dependence of the maximum absorbance (and hence the FO_2 yield) on the oxygen partial pressure for the same series of experiments used to derive the kinetic data presented in Fig. 4A. For experiments performed using partial pressures of O_2 greater than 35 mbar, variation of the oxygen concentration had no discernable effect on the maximum absorbance. However, the absorbance decreased by a factor of 3 as the O_2 partial pressure was reduced from 35 to 2 mbar.

At this point we need to consider the possible radiolysis of O_2 in the reaction cell to generate O atoms. As reported previously, the radiolysis of 1000 mbar of O_2 using full radiolysis dose results in the formation of 9.4×10^{14} molecule cm^{-3} of ozone [1]. Ozone is formed by the reaction of O atoms with O_2 and serves as a measure of the efficiency of O atom production in the system. The maximum O_2 partial pressure used in the present work was 50 mbar. The maximum O atom yield in the present experiments will then be 4.7×10^{13} cm^{-3} (a factor of 70 less than the initial F atom concentration). At this low concentration, O atoms are not expected to pose a complication in the present work.

Possible secondary reactions which could account for the observed trend in Fig. 4B are

$$F+F+M \rightarrow F_2+M, \quad (5)$$

$$F+FO_2+M \rightarrow F_2O_2+M, \quad (6a)$$

$$F+FO_2 \rightarrow F_2+O_2, \quad (6b)$$

$$FO_2 + FO_2 + M \rightarrow F_2O_4 \text{ (or } F_2 + 2O_2) + M . \quad (7)$$

$$F + SF_4 \rightarrow SF_5 + M . \quad (8)$$

$$F + SF_5 \rightarrow SF_6 + M . \quad (9)$$

To provide insight into the potential importance of these reactions the Acuchem program [16] was used with the mechanism given in Table 1 to model the chemical system. With the exception of reaction (8), kinetic data were taken from the literature [5,9,23,24]. The rate constant for reaction (8) was taken from a recent study in our laboratory [25]. There are no data available concerning the rate of decomposition of FO_2 radicals in SF_6 diluent. Pagsberg et al. [5] report $K_{eq} = k_1/k_{-1} = 2.38 \times 10^{-16}$ cm^3 molecule^{-1} at 293 K [5]. Using the value of $k_1 = (2.0 \pm 0.3) \times 10^{-13}$ cm^3 molecule^{-1} s^{-1}, we derive $k_{-1} = 810$ s^{-1} at 1000 mbar total pressure of SF_6 diluent; this value was used in the mechanism. The initial conditions used in the simulation were $[F]_0 = 3.3 \times 10^{15}$ cm^{-3}, $[SF_6] = 950$ mbar and $[O_2] = 2$–60 mbar. In addition to F atoms, the pulse radiolysis of SF_6 produces SF_4 [20]. The initial concentration of SF_4 used in the model was set equal to one half of that of F atoms.

The behavior of the absorption maximum with changes in $[O_2]$ predicted using the chemical mechanism in Table 1 is represented by the dotted line in Fig. 4B. It can be seen that while the mechanism does not precisely fit the observed data it does reproduce the gross features. At this point it should be noted that the kinetic data in Table 1 were taken from the literature; no attempt was made to fit the data by the adjustment of any of the parameters. The fact that the mechanism overpredicts the maximum absorption at low O_2 concentrations by approximately 10% indicates that either the mechanism is incomplete, or that one of the rate parameters used is in error, or both. It seems likely that the small difference between the observed and predicted behavior in Fig. 4B lies in uncertainties in the kinetic data used in the mechanism. Reaction (8) is the most important secondary reaction. If k_8 is increased by 10% and k_1 is decreased by 5% (both changes are within the quoted uncertainties of the reported rate constants) then the predicted absorption at 2 mbar O_2 concentration drops by 10%, i.e. within the range observed experimentally.

The aim of the present work is to investigate the kinetics of the reaction of F atoms with O_2, not to study the secondary reactions (5)–(9). The modelling exercise was not pursued further. To determine the effect of reactions (5)–(9) on the kinetic data shown in Fig. 4A first-order fits were made to the simulated FO_2 rise curves. The dotted line in Fig. 4A represents the results from the modelling study. The slope of the dotted line in Fig. 4A returns a value of k_1 equal to that used in the model. Hence, secondary reactions (5)–(9) should not affect the value k_1 derived from the experimental data.

As an additional check that secondary reactions do not influence the measured value of k_1 a series of kinetic experiments were performed using $[O_2] = 50$ mbar, $[SF_6] = 950$ mbar, and radiolysis doses of less

Table 1
Chemical mechanism

Reaction	k (cm^3 molecule^{-1} s^{-1})	Ref.
$F + O_2 + M \rightarrow FO_2 + M$	2.0×10^{-13}	this work
$FO_2 + M \rightarrow F + O_2 + M$	810 [a]	see text
$F + F + M \rightarrow F_2 + M$	4.0×10^{-15}	[22] [b]
$F + FO_2 + M \rightarrow F_2O_2 + M$	8.8×10^{-13}	[9] [c]
$F + FO_2 \rightarrow F_2 + O_2$	9.5×10^{-14}	[9]
$FO_2 + FO_2 + M \rightarrow F_2O_4$ (or $F_2 + 2O_2$) + M	1.7×10^{-17}	[5]
$F + SF_4 \rightarrow SF_5 + M$	1.2×10^{-11}	[23]
$F + SF_5 \rightarrow SF_6 + M$	1.7×10^{-11}	[24]

[a] Units of s^{-1}.
[b] We assume that the third-body efficiency of SF_6 is twice that of Ar.
[c] Assumed to be at high-pressure limit in 1000 mbar of SF_6.

than, or equal to, one third of the maximum. As shown in Figs. 2A and 4B, under these conditions the impact of secondary reactions is negligible. The measured half-lives for the formation of FO_2 radicals at different monitoring wavelengths and radiolysis doses are shown in Table 2. The measured formation half-lives do not change significantly with a threefold change of the irradiation dose (and hence initial fluorine atom concentration), confirming that any secondary chemistry has negligible influence here. The formation kinetics were independent of wavelength, suggesting the presence of only one absorbing species. A value of $k_1 = (1.96 \pm 0.40) \times 10^{-13}$ cm^3 molecule^{-1} s^{-1} at 950 mbar of SF_6 was determined from a mean of the experiments listed in Table 2, which is in agreement with the result obtained from the pseudo-first-order plot in Fig. 4A.

Finally, k_1 was determined at five different pressures in the range 200–1000 mbar. The results shown in Fig. 5 and given in table 3 show that k_1 is in the falloff region at 200–1000 mbar SF_6. The solid line in Fig. 5 is a two-parameter fit to the Troe expression for the pressure dependence of termolecular reactions [26]. Using $F_c = 0.6$, k_0 and k_∞ were determined to be 1.4×10^{-32} cm^6 molecule^{-1} s^{-1} and 2.0×10^{-12} cm^2 molecule^{-1} s^{-1}, respectively. The extrapolation to the high-pressure limit is uncertain. Experiments are needed at pressures significantly greater than 1000 mbar to better determine k_∞. The value determined for k_0 was insensitive to changes in k_∞. Fixing k_∞ a factor of 5 higher, or a factor of 2 lower only resulted in a 20% change in the best fit value of k_0. Hence, ±20% can be taken as an estimate of the uncertainty for k_0. Calculated falloff curves in both cases provide a reasonable fit of the data in Fig. 5. The value for k_0 determined in this work is consistent with k_0^{298} obtained by Lyman and Holland (He: 2.8×10^{-33}; Ar: 3.1×10^{-33}; F_2: 1.1×10^{-32}; in units of cm^6 molecule^{-1} s^{-1}) and Pagsberg and co-workers (Ar: 4.5×10^{-33} cm^6 molecule^{-1} s^{-1}) when the difference in third body is taken into account.

Table 2
Formation half-lives for FO_2

Dose (fraction of maximum)	Wavelength (nm)	Half-life (μs)
0.32	230	2.82
0.22	230	2.91
0.18	230	3.10
0.14	230	3.05
0.11	230	3.30
0.32	215	2.50
0.32	220	2.43
0.32	235	2.70
		average 2.87 ± 0.59

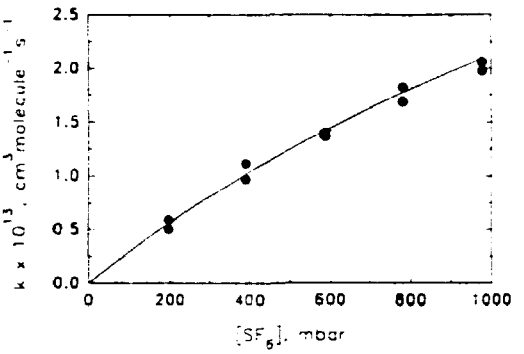

Fig. 5. Values of the rate constant for the reaction $F + O_2 + SF_6 \rightarrow FO_2 + SF_6$ as a function of total pressure as determined in the pulse radiolysis of mixtures of 5% O_2 in SF_6.

Table 3
Measured pseudo-second-order rate constants for the $F + O_2$ reaction

Total pressure (mbar)	$10^{13} k$ (cm^3 molecule^{-1} s^{-1})
200	0.55
400	1.04
600	1.38
800	1.75
1000	1.93

Recently, Hippler [27], using a flash photolysis technique, has reported $\sigma(FO_2)$ at 220 nm = $(1.5 \pm 0.1) \times 10^{-17}$ cm^2 molecule^{-1}. This result is approximately 50% larger than measured in our work. The origin of the discrepancy is unclear.

4. Acknowledgement

Financial support from the Commission of the European Communities is gratefully acknowledged.

5. References

[1] T.J. Wallington, M.M. Maricq, T. Ellermann and O.J. Nielsen, J. Phys. Chem. 96 (1992) 982.
[2] T.J. Wallington, J.C. Ball, O.J. Nielsen and E. Bartkiewicz, J. Phys. Chem. 96 (1992) 1241.
[3] O.J. Nielsen, T. Ellermann, E. Bartkiewicz, T.J. Wallington and M.D. Hurley, Chem. Phys. Letters 192 (1992) 82.
[4] O.J. Nielsen, T. Ellermann, J. Sehested, E. Bartkiewicz, T.J. Wallington and M.D. Hurley, Intern. J. Chem. Kinetics 24 (1992) 1009.
[5] P. Pagsberg, E. Ratajcak, A. Sillesen and J. Jodkowski, Chem. Phys. Letters 141 (1987) 88.
[6] C. Zetzch, in First European symposium on combustion, ed. F.J. Weinberg (Academic Press, New York, 1973), p 35.
[7] I.W.M. Smith and D.J. Wrigley, Chem. Phys. Letters 70 (1980) 481.
[8] I.W.M. Smith and D.J. Wrigley, Chem. Phys. 63 (1981) 321.
[9] J.L. Lyman and R. Holland, J. Phys. Chem. 92 (1988) 7232.
[10] M.M. Matchuk, V.I. Tupikov, A.I. Malkova and S.Ya. Pshezhetskii, Opt. Spectry. 40 (1967) 7.
[11] M.M. Maricq and J.J. Szente, J. Phys. Chem. 96 (1992) 4925.
[12] K.B. Hansen, R. Wilbrandt and P. Pagsberg, Rev. Sci. Instr. 50 (1979) 1532.
[13] O.J. Nielsen, Risø R-480 (1984).
[14] T. Ellermann, Risø-M-2932 (1991).
[15] O.L. Rasmussen and E. Bjergbakke, Risø-R-395 (1984).
[16] W. Braun, J.T. Herron and D.K. Kahaner, Intern. J. Chem Kinetics 20 (1988) 51.
[17] T.J. Wallington, P. Dagaut and M.J. Kurylo, Chem. Rev. 92 (1992) 667.
[18] M.M. Maricq and T.J. Wallington, J. Phys Chem. 96 (1992) 986.
[19] J. Czarnowski and H.J. Schumacher, Intern. J. Chem. Kinetics 11 (1979) 613.
[20] C. Anastasi, D.J. Muir, V.J. Simpson and P. Pagsberg, J. Phys. Chem. 95 (1991) 5791.
[21] O.J. Nielsen, J. Munk, G. Locke and T.J. Wallington, J. Phys. Chem. 95 (1991) 8714.
[22] T.J. Wallington, M.D. Hurley, J. Shi, M.M. Maricq, J. Sehested, O.J. Nielsen and T. Ellermann, Intern. J. Chem. Kinetics, in press.
[23] J.T. Herron, Intern. J. Chem. Kinetics 19 (1987) 129.
[24] P.S. Ganguli and M. Kaufman, Chem. Phys. Letters 25 (1974) 221.
[25] J. Sehested, T. Ellermann, O.J. Nielsen and T.J. Wallington, Intern. J. Chem. Kinetics, submitted for publication.
[26] J. Troe, J. Phys. Chem. 83 (1979) 1.
[27] H. Hippler, private communication (1993).

Reprinted from The Journal of Physical Chemistry, 1994, 98.

Atmospheric Chemistry of FO_2 Radicals: Reaction with CH_4, O_3, NO, NO_2, and CO at 295 K

Jens Sehested, Knud Sehested, and Ole John Nielsen*

Chemical Reactivity Section, Environmental Science and Technology Department, Risø National Laboratory, DK-4000 Roskilde, Denmark

Timothy John Wallington*

Sci. Res. Labs. E3083, Ford Motor Co. P.O. 2053, Dearborn, Michigan 48121

*Received: February 10, 1994; In Final Form: May 12, 1994**

Using pulse radiolysis combined with UV absorption spectroscopy, upper limits for the rate constants of the reaction of the FO_2 radical with O_3, CH_4, and CO were determined to be $<3.4 \times 10^{-16}$, $<4.1 \times 10^{-15}$, and $<5.1 \times 10^{-16}$ cm^3 molecule^{-1} s^{-1}, respectively. The rate constants for the reactions of FO_2 radicals with NO and NO_2 were measured: $FO_2 + NO \rightarrow FNO + O_2$ (10a); $FO_2 + NO_2 \rightarrow$ products (11). The rate constants for reactions 10 and 11 were determined to be $(1.47 \pm 0.08) \times 10^{-12}$ and $(1.05 \pm 0.15) \times 10^{-13}$ cm^3 molecule^{-1} s^{-1}, respectively. Reaction 10a was found to give FNO in a yield of $100 \pm 14\%$. As a part of this work, an upper limit of the reaction of FO radicals with O_3 was determined to be $<1.2 \times 10^{-12}$ cm^3 molecule^{-1} s^{-1}. Results are discussed in the context of the atmospheric chemistry of the FO_2 radical and hydrofluorocarbons.

Introduction

Recognition of the adverse environmental effect of chlorofluorocarbon (CFC) release into the atmosphere has led to an international agreement to phase out CFCs by the end of 1995. Efforts have been made to find environmentally acceptable alternatives. Among these alternatives are hydrofluorocarbons (HFCs). Prior to their large-scale industrial use, the environmental impact of HFCs must be investigated.

HFCs, when released into the atmosphere, will react with OH to form alkyl radicals which will, in turn, react with O_2 to form peroxy radicals.[1,2] The degradation of these fluorinated peroxy radicals in the atmosphere is known to produce a variety of products and radicals such as FO_2, FO, CF_3O, CF_3O_2, CF_2HO_2, CFH_2O_2, CF_3OH, FNO, CF_3COF, CF_3COH, HCOF, CF_2O, and HF.[1,2]

It has been discussed whether the CF_3O and CF_3O_2 radicals could destroy ozone in a catalytic cycle.[3] It is now well accepted that the ozone depletion effect of CF_3O_x radicals is negligible.[3,4] Attention has also been drawn to the atmospheric chemistry of the FO_x radicals. It has been suggested by Francisco and Su[5] and Francisco[6] that FO_2 and FO radicals formed in the atmospheric degradation of HFCs could destroy ozone in chain reaction processes:

$$FO + O_3 \rightarrow FO_2 + O_2 \quad (1)$$

$$FO_2 + O \rightarrow FO + O_2 \quad (2)$$

$$\text{net: } O + O_3 \rightarrow 2O_2$$

and

$$FO + O_3 \rightarrow FO_2 + O_2 \quad (1)$$

$$FO_2 + O_3 \rightarrow FO + 2O_2 \quad (3)$$

$$\text{net: } O_3 + O_3 \rightarrow 3O_2$$

A necessary but not sufficient condition for these two ozone destruction cycles to be efficient is that the FO_2 radical reacts rapidly with O_3 or O and that the loss processes for FO_x radicals are slow. Some reactions of the FO_2 radical are investigated in this work.

The equilibrium between F atoms, O_2, and FO_2 has been studied by Pagsberg et al.,[7] Lyman and Holland,[8] Ellermann et al.,[9] and Hippler.[10]

$$F + O_2 + M \rightleftharpoons FO_2 + M \quad (4,-4)$$

The following values have been reported: Pagsberg et al.,[7] $k_4 = 4.4 \times 10^{-33}$ cm^6 molecule^{-2} s^{-1} (298 K) and $K_p = 3.2 \times 10^{-25}$ exp(6100/T) cm^3 molecule^{-1}; Lyman and Holland,[8] $k_4 = (3.1 \pm 0.3) \times 10^{-33}$ cm^6 molecule^{-2} s^{-1} and $K_p = 1.2 \times 10^{-15}$ (298 K) cm^3 molecule^{-1}; Ellermann et al.,[9] $k_4 = (1.9 \pm 0.3) \times 10^{-33}$ cm^3 molecule^{-1} s^{-1} (295 K, 1 bar SF_6); Hippler et al.,[10] $K_p = 1.17 \times 10^{-25}$ exp(6712/T) cm^3 molecule^{-1}. In the following, the value of k_4 from Pagsberg et al.[7] and the K_p from Hippler[10] will be used.

The objective of this work is to study atmospherically significant reactions of the FO_2 radical. We have studied reactions of the FO_2 radical with NO, NO_2, CO, CH_4, and O_3 using pulse radiolysis coupled with time-resolved UV absorption spectroscopy.

Experimental Section

Two setups using pulse radiolysis coupled with time-resolved UV absorption spectroscopy were used in the present work. In the first setup a Febetron 705B accelerator was used to initiate the reactions. This experimental system has been described in detail previously[11,12] and has been used routinely for several years. The second setup applied a linear 10 MeV electron accelerator to initiate the reactions in a new 0.33 L stainless steel high-pressure cell. Results from this setup have not been reported previously in the literature. Both experimental setups are described below.

In the first system, radicals were produced in a 1 L stainless steel reaction cell using a 30 ns pulse of 2 MeV electrons from a Febetron 705B field emission accelerator. Pressures of up to 1 bar could be used in the reaction cell. The pressure was measured by a Baratron absolute membrane manometer. A chromel/alumel thermocouple measured the temperature inside the reaction cell close to the center.

The gas mixture was analyzed using UV light from a pulsed xenon lamp. The light beam from the xenon lamp was reflected 3, 7, or 11 times in the gas cell by internal White-type optics,

* Abstract published in *Advance ACS Abstracts*, June 15, 1994.

0022-3654/94/2098-6731$04.50/0

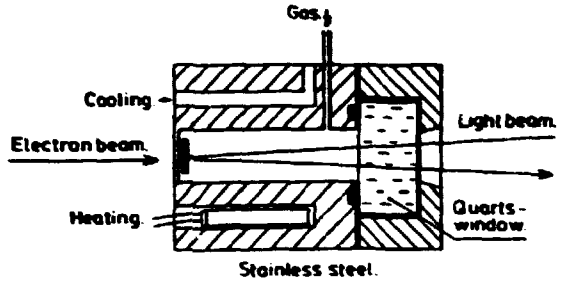

Figure 1. Outline of the high-pressure cell.

giving total optical pathlengths of 40, 80, or 120 cm. The analyzing light was passed into a McPherson 1 m grating monochromator operated at a spectral resolution of 0.8 nm and was detected by a Hamamatsu photomultiplier coupled to a Biomation digitizer. Data handling and storage were performed using a PDP11 computer.

In Figure 1 an outline of the high-pressure cell is shown. The cell is a stainless steel gas cell built for pressures up to 150 bar. Partial pressures of less than 1 bar were measured by a Juno 4ADM-22 pressure transducer coupled to a Juno PDA-48/k instrument. Pressures above 1 bar were measured by a Juno 4AP-30 pressure transducer coupled to a 4PDE-48 instrument. The cell may be heated up to 590 K, but in the present experiments, ambient temperature, 295 K, was used. Reactions were initiated by a 10 MeV HRC Linarc electron accelerator delivering a 0.5–4 μs electron pulse into the reaction cell. To obtain acceptable S/N ratios, up to five electron pulses were added. No changes in the observed transients were detected by comparing the obtained transients from the first and the last electron pulses.

The electron beam enters the cell through a thin metal window of 1.5 mm stainless steel at the left side of the cell. The diameter of the electron beam was close to the diameter of the cell, ensuring that the radiation was evenly distributed on the area entering the cell. The longitudinal distribution of radiation in the cell is also uniform since only a small fraction of the radiation is absorbed in the cell.

A 150 W Varian xenon lamp delivered the analyzing light. The xenon lamp could be pulsed to obtain better signal to noise ratios if a full time scale of less than or equal to 2 ms was applied. The analyzing light entered the cell through a quartz window and was reflected by a mirror mounted in the cell, giving a total optical pathlength of 20 cm. The light was detected by a Perkin-Elmer double-quartz prism monochromator with an optical resolution of 2–5 nm, and a IP28 photomultiplier and a LeCroy 9400 digital oscilloscope. Data handling and storage were performed using a IBM personal computer.

The gas mixtures used for both setups contained SF_6 in great excess. F atoms are known to be produced upon radiolysis of SF_6 with high-energy electrons:[12]

$$SF_6 + 2 \text{ or } 10 \text{ MeV } e^- \rightarrow F + \text{products} \quad (5)$$

The yield of F atoms has been determined routinely[13,14] in the first system by radiolysis of gas mixtures of CH_4, O_2, and SF_6 and subsequent observation of the absorbance at 260 nm ascribed to CH_3O_2 formed by reaction 5 and the following two reactions:

$$F + CH_4 \rightarrow CH_3 + HF \quad (6)$$

$$CH_3 + O_2 + M \rightarrow CH_3O_2 + M \quad (7)$$

In the present study the F atom yield in the low-pressure cell at full dose and 1000 mbar SF_6 was determined to be $(2.8 \pm 0.3) \times 10^{15}$ molecules cm^{-3}.

The F atom yield in the high-pressure cell was determined in a similar way. Mixtures of 50 mbar CH_4, 100 mbar at O_2, and 0–19.5 bar of SF_6 were radiolyzed by a 2 μs pulse of 10 MeV

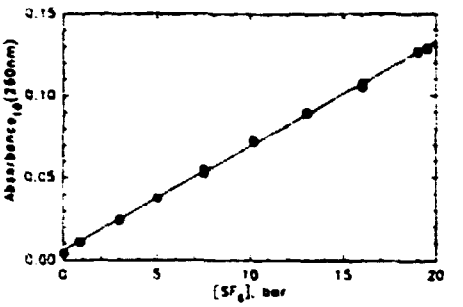

Figure 2. Transient absorption at 260 nm following pulse radiolysis of 50 mbar CH_4, 100 mbar O_2, and 0–19.5 bar of SF_6. The straight line is determined by linear regression of the data.

electrons. The absorbance due to CH_3O_2 radicals was measured at 260 nm as a function of the SF_6 pressure and is plotted in Figure 2. It is seen from the figure that the absorbance is proportional to the SF_6 concentration and thereby to the F atom concentration in the gas cell. By linear regression, the slope of the straight line in Figure 2 is determined to be $(6.36 \pm 0.08) \times 10^{-3}$ bar^{-1}. From this slope and the absorption cross section of the CH_3O_2 radical at 260 nm of 3.18×10^{-18} cm^2 molecule^{-1},[15] and taking into account a small correction due to the reaction of F atoms with O_2 (k_4 at 18 bar SF_6 is later determined to be 2.7×10^{-12} cm^3 molecule^{-1} s^{-1}), an estimate of the fluorine atom yield at 18 bar SF_6 of $(4.5 \pm 0.5) \times 10^{15}$ molecules cm^{-3} was derived. The uncertainty includes 10% uncertainty in $\sigma_{CH_3O_2}$ (260 nm) and the uncertainty in the slope in Figure 2.

FO_2 radicals were generated in both setups by radiolysis of mixtures of O_2 and SF_6:

$$SF_6 + 2 \text{ or } 10 \text{ MeV } e^- \rightarrow F + \text{products} \quad (5)$$

$$F + O_2 + M \rightarrow FO_2 + M \quad (4)$$

The pseudo-second-order rate constant for reaction 4 is well-known at 1 bar of SF_6 total pressure, $k_4 = (1.9 \pm 0.3) \times 10^{-13}$ cm^3 molecule^{-1} s^{-1}.[9] SF_6 pressures were 1 bar (within 5%) in all experiments in the low-pressure cell. The SF_6 pressure applied in the high-pressure cell was 18 bar. k_4 at 18 bar SF_6 is determined later to be $(2.7 \pm 0.7) \times 10^{-12}$ cm^3 molecule^{-1} s^{-1}.

Reagents and concentrations used were as follows: SF_6 (>99.97%), 0.9–19 bar; CH_4 (>99%), 0–600 mbar; and CO (>99.9%), 0–500 mbar; O_2, ultrahigh purity, 50–1000 bar; NO (>99.8%), 0–0.65 mbar; and NO_2 (>98%), 0–3 mbar. SF_6, CH_4, and CO were supplied by Gerling and Holz. O_2 was supplied by L'Air Liquide. NO was obtained from Messer Griesheim, and NO_2 was supplied by Linde Technische Gase. All reagents were used as received.

Ozone was produced by flowing O_2 through a conventional discharge ozonizer. The O_2 was purified before it entered the ozonizer by flowing it through a silica gel trap. The ozone/oxygen mixture was flowed through a silica gel trap cooled to −78 °C by an ethanol and dry ice bath. After ozone was collected on the silica gel trap for 3 h, the silica gel trap with ozone was hooked directly to the gas inlet on the high-pressure cell. The ozone/oxygen gas mixture in the silica gel trap flowed directly into the cell. Ozone concentrations were determined by measurements of the absorption at 220 or 288 nm in the cell before and after the gas cell was filled with the ozone/oxygen mixture. The ozone absorption cross sections used for quantifications of ozone were 1.80×10^{-18} cm^2 at 220 nm and 1.79×10^{-18} cm^2 at 288 nm.[16] Ozone concentrations were in the range 0–4 mbar.

Results

The reactions of the FO_2 radical with NO and NO_2 were investigated using the low-pressure cell. The rate constant of the

reaction of FO_2 with NO was determined from the formation kinetics of FNO at 310.5 nm. The rate constant of the reaction between FO_2 and NO_2 was determined by the decays of NO_2 at 400 nm and FO_2 at 220 nm.

The high-pressure cell was used to study the reactions of FO_2 with NO_2, O_3, CH_4, and CO. Performing the experiments in the high-pressure cell had two advantages: (i) high O_2 concentrations could be used, and (ii) k_4 is greater at the high total pressures that could be used in this cell. Therefore it was easier to avoid the reaction of F atoms with the reactant species CH_4, NO_2, O_3, and CO. As a preliminary exercise, the rate of the reaction of F atoms with O_2 at 18 bar SF_6 was determined by a relative rate technique. To determine the rate constants of the reactions of FO_2 radicals with NO_2, O_3, CO, and CH_4, the decay of FO_2 was followed at 220 nm.

It is important in both systems to work under conditions where the initially formed F atoms react mainly with O_2 and not with the species X we have added to the reaction mixture to study the reaction between FO_2 and X:

$$F + O_2 + M \rightarrow FO_2 + M \quad (4)$$

$$F + X \rightarrow \text{products} \quad (8)$$

$$FO_2 + X \rightarrow \text{products} \quad (9)$$

It is therefore necessary to know the reactivity of F atoms toward O_2 and the substance X to evaluate this potential complication. The percentage of F atoms reacting with X may be calculated from eq I:

$$\text{importance of reaction 8} = 100\% k_8[X]/(k_8[X] + k_4[O_2]) \quad (I)$$

The influence of reaction 8 can be calculated from k_8, k_4, and the concentrations of X and O_2.

Another possible complication is the decomposition of FO_2 producing F atoms which might react with the species X:

$$FO_2 + M \rightarrow F + O_2 + M \quad (-4)$$

$$F + O_2 + M \rightarrow FO_2 + M \quad (4)$$

$$F + X \rightarrow \text{products} \quad (8)$$

The rate constant of reaction 4 has been measured previously at 1 bar SF_6 to be $k_4 = (1.9 \pm 0.3) \times 10^{-13}$ cm^3 molecule^{-1} s^{-1}.[9] In the following, the rate constant at 18 bar SF_6 has been determined as $(2.7 \pm 0.7) \times 10^{-12}$ cm^3 molecule^{-1} s^{-1}. From these two values and the equilibrium constant for reaction 4, $K_p(295K) = 8.9 \times 10^{-16}$ cm^3 molecule^{-1},[10] values of k_{-4} at 1 bar SF_6 and 18 bar SF_6 of 213 and 3027 s^{-1} are derived. All studies of K_p indicate it is pressure independent.

We can now determine the rate of decay of FO_2 in the presence of a substance X if FO_2 does not react with X via reaction 9 but F atoms react with X via reaction 8. If all F atoms produced by the decomposition of FO_2 react with X, the decay of FO_2 would be equal to k_{-4}. However, only a fraction of the F atoms react with X in competition with O_2. This fraction is given by the equation $k_8[X]/(k_8[X] + k_4[O_2])$. The first-order decay rate coefficient is then

$$k_{decay} = k_{-4}k_8[X]/(k_8[X] + k_4[O_2]) \quad (II)$$

In the experiments reported in the present study we have used conditions where $k_8[X] \ll k_4[O_2]$. Therefore k_{decay} can be written:

$$k_{decay} \approx k_8[X]/K_p[O_2] \quad (III)$$

TABLE 1: Comparison of Measured Rate Constants and $k_{decay}/[X]$

compd X	exp rate, 10^{-16} cm^3 molecule^{-1} s^{-1}	k_9, 10^{-11} cm^3 molecule^{-1} s^{-1}	$k_{decay}/[X]$,[a] 10^{-16} cm^3 molecule^{-1} s^{-1}
O_3[b]	2.8 ± 0.6	1.0[3,23]	4.6
CH_4[b]	36 ± 5	6.8[19]	31
CO[b]	4.8 ± 0.3	1.2[d]	5.5
NO_2[b]	$(1.0 \pm 0.1) \times 10^3$	3.0[16]	14
NO_2[c]	$(1.1 \pm 0.1) \times 10^3$	3.0[16]	14
NO[c]	$(1.5 \pm 0.1) \times 10^4$	0.5[13]	2.3

[a] $k_{decay}/[X] = k_9/K_p[O_2]$. [b] High-pressure cell. [c] Low-pressure cell. [d] This work.

k_{decay} is the first-order decay rate coefficient of FO_2 radicals in the presence of X if the FO_2 radical does not react with X. $k_{decay}/[X]$ will then be the rate constant for the decay of the FO_2 even though FO_2 radicals do not react with the species X. $k_{decay}/[X]$ is the lowest possible result of a measurement of k_9. In Table 1 we have listed values of k_9 and $k_{decay}/[X]$. By comparison of the experimentally measured value of k_9 with the values of $k_{decay}/[X]$ given in Table 1 we can determine whether the measured rate constant is a real k_9 or just the result of the reaction mechanism, k_4, k_{-4}, and k_8. The results are discussed in the paragraphs dealing with the specific reactions.

Rate Constant for the Reaction of FO_2 Radicals with NO. In the low-pressure cell, radiolysis of 50 mbar O_2, 0.21–0.65 mbar NO, and 1000 mbar SF_6 was used to study the reaction between the FO_2 radical and NO. This reaction has two possible reaction pathways:

$$FO_2 + NO \rightarrow FNO + O_2 \quad (10a)$$

$$FO_2 + NO \rightarrow FO + NO_2 \quad (10b)$$

Reaction 10a is 43.6 kcal mol^{-1} exothermic[16] while reaction 10b is 6 kcal mol^{-1} endothermic.[16] To evaluate the branching of reaction 10, the yield of FNO was determined by the absorption at 310.5 nm. The transient absorbance at 310.5 nm following radiolysis of a mixture of 0.44 mbar NO, 50 mbar O_2, and 1000 mbar SF_6 is shown in Figure 3A. The average absorbance of the six recorded FNO transients was 0.044 ± 0.006. Using σ_{FNO} (310.5 nm) $= 5.7 \times 10^{-19}$ cm^2 molecule^{-1},[17] path length = 120 cm, dose 0.527, and an F atom yield at full dose and 1000 mbar of SF_6 of $(2.8 \pm 0.3) \times 10^{15}$ molecule cm^{-3}, we obtain a yield of FNO of $100 \pm 14\%$. Clearly, a is the major reaction channel for reaction 10. Channel 10a could proceed through a 4-center rearrangement.

The rate of reaction 10 was determined by fitting a first-order rise expression to the formation of FNO at 310.5 nm. The transients were always fitted well by a first-order expression. The pseudo-first-order rates obtained in this way are plotted in Figure 4 as a function of the NO concentration. The slope of a straight line through the data points gives $k_{10} = (1.5 \pm 0.1) \times 10^{-12}$ cm^3 molecule^{-1} s^{-1}.

Rate Constant for the Reaction of FO_2 Radicals with NO_2 Using the Low-Pressure Cell. The rate constant for the reaction of FO_2 with NO_2 was determined by monitoring the decay of NO_2 and FO_2 following radiolysis of 0.3–3.0 mbar NO_2, 50 mbar of O_2, and 1000 mbar of SF_6:

$$FO_2 + NO_2 \rightarrow \text{products} \quad (11)$$

The final absorption in Figure 3B is less than that before the radiolysis pulse. This is not surprising since the absorption at 220 nm is a combination of that from FO_2 radicals and NO_2. NO_2 is consumed by reaction 11, leading to a final absorbance which is less than that observed before the radiolysis pulse. As seen from Figure 3C, the transient absorption observed at 400 nm has an interesting shape. The absorption at 400 nm is due solely to NO_2. The large initial drop in absorption is caused by

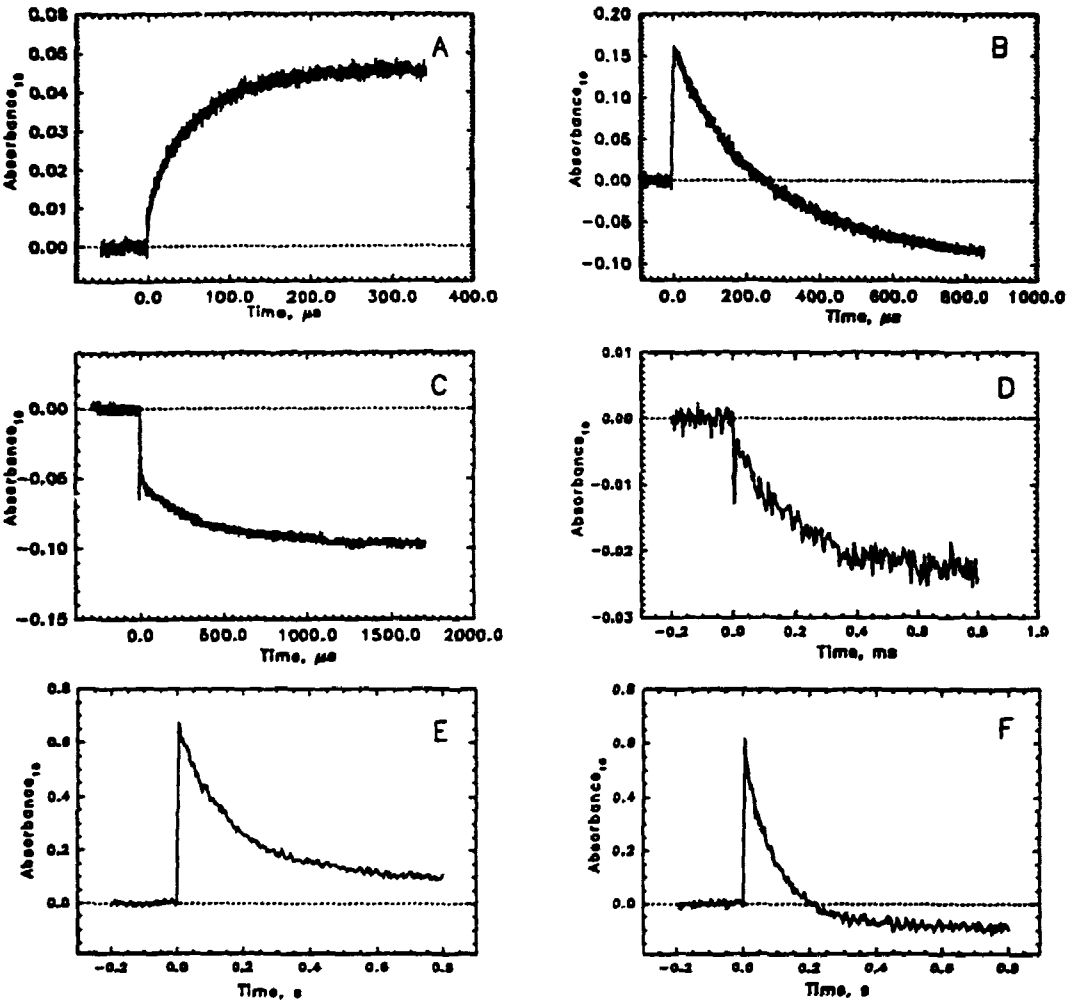

Figure 3. Transient absorptions observed at the following wavelengths and conditions: (A) at 310.5 nm with 0.44 mbar NO, 50 mbar O_2, and 950 mbar SF_6; (B) at 220 nm with 1.0 mbar NO_2, 50 mbar of O_2, and 950 mbar of SF_6; (C) at 400 nm with 0.5 mbar NO_2, 50 mbar of O_2, and 950 mbar of SF_6; (D) at 400 nm with 2 mbar NO_2, 1000 mbar O_2, and 18 bar SF_6; (E) at 220 nm with 1000 mbar O_2 and 18 bar SF_6; (F) at 220 nm with 1.3 mbar O_3, 1000 mbar O_2, and 18 bar SF_6.

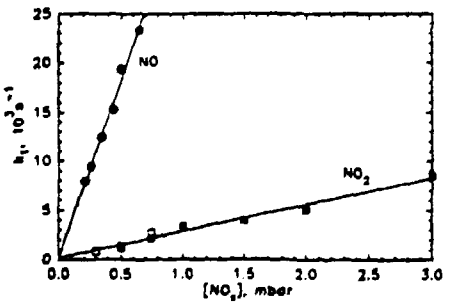

Figure 4. First-order formation rates of FNO at 310.5 nm (●) and first-order decay rates of FO_2 at 220 nm (■) and NO_2 at 400 nm (□). The straight lines are found by linear regressions of the data.

the scavenging of some of the F atoms by NO_2. The subsequent decay is caused by the reaction of FO_2 radicals with NO_2. In considering the transient in Figure 3C, it should be noted that the observed change in absorption represents only a small fraction (<20%) of the total absorption at this wavelength.

Pseudo-first-order decay rate constants obtained from traces such as those shown in Figure 3B and 3C are plotted as a function of the NO_2 concentration in Figure 4. As seen in Figure 4, the kinetic data obtained by monitoring the decay of absorption at 220 and 400 nm were in good agreement. A linear regression of the data in Figure 4 gives $k_{11} = (1.1 \pm 0.1) \times 10^{-13}$ cm^3 molecule^{-1} s^{-1}. The products of reaction 11 are unknown. Reaction 11 may proceed via a mechanism involving a 4-center rearrangement to give FNO_2 and O_2. Alternatively, reaction 11 may proceed to give the adduct FO_2NO_2.

At this point we need to consider potential complications in our measurement of k_{11}. One complication could be the formation of FNO_2 via reaction 11 or via the direct reaction of F atoms with NO_2 (as evidenced by the initial drop in absorption seen in Figure 3C). FNO_2 is a stable compound which absorbs only weakly in the UV (σ(max) = 2.6×10^{-20} cm^2 molecule^{-1} at 230 nm[18]). The formation of FNO_2 is not expected to complicate the present kinetic analysis. In light of the excellent agreement in the kinetic data derived using the two different wavelengths (220 and 400 nm) shown in Figure 4, it seems unlikely that the present work is subject to significant complications caused by unwanted radical species.

The Reaction of F Atoms with O_2 at 18 bar SF_6. At a pressure of 18 bar of SF_6 the rate constant for reaction 4 is expected to be significantly elevated as compared to k_4 at 1 bar SF_6 since the pseudo-second-order rate constant, k_4, is pressure dependent up to pressures higher than 1000 bar of He.[10] Therefore we have measured k_4 at 18 bar of SF_6.

It was not possible to measure k_4 directly by the 220 nm absorption of FO_2 that is formed in the reaction. At the low oxygen concentrations necessary to measure the formation kinetics, radical–radical reactions such as the reaction of F atoms with the FO_2 radical become important. This increases the apparent formation kinetics of FO_2 so much that it was impossible to derive a meaningful reaction rate from direct measurements. Therefore a relative rate method was applied.

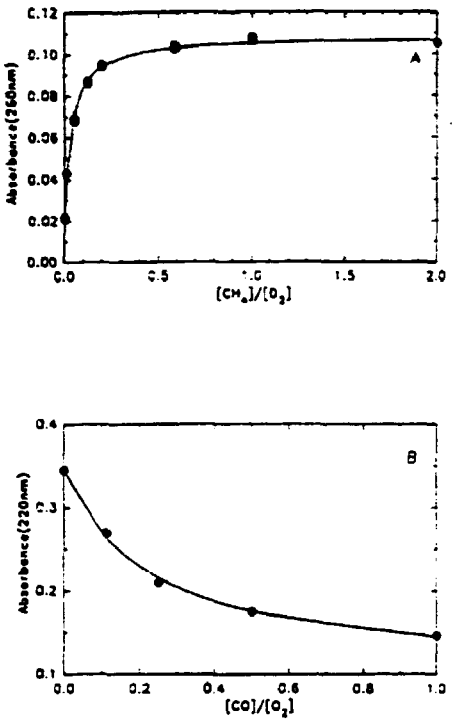

Figure 5. (A) Maximum transient absorbance at 260 nm following pulse radiolysis of 0–600 mbar CH_4, 300–1000 mbar O_2, and 18 bar SF_6 as a function of the concentration ratio $[CH_4]/[O_2]$. (B) Maximum transient absorbance at 220 nm following pulse radiolysis of 0–500 mbar CO, 500–1000 mbar O_2, and 18 bar SF_6 as a function of the concentration ratio $[CO]/[O_2]$. Solid lines are fits to the data; see text.

The pseudo-second-order rate constant, k_4, at 18 bar SF_6 was determined relative to the rate constant for reaction of F atoms with CH_4, k_6. The literature data on the reactivity of F atoms toward methane are discussed by Wallington et al.,[19] and a value of $(6.8 \pm 1.4) \times 10^{-11}$ cm^3 molecule^{-1} s^{-1} was derived. This rate constant is not pressure dependent.

When mixtures of $O_2/CH_4/SF_6$ are radiolyzed, FO_2 and CH_3O_2 are formed from the following set of reactions:

$$SF_6 + 10\ \text{MeV}\ e^- \rightarrow F + \text{products} \quad (5)$$

$$F + O_2 + M \rightarrow FO_2 + M \quad (4)$$

$$F + CH_4 \rightarrow CH_3 + HF \quad (6)$$

$$CH_3 + O_2 + M \rightarrow CH_3O_2 + M \quad (7)$$

The amounts of FO_2 radicals relative to the amount of CH_3O_2 radicals formed depends only on the ratio between the rate constant of F atom reactions with CH_4 and O_2, k_6/k_4, and the ratio between the methane concentration and the oxygen concentration, $[CH_4]/[O_2]$.

As a measure of the CH_3O_2 concentration, the absorbance at 260 nm following pulse radiolysis of mixtures of 300–500 mbar of O_2, 0–600 mbar CH_4, and 18 bar SF_6 was used. In these experiments the radiolysis time of 2 μs and a SF_6 concentration of 18 bar were held constant ($[F]_0 = 4.5 \times 10^{15}$ molecules cm^{-3}).

Figure 5A shows the observed variation of the maximum transient absorption as function of the concentration ratio $[CH_4]/[O_2]$. As seen from this figure, the absorbance at low $[CH_4]/[O_2]$ ratio was small, around 0.02. As the concentration ratio increased, the absorption increased until a ratio $[CH_4]/[O_2]$ of 1 was reached. Further increase in the ratio $[CH_4]/[O_2]$ had no discernible effect on the absorption. This behavior is rationalized in terms of the competition between CH_4 and O_2 for the available F atoms. At low CH_4 concentrations, an appreciable amount of

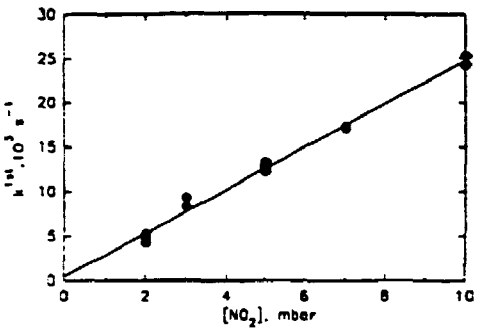

Figure 6. First-order decay rates of NO_2 measured at 400 nm following pulse radiolysis of 2–10 mbar NO_2, 1000 mbar O_2, and 18 bar SF_6 plotted as a function of $[NO_2]$. The solid line is a linear regression of the data.

FO_2 is formed; hence, a small initial absorption at 260 nm is seen. As the CH_4 concentration is increased, an increasing fraction of the F atoms reacts with CH_4 at the expense of O_2, and the initial maximum absorption increases.

The solid line in Figure 5A represents a three-parameter fit of the following expression to the data:

$$A_{max} = \{A_{FO2} + (A_{CH3O2}(k_6/k_4)[CH_4]/[O_2])/(1 + (k_6/k_4)[CH_4]/[O_2])\} \quad (IV)$$

where A_{max} is the observed maximum transient absorbance, A_{FO2} is the maximum absorbance expected if only FO_2 is produced, and A_{CH3O2} is the maximum absorbance expected if all F atoms react with CH_4. Parameters A_{FO2}, A_{CH3O2}, and k_6/k_4 were simultaneously varied. The best fit was obtained with $k_6/k_4 = 25.1 \pm 3.4$, $A_{FO2} = 0.023 \pm 0.003$, and $A_{CH3O2} = 0.108 \pm 0.018$. Errors are two standard deviations. Using our value of $k_6 = (6.8 \pm 1.4) \times 10^{-11}$ cm^3 molecule^{-1} s^{-1}, k_4 is $(2.7 \pm 0.7) \times 10^{-12}$ cm^3 molecule^{-1} s^{-1} (quoted errors reflect uncertainty in k_6 and the ratio k_6/k_4). This is concluded to be the pseudo-second-order rate constant for the reaction of F atoms with O_2 at 18 bar SF_6.

Rate Constant for the Reaction of FO_2 Radicals with NO_2 Using the High-Pressure Cell. The decay of NO_2 was used to study the reaction between FO_2 and NO_2 in the high-pressure cell. These experiments were performed to verify the result from the low-pressure cell and to check for any pressure dependence of the reaction between FO_2 and NO_2. The pseudo-first-order rate constant for the reaction of FO_2 with NO_2 was derived by observing the decay of NO_2 and by plotting $\ln\{(Abs_t - Abs_\infty)/Abs_t\}$ against the time. Abs_t and Abs_∞ are the absorbances at time t and $t = \infty$, respectively. If the reaction is first order, then a plot of $\ln\{(Abs_t - Abs_\infty)/Abs_t\}$ versus time gives a straight line with a slope of the pseudo-first-order rate constant. Following radiolysis of 2 mbar NO_2, 1000 mbar O_2, and 18 bar SF_6, the transient absorbance observed at 400 nm is displayed in Figure 3D. The pseudo-first-order rates found from the experimental transients at 400 nm as described above are plotted as a function of $[NO_2]$ in Figure 6. A linear regression of the data gives a rate constant of $(1.05 \pm 0.10) \times 10^{-13}$ cm^3 molecule^{-1} s^{-1}. It should be noted that the same value of k_{11} is obtained by both the high- and the low-pressure techniques. Reaction 11 shows no pressure dependence in the range of 1–18 bar SF_6.

It is expected that the products of the reaction of FO_2 with NO_2 are either FO_2NO_2 or FNO_2 and O_2. Formation of FO and NO_3 is not feasible since this reaction is 29 kcal mol^{-1} endothermic.[16] The two first mentioned product channels give stable products, and it is therefore not expected that these products change the apparent decay of NO_2. Hence, we do not expect any interference with secondary chemistry on the experimental data.

As seen from Table 1, $k_{decay}/[NO_2] \ll k_{11}$, so the interference from the direct reaction of F atoms with NO_2 is negligible. We choose to quote a value for k_{11} of $(1.05 \pm 0.10) \times 10^{-13}$ cm^3 molecule^{-1} s^{-1} from the present work.

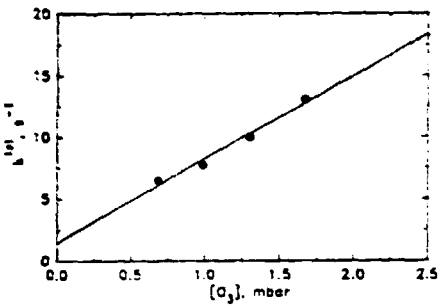

Figure 7. First-order decay rates of FO_2 measured at 220 nm following pulse radiolysis of 0.65–1.7 mbar O_3, 1000 mbar O_2, and 18 bar SF_6 plotted as a function of $[O_3]$. The solid line is a linear regression fit of the data.

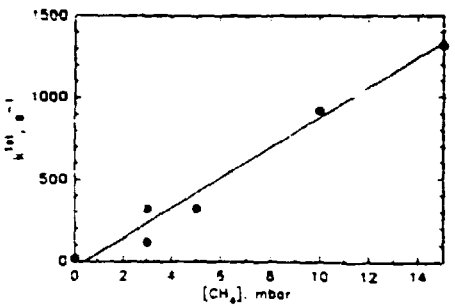

Figure 8. First-order decay rates of FO_2 measured at 220 nm following pulse radiolysis of 0–15 mbar CH_4, 1000 mbar O_2, and 18 bar SF_6 plotted as a function of $[CH_4]$. The solid line is a linear regression fit of the data.

The Reaction of FO_2 with O_3. Displayed in Figure 3E and 3F are two FO_2 transients recorded at 220 nm without and with 1.3 mbar of ozone, respectively. It is seen from the figure that small amounts of ozone increase the apparent decay of FO_2. Pseudo-first-order decay rates were determined from the slope of a plot of $\ln\{(Abs_t - Abs_\infty)/Abs_t\}$ versus time as described above. The rates are plotted in Figure 7 against the ozone concentration. The slope found by linear regression of the data gives a reaction rate of $(2.8 \pm 0.6) \times 10^{-16}$ cm^3 molecule^{-1} s^{-1}. The plot in Figure 7 has a significant intercept, 1.5 ± 1.4 s^{-1}. This intercept corresponds to the decay of the FO_2 radicals in the cell without any other substances present.

As shown in Table 1, $k_{decay}/[O_3]$ is close to the value found for the rate constant of the reaction of FO_2 with ozone. Hence, within the uncertainty, the FO_2 radicals do not react with ozone and an upper limit of 3.4×10^{-16} cm^3 molecule^{-1} s^{-1} can be derived from the data.

As an additional check on the system, the behavior of ozone was recorded by measuring the absorbance at 288 nm. A loss of ozone was observed. This may be explained by the reaction of F atoms, formed in the decomposition of the FO_2 radical, with ozone:

$$FO_2 + M \rightarrow F + O_2 + M \qquad (-4)$$

$$F + O_3 \rightarrow FO + O_2 \qquad (12)$$

The loss of ozone was in all cases $100 \pm 16\%$ of the initial F atom yield including an uncertainty of 10% in the F atom calibration. The upper limit of the ozone loss of 116% gives us an upper limit for the reaction of FO with ozone,

$$FO + O_3 \rightarrow FO_2 + O_2 \qquad (1)$$

because if this reaction were fast the result would be more than 100% ozone loss. The highest ozone concentration used in the present work was 4 mbar. At this ozone concentration the decay of the 4.5×10^{15} molecule cm^{-3} FO_2 radicals will produce almost the same amount of FO radicals by decomposition of FO_2 followed by reaction of F atoms with ozone. A maximum of 16% of these FO radicals will react with ozone. The other 84% will be consumed by some other loss reactions. The fastest possible loss reaction of FO radicals apart from reaction with O_3 is the reaction with FO_2:

$$FO + FO_2 \rightarrow \text{products} \qquad (13)$$

The maximum rate constant for this reaction is the diffusion limit, about 10^{-10} cm^3 molecule^{-1} s^{-1}. This reaction will, however, reduce the amount of FO radicals formed to half of the amount of FO_2 radicals formed. Therefore, up to 32% of the FO radicals may react with ozone. This gives us the following equation:

$$k_1[O_3]/(k_1[O_3] + k_{13}[FO_2]) = 1/(1 + k_{13}[FO_2]/(k_1[O_3])) < 0.32 \quad (V)$$

Using $k_{13} = 10^{-10}$ cm^3 molecule^{-1}, $[FO_2] \approx 0.2$ mbar, and $[O_3] = 4$ mbar,

$$1/(1 + 5 \times 10^{-12}/k_1) < 0.32 \Rightarrow k_1 < 1.2 \times 10^{-12}$$

The upper limit for k_1 at 295 K is therefore 1.2×10^{-12} cm^3 molecule^{-1} s^{-1}. Recently, Bedzhanyan et al.[20] reported an upper limit for reaction 1 of 2×10^{-16} cm^3 molecule^{-1} s^{-1}.

The Reaction of FO_2 with CH_4. The reaction of FO_2 radicals with methane was studied using the decay of the FO_2 radical by following the transient absorption at 220 nm. An initial rate method was applied for this study: 0–15 mbar CH_4, 1000 mbar O_2, and 18 bar SF_6 were used. The initial rates of FO_2 loss at different methane concentrations divided by the initial FO_2 radical concentration gives the pseudo-first-order rate constants. These are plotted as a function of $[CH_4]$ in Figure 8. The slope of a straight line through the data gives a rate constant of $(3.6 \pm 0.5) \times 10^{-15}$ cm^3 molecule^{-1} s^{-1}. As seen in Table 1, this value is similar to $k_{decay}/[CH_4]$, indicating that the determined value is not a "true" rate constant for the reaction of the FO_2 radical with CH_4 but rather an upper limit.

Possible complications of the measurement above included (i) reactions of products of the methane degradation with FO_2 and (ii) reaction of F atoms formed initially with CH_4. The first complication cannot be ruled out but probably is not a serious complication since FO_2 radicals seem to react slowly with most species. However, if this reaction is important, it will tend to speed the decay of the FO_2 radicals; hence the upper limit above is still valid. The second complication will also tend to increase the apparent decay at 220 nm since the decay of CH_3O_2 is faster than that of FO_2. Using $k_4 = 2.7 \times 10^{-12}$ cm^3 molecule^{-1} s^{-1} and $k_6 = 6.8 \times 10^{-11}$ cm^3 molecule^{-1} s^{-1}, we calculate for the highest methane concentration used a yield of 27% of initially formed CH_3 radicals by direct reaction of the initially formed F atoms with CH_4. This will, as stated previously, increase the apparent decay rate at 220 nm, and hence the upper limit is still valid.

The Reaction of FO_2 with CO. The reaction of FO_2 with CO was studied by monitoring the FO_2 decay at 220 nm. In a set of preliminary experiments, the rate of reaction of F atoms with CO was measured at 18 bar SF_6. The maximum transient absorbance at 220 nm was measured following radiolysis of 0–500 mbar CO, 500–1000 mbar O_2, and 18 bar SF_6. The absorbance data are shown as a function of $[CO]/[O_2]$ in Figure 5B. In the system, CO and O_2 compete for the available F atoms in the two reactions

$$F + CO + M \rightarrow FCO + M \qquad (14)$$

$$F + O_2 + M \rightarrow FO_2 + M \qquad (4)$$

FCO radicals react rapidly with O_2 to give $FC(O)O_2$:[13]

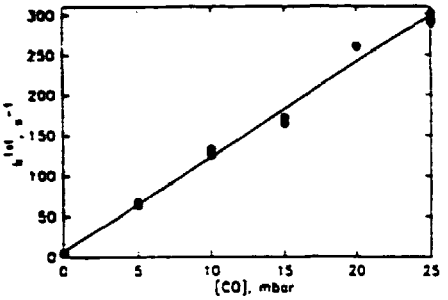

Figure 9. First-order decay rates of FO_2 measured at 220 nm following pulse radiolysis of 0–25 mbar CO, 1000 mbar O_2, and 18 bar SF_6 plotted as a function of [CO]. The solid line is a linear regression fit of the data.

$$FCO + O_2 + M \rightarrow FC(O)O_2 + M \qquad (15)$$

The absorbance at 220 nm is therefore a combination of the absorbances of FO_2 and $FC(O)O_2$. At low CO concentrations the absorbance at 220 nm is mainly due to FO_2. As the concentration of CO is increased, more and more $FC(O)O_2$ is formed relative to FO_2. We can now rationalize the absorbance behavior in Figure 5B since the absorption cross section of FO_2 at 220 nm is larger than that of $FC(O)O_2$.[13] By analogy with the determination of k_4, the data in Figure 5B may be fitted by the following expression:

$$A_{max} = \{A_{FO2} + (A_{FC(O)O2}(k_{14}/k_4)[CO]/[O_2])/(1 + (k_{14}/k_4)[CO]/[O_2])\} \qquad (VI)$$

where A_{FO2} and $A_{FC(O)O2}$ are the absorbances if all F atoms were converted into FO_2 or $FC(O)O_2$ radicals, respectively. A three-parameter fit of A_{FO2}, $A_{FC(O)O2}$, and k_{14}/k_4 gave a ratio between the two rate constants of 4.5 ± 1.4. The fit may be seen as the solid line in Figure 5B. Using $k_4 = (2.7 \pm 0.7) \times 10^{-12}$ cm^3 molecule^{-1} s^{-1}, we derive $k_{14} = (1.2 \pm 0.5) \times 10^{-11}$ cm^3 molecule^{-1} s^{-1}; the quoted error reflects the cumulative uncertainties in the measured ratio k_{14}/k_4 and k_4.

In the following, concentration ratios [CO]/[O_2] of up to 0.025 were used to determine the rate constant for the reaction of FO_2 with CO. Using $k_{14}/k_4 = 4.5$, we discover that the amount of initially formed $FC(O)O_2$ is less than 10% of the initial amount of F atoms formed in the system.

To measure the rate constant for the reaction of FO_2 radicals with CO, mixtures of 0–25 mbar CO, 1000 mbar O_2, and 18 bar SF_6 were radiolyzed, and the first-order rate of decay of the absorption at 220 nm was determined. The first-order decay rates were determined from the slope of a plot of $\ln\{(Abs_t - Abs_\infty)/Abs_i\}$ versus time, as described above. The first-order rates are plotted against [CO] in Figure 9. The slope found by linear regression of the data gives a rate constant for the reaction of FO_2 with CO of $(4.8 \pm 0.3) \times 10^{-16}$ cm^3 molecule^{-1} s^{-1}.

This rate constant may be influenced by reactions of FO_2 with $FC(O)O_2$ and other CO degradation products. However, it is seen from this work that the FO_2 radical is very unreactive, so it seems likely that the kinetics of the FO_2 radical are not significantly perturbated by the degradation products. As seen in Table 1, the measured rate constant for the reaction of FO_2 with CO is equal to $k_{decay}/[CO]$. This indicates that the reaction rate of FO_2 with CO may be zero within the uncertainty of the experiment. The value of $(4.8 \pm 0.3) \times 10^{-16}$ cm^3 molecule^{-1} s^{-1} is therefore an upper limit.

Discussion

As seen from the results of this work, FO_2 reactions are generally very slow. There are two possible reaction pathways of the reaction of FO_2 radicals with the species X: (i) Reactions where the F atom is the active part of the FO_2 radical. For example in the reaction with NO, >86% of the products were FNO and O_2, probably formed via the reaction complex ON–FO_2; (ii) reactions where the O–O* moiety of the FO_2 radical is the active part (i.e. where FO_2 reacts as a peroxy radical). We have not detected any evidence for peroxy radical type behavior for FO_2.

Reaction channel i is expected to be slow because of the large activation energy involved in the abstraction of an F atom from the FO_2 radical (~12.6 kcal mol^{-1}).[7] However, if the species X is capable of forming a low-energy reaction complex where the activation barrier is lowered effectively, a reaction is possible. It seems likely that NO is capable of doing this, while CH_4 does not effectively lower the activation barrier. A study of the temperature dependence of the reaction of FO_2 with NO and NO_2 would be of interest in this connection.

The FO_2 radical also seems very unreactive through reaction channel ii. As stated above, no experimental evidence for this reaction pathway was found in this work. No rates have been measured for reactions of FO_2 with other peroxy radicals. However, FO_2 seems stable in the presence of other peroxy radicals.[21] The conclusion is that FO_2 is not a very reactive radical.

Atmospheric Implications. The known reactions of F, FO, and FO_2 of importance in the atmosphere are displayed in Table 2. Apart from the unimolecular decomposition of the FO_2 radical, all known activation energies are small. The rate constants at 295 and 220 K differ by less than a factor of 2. For simplicity we have therefore only considered the temperature dependence of the self-decomposition of the FO_2 radicals in the following. While the temperature dependences of the rate constants of the first five reactions in Table 2 are not known, it is expected that the rates of these reactions will slow down at lower temperatures because of the significant energy involved in abstraction of F atoms from the FO_2 radical.

To evaluate the importance of the reactions of the F, FO, and FO_2 radicals in the atmosphere, knowledge of the atmospheric concentrations of the reactants is necessary. We have used known values of NO, NO_2, CO, O_3, O, and M and the temperature from Brasseur and Solomon.[22] These are known concentrations at mid latitudes. Figure 10A–C shows the lifetimes of F atoms (Figure 10A), FO radicals (Figure 10B), and FO_2 radicals (Figure 10C) with respect to reactions with atmospheric-important species at different altitudes. There are reactions in Table 2 which directly or indirectly destroy odd oxygen (O atoms or O_3 molecules):

$$F + O_3 \rightarrow FO + O_2 \qquad (12)$$

$$FO + O_3 \rightarrow FO_2 + O_2 \qquad (1)$$

TABLE 2: FO_x Reactions

reaction	rate constant (295 K), cm^3 molecule^{-1} s^{-1}	ref
$FO_2 + NO \rightarrow FNO + O_2$	$(1.5 \pm 0.1) \times 10^{-12}$	this work
$FO_2 + O_3 \rightarrow FO + 2O_2$	$<3.4 \times 10^{-16}$	this work
$FO_2 + NO_2 \rightarrow$ products	$(1.05 \pm 0.10) \times 10^{-13}$	this work
$FO_2 + CO \rightarrow$ products	$<5.1 \times 10^{-16}$	this work
$FO_2 + CH_4 \rightarrow$ products	$<4.1 \times 10^{-15}$	this work
$FO_2 + M \rightarrow F + O_2 + M$	3.75×10^{-9}[M] exp(−6711/T)[b]	10,7
$FO_2 + O \rightarrow FO + O_2$	5.0×10^{-11}[a]	16
$FO + NO \rightarrow NO_2 + F$	2.6×10^{-11}	16
$FO + O \rightarrow F + O_2$	2.7×10^{-11}	20
$FO + O_3 \rightarrow$ products	$<2 \times 10^{-16}$	20
$FO + O_3 \rightarrow$ products	$<1.2 \times 10^{-12}$	this work
$FO + ClO \rightarrow F + Cl + O_2$	5×10^{-11}	c
$F + CH_4 \rightarrow CH_3 + HF$	$(6.8 \pm 1.4) \times 10^{-11}$	19
$F + H_2O \rightarrow OH + HF$	1.4×10^{-11}	16
$F + O_3 \rightarrow FO + O_2$	1.0×10^{-11}	3,23
$F + O_2 + M \rightarrow FO_2 + M$	4.4×10^{-33}[M]	7

[a] Uncertain, no experimental data. [b] Calculated from $k_{-4} = k_4/K_4$. k_4 is taken from ref 7 and K_4 from ref 10. [c] Rate and products found by analogy to other halogen oxide self-reactions.

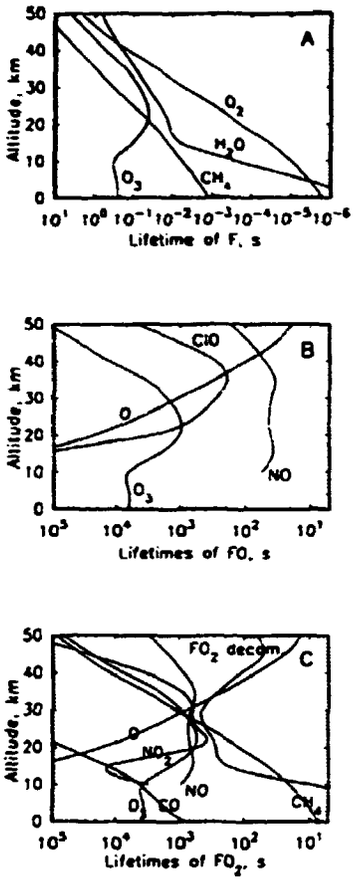

Figure 10. Lifetimes, $t = 1/(k_{FO_x+X}[X])$, of F atoms (A), FO radicals (B), and FO_2 radicals (C) with respect to reaction with atmospheric-important species at different altitudes. The concentrations are taken from Brasseur and Solomon[22] and the rate constants from Table 2.

$$FO + O \rightarrow F + O_2 \quad (16)$$

$$FO + ClO \rightarrow F + Cl + O_2 \quad (17)$$

$$FO_2 + O_3 \rightarrow FO + 2O_2 \quad (3)$$

$$FO_2 + O \rightarrow FO + O_2 \quad (2)$$

There are two reactions which remove the F atoms efficiently from the FO_x catalytic cycle:

$$F + CH_4 \rightarrow HF + CH_3 \quad (6)$$

$$F + H_2O \rightarrow HF + OH \quad (18)$$

HF is unreactive in the stratosphere and is transported to the troposphere where it is incorporated into rain droplets and rained out.

In the following we will establish an upper limit for the number of ozone molecules destroyed by one F atom formed in the atmosphere. The mechanism we will use to evaluate this is shown in Figure 11. The main reaction of F atoms in the atmosphere is reaction with O_2 to form FO_2. F atoms are then reformed by unimolecular decomposition of FO_2. FO radicals may be formed from the reaction of FO_2 radicals with O atoms and O_3 molecules and by the reaction of F atoms with ozone. FO radicals reform F atoms or FO_2 radicals by reaction with NO, O atoms, ClO, or ozone. F atoms are removed from the cycle by reaction with CH_4 and H_2O.

The number of times FO_2 is reformed through equilibrium 4 before its removal by reaction with H_2O or CH_4 is

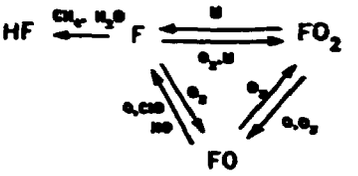

Figure 11. Reaction scheme of the kinetic model used in the calculation of the ozone destruction effectiveness of F atoms released to the stratosphere.

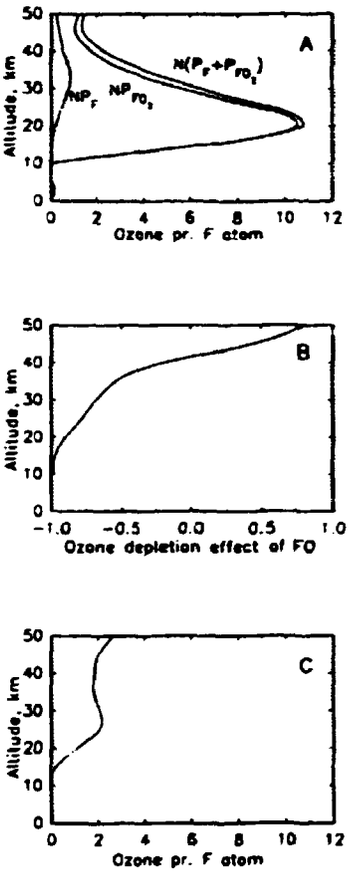

Figure 12. Plot of the number of ozone molecules destroyed by an F atom released to the stratosphere: simple model (A) and advanced model (C). Effect of an FO radical on the ozone layer before it forms FO_2 or F atoms (B). See text for details.

$$N = k_4[O_2]/(k_6[CH_4] + k_{18}[H_2O]) \quad (VII)$$

The probability that FO_2 or F destroys an ozone molecule either as O_3 or O, before reaction with O_2 or decomposition, respectively, is

$$P_F = k_{12}[O_3]/k_4[O_2] \quad (VIII)$$

$$P_{FO2} = (k_3[O_3] + k_2[O])/k_{-4} \quad (IX)$$

Under the assumption that FO neither destroys nor forms ozone before it forms FO_2 radicals or F atoms, we can now derive an upper limit for the number of ozone molecules destroyed by one F atom released into the stratosphere. The upper limit is the product of the probability that FO_2 or F will destroy an ozone molecule before it is removed by decomposition or reaction with O_2, P_{FO2} or P_F, and the number of times F and FO_2 are reformed before F reacts with CH_4 or H_2O, $N(P_F + P_{FO2})$. NP_F, NP_{FO2}, and $N(P_F + P_{FO2})$ are plotted in Figure 12A at different altitudes. As seen from Figure 12A, the maximum number of ozone molecules destroyed per F atom formed in the stratosphere from this simple model is 11 at 20 km altitude.

Now we will make our model a little more sophisticated. We will consider the FO reactions and include a reaction which has an analog in ClO chemistry.

$$FO + ClO \rightarrow F + Cl + O_2 \quad (17)$$

This reaction could be fast with a rate constant of up to 5×10^{-11} cm^3 $molecule^{-1}$ s^{-1}. The lifetime of FO with respect to the reaction with ClO is plotted in Figure 10B. The maximum ozone destruction potential of a FO radical before it is converted into FO_2 or F atoms is determined by reaction with ClO, O atoms, O_2, and NO_2. FO destroys one ozone molecule before it forms F or FO_2 if it reacts with ClO, O_3, or O atoms. If it reacts with NO, it actually reforms an ozone molecule because the product, NO_2, photolyzes to give NO and an O atom. The effect of FO radicals on the stratospheric ozone layer may be calculated from

$$(k_{FO+NO}[NO] - k_{17}[ClO] - k_1[O_3] - k_{16}[O])/(k_{FO+NO}[NO] + k_{17}[ClO] + k_1[O_3] + k_{16}[O]) \quad (X)$$

The values determined by eq X at different altitudes are plotted in Figure 12B; −1 means that an ozone molecule is formed, by reaction with NO, before FO is converted into F atoms or FO_2 radicals, and +1 means that one ozone molecule is destroyed before FO is converted into FO_2 or F.

The real potential ozone destroying effect of the FO_x cycle may now be calculated as $N(P_F + P_{FO2})(1 + FO\ effect)$ because every time a FO radical is produced an ozone molecule is lost and the effects of reforming F or FO_2 from FO may be calculated from eq V. As seen from Figure 12C, the maximum possible effect of the FO_x cycle is small. Less than about 2 ozone molecules are destroyed per F atom released into the stratosphere. This number should be compared to 10^3–10^4 for Cl atoms. The effect of F atoms on the stratospheric ozone layer is therefore likely to be negligible.

The method used to calculate the upper limit for the number of ozone molecules destroyed per F atom released into the stratosphere is not exact. However, it gives a good estimate of the ozone-depleting effect of F atoms and shows that, with the currently known FO_x reactions, FO_x cycles do not pose a threat to the stratospheric ozone layer.

From the discussion above we may now estimate an upper limit for the ODP (ozone depletion potential) of HFCs (hydrofluorocarbons) due to the ozone destruction by F atoms. Most HFCs have atmospheric lifetimes with respect to reaction with OH radicals of >5 years. Only 5–10% of the HFCs are degradated in the stratosphere, hence reducing the ODP of these compounds by a factor of at least 10 as compared to CFCs. As indicated above, F atoms are at least 1000 times less efficient than Cl atoms in destroying ozone in the stratosphere. An upper limit for the ozone depletion potential due to the FO_x cycles of HFC-134a (CF_3-CFH_2), an important CFC substitute, is $\sim 10^{-4}$. This value is determined under the worst case assumption that all the fluorine atoms in HFC-134a are released as F atoms. We therefore believe that the ozone depletion potential of HFCs due to F atoms formed in the stratosphere is negligible.

Acknowledgment. J.S. thanks the Danish Research Academy for a research scholarship. O.J.N. thanks the Commission of the European Communities for financial support. O.J.N. and J.S. thank, for financial support, the AFEAS under Contract CTR93-45/P93-120. The authors also thank Steve Japar (Ford Motor Co.) for helpful discussions. The authors are indebted to E. E. Larsen for the construction of the high-pressure gas cell and to T. Johansen for skillful operation of the linarc accelerator.

References and Notes

(1) Alternative Fluorocarbon Environmental Acceptability Study, W.M.O. Global Ozone Research and Monitoring Project, Report No. 20; Scientific Assessment of Stratospheric Ozone, Vol. 2, 1989.
(2) Scientific Assessment of Stratospheric Ozone Depletion: 1991, World Meteorological Organization Global Ozone Research and Monitoring Project, Report No. 25.
(3) Nielsen, O. J.; Sehested, J. *Chem. Phys. Lett.* **1993**, *213*, 433 and references therein.
(4) Ravishankara, A. R.; Turnipseed, A. A.; Jensen, N. R.; Barone, S.; Mills, M.; Howard, C. J.; Solomon, S. *Science* **1994**, *263*, 71.
(5) Francisco, J. S.; Sin, Y. *Chem. Phys. Lett.* **1993**, *215*, 58.
(6) Francisco, J. S. *J. Phys. Chem.* **1993**, *98*, 2198.
(7) Pagsberg, P.; Ratajczak, E.; Sillesen, A.; Jodkowski, J. T. *Chem. Phys. Lett.* **1987**, *141*, 88.
(8) Lyman, J. L.; Holland, R. *J. Phys. Chem.* **1988**, *92*, 7232.
(9) Ellermann, T.; Sehested, J.; Nielsen, O. J.; Wallington, T. J.; Pagsberg, P. *Chem. Phys. Lett.* **1993**, *218*, 287.
(10) Hippler, H. Private communication, 1993.
(11) Nielsen, O. J. Risø National Laboratory Report Risø-R-480, 1984.
(12) Ellermann, T. Risø National Laboratory Report Risø-M-2932, 1991.
(13) Wallington, T. J.; Ellermann, T.; Nielsen, O. J.; Sehested, J. *J. Phys. Chem.* **1993**, *98*, 2346.
(14) Sehested, J. *Int. J. Chem. Kinet.*, accepted for publication.
(15) Wallington, T. J.; Dagaut, P.; Kurylo, M. J. *Chem. Rev.* **1992**, *92*, 667.
(16) DeMore, W. B.; Sander, S. P.; Golden, D. M.; Molina, M. J.; Hampson, R. F., Jr.; Kurylo, M. J.; Howard, C. J.; Ravishankara, A. R.; Kolb, C. E. JPL Publication 92-20, 1992.
(17) Sehested, J.; Nielsen, O. J. Unpublished results.
(18) Uthman, A. P.; Sherman, G. A.; Takacs, G. A. *Spectrochim. Acta* **1977**, *34A*, 1109.
(19) Wallington, T. J.; Hurley, M. D.; Shi, J.; Maricq, M. M.; Sehested, J.; Nielsen, O. J.; Ellermann, T. *Int. J. Chem. Kinet.* **1993**, *25*, 651.
(20) Bedzhanyan, Y. R.; Markin, E. M.; Gershenzon, Y. M. *Kinet. Catal.* **1992**, *33*, 591.
(21) Nielsen, O. J.; Ellermann, T.; Sehested, J.; Bartkiewicz, E.; Wallington T. J.; Hurley, M. D. *Int. J. Chem. Kinet.* **1992**, *24*, 1009.
(22) Brasseur, G.; Solomon, S. *Aeronomy of the Middle Atmosphere*; Reidel: Dordrecht, The Netherlands, 1986.
(23) Maricq, M. M.; Szente, J. J. *Chem. Phys. Lett.* **1993**, *213*, 449.

2346 Reprinted from The Journal of Physical Chemistry, 1994, 98.

Atmospheric Chemistry of FCO_x Radicals: UV Spectra and Self-Reaction Kinetics of FCO and $FC(O)O_2$ and Kinetics of Some Reactions of FCO_x with O_2, O_3, and NO at 296 K

Timothy J. Wallington*

Research Staff, SRL-E3083, Ford Motor Company, Dearborn, Michigan 48121-2053

Thomas Ellermann,† Ole J. Nielsen,* and Jens Sehested

Section for Chemical Reactivity, Environmental Science and Technology Department, Risø National Laboratory, DK-4000 Roskilde, Denmark

Received: September 28, 1993; In Final Form: December 24, 1993[⊗]

A pulse radiolysis technique has been used to measure the UV spectra of FCO and $FC(O)O_2$ radicals over the ranges 265–275 and 220–290 nm, respectively. At 269.6 nm, $\sigma_{FCO} = (1.7 \pm 0.2) \times 10^{-18}$ cm^2 molecule^{-1}; at 250 nm, $\sigma_{FC(O)O_2} = (2.1 \pm 0.2) \times 10^{-18}$ cm^2 molecule^{-1}. The decay of UV absorption was used to study the kinetics of the self-reactions of FCO and $FC(O)O_2$ radicals at 296 ± 2 K. Observed self-reaction rate constants, defined as $-d[FCO]/dt = 2k_7[FCO]^2$ and $-d[FC(O)O_2]/dt = 2k_{obs8}[FC(O)O_2]^2$, were $k_7 = (1.6 \pm 0.2) \times 10^{-11}$ and $k_{obs8} = (6.0 \pm 0.7) \times 10^{-12}$ cm^3 molecule^{-1} s^{-1}. A rate constant, $k_1 = (1.2 \pm 0.2) \times 10^{-12}$ cm^3 molecule^{-1} s^{-1}, was derived for the addition reaction $FCO + O_2 \rightarrow FC(O)O_2$ in 1000 mbar of SF_6 diluent. Rate constants for the reactions of FCO, FC(O)O, and $FC(O)O_2$ radicals with NO were determined to be $(1.0 \pm 0.2) \times 10^{-12}$, $(1.3 \pm 0.7) \times 10^{-10}$, and $(2.5 \pm 0.8) \times 10^{-11}$, cm^3 molecule^{-1} s^{-1}, respectively. An upper limit of $k_3 < 6 \times 10^{-14}$ cm^3 molecule^{-1} s^{-1} was measured for the reaction of FC(O)O radicals with O_3. Finally, a rate constant of $(5.5 \pm 0.7) \times 10^{-12}$ cm^3 molecule^{-1} s^{-1} was measured for the association reaction of F atoms to NO in 1000 mbar of SF_6 diluent. All experiments were performed at 296 ± 2 K. Results are discussed with respect to the atmospheric chemistry of hydrofluorocarbons.

Introduction

An international effort is taking place to replace chlorofluorocarbons (CFCs) with environmentally acceptable alternatives.[1-3] Hydrofluorocarbons (HFCs) are one class of CFC replacements. For example, HFC-134a (CF_3CFH_2) is a replacement for CFC-12 (CF_2Cl_2) in air conditioning and refrigeration units. Prior to their large-scale industrial use, the environmental consequences of HFC release into the atmosphere need to be considered.

To define the environmental impact of the release of HFCs, two main questions need to be answered. First, what will be the effect on the ozone layer? Second, what will be the effect on potential global climate change? For each of these questions a subquestion needs to be considered: what effect will the atmospheric degradation products of HFCs have on the ozone layer and potential global climate change? The answer to the first question is straightforward: HFCs contain no chlorine and therefore are not expected to impact the ozone layer. The second question has been addressed by atmospheric modeling studies.[4,5] Because of the ability of OH radicals to scavenge HFCs in the lower atmosphere, the atmospheric lifetimes of HFCs are, in general, much shorter than CFCs. With shorter lifetimes the HFCs have smaller global warming potentials. For example, the global warming potential of HFC-134a is approximately an order of magnitude less than for CFC-12. Part of the subquestion has been addressed in our laboratories by identifying the atmospheric degradation products for a series of HFCs (HFC-23,[6] HFC-32,[7] HFC-41,[8] HFC-125,[9] HFC-134,[10] and HFC-134a[11,12]).

From work performed in our laboratories, and elsewhere,[13-15] it is clear that either HC(O)F or COF_2, or both, are formed during the atmospheric oxidation of every HFC. The atmospheric chemistries of HC(O)F and COF_2 are believed to be dominated by incorporation into rain–cloud–sea water followed by hydrolysis. Photolysis, which is a minor loss process for both HC(O)F and COF_2 overall, may be important in the stratosphere. Photolysis of HC(O)F and COF_2 is expected to produce FCO radicals which will add O_2 to give $FC(O)O_2$ radicals.

There has been speculation that $FC(O)O_x$ radicals could participate in catalytic ozone destruction cycles,[16] for example:

$$FC(O)O_2 + O_3 \rightarrow FC(O)O + 2O_2$$

$$FC(O)O + O_3 \rightarrow FC(O)O_2 + O_2$$

Detailed information regarding the atmospheric chemistry of FCO_x radicals, especially their reaction with O_3, is needed to place discussions of the environmental impact of HFC usage on a sound scientific basis. Unfortunately, there is little data available concerning the atmospheric chemistry of FCO_x radicals. We have used pulse radiolysis combined with transient UV absorption spectroscopy to provide such information. Results concerning the UV absorption spectra and self-reaction kinetics of FCO, FC(O)O, and $FC(O)O_2$ radicals and the kinetics of reactions 1–4 are reported herein.

$$FCO + O_2 + M \rightarrow FC(O)O_2 + M \quad (1)$$

$$FC(O)O_2 + NO \rightarrow FC(O)O + NO_2 \quad (2)$$

$$FC(O)O + O_3 \rightarrow \text{products} \quad (3)$$

$$FC(O)O + NO \rightarrow FNO + CO_2 \quad (4)$$

Experimental Section

The pulse radiolysis transient UV absorption spectrometer used in the present experiments has been described previously.[17] FCO radicals were generated by the radiolysis of SF_6/CO gas mixtures in a 1-L stainless steel reactor with a 30-ns pulse of 2-MeV electrons from a Febetron 705B field emission accelerator. SF_6

* Authors to whom correspondence may be addressed.
† Permanent address: NERI, DK-4000, Roskilde, Denmark.
⊗ Abstract published in *Advance ACS Abstracts*, February 1, 1994.

0022-3654/94/2098-2346$04.50/0

was always in great excess and was used to generate fluorine atoms:

$$SF_6 + e^- \rightarrow F + \text{products} \quad (5)$$

$$F + CO \rightarrow FCO \quad (6)$$

Five sets of experiments were performed. First, the ultraviolet absorption spectra of FCO and $FC(O)O_2$ radicals were determined by observing the maximum in the transient UV absorption at short times (10–40 μs) following the pulse radiolysis of SF_6/CO and $SF_6/CO/O_2$ mixtures, respectively. Second, using a longer time scale (100–400 μs), the subsequent decay of the absorption was monitored to determine the kinetics of reactions 7 and 8:

$$FCO + FCO \rightarrow \text{products} \quad (7)$$

$$FC(O)O_2 + FC(O)O_2 \rightarrow \text{products} \quad (8)$$

Third, the rate of conversion of FCO into $FC(O)O_2$ radicals was monitored, as a function of the concentration of O_2 present, to derive a value for the rate constant of reaction 1. Fourth, the rate of NO_2 formation and the behavior of FC(O)O following the pulse radiolysis of $SF_6/CO/O_2/NO$ mixtures were used to measure k_2 and k_4. Finally, the radiolysis of $SF_6/CO/O_2/O_3$ mixtures was used to study the behavior of FC(O)O radicals in the presence of O_3 and, hence, to derive kinetic data for reaction 3.

To monitor the transient UV absorption, the output of a pulsed 150-W xenon arc lamp with multipassed through the reaction cell using internal White cell optics (40-, 80-, or 120-cm path length). A McPherson grating spectrometer, Hamamatsu R 955 photomultiplier, and Biomation 8100 waveform digitizer were used to detect and record the light intensity at the desired wavelength. The spectral resolution used was 0.8 nm. Data transfer and storage were controlled by a PDP11 minicomputer. The following reagent concentrations were used: SF_6, 95–1000 mbar; O_2, 0–40 mbar; CO, 40 mbar; NO, 0–10 mbar (1 mbar = 2.46×10^{16} molecules cm^{-3}). All experiments were performed at 296 ± 2 K. Ultrahigh-purity O_2 was supplied by L'Air Liquide, SF_6 (99.97%) and CO (>99.9%) were supplied by Gerling and Holz, and NO (>99.8%) was supplied by Messer Griesheim. All reagents were used as received.

Ozone was produced by flowing O_2 through a conventional discharge ozonizer. The O_2 was purified before entering the ozonizer by flowing through silica gel. Trace amounts of NO_2, N_2O_5, and HNO_3 were removed from the ozone/oxygen mixture by flowing through a silica gel trap cooled to −80 °C. Up to 1.0% O_3 in O_2 was produced in this way.

Ozone concentrations in the reaction cell were determined by measurement of the absorption at 272 or 288 nm before and after filling with reaction mixtures. Ozone absorbs strongly at these wavelengths (σ_{O_3}(272 nm) = 6.92×10^{-18} and σ_{O_3}(288 nm) = 1.79×10^{-18} cm^2 $molecule^{-1}$).[18] No absorption at these wavelengths was detected when the reaction cell was filled with reactant gases other than O_3. Ozone concentrations used were in the range 0.25–0.39 mbar.

Immediately prior to the conclusion of the experimental work described herein, a Princeton Applied Research OMA-II diode array was installed at the exit slit of the monochromator in place of the photomultiplier which has been routinely used to measure the transient absorptions. The system consisted of the diode array, an image amplifier (type 1420-1024HQ), a controller (type 1421), and a conventional PC computer for data handling and storage. Spectral calibration was achieved using Hg and Ne pen ray lamps. Diode array spectra of FCO and FC(O)O radicals were recorded and are presented herein.

Results and Discussion

Spectrum of FCO Radicals. Following the pulse radiolysis of SF_6/CO mixtures a rapid increase in the UV absorption was observed, followed by a slower decay. Figure 1 shows the transient absorption at 269.6 nm observed for the first 180 μs following the radiolysis of a mixture of 40 mbar of CO and 960 mbar of SF_6 (1 mbar = 2.46×10^{16} molecules cm^{-3}). The UV path length was 120 cm. No absorption was observed when either 40 mbar of CO or 960 mbar of SF_6 was radiolyzed separately. We ascribe the absorption shown in Figure 1 to the formation of FCO radicals and their subsequent loss by self-reaction.

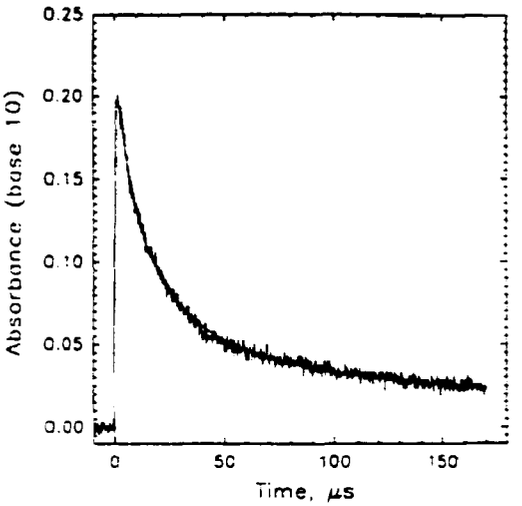

Figure 1. Transient absorption at 269.6 nm following the radiolysis of a mixture of 40 mbar of CO and 960 mbar of SF_6 using a UV path length of 120 cm. The solid line is a second-order decay fit.

Measurement of the absolute absorption spectrum of FCO radicals requires calibration of the initial F atom concentration. Additionally, experimental conditions are needed to ensure that there is 100% conversion of F atoms to FCO radicals. The yield of F atoms was established by monitoring the transient absorption at 260 nm due to methylperoxy radicals produced by radiolysis of $SF_6/CH_4/O_2$ mixtures as described previously.[19] Using a value of 3.18×10^{-18} cm^2 $molecule^{-1}$ for $\sigma(CH_3O_2)$ at 260 nm,[20] the yield of F atoms at 1000 mbar of SF_6 was measured to be (2.92 ± 0.15) × 10^{15} cm^{-3} at full irradiation dose. The quoted error represents statistical uncertainty (2 standard deviations). Potential systematic error associated with the uncertainty in $\sigma(CH_3O_2)$ is estimated to be ±10%. Combining the statistical and potential systematic uncertainties, we arrive at a calibrated F atom yield of (2.92 ± 0.33) × 10^{15} cm^{-3}.

To work under conditions where the F atoms are converted stoichiometrically into FCO, it is necessary to consider potential interfering secondary chemistry such as reaction 9.

$$F + FCO \rightarrow \text{products} \quad (9)$$

To check for such a complication, the maximum transient absorption at 269.6 nm was measured in experiments using [CO] = 40 mbar and [SF_6] = 960 mbar, with the radiolysis dose varied over a wide range. Figure 2 shows the maximum absorption at 269.6 nm as a function of the radiolysis dose. (The UV path length was 80 cm.) For doses less than one-half of maximum, the absorption increased linearly with radiolysis dose (and hence initial radical concentration), suggesting that unwanted secondary radical–radical reactions are unimportant. The absorption observed using maximum dose was approximately 10% less than that expected from a linear extrapolation of the low-dose data. We ascribe this behavior to incomplete conversion of F atoms into FCO radicals at the highest initial F atom concentration used. Linear least-squares analysis of the data in Figure 2 (full dose experiment excepted) gives a slope of 0.168 ± 0.005. Combining this value with the calibrated yield of F atoms of (2.92 ± 0.33) × 10^{15} molecules cm^{-3} (full dose and [SF_6] = 1000 mbar) gives σ(FCO) = (1.73 ± 0.20) × 10^{-18} cm^2 $molecule^{-1}$ at

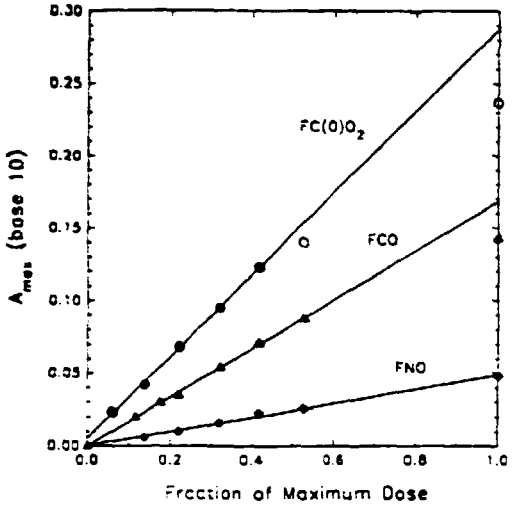

Figure 2. Maximum transient absorptions at 250 (●), 269.6 (▲), and 310.5 nm (◆) observed following the pulsed radiolysis of mixtures of 40 mbar of CO, 40 mbar of O_2, and 920 mbar of SF_6; 40 mbar of CO and 960 mbar of SF36; and 2 mbar of NO and 998 mbar of SF_6, respectively, as a function of the radiolysis dose. Solid lines are linear least-squares fits to the filled data points. Dotted lines are second-order fits to aid in visual inspection of the data trend.

TABLE 1: Measured UV Absorption Cross Sections

FCO		FC(O)O$_2$	
λ (nm)	$\sigma \times 10^{20}$ (cm^2 molecule^{-1})	λ (nm)	$\sigma \times 10^{20}$ (cm^2 molecule^{-1})
265.4	152	220	272
365.9	105	225	315
266.4	69	230	297
266.9	62	235	301
267.0	74	240	269
267.5	57	245	264
268.0	57	250	213
268.5	87	255	181
269.0	139	260	155
269.4	161	265	117
269.6	173	270	83
269.9	184	275	66
270.4	130	280	41
270.9	94	285	26
271.4	71	290	19
271.9	62		
272.4	57		
272.9	59		
273.4	81		
273.9	127		
274.4	159		

269.6 nm. Quoted errors reflect statistical and possible systematic uncertainties.

To map out the absorption spectrum of FCO radicals, experiments were performed to measure the initial absorption between 265 and 275 nm following the pulsed irradiation of mixtures of 40 mbar of CO and 960 mbar of SF_6. Initial absorptions were then scaled to that at 269.6 nm and converted into absolute absorption cross sections. Values so obtained are given in Table 1 and shown in Figure 3, where they are compared to the data reported recently by Maricq et al.[21]

Finally, a diode array camera was used to obtain the spectrum given in Figure 3. The conditions were as follows: spectral resolution, 0.15 nm; gate, 30 μs; delay, 1 μs; [CO], 40 mbar; [SF_6], 960 mbar; full radiolysis dose. As seen from this figure, the band positions measured in the present work are in good agreement with the results from ref 21. The sharper nature of the spectrum measured here is explained by the greater spectral resolution used in the present work: 0.8 nm compared to ≈1–2 nm.[21] The integrated absorption measured in the present work is approximately 10–20% lower than reported previously.[21] Such

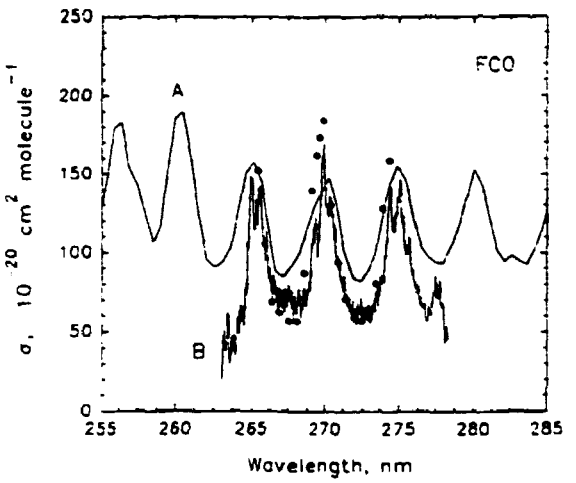

Figure 3. Absorption cross section data for FCO radicals measured in this work (●). The solid line A is the spectrum reported by Maricq et al.[21] The solid line B is the diode array spectrum recorded in this work.

a difference is well within the combined experimental uncertainties inherent in both studies. The spectral features measured here are also consistent with those reported by Milligan et al.[22] and Wang and Jones.[23]

Kinetic Study of the Self-Reaction of FCO Radicals. Figure 1 shows a typical transient absorption trace obtained for the self-reaction of FCO radicals, together with a nonlinear least-squares second-order fit. As discussed in previous publications,[24,25] kinetic analysis of second-order decays can be complicated by the formation of products which absorb at the monitoring wavelength, leading to a postradiolysis transmitted light intensity which is lower than the preradiolysis value. Accordingly, the experimental data were fit to the three-parameter expression

$$1/B - 1/B_0 = 2kt/\sigma_{eff}L \qquad (I)$$

where $B = \ln(I_\infty/I)$, $B_0 = \ln(I_\infty/I')$, k is the second-order rate constant for the self-reaction of the radicals, σ_{eff} is the absorption cross section of the radical minus that of any absorbing product formed at the monitoring wavelength (in the case of FCO there was no residual absorption and $\sigma_{eff} = \sigma_{FCO}$), L is the monitoring UV path length (either 80 or 120 cm), I' is the minimum transmitted light intensity following the radiolysis pulse, I_∞ is the final light intensity, and I is the transmitted light intensity at time t. In the fitting algorithm the three parameters B, B_0, and k/σ_{eff} were fit simultaneously.

The decay of the transient absorption following radiolysis of SF_6/CO mixtures was monitored at wavelengths between 265 and 275 nm. At all wavelengths the decay was well represented by a second-order least-squares fit. No residual absorption was observed, indicating the absence of any long-lived product which absorbs significantly in the 265–275-nm region. The reciprocal of the observed half-life for the decay of absorption is plotted as a function of the initial FCO radical concentration in Figure 4. The initial radical concentration was calculated from the observed initial absorption using the cross sections given in Figure 3.

As shown in Figure 4, the reciprocal of the observed half-life for the decay of absorption was a linear function of $[FCO]_0$. This linearity suggests that only one species is responsible for the absorption in this wavelength region, and so the kinetic analysis is not complicated by the presence of other absorbing species. Linear least-squares analysis of the data in Figure 4 gives a y-axis intercept which is not statistically different from zero and a slope $= 2k_7 = (3.20 \pm 0.12) \times 10^{-11}$ cm^3 molecule^{-1} s^{-1}. Hence, $k_7 = (1.60 \pm 0.06) \times 10^{-11}$ cm^3 molecule^{-1} s^{-1}. Quoted errors are 2 standard deviations. Including our estimate of potential uncertainty in the absolute radical yield calibration (11%) gives $k_7 = (1.6 \pm 0.2) \times 10^{-11}$ cm^3 molecule^{-1} s^{-1}. There have been two

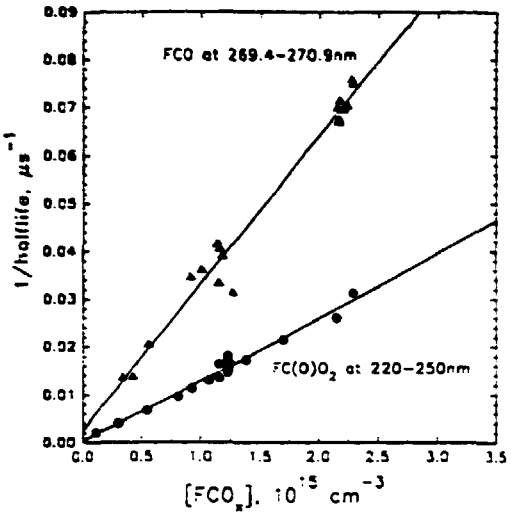

Figure 4. Reciprocal of the half-lives for the decay of absorption at 269.4–270.9 (▲) and 220–250 nm (●), attributed to FCO and $FC(O)O_2$ radicals, as a function of the initial radical concentration. Solid lines are linear least-squares fits.

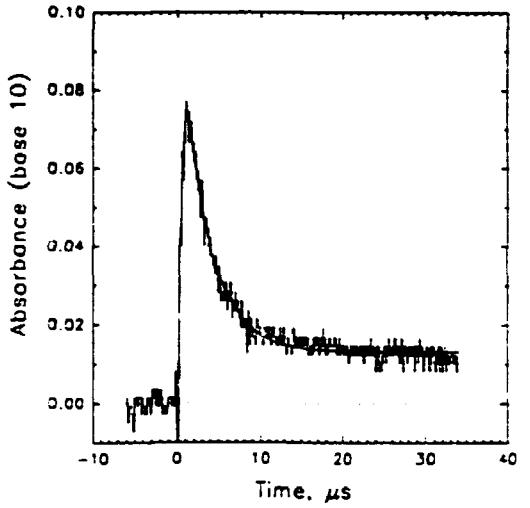

Figure 5. Transient absorption at 300 nm observed following the pulsed radiolysis (full dose) of a mixture of 40 mbar of CO, 9.8 mbar of O_2, and 950 mbar of SF_6. The solid line is a first-order decay fit which gives $k^{1st} = 3.1 \times 10^5$ s^{-1}.

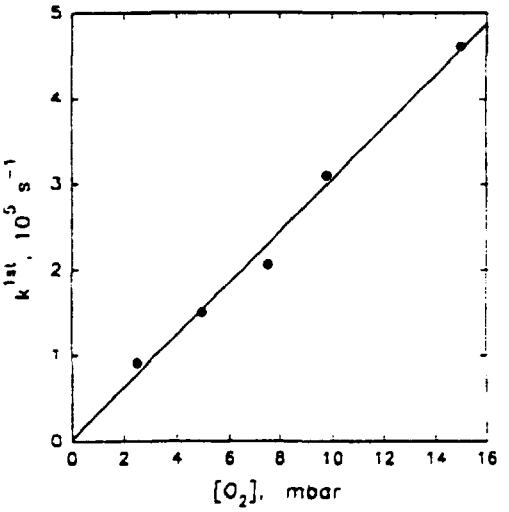

Figure 6. Plot of k^{1st} versus the concentration of O_2.

reported values of k_7 with which we can compare our measurement. In the work of Maricq et al.,[21] the self-reaction of FCO radicals was studied in the presence of 5 Torr of F_2, 95 Torr of He, 100 Torr of CO, and 100 Torr of N_2. A value of $k_7 = (1.9 \pm 0.2) \times 10^{-11}$ cm^3 $molecule^{-1}$ s^{-1} was reported, which is consistent with that measured in the present work. In the work of Behr et al.[26] reaction 7 was studied in the presence of 1.5–2.5 Torr of helium diluent, and a value of $k_7 = (4.9 \pm 2.0) \times 10^{-11}$ $molecule^{-1}$ s^{-1} was reported. It is interesting to note the apparent inverse pressure effect, with reported values of k_7 increasing with decreasing total pressure. A possible explanation for this observation is the presence of vibrationally excited FCO radicals at lower pressures. There are no available data concerning the rate at which collisions with He, N_2, or SF_6 deactivate vibrationally excited FCO. However, the rate of energy transfer from vibrationally excited CO has been studied extensively[27] and can serve as a rough guide for the behavior of FCO. The rate constant for collisional relaxation of CO(v=1) at 298 K by N_2 is of the order of 10^{-14} cm^3 $molecule^{-1}$ s^{-1}. At 1 Torr total pressure the lifetime of CO(v=1) is then approximately 3 ms. At 760 Torr the lifetime is approximately 4 μs. Helium is a less efficient third body than N_2, whereas SF_6 is more efficient than N_2. The experiments described by Behr et al.[26] were performed using 1.5–2.5 Torr of helium diluent with the FCO kinetics monitored on times scales of the order of milliseconds. It is possible that vibrationally excited FCO played an important role in these experiments. The experiments described by Maricq et al.[21] were performed at 300 Torr total pressure with the FCO kinetics monitored for several hundred microseconds. It seems unlikely that vibrationally excited FCO played a major role in these experiments; however, a minor role cannot be excluded. In the present work 1000 mbar of SF_6 diluent was used, and the decay of FCO radicals was monitored over 200 μs. Vibrationally excited FCO radicals produced in reaction 6 will be rapidly thermalized and are not expected to interfere with the measurement of k_7 in the present work.

Finally, it is worth noting that the diluent N_2 gas used by Maricq et al.[21] was industrial grade (99%) and may have contained traces of O_2. The presence of a small O_2 impurity would augment the FCO loss via reactions 1 and 10, thereby explaining why the value reported by Maricq et al.[21] is slightly larger than that measured in the present work.

$$FCO + O_2 \rightarrow FC(O)O_2 \qquad (1)$$

$$FCO + FC(O)O_2 \rightarrow FC(O)O + FC(O)O \qquad (10)$$

Spectrum of $FC(O)O_2$ Radicals and Kinetics of the FCO + O_2 Reaction. The UV spectrum of $FC(O)O_2$ radicals was studied using the pulsed radiolysis of $SF_6/CO/O_2$ mixtures. Following radiolysis a rapid increase in absorption in the ultraviolet at 260–300 nm was observed followed by a rapid decay and then a slower decay. The observed absorption is ascribed to the formation of FCO radicals, their conversion into $FC(O)O_2$ radicals, and then the loss of $FC(O)O_2$ via self-reaction. The rapid decay of the initial absorption displayed first-order kinetics. To measure k_1, experiments were performed using a monitoring wavelength of 300 nm to measure the first-order loss of FCO following the pulse radiolysis (maximum dose) of 950 mbar of SF_6, 40 mbar of CO, and 2.5–15 mbar of O_2. Figure 5 shows the transient absorption at 300 nm observed for the first 40 μs following the radiolysis of a mixture containing 9.8 mbar of O_2. The solid line is a first-order fit to the data which gives a first-order loss rate, k^{1st}, of 3.1×10^5 s^{-1}. Figure 6 shows a plot of k^{1st} versus $[O_2]$. Linear least-squares analysis of the data in Figure 6 gives $k_1 = (1.23 \pm 0.14) \times 10^{-12}$ cm^3 $molecule^{-1}$ s^{-1}. (Quoted errors are 2 standard deviations.) This result is approximately 50% larger than that reported in the presence of 330 Torr of N_2/He/CO mixtures[28] and presumably reflects the greater third-body efficiency of the 1000 mbar of SF_6 diluent used in our work.

In experiments to measure $\sigma(FC(O)O_2)$ the concentration of O_2 was 40 mbar. At this oxygen concentration the conversion of FCO into $FC(O)O_2$ radicals will be >98% complete within 4

μs. Accordingly, in experiments to measure $\sigma(FC(O)O_2)$, the transient absorption 4 μs after the radiolysis pulse was ascribed to absorption due to the peroxy radical.

To measure the UV absorption spectrum of $FC(O)O_2$ radicals, experimental conditions have to be chosen to minimize unwanted reactions such as reactions 9–12 which interfere with conversion of F atoms into $FC(O)O_2$.

$$F + O_2 + M \rightarrow FO_2 + M \quad (11)$$

$$F + FCO \rightarrow \text{products} \quad (9)$$

$$F + FC(O)O_2 \rightarrow \text{products} \quad (12)$$

$$FCO + FC(O)O_2 \rightarrow FC(O)O + FC(O)O \quad (10)$$

Reaction 11 competes with reaction 6 for the available F atoms. The kinetics of both reactions have been studied in our laboratory. In 1000 mbar of SF_6, $k_6 = (1.8 \pm 0.2) \times 10^{-12}$ [29] and $k_{11} = (1.9 \pm 0.3) \times 10^{-13}$ cm^3 molecule^{-1} s^{-1}.[30] The importance of reaction 11 can be minimized by lowering $[O_2]$. However, as $[O_2]$ is decreased, reaction 10 becomes more significant. Clearly, a compromise is needed. Experiments were performed using [CO] = 40 mbar, $[O_2]$ = 40 mbar, and $[SF_6]$ = 920 mbar. Under these conditions, 90.5% of the F atoms are converted into FCO radicals and 9.5% into FO_2 radicals.

Kinetic data for reactions 9, 10, and 12 are not available, and so it is difficult to estimate their impact. To check for these unwanted radical–radical reactions, the maximum transient absorption at 250 nm was measured in experiments using [CO] = 40 mbar, $[O_2]$ = 40 mbar, and $[SF_6]$ = 920 mbar with the radiolysis dose varied by an order of magnitude. The UV path length was 120 cm. Figure 2 shows the observed maximum of the transient absorption at 250 nm as a function of the dose. For doses less than one half of maximum the absorption increased linearly with radiolysis dose (and hence initial F atom concentration), suggesting the absence of unwanted radical–radical reactions such as (9), (10), and (12). Linear least-squares analysis of the data in Figure 2 (full and half dose experiments excepted) gives a slope = 0.283 ± 0.010. Quoted errors are 2 standard deviations. Combining this value with three additional pieces of information, (i) the calibrated yield of F atoms of (2.92 ± 0.33) × 10^{15} cm^{-3} (full dose and $[SF_6]$ = 1000 mbar), (ii) the calculated conversion of F atoms into 90.5% FCO radicals and 9.5% FO_2 radicals, and (iii) the absorption cross section for FO_2 at 250 nm (σ = 1.11 × 10^{-18} cm^2 molecule^{-1} [30], gives $\sigma(FC(O)O_2)$ at 250 nm = (2.13 ± 0.25) × 10^{-18} cm^2 molecule^{-1}. The quoted errors include uncertainty in the calibrated F atom yield and reflect the accuracy of the measurement.

To map out the spectrum of $FC(O)O_2$ radicals, experiments were performed to measure the absorption at 220–290 nm following the pulsed irradiation of $SF_6/CO/O_2$ mixtures. The absorptions were then scaled to that at 250 nm to obtain absolute absorption cross sections and corrected for the component of absorption attributable to FO_2 radicals. The correction was calculated using the expression $\sigma(FC(O)O_2) = [\sigma(\text{observed}) - 0.095\sigma(FO_2)]/0.905$. Values for $\sigma(FO_2)$ were taken from the literature.[30] Measured absorption cross sections are given in Table 1 and shown in Figure 7, where they are compared to those available in the literature;[28] the agreement is excellent.

Kinetic Study of the Self-Reaction of $FC(O)O_2$ Radicals. Transient absorption traces at 220–250 nm obtained 4–400 μs after the pulsed radiolysis of mixtures of 40 mbar of O_2, 40 mbar of CO, and 920 mbar of SF_6 (full radiolysis dose) were fit using expression I. In all cases, within the experimental uncertainties, the decays followed second-order kinetics. There was no significant residual absorption above that expected from the absorption attributed to FO_2 radicals. Figure 4 shows a plot of the reciprocal of the observed half-lives for the decay of absorption,

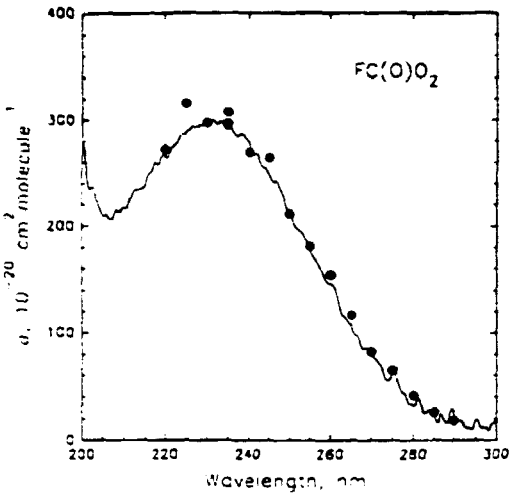

Figure 7. Absorption cross-section data for $FC(O)O_2$ radicals measured in this work (●). The solid line is the spectrum reported by Maricq et al.[28]

as determined by fitting expression I to the transient, plotted as a function of the initial $FC(O)O_2$ radical concentration. Linear least-squares analysis gives a slope = $2k_{8obs}$ = (1.20 ± 0.04) × 10^{-11}; hence k_{8obs} = (6.0 ± 0.2) × 10^{-12} cm^3 molecule^{-1} s^{-1}. Quoted errors are 2 standard deviations. Including our estimate of a potential 11% uncertainty in the absolute radical yield calibration gives k_{8obs} = (6.0 ± 0.7) × 10^{-12} cm^3 molecule^{-1} s^{-1}. This result is in excellent agreement with a recent report of k_8 = 6.6 × 10^{-12} cm^3 molecule^{-1} s^{-1} at 295 K.[28]

The products of the self-reaction of $FC(O)O_2$ radicals have been studied recently using the FTIR–Smog chamber technique.[31] From the observed product yields it was determined that reaction 8 proceeds predominantly (80 ± 20%), if not exclusively, via channel 8a with a minor, or zero, contribution by channel 8b:

$$FC(O)O_2 + FC(O)O_2 \rightarrow FC(O)O + FC(O)O + O_2 \quad (8a)$$

$$FC(O)O_2 + FC(O)O_2 \rightarrow FC(O)OOC(O)F + O_2 \quad (8b)$$

The lifetime of FC(O)O radicals with respect to thermal dissociation into F atoms and CO_2 at 298 K is at least 3 s.[31] In the present experiments FC(O)O radicals produced in reaction 8a are expected to either undergo self-reaction to give the dimer (FC(O)OOC(O)F) or react with $FC(O)O_2$ to give the trioxide:

$$FC(O)O + FC(O)O \rightarrow FC(O)OOC(O)F \quad (13)$$

$$FC(O)O + FC(O)O_2 \rightarrow FC(O)OOOC(O)F \quad (14)$$

The fact that no trioxide end product was observed in the FTIR–Smog chamber study of reaction 8[31] places an upper limit of approximately 2 min on the lifetime of the trioxide. It is possible that the trioxide is formed as a stable product within the time scales used in the present pulse radiolysis experiments. If so, then the observed second-order rate constant k_{8obs} measured here is not the true bimolecular rate constant, but rather it is an overestimate. In a worst case where $k_{14} \gg k_8$ each FC(O)O radical formed in reaction 8a will consume an additional $FC(O)O_2$ radical via reaction 14. Hence, k_{8obs} could be up to a factor of 1.8 greater than the true bimolecular rate constant k_8. Kinetic data for reaction 14 and information regarding the lifetime of the trioxide are needed to fully assess the role played by reaction 14. We will present kinetic data for reaction 14 in a subsequent section dealing with the study of the reaction of FC(O)O radicals with O_3. Unfortunately, there are no available data concerning the lifetime of the trioxide. Thus, it is not possible to fully assess

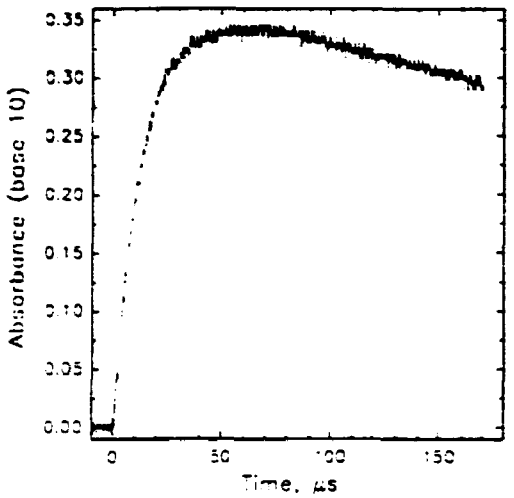

Figure 8. Transient absorption at 696.1 nm following the radiolysis of a mixture of 40 mbar of CO, 40 mbar of O_2, and 920 mbar of SF_6 (full dose, UV path length = 80 cm).

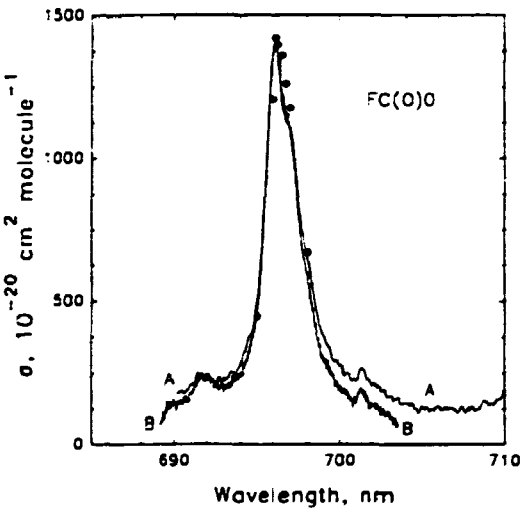

Figure 9. Absorption cross-section data for FC(O)O radicals measured in this work (●). The solid line A is the spectrum reported by Maricq et al.[28] The solid line B is the diode array spectrum recorded in this work.

the impact of reaction 14 on kinetic studies of k_8. This point is discussed further in the following section.

Study of FC(O)O Radicals. The self-reaction of $FC(O)O_2$ radicals produces FC(O)O radicals in a yield of 80 ± 20%.[31] FC(O)O radicals absorb strongly in the visible at 500–700 nm.[28] The formation and decay of FC(O)O radicals can be studied by radiolyzing $SF_6/CO/O_2$ mixtures and monitoring the increase in absorption in the visible. Figure 8 shows the observed transient absorption at 696.1 nm following the radiolysis of a mixture of 40 mbar of CO, 40 mbar of O_2, and 920 mbar of SF_6 (full dose, UV path length = 80 cm). Control experiments were performed in which either SF_6, SF_6/O_2, or SF_6/CO mixtures were radiolyzed separately. No absorption at 696.1 nm was detected. We ascribe the transient absorption shown in Figure 8 to the formation of FC(O)O radicals via reaction 8a. To map out the spectrum of FC(O)O radicals, the monitoring wavelength was increased in 0.2–0.5-nm steps over the range 694–697 nm. As shown in Figure 9, the shape of the resulting spectrum was in good agreement with that given in ref 28.

To place our measured spectrum on an absolute basis, the initial rate of increase in absorption at 696.1 nm was combined with the calculated $FC(O)O_2$ loss rate ($2k_{8obs}[FC(O)O_2]_0^2$) and the branching ratio $k_{8a}/k_8 = 0.8$[31] to give $\sigma(FC(O)O)$. For the data shown in Figure 8 a value of $\sigma(FC(O)O) = 1.4 \times 10^{-17}$ cm² molecule^{-1} is derived. As discussed in the previous section, because of the possible interference of reaction 14, the value of k_{8obs} measured in the present work may be an overestimate of the true bimolecular rate constant k_8. Hence, $2k_{8obs}[FC(O)O_2]_0^2$ may be an overestimate of the rate of production of FC(O)O radicals. Consequently, the value of $\sigma(FC(O)O)$ derived above is a lower limit. In principle, the $\sigma(FC(O)O)$ could be up to a factor of 1.8 greater than derived above. According, we choose to quote $\sigma(FC(O)O) = (2.0 \pm 0.6) \times 10^{-17}$ cm² molecule^{-1}. Maricq et al.[28] have reported absolute absorption cross sections for FC(O)O measured using a technique which was similar to that described above. In their analysis Maricq et al. assumed there were no interferences caused by reaction 14. As stated above, this assumption is not necessarily justified. Nevertheless, a direct comparison of the results obtained in our work and that of Maricq et al.[28] can be made by using $\sigma(FC(O)O) = 1.4 \times 10^{-17}$ cm² molecule^{-1} at 696.1 nm to calibrate our absorption spectrum. As seen from Figure 9 the agreement is excellent. From a detailed consideration of the formation and decay of the transient absorption at 696.1 nm, kinetic data concerning reactions 13 and 14 can be derived. Discussion of these results can be found in the section describing the study of the reaction of FC(O)O radicals with O_3.

Finally, the diode array system was used to obtain the spectrum of FC(O)O radicals given in Figure 9. The conditions were as follows: spectral resolution, 0.13 nm; gate, 7 μs; delay, 50 μs; [CO], 40 mbar; [O_2], 40 mbar; [SF_6], 920 mbar, full radiolysis dose. As seen from this figure, the band positions measured in the present work are in good agreement with the results from ref 28.

Kinetic Studies of the Reactions F + NO → FNO and FCO + NO → Products. As a preliminary exercise prior to the investigation of the reaction of $FC(O)O_2$ radicals with NO, a series of experiments were performed to investigate the reactions of NO with both F atoms and FCO radicals. The reaction of F with NO was measured by observing the first-order rise of the absorption of FNO at 310.5 nm following the radiolysis of mixtures of 1000 mbar of SF_6 and 2–10 mbar of NO. The available literature UV spectra of FNO[32,33] do not report absolute absorption cross sections. To provide such, the maximum absorption following the radiolysis of 1000 mbar of SF_6 and 2 mbar of NO was measured as a function of the radiolysis dose (UV path length = 80 cm); results are shown in Figure 2, from which we derive $\sigma(FNO)$ at 310.5 nm = $(4.73 \pm 0.66) \times 10^{-19}$ cm² molecule^{-1}. The formation of FNO followed first-order kinetics, allowing a value of $k(F+NO) = (5.5 \pm 0.7) \times 10^{-12}$ cm³ molecule^{-1} s^{-1} to be measured. Variation of the radiolysis dose by an order of magnitude and the NO concentration by a factor of 5 had no discernible effect on the value of $k(F+NO)$.

The reaction of FCO radicals with NO is expected to produce either CO + FNO or the adduct FCONO, or both. FNO exhibits a structured UV absorption in the wavelength region 275–350 nm,[32,33] as does FCO. A monitoring wavelength of 303 nm was chosen to measure the decay of FCO in the presence of NO because at this wavelength the difference in the absorption cross sections of FCO and FNO radicals is large. Following the radiolysis of mixtures of 960 mbar of SF_6, 40 mbar of CO, and 0.5–2.2 mbar of NO, a rapid initial increase in absorption at 303 nm was observed followed by a slow decay. The decay of absorption followed first-order kinetics. The observed first-order loss rate, k^{1st}, is plotted as a function of the NO concentration in Figure 10. The y-axis intercept is not statistically significant. Linear least-squares analysis gives $k(FCO+NO) = (1.03 \pm 0.22) \times 10^{-12}$ cm³ molecule^{-1} s^{-1} at 1000 mbar of SF_6 diluent. To the best of our knowledge, there are no literature data with which to compare this result.

Kinetic Study of the Reaction $FC(O)O_2 + NO \rightarrow FC(O)O + NO_2$. The kinetics of reaction 2 were studied by monitoring the rate of increase in absorption at 400 nm (attributed to the

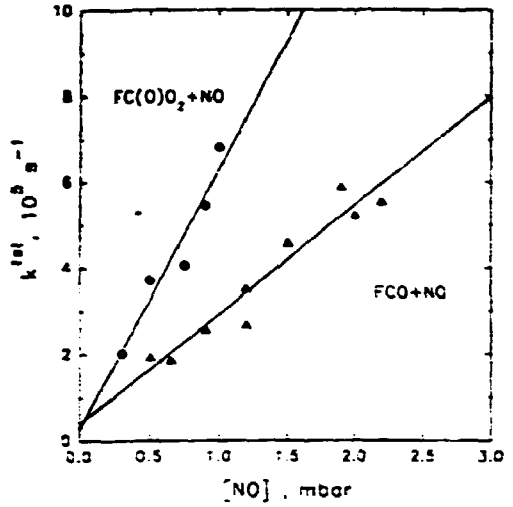

Figure 10. Plot of the pseudo-first-order decay rate of FCO radicals in the reaction of FCO with NO (▲) and the pseudo-first-order appearance rate of NO_2 in the reaction of $FC(O)O_2$ with NO (●), as functions of the NO concentrations.

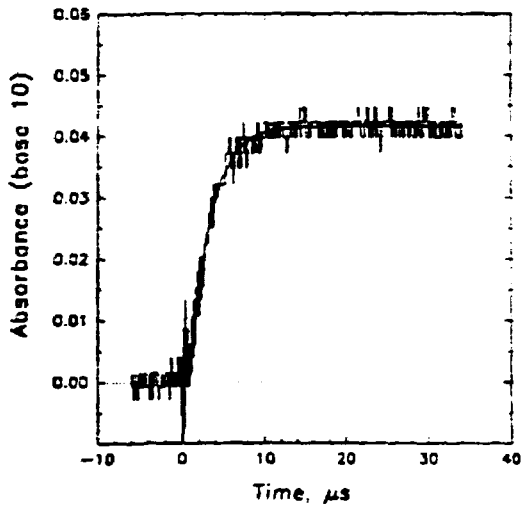

Figure 11. Transient absorption at 400 nm observed following the pulse radiolysis (full dose) of a mixture of 0.75 mbar of NO, 40 mbar of CO, 40 mbar of O_2, and 920 mbar of SF_6. The solid line is a first-order rise fit which gives $k^{1st} = 4.05 \times 10^5\ s^{-1}$.

formation of NO_2) following the radiolysis of mixtures of 0.3–1.0 mbar of NO, 40 mbar of CO, 40 mbar of O_2, and 920 mbar of SF_6. This method of measuring the kinetics of the reaction of peroxy radicals with NO has been used extensively in our laboratory and is discussed in detail elsewhere.[11,34] Figure 11 shows the results from a mixture with [NO] = 0.75 mbar. The smooth curve in Figure 11 is a first-order fit using the expression $Abs(t) = (A_{inf} - C)[1 - \exp(-k^{1st}t)] + C$, where $Abs(t)$ is the absorbance as a function of time, A_{inf} is the absorbance at infinite time, k^{1st} is the pseudo-first-order appearance rate of NO_2, and C is the extrapolated absorbance at $t = 0$. For the data shown in Figure 11, $k^{1st} = 4.05 \times 10^5\ s^{-1}$. In all cases, the rise in absorption followed first-order kinetics. Control experiments were performed in which SF_6/CO, $SF_6/CO/O_2$, SF_6/O_2, or just SF_6 was radiolyzed; no change in absorption at 400 nm was observed. It seems reasonable to conclude that NO_2 is the species responsible for the absorption change following radiolysis of $SF_6/CO/O_2/NO$ mixtures.

As seen from Figure 10, the pseudo-first-order rate constant, k^{1st}, increased linearly with [NO]. The y-axis intercept is not statistically significant. Linear least-squares analysis gives $k_2 = (2.5 \pm 0.8) \times 10^{-11}\ cm^3\ molecule^{-1}\ s^{-1}$. Errors are 2 standard deviations.

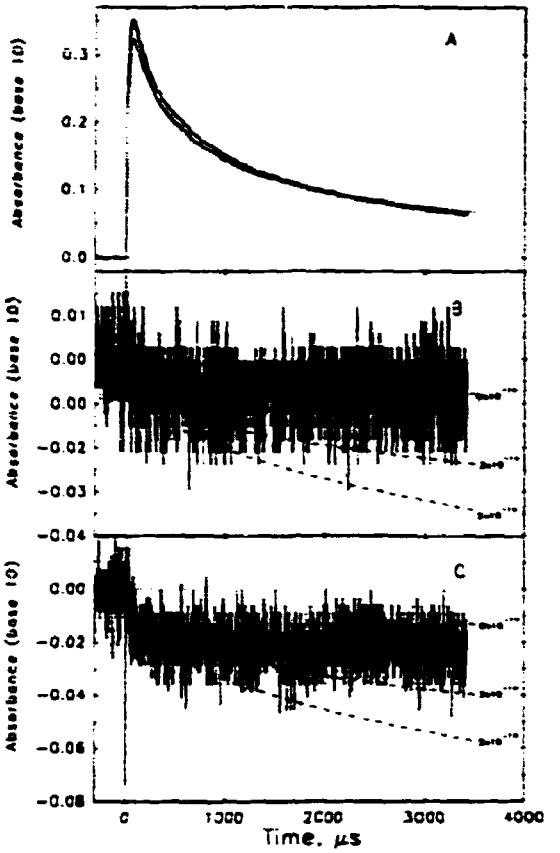

Figure 12. Transient absorptions at 696.1 (A), 288 (B), and 272 nm (C) following the pulse radiolysis of $SF_6/CO/O_2/O_3$ mixtures; see text for details. The path length for the analysis light was 80 cm. There are three traces in panel A. The dotted smooth curve in (A) is that predicted using the chemical mechanism given in Table 2; see text. The two experimental traces shown in (A) are transient absorptions at 696.1 nm observed in the presence and absence of O_3. The trace with the largest maximum absorbance was recorded in the absence of O_3. In panels B and C the dotted lines are the behavior predicted using the chemical model given in Table 2 with $k_4 = 0$, 3×10^{-16}, and $5 \times 10^{-16}\ cm^3\ molecule^{-1}\ s^{-1}$.

The increase in absorbance at 400 nm can be combined with the literature value of σ_{NO_2} (400 nm) = $5.9 \times 10^{-19}\ cm^2\ molecule^{-1}$ [18] to calculate the yield of NO_2 in this system. The yield of NO_2 in the five experiments given in Figure 10, expressed as moles of NO_2 produced per mole of $FC(O)O_2$ radicals consumed, was 91 ± 13%, suggesting that the majority of reaction 2 proceeds to give NO_2 and, by implication, FC(O)O radicals. In this calculation allowance was made for loss of F atoms via reaction with O_2, and loss of FCO radicals via reaction with NO, using rate data measured in the present work.

Kinetic Study of the Reaction FC(O)O + O_3. As discussed above, the self-reaction of $FC(O)O_2$ radicals is believed to give FC(O)O radicals as the major, if not sole, product.[31] The self-reaction of $FC(O)O_2$ radicals can be used to prepare FC(O)O radicals in the presence or absence, of O_3. FC(O)O radicals can be readily monitored using their absorption in the visible; see Figure 9. The difference in the temporal behavior of FC(O)O radicals with, and without, O_3 provides information on the kinetics of reaction 3.

$$FC(O)O + O_3 \rightarrow \text{products} \qquad (3)$$

Figure 12A shows the transient absorptions at 696.1 nm following the pulse radiolysis of 40 mbar of CO, 40 mbar of O_2, and 920 mbar of SF_6 with, and without, 0.26 mbar of O_3. As seen from Figure 12A, the maximum FC(O)O concentration observed when O_3 is present is slightly less than that when O_3 is absent. However,

there is little or no discernible difference in the decay of FC(O)O radicals in the presence, or absence, of O_3. Experiments were also performed using a UV monitoring wavelength of 288 and 272 nm; see panels B and C of Figure 12, respectively. Ozone absorbs strongly at these wavelengths (σ_{O_3}(288 nm) = 1.79 × 10^{-18} and σ_{O_3}(272 nm) = 6.92 × 10^{-18} cm^2 $molecule^{-1}$ [18]), and the transient absorption provides information on the temporal behavior of O_3 in the presence of FCO_x radicals. As seen from Figure 12, there is a small decrease in the absorption at 272 and 288 nm following radiolysis of $CO/O_2/O_3/SF_6$ mixtures. The effect is most pronounced at 272 nm with a change of 0.021 absorbance units; at 288 nm the change is 0.006 units. At both wavelengths the change occurs very shortly after the radiolysis pulse (within 50 μs), and subsequently there is little or no observable loss of O_3. The change in absorption at 288 and 272 nm can be equated with an ozone loss of 9.6 × 10^{13} and 8.7 × 10^{13} cm^{-3}, respectively. The initial ozone concentrations used in the experiments given in Figure 12B,C were 0.39 and 0.30 mbar. The initial F atom concentration employed was 2.69 × 10^{13} cm^{-3}. In the present experiments there is competition for available F atoms between reactions 6, 11, and 15.

$$F + CO \rightarrow FCO \quad (6)$$

$$F + O_2 + M \rightarrow FO_2 + M \quad (11)$$

$$F + O_3 \rightarrow FO + O_2 \quad (15)$$

M represents a third body (SF_6 in our case). Using k_6 = 1.8 × 10^{-12},[29] k_{11} = 1.9 × 10^{-13},[30] and k_{15} = 1.0 × 10^{-11} cm^3 $molecule^{-1}$ s^{-1},[35] the loss of O_3 through reaction 15 following the radiolysis of mixtures containing 40 mbar of CO, 40 mbar of O_2, and either 0.39 or 0.30 mbar of O_3 is expected to be 1.26 × 10^{14} and 9.77 × 10^{13} cm^{-3}, respectively. The expected ozone losses in the experiments given in Figure 12B,C are then somewhat more than those experimentally observed. However, after considering the experimental difficulties associated with the measurement of the small absorption changes evident in Figure 12B,C, we conclude that the observed loss of ozone is indistinguishable, within the experimental uncertainties, from that expected from the above analysis. The fact that the O_3 loss evident in Figure 12B,C can be entirely explained by reaction 15 shows that loss of O_3 by reaction with FC(O)O radicals (or indeed by any other process) is negligible in the present work. To derive an upper limit for k_3, the experimental traces given in Figure 12 were simulated using the CHEMSIMUL program[36] with the mechanism given in Table 2.

The first task was to simulate the behavior of FC(O)O radicals in the absence of O_3. As shown in Figure 12A, the base model given in Table 2 reproduces the observed behavior adequately. In this model k_{13} and k_{14} were varied to provide a satisfactory fit to the data, k_6 and k_{11} were taken from previous work,[29,30] and k_7, k_8, and k_9 were taken from results obtained in the present work. Reactions 16, −13, and −14 were not included in the mechanism but merit discussion.

$$FC(O)O \rightarrow F + CO_2 \quad (16)$$

$$FC(O)OOC(O)F \rightarrow FC(O)O + FC(O)O \quad (-13)$$

$$FC(O)OOOC(O)F \rightarrow FC(O)O + FC(O)O_2 \quad (-14)$$

At ambient temperature, FC(O)O radicals and the peroxide, FC(O)OOC(O)F, have lifetimes with respect to thermal decomposition of at least 3 s and 800 min, respectively.[31] Hence, reactions 16 and −13 can be excluded from the mechanism.

The absence of the trioxide, FC(O)OOOC(O)F, as a stable product in the FTIR–Smog chamber study of the $FC(O)O_2$ self-reaction[31] places an upper limit of 2 min for the lifetime of FC(O)OOOC(O)F at ambient temperature. It is possible that reaction −14 occurs on the millisecond time scale of the present pulse radiolysis experiments, and if so, then the value of k_{13} derived from the base model given in Table 2 is a lower limit. In the absence of data concerning k_{-14} we choose to exclude this reaction from the model. The aim of the present study is to measure the reactivity of FC(O)O radicals toward O_3. Inadequacies in the model in Table 2 caused by ignoring reaction −14 should have a negligible effect on conclusions relating to k(FC(O)O+O_3).

TABLE 2: Reaction Mechanism

reaction	rate constant[a]	reference
Base Model		
F + CO + M → FCO + M[c]	1.8 × 10^{-12} [b]	29
F + O_2 + M → FO_2 + M	1.9 × 10^{-13} [b]	30
FCO + FCO → COF_2 + CO	1.6 × 10^{-11}	this work
FCO + O_2 + M → $FC(O)O_2$ + M	1.2 × 10^{-12} [b]	this work
$FC(O)O_2$ + $FC(O)O_2$ → FC(O)O + FC(O)O + O_2	4.8 × 10^{-12}	this work, 31
$FC(O)O_2$ + $FC(O)O_2$ → FC(O)OOC(O)F + O_2	1.2 × 10^{-12}	this work, 31
FC(O)O + FC(O)O + M → FC(O)OOC(O)F + M	7.0 × 10^{-13} [b]	this work
FC(O)O + $FC(O)O_2$ + M → FC(O)OOC(O)F + M	8.0 × 10^{-12} [b]	this work
O_3 Chemistry		
FC(O)O + O_3 → products	[d]	
F + O_3 → FO + O_2	1.0 × 10^{-11}	35
NO_x Chemistry		
F + NO + M → FNO + M	5.5 × 10^{-12} [b]	this work
FCO + NO → FNO + CO	1.0 × 10^{-12}	this work
$FC(O)O_2$ + NO → FC(O)O + NO_2	2.5 × 10^{-11}	this work
FC(O)O + NO → FNO + CO_2	[d]	

[a] Units of cm^3 $molecule^{-1}$ s^{-1}. [b] Pseudo-second-order rate constant, value appropriate for 1000 mbar of SF_6. [c] M represents a third body (SF_6 in the present system). [d] Varied, see text.

The lower limit of $k_{13} > 7 \times 10^{-13}$ cm^3 $molecule^{-1}$ s^{-1} obtained in the present work can be compared to the value of k_{13} = (2.3–6.5) × 10^{-12} cm^3 $molecule^{-1}$ s^{-1} reported by Maricq et al.[28] While the two values are consistent, this may be fortuitous as the chemical mechanisms used to derive k_{13} differ in two important respects. First, in the study of Maricq et al.[28] reaction 14 was not included in the mechanism. Second, to fit their data, Maricq et al.[28] found it necessary to include reaction −13 with k_{-13} = 700 s^{-1}. As discussed above, such a rate is inconsistent with the stability of FC(O)OOC(O)F reported in ref 31. In both the present work and that of Maricq et al.[28] the FC(O)O radicals are formed indirectly in complex chemical systems containing $FC(O)O_2$ radicals. Further studies of the kinetics of reaction 13 are required using more direct methods to produce FC(O)O radicals in the absence of $FC(O)O_2$ radicals, thereby removing complications caused by reactions 14 and −14.

As shown in Figure 12A, the decay of the transient absorption attributed to FC(O)O radicals is unaffected by the presence of O_3. This observation suggests that reaction 3 is not a significant loss process for FC(O)O radicals. Figure 12B,C shows that in the time period from 0.1 to 4.0 ms after the radiolysis pulse the concentration of O_3 is essentially constant, and yet as evidenced in Figure 12A during this time there is a significant exposure of the O_3 to FC(O)O radicals. The dashed lines in Figure 12B,C show the expected behavior when reactions 3 and 15 are added to the base model. As seen from Figure 12, the lack of any discernible O_3 loss in the period 0.1–4.0 ms enables an upper limit of $k_3 < 3 \times 10^{-14}$ cm^3 $molecule^{-1}$ s^{-1} to be established. At this point we need to consider the impact that uncertainties in σ(FC(O)O) have on k_3. The dotted lines in Figure 12B,C were derived assuming σ(FC(O)O) = 1.4 × 10^{-17} cm^2 $molecule^{-1}$. As discussed previously, this value is actually a lower limit; in principle σ(FC(O)O) could be as much as a factor of 1.8 larger. If σ-

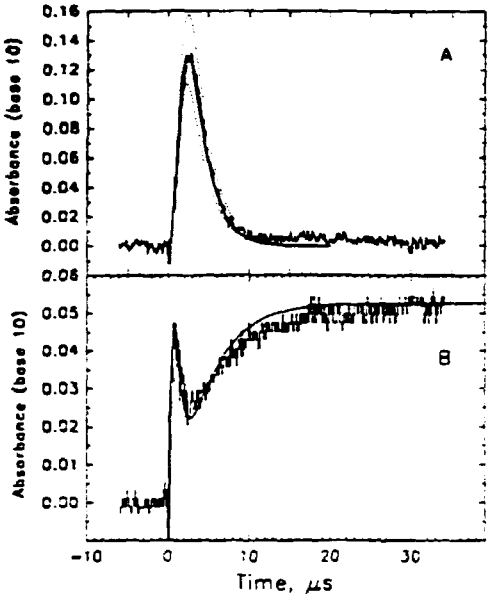

Figure 13. Transient absorptions at 696.1 (A) and 310.5 nm (B) observed following the pulsed radiolysis (full dose) of mixtures of 40 mbar of CO, 40 mbar of O_2, and 920 mbar of SF_6 with 1.0 (A) or 0.5 mbar (B) of NO. The solid smooth curves are those predicted using the chemical mechanism given in Table 2; see text. The UV path length was 80 cm.

(FC(O)O) was 2.5×10^{-17} cm^2 molecule^{-1}, then the exposure of O_3 to FC(O)O radicals would be about one-half of that used to derive the dotted lines in Figure 12B,C. Hence, we chose to increase our upper limit by a factor of 2, giving $k_3 < 6 \times 10^{-14}$ cm^3 molecule^{-1} s^{-1}. There have been no other studies of this reaction with which we can compare this result.

Kinetic Study of the Reaction FC(O)O + NO. The reaction of $FC(O)O_2$ radicals with NO produces FC(O)O radicals as the major (91 ± 13%), if not sole, carbon-containing product and thus provides a convenient method of preparing FC(O)O radicals in the presence of NO. By monitoring the temporal behavior of FC(O)O radicals in the presence of NO, kinetic information regarding the reaction of FC(O)O with NO can be derived. Experiments were performed using the radiolysis of SF_6/CO/O_2/NO mixtures with the transient absorption monitored at 696.1 and 310.5 nm.

The temporal profiles of FC(O)O radicals were found to be significantly perturbed in the presence of NO. Experiments were performed with NO concentrations varied over the range 0.21–1.45 mbar. As the NO concentration was increased, the maximum in the transient absorption at 696.1 nm attributed to FC(O)O radicals was found to decrease and shift to shorter times. The rate of decay of the absorption (and hence FC(O)O concentration) increased with increasing NO concentration. A comparison of the transient absorption given in Figure 13A (obtained in the presence of 1 mbar of NO) with that given in Figure 8 (obtained in the absence of NO) illustrates these effects. It is worth emphasizing that with the exception of the addition of 1.0 mbar of NO in the mixture used to obtain the trace given in Figure 13A, all experimental conditions used to derive the traces shown in Figures 8 and 13A were identical.

Clearly, additional loss processes for FC(O)O radicals are present when NO is added to the reaction mixture. There are three possibilities: FC(O)O radicals could react with NO, NO_2 (produced in reaction 2), or both. To investigate the relative importance of reactions 4 and 17, the transient absorption at 696.1 nm was simulated using the model given in Table 2.

$$FC(O)O + NO \rightarrow FNO + CO_2 \quad (4)$$

$$FC(O)O + NO_2 \rightarrow FNO_2 + CO_2 \quad (17)$$

As shown in Table 2, the reactions of NO with F, FCO, FC(O)O, and $FC(O)O_2$ were included in the model. All rate constant in the model were fixed, while k_4 was then varied to provide the best fit with the experimental data. The solid line in Figure 13A represents the predicted behavior using the mechanism in Table 2 with $k_4 = 9.0 \times 10^{-11}$ cm^3 molecule^{-1} s^{-1} and provides a reasonable fit to the experimental data. The dotted lines in Figure 13A show the effect of varying k_4 by ±20%. Experiments were performed using initial NO concentrations in the range 0.21–1.45 mbar, and in all experiments the observed FC(O)O temporal profile was well described by the mechanism given in Table 2 using $k_4 = (1.0 \pm 0.3) \times 10^{-10}$ cm^3 molecule^{-1} s^{-1}.

The chemical mechanism given in Table 2 does not contain reactions of NO_2 with FCO_x radicals or with F atoms. Reaction of F atoms and FCO radicals with NO_2 can be neglected because NO_2 is only formed by the reaction of $FC(O)O_2$ radicals with NO, and the concentrations of F atoms and FCO radicals have decayed to low levels before significant production of NO_2 has occurred. The fact that the yield of NO_2 following reaction of $FC(O)O_2$ with NO is 91 ± 13% suggests that NO_2 is not effectively scavenged by $FC(O)O_2$ radicals. There are two experimental observations that suggest that reaction of FC(O)O radicals with NO_2 is not a major complicating factor in our data analysis. First, the value of k_4 derived from fitting the observed transients at 696.1 nm to the mechanism in Table 2 was found to be independent of the initial NO concentration over the range 0.21–1.45 mbar at a constant initial radical concentration. With a constant initial radical concentration the NO_2 produced via reaction 2 will also be constant. If reaction 17 augmented the loss of FC(O)O radicals, then values of k_4 derived in the above analysis should appear to increase as the initial NO concentration is decreased; no such effect was observed. Second, the value of k_4 derived in the present work is within a factor of 3 of the gas kinetic limit. The NO_2 concentration present during the FC(O)O decay was up to a factor of 14 times less than that of NO. For reaction with NO_2 to account for a substantial fraction of the observed FC(O)O decay would require a rate constant k(FC(O)O+NO_2) in excess of the gas kinetic limit which is not physically reasonable. While it is clear that the reaction of FC(O)O with NO_2 does not play a major role in the observed FC(O)O decay, we cannot exclude a small contribution from this reaction. Accordingly, we choose to add an additional 10% uncertainty range to k_4 to give $k_4 = (1.0 \pm 0.4) \times 10^{-10}$ cm^3 molecule^{-1} s^{-1}. Finally, the impact of uncertainties in σ(FC(O)O) on k_4 needs consideration. The modeled traces in Figure 13A were derived using $\sigma(FC(O)O) = 1.4 \times 10^{-17}$ cm^2 molecule^{-1}. As discussed previously, this value is actually a lower limit; in principle, σ(FC(O)O) could be as much as a factor of 1.8 larger. To assess the maximum possible impact that uncertainties in σ(FC(O)O) could have upon the derived values of k_4, the modeling procedure was repeated using $\sigma(FC(O)O) = 2.5 \times 10^{-17}$ cm^2 molecule^{-1}. With this larger absorption cross section, values of k_4 of (1.5–2.0) $\times 10^{-10}$ cm^3 molecule^{-1} s^{-1} were needed to fit the experimental traces. To account for uncertainties in σ(FC(O)O), we choose to quote $k_4 = (0.6–2.0) \times 10^{-10}$ cm^3 molecule^{-1} s^{-1}, i.e., $k_4 = (1.3 \pm 0.7) \times 10^{-10}$ cm^3 molecule^{-1} s^{-1}. There have been no other studies of this reaction with which we can compare this result.

The chemistry following the pulsed radiolysis of SF_6/CO/NO/O_2 mixtures was also probed at a monitoring wavelength of 310.5 nm. This wavelength was selected because it is where FNO absorbs strongly[32,33] (σ(FNO) at 310.5 nm = (4.73 ± 0.66) × 10^{-19} cm^2 molecule^{-1} (this work)), and by analogy to the reaction of CF_3O radicals with NO,[37] we expect that FNO is a likely product of the reaction of FC(O)O radicals with NO. Figure 13B shows the transient absorption at 310.5 nm following the radiolysis (full dose) of a mixture of 40 mbar of CO, 40 mbar of O_2, 0.5 mbar of NO, and 920 mbar of SF_6. The UV absorption

path length was 80 cm. The transient absorption has an interesting shape. There is an initial rapid rise which is complete within the first 0.3 μs. This is ascribed to the rapid formation of FCO radicals which absorb at 310.5 nm (σ(FCO) at 310.5 nm = 1.1×10^{-18} cm^2 $molecule^{-1}$ [21]). Over the next 2 μs the absorption decays fairly rapidly, which can be ascribed to the conversion of FCO into $FC(O)O_2$ radicals via reaction 1. $FC(O)O_2$ radicals do not absorb significantly at 310.5 nm. At times greater than 2.5 μs the absorption slowly increases because of the reaction of $FC(O)O_2$ radicals with NO to produce NO_2 and FC(O)O radicals. NO_2 absorbs weakly at 310.5 nm ($\sigma = 1.9 \times 10^{-19}$ cm^2 $molecule^{-1}$ [18]). FC(O)O radicals then react with NO to give FNO, which absorbs more strongly at 310.5 nm. The solid line shown in Figure 13B is the behavior predicted using the CHEMSIMUL program with the chemical mechanism given in Table 2 ($k_4 = 8.0 \times 10^{-11}$ cm^3 $molecule^{-1}$ s^{-1}). As seen from Figure 13B, the mechanism in Table 2 describes the observed transient absorption at 310.5 nm adequately. It should be noted that the reaction of FC(O)O radicals with NO is assumed in Table 2 to yield FNO and CO_2 as the sole products. The agreement evident in Figure 13B supports this assumption. Four experiments were performed with NO varied over the range 0.3–1.0. In all cases the transient absorption at 310.5 nm was well described by the chemical mechanism in Table 2. The final absorption, when corrected for the contribution from NO_2, provides a yield of 78 ± 4% for the yield of FNO (moles of FNO produced per mole of FC(O)O radicals lost) from reaction 4. Quoted errors reflect statistical uncertainties (2 standard deviations), and we estimate that potential systematic errors could add an additional 20% range.

It is interesting to compare the kinetic and mechanistic data for the reaction of FC(O)O radicals with NO derived in the present work with the available literature data concerning the analogous reaction of CF_3O radicals with NO. While FC(O)O and CF_3O radicals both react with NO to give FNO as a major product,[37] FC(O)O radicals react significantly more rapidly ($k(CF_3O+NO) \approx 3 \times 10^{-11}$ cm^3 $molecule^{-1}$ s^{-1} [38-40]. That FC(O)O radicals are more reactive toward NO than CF_3O is probably a reflection of the relatively weak F–C bond energy in FC(O)O compared to CF_3O radicals.

Implications for Atmospheric Chemistry

The results presented here substantially improve our understanding of the atmospheric chemistry of FCO_x radicals. As demonstrated here and elsewhere,[28] FCO radicals react rapidly with O_2 to give $FC(O)O_2$ radicals. Using $k_1 = 1 \times 10^{-12}$ cm^3 $molecule^{-1}$ s^{-1}, we calculate a lifetime of 0.2 μs for FCO radicals with respect to conversion into $FC(O)O_2$ in 760 Torr of air. Reaction with O_2 is the sole atmospheric fate of FCO radicals. We have shown that $FC(O)O_2$ radicals react rapidly with NO to give FC(O)O radicals and NO_2. Using $k_2 = 2.5 \times 10^{-11}$ cm^3 $molecule^{-1}$ s^{-1} together with a background tropospheric NO level of 2.5×10^8 cm^{-3}, the lifetime of $FC(O)O_2$ with respect to reaction with NO is 3 min. Reaction with NO is likely to be a major fate of $FC(O)O_2$ radicals. It has been shown in the present work that FC(O)O radicals react rapidly with NO. Using $k_4 = 1.3 \times 10^{-10}$ cm^3 $molecule^{-1}$ s^{-1} and [NO] = 2.5×10^8 cm^{-3}, the lifetime of FC(O)O radicals with respect to reaction with NO is calculated to be 30 s. This lifetime is of the same order of magnitude as that for thermal decomposition of FC(O)O radicals into F atoms and CO_2.[31,41] Under ambient conditions it is possible that both thermal decomposition and reaction with NO are important fates of FC(O)O radicals. From the viewpoint of establishing the atmospheric chemistry of FC(O)O radicals, the issue of whether thermal decomposition or reaction with NO dominates the loss of FC(O)O radicals is moot as the product of reaction with NO, FNO, will photolyze to give F atoms and NO. F atoms will abstract H atoms from hydrogen-containing compounds (e.g., H_2O or CH_4) to give HF, which will then be rained out.

In contrast to the reactivity of FC(O)O radicals toward NO, we have shown here that FC(O)O radicals react slowly (if at all) with O_3. While the kinetic data reported here were measured at ambient temperature and not at the low temperatures applicable to the stratosphere, the data presented serve as a guide to the relative importance of these reactions at lower temperatures. At 20 km the concentrations of O_3 and NO are 7×10^{12} and 5×10^8 cm^{-3} (24-h average), respectively.[18] Multiplying the concentrations by the room temperature rate constants measured here ($<6 \times 10^{-14}$ and 1.3×10^{-10}) gives pseudo-first-order loss rates for FC(O)O radicals with respect to reaction with O_3 and NO of <0.42 and 0.07 s^{-1}, respectively. Thus, it appears from our work that the reaction of FC(O)O radicals with O_3 is less than a factor of 7 times more important in terms of a loss of FC(O)O radicals than reaction with NO. This implies a chain length of 7, or less, for any catalytic ozone destruction cycle involving reaction 4. This chain length can be compared to the Cl/ClO chain length, which is of the order of 1000–10 000. Clearly, FC(O)O radicals will have a minimal impact on stratospheric ozone levels. Further work is needed to conduct kinetic studies of reactions 3 and 4 at lower temperatures which are more representative of stratospheric conditions. Such work is underway in our laboratories.

Finally, the results from the present work need to be placed within the broader perspective of assessing the environmental impact of HFCs. As stated in the Introduction, HFCs have been chosen as CFC replacements in certain applications. The choice of HFCs was motivated by a number of factors, not the least of which is the fact that HFCs do not contain chlorine and so have no ozone depletion potential associated with the well-established chlorine catalytic cycles. Recently, there has been speculation regarding the possibility of an impact of HFCs on stratospheric ozone by virtue of their degradation into CF_3O_x and FCO_x radicals which could participate in catalytic ozone destruction cycles. Recent work in our laboratories led to the conclusion that CF_3O_x radicals do not pose a threat to stratospheric ozone.[35,42,43] The results presented in the present work suggest that the same conclusion applies to FCO_x radicals. At present there appears to be no credible scientific evidence to support the notion that the use of HFCs will impact stratospheric ozone.

Acknowledgment. We thank Matti Maricq and Steve Japar (Ford) for helpful discussions and AFEAS for financial support under Contract CTR93-45/P93-120. We thank Alfred Sillesen (Risø) for assistance in recording the diode array spectra.

Note Added in Proof. Burley et al.[44] have reported UV absorption cross sections for FNO. The results of Burley et al.[44] are consistent with the results from the present work.

References and Notes

(1) Farman, J. D.; Gardiner, B. G.; Shanklin, J. D. *Nature* **1985**, *315*, 207.
(2) Solomon, S. *Nature* **1990**, *347*, 6291 and references therein.
(3) World Meteorological Organization Global Ozone Research and Monitoring Project, Report No. 20; Scientific Assessment of Stratospheric Ozone, 1989; Vol. 1.
(4) Fisher, D. A.; Hales, C. H.; Wang, W. C.; Ko, M. K. W.; Dak Sze, N. *Nature* **1990**, *344*, 529.
(5) Shine, K.; Derwent, R. G.; Wuebbles, D. J.; Morcrette, J.-J. Assessment for WG1 Plenary, 27th April 1990.
(6) Nielsen, O. J.; Ellermann, T.; Sehested, J.; Bartkiewicz, E.; Wallington, T. J.; Hurley, M. D. *Int. J. Chem. Kinet.* **1992**, *24*, 1009.
(7) Nielsen, O. J.; Ellermann, T.; Bartkiewicz, E.; Wallington, T. J.; Hurley, M. D. *Chem. Phys. Lett.* **1992**, *192*, 82.
(8) Wallington, T. J.; Ball, J. C.; Nielsen, O. J.; Bartkiewicz, E. *J. Phys Chem.* **1992**, *96*, 1241.
(9) Sehested, J.; Ellermann, T.; Nielsen, O. J.; Wallington, T. J.; Hurley, M. D. *Int. J. Chem. Kinet.* **1993**, *25*, 701.
(10) Nielsen, O. J.; Ellermann, T.; Sehested, J.; Wallington, T. J. *J. Phys. Chem.* **1992**, *96*, 10875.
(11) Wallington, T. J.; Nielsen, O. J. *Chem. Phys. Lett.* **1991**, *187*, 33.

(12) Wallington, T. J.; Hurley, M. D.; Ball, J. C.; Kaiser, E. W. *Environ. Sci. Technol.* **1992**, *26*, 1318.
(13) Edney, E. O.; Gay, B. W.; Driscoll, D. J. *J. Atmos. Chem.* **1991**, *12*, 105.
(14) Edney, E. O.; Driscoll, D. J. *Int. J. Chem Kinet.* **1991**, *24*, 1067.
(15) Tuazon, E. C.; Atkinson, R. *J. Atmos. Chem.* **1993**, *17*, 179.
(16) Francisco, J. S.; Goldstein, A. N.; Li, Z.; Zhao, Y.; Williams, I. H. *J. Phys. Chem.* **1990**, *94*, 4791.
(17) Nielsen, O. J. Risø-R-480, 1984.
(18) DeMore, W. B.; Sander, S. P.; Golden, D. M.; Hampson, R. F.; Kurylo, M. J.; Howard, C. J.; Ravishankara, A. R.; Kolb, C. E.; Molina, M. J. Jet Propulsion Laboratory Publication 92-20, Pasadena, CA, 1992.
(19) Wallington, T. J.; Maricq, M. M.; Ellermann, T.; Nielsen, O. J. *J. Phys. Chem.* **1992**, *96*, 982.
(20) Wallington, T. J.; Dagaut, P.; Kurylo, M. J. *Chem. Rev.* **1992**, *92*, 667.
(21) Maricq, M. M.; Szente, J. J.; Khitrov, G. A.; Francisco, J. S. *Chem. Phys. Lett.* **1992**, *199*, 71.
(22) Milligan, D. E.; Jacox, M. E.; Bass, A. M.; Comeford, J. J.; Mann, D. E. *J. Chem. Phys.* **1965**, *42*, 3187.
(23) Wang, D. K. W.; Jones, W. E. *J. Photochem.* **1972**, *1*, 47.
(24) Kurylo, M. J.; Ouellette, P. A.; Laufer, A. H. *J. Phys. Chem.* **1986**, *90*, 437.
(25) Sander, S. P.; Watson, R. T. *J. Phys. Chem.* **1981**, *85*, 2960.
(26) Behr, P.; Goldbach, K.; Heydtmann, H. *Int. J. Chem. Kinet.* **1993**, *25*, 957.
(27) Maricq, M. M.; Gregory, E. A.; Simpson, C. J. S. M. *Chem. Phys* **1985**, *95*, 43 and references therein.
(28) Maricq, M. M.; Szente, J. J.; Khitrov, G. A.; Francisco, J. S. *J. Chem. Phys.* **1993**, *98*, 9522.
(29) Ellermann, T. Unpublished results.
(30) Ellermann, T.; Sehested, J.; Nielsen, O. J.; Pagsberg, P.; Wallington, T. J. *Chem. Phys. Lett.*, in press.
(31) Wallington, T. J.; Hurley, M. D.; Maricq, M. M. *Chem. Phys. Lett.* **1993**, *205*, 62.
(32) Johnston, H. S.; Bertin, H. J. *J. Mol. Spectrosc.* **1959**, *3*, 683.
(33) Ogai, A.; Brandon, J.; Reisler, H.; Suter, H. U.; Huber, J. R.; von Dirke, M.; Schinke, R. *J. Chem. Phys.* **1992**, *96*, 6643.
(34) Sehested, J.; Nielsen, O. J.; Wallington, T. J. *Chem. Phys. Lett.* **1993**, *213*, 457.
(35) Nielsen, O. J.; Sehested, J. *Chem. Phys. Lett.* **1993**, *213*, 433.
(36) Rasmussen, O. L.; Bjergbakke, E. CHEMSIMUL—A Program Package for Numerical Simulation of Chemical Reaction Systems, Risø-R-395, 1984.
(37) Chen, J.; Zhu, T.; Niki, H. *J. Phys. Chem.* **1992**, *96*, 6115.
(38) Bevilacqua, T. J.; Hanson, D. R.; Howard, C. J. *J. Phys. Chem.* **1993**, *97*, 3750.
(39) Zellner, R. Private communication, 1993.
(40) Sehested, J.; Nielsen, O. J. *Chem. Phys. Lett.* **1993**, *206*, 369.
(41) Francisco, J. S.; Goldstein, A. N. *Chem. Phys.* **1988**, *127*, 73.
(42) Wallington, T. J.; Hurley, M. D.; Schneider, W. F. *Chem. Phys. Lett.* **1993**, *213*, 442.
(43) Maricq, M. M.; Szente, J. J. *Chem. Phys. Lett.* **1993**, *213*, 449.
(44) Burley, J. D.; Miller, C. E.; Johnston, H. S. *J. Mol. Spectrosc.* **1993**, *158*, 377.

Atmospheric Chemistry of CF_3O Radicals: Reaction with H_2O

Timothy J. Wallington,* Michael D. Hurley, and William F. Schneider

Research Staff, SRL-3083, Ford Motor Company, Dearborn, P.O. Box 2053, Michigan 48121-2053

Jens Sehested and Ole John Nielsen

Section for Chemical Reactivity, Environmental Science and Technology Department, Risø National Laboratory, DK-4000 Roskilde, Denmark

Received: February 19, 1993; In Final Form: April 7, 1993

Evidence is presented that CF_3O radicals react with H_2O in the gas phase at 296 K to give CF_3OH and OH radicals. This reaction is calculated to be exothermic by 1.7 kcal mol^{-1} implying a surprisingly strong CF_3O–H bond energy of 120 ± 3 kcal mol^{-1}. Results from a relative rate experimental study suggest that the rate constant for the reaction of CF_3O radicals with H_2O lies in the range (0.2–40) × 10^{-17} cm^3 $molecule^{-1}$ s^{-1}. Implications for the atmospheric chemistry of CF_3O radicals are discussed.

Introduction

Recognition of the adverse effect of chlorofluorocarbon (CFC) release into the atmosphere has led to an international effort to replace CFCs with environmentally acceptable alternatives.[1-3] Hydrofluorocarbons (HFCs) are under consideration as CFC substitutes. For example, HFC-134a is a replacement for CFC-12 in automotive air conditioning systems. Prior to large-scale industrial use, the environmental consequences of release of HFCs into the atmosphere are being considered.[4] To define the environmental impact of HFC release, the atmospheric photooxidation products of HFCs need to be determined.

CF_3 radicals are produced during the oxidation of HFC-134a,[5,6] HFC-125,[7-9] and HFC-23.[10] In the atmosphere, CF_3 radicals react with O_2 to give CF_3O_2 radicals which, in turn, react rapidly with NO to form CF_3O radicals:[11,12]

$$CF_3 + O_2 + M \rightarrow CF_3O_2 + M \quad (1)$$

$$CF_3O_2 + NO \rightarrow CF_3O + NO_2 \quad (2)$$

The atmospheric fate of CF_3O radicals is uncertain and the subject of a significant current research effort. Recently, it has been shown that CF_3O radicals react with NO[13,14] and organic compounds.[14-16] To the best of our knowledge, the reaction of CF_3O with H_2O has not been considered as an atmospheric loss mechanism for CF_3O radicals. We report herein results from a computational and experimental study of reaction (3). Our results suggest that reaction (3) may play an important role in the atmospheric chemistry of CF_3O radicals.

$$CF_3O + H_2O \rightarrow CF_3OH + OH \quad (3)$$

Computational and Experimental Details

Experimental Details. The experimental setup used for the present work has been described previously[17] and is only briefly discussed here. The apparatus consists of a Mattson Instruments Inc. Sirius 100 FT-IR spectrometer interfaced to a 140-L, 2-m long evacuable Pyrex chamber. White type multiple reflection optics were mounted in the reaction chamber to provide a total path length of 26.6 m for the IR analysis beam. The spectrometer was operated at a resolution of 0.25 cm^{-1}. Infrared spectra were derived from 32 co-added interferograms.

CF_3O radicals were generated by the chlorine-initiated oxidation of HFC-134a. Chlorine atoms were generated by the photolysis of molecular chlorine using the output of 22 UV fluorescent lamps (GTE F40BLB). CF_3O radicals are formed by the following reactions:[6,16]

$$Cl_2 + h\nu(\lambda > 300\ nm) \rightarrow 2Cl \quad (4)$$

$$Cl + CF_3CFH_2\ (HFC\text{-}134a) \rightarrow CF_3CFH + HCl \quad (5)$$

$$CF_3CFH + O_2 \rightarrow CF_3CFHO_2 \quad (6)$$

$$CF_3CFHO_2 + CF_3CFHO_2 \rightarrow CF_3CFHO + CF_3CFHO + O_2 \quad (7a)$$

$$CF_3CFHO_2 + CF_3CFHO_2 \rightarrow CF_3COF + CF_3CFHOH + O_2 \quad (7b)$$

$$CF_3CFHO \rightarrow CF_3 + HC(O)F \quad (8)$$

$$CF_3 + O_2 \rightarrow CF_3O_2 \quad (1)$$

$$CF_3O_2 + CF_3O_2 \rightarrow CF_3O + CF_3O + O_2 \quad (9)$$

Initial concentrations used were as follows: HFC-134a, 10–1040 mTorr; Cl_2, 296–447 mTorr; and H_2O, 0–916 mTorr. In all experiments, ultrapure air was used as diluent at a total pressure of 700 Torr. The temperature was 296 ± 2 K.

With the exception of CF_3OH, products were quantified by fitting reference spectra of the pure compounds to the observed product spectra using integrated absorption features. Reference spectra were obtained by expanding known volumes of the reference material into the long-path-length cell. Systematic uncertainties associated with quantitative analyses using these reference spectra are estimated to be <10%. CF_3OH was identified by virtue of its characteristic absorption at 3600–3700 cm^{-1} and quantified using $\sigma_{3664cm^{-1}}(CF_3OH) = 9 \times 10^{-19}$ cm^2 $molecule^{-1}$.[16] Systematic uncertainties in the analysis of CF_3OH are estimated to be <15%.

The procedure was as follows. HFC-134a was first quantified and subtracted from the product spectra using characteristic absorption features over the wavelength region 800–1500 cm^{-1}. HC(O)F, CF_3COF, COF_2, $CF_3O_3CF_3$, and CF_3OH were then identified and quantified using features over the following wavelength ranges: 1700–1900, 1000–1200 and 1800–2000, 700–800 and 1800–2000, 700–900 and 1100–1400, and 3600–3700 cm^{-1}, respectively.

HFC-134a, Cl_2, CF_3COF, and COF_2 were purchased from commercial vendors at purities ≥99%. HC(O)F was prepared

* To whom correspondence should be addressed.

0022-3654/93/2097-7606$04.00/0

TABLE I: MP2/6-31G*(d,p) Optimized Bond Distances (angstroms) and Bond Angles (degrees). X_{ip} (In-Plane) and X_{op} (Out-of-Plane) Refer to the Two Symmetry-Unique Sets of C-Bound F or H Atoms under C_s Symmetry

	CF_3OH	CF_3O	CH_3OH	CH_3O
r(C–O)	1.3493	1.3662	1.4198	1.3850
r(C–X_{ip})	1.3307	1.3364	1.0852	1.0956
r(C–X_{op})	1.3502	1.3367	1.0919	1.0911
r(O–H)	0.9655		0.9622	
$\angle$(O–C–X_{ip})	108.30	105.81	106.52	104.93
$\angle$(O–C–X_{op})	112.19	111.78	112.43	112.54
$\angle$(H–O–C)	108.11		107.32	
$\angle$(X_{ip}–C–X_{op})	108.78	109.87	108.35	107.76
$\angle$(X_{op}–C–X_{op})	106.52	107.75	108.58	110.90

TABLE II: MP4(FC)/6-311+G(d,p)//MP2/6-31G(d,p) Electronic Energies, along with Zero-Point and Internal Energy Corrections to 298.15 K Obtained from the MP2/6-31G(d,p) Geometries and Vibrational Spectra (All Energies in au)

	sym	state	MP4 energy	ZPE	$\Delta E^{298.15}$	total
CF_3OH	C_s	$^1A'$	−412.726 47	0.029 69	0.004 38	−412.731 09
CF_3O	C_s	$^2A'$	−412.071 23	0.016 64	0.004 18	−412.050 42
CH_3OH	C_s	$^1A'$	−115.477 29	0.053 04	0.003 39	−115.420 86
CH_3O	C_s	$^2A'$	−114.803 09	0.038 58	0.002 97	−114.761 55
H_2O	C_{2v}	$^1A_1$	−76.287 03	0.021 90	0.002 83	−76.262 30
HO	$C_{\infty v}$	$^2\Pi$	−75.595 39	0.008 76	0.002 36	−75.584 28
CH_4	T_d	^1A	−40.405 14	0.046 61	0.020 86	−40.355 67
CH_3	D_{3h}	$^2A_2''$	−39.731 91	0.030 76	0.003 31	−39.697 84
H_2	$D_{\infty h}$	$^1\Sigma^+_g$	−1.167 69	0.010 50	0.002 36	−1.154 83
H	K_h	^2S	−0.499 81	0.0	0.001 42	−0.498 39

from the reaction of benzoyl chloride with dry formic acid and anhydrous potassium fluoride.[18] $CF_3O_3CF_3$ was prepared by the UV irradiation of CF_3H–F_2–O_2–He mixtures.[19]

Computational Details. All calculations were performed with the Gaussian 88 program and employed standard basis sets.[20] The structures of all molecules were obtained by gradient optimization at the MP2/6-31G(d,p) level (unrestricted MP2 for the radicals). The structures of the first-row hydrides are consistent with MP2/6 31G(d) geometries reported previously, with the addition of a small but uniform decrease in all X–H bond distances arising from the additional hydrogen polarization functions included in our calculations.[21] Table I contains the optimized parameters for trifluoromethanol,[22] trifluoromethoxy radical,[23] methanol,[21] and methoxy radical.[24] Again, all are consistent with earlier results at various lower levels of theory. Using the MP2/6-31G(d,p) geometries, single-point energies were evaluated at the UMP4/6-311+G(d,p) level, keeping the core orbitals frozen in the perturbation calculation. The resultant total energies for all molecules included in this study are reported in Table II.

The force constant matrices and harmonic vibrational frequencies for all molecules were obtained by numerical differentiation of the analytical MP2/6-31G(d,p) gradients. Again, the results parallel those reported earlier for the first-row hydrides.[25] The vibrational frequencies were used unscaled to obtain zero point vibrational energies. Internal translational, rotational, and vibrational energy corrections to 298.15 K were calculated using standard statistical mechanical methods.[26,27] The low-frequency torsions in the two alcohol molecules, along with the umbrella mode of methyl radical, were treated as free rotations and thus contributed $RT/2$ to the internal energy. While inclusion of zero point energies has a substantial (up to 3 kcal/mol) effect on the calculated reaction heats, the thermal corrections have a fairly minor impact (<0.5 kcal/mol) on our final results.

Experimental Results

Ten experiments were performed as part of the present work. The experimental conditions and observed product yields are given in Table III. The first experiment involved the UV irradiation of a mixture of 1.04 Torr of HFC-134a and 300 mTorr of Cl_2, in 700 Torr of air diluent. Figure 1A,B show spectra taken before and after 240 s irradiation of the mixture in experiment no. 1. Comparison with reference spectra of HC(O)F and CF_3OH given in panel 1C clearly shows the formation of these two products. In addition, CF_3COF, COF_2, and $CF_3O_3CF_3$ were detected. The observed product yields are given in Table III. In experiments with initial HFC-134a concentrations of 1 Torr the IR features attributable to HFC-134a were saturated; consequentially the loss of HFC-134a could not be quantified. When the reaction mixture from experiment no. 1 was allowed to stand in the dark the CF_3OH was observed to decay rapidly to give COF_2. The decay is attributed to heterogeneous decomposition on the reactor walls:[16]

$$CF_3OH \rightarrow COF_2 + HF \qquad (10)$$

Within the experimental uncertainties, the decay of CF_3OH followed first-order kinetics with a lifetime of 100 ± 10 s. This loss rate is nearly 200 times faster than we observed in our previous study of CF_3OH.[16] Clearly, the walls of the reaction chamber are now much more reactive toward CF_3OH decomposition. The explanation of the dramatic increase in the wall reactivity probably lies in the recent movement of the experimental system from one building to another. During the move the chamber was exposed to room air for a period of 1 month. In an attempt to recondition the chamber, several experiments were performed in which mixtures of 5–10 Torr of HFC-134a and 1 Torr of Cl_2 were irradiated to expose the chamber walls to high concentrations of CF_3OH. Unfortunately, no conditioning was observed. Throughout the present work the lifetime of CF_3OH remained at 100 ± 10 s.

Experiment no. 2 was essentially a repeat of no. 1 with the addition of 460 mTorr of H_2O. Figure 1D,E show IR spectra before and after 240 s irradiation. For clarity the H_2O features have been removed from 1E. Comparison of panels 1B and 1E shows that the yields of HC(O)F and CF_3OH were unaffected by the presence of H_2O. Similarly, the yields of CF_3COF, COF_2, and $CF_3O_3CF_3$ were unchanged by the presence of H_2O. In a recent study of the products from the simulated atmospheric oxidation of HFC-134a we have shown that CF_3OH is produced from the reaction of CF_3O radicals with HFC-134a, and that this reaction has a rate constant of $k_{11} = (1.1 \pm 0.7) \times 10^{-15}$ cm^3 molecule^{-1} s^{-1}.[16] Reaction 11 competes with reaction 12 for the

$$CF_3O + CF_3CFH_2 \text{ (HFC-134a)} \rightarrow CF_3OH + CF_3CFH \qquad (11)$$

$$CF_3O + CF_3O_2 \rightarrow CF_3O_3CF_3 \qquad (12)$$

available CF_3O radicals. From experiment nos. 1 and nos. 2 it is clear that the addition of 460 mTorr of H_2O to a reaction mixture containing approximately 1 Torr of HFC-134a causes no observable change (<10%) of CF_3OH formation when the mixtures are irradiated. Hence, 460 mTorr of H_2O is less than 10% as effective as 1030 mTorr of HFC-134a. As $k_{11} < 1.8 \times 10^{-15}$ cm^3 molecule^{-1} s^{-1}, then $k_3 < 4 \times 10^{-16}$ cm^3 molecule^{-1} s^{-1}.

Further investigation of the kinetics of reaction 3 requires use of larger values of the $[H_2O]/[HFC\text{-}134a]$ concentration ratio. The presence of moisture-sensitive optical components in the reaction chamber makes the use of significantly increased $[H_2O]$ undesirable. Therefore, the ratio $[H_2O]/[HFC\text{-}134a]$ was increased by decreasing [HFC-134a]. Experiment nos. 3–10 were conducted using $[HFC\text{-}134a]_0$ = 9.9–24.1 mTorr. With such low initial concentrations the expected yields of CF_3OH are close to, or below, the detection limit of approximately 1 mTorr, which precludes direct measurement of the CF_3OH yield. Instead, the formation of CF_3OH was measured indirectly by observing the yield of COF_2 formed after reaction mixtures were left to stand

TABLE III: Product Yields[a] following the Irradiation of HFC-134a/Cl_2/H_2O Mixtures in 700 Torr of Air

expt	$[HFC\text{-}134a]_0$	$[Cl_2]_0$	$[H_2O]_0$	t_{UV} (s)	Δ[HFC-134a]	Δ[HC(O)F]	Δ[CF_3COF]	Δ[$CF_3O_2CF_3$]	Δ[COF_2]	Δ[CF_3OH]
1	1040	296	0	75[b]	nm[c]	11.1	3.3	3.9	1.0	2.4
				240[b]	nm	35.7	10.2	9.7	9.6	4.3
2	1030	296	460	75[b]	nm	10.6	3.0	2.4	0.9	2.1
				240[b]	nm	35.7	10.2	10.2	9.7	4.0
3	9.9	438	0	180[c]	2.28	1.38	0.51	0.58	0.47	
						(61%)[d]	(22%)	(25%)	(21%)	
4	10.1	444	502	180[c]	2.42	1.39	0.49	0.53	0.57	
						(57%)	(20%)	(22%)	(24%)	
5	10.1	444	786	180[c]	2.32	1.35	0.51	0.50	0.67	
						(58%)	(22%)	(22%)	(29%)	
6	10.1	444	916	180[c]	2.12	1.46	0.45	0.39	0.68	
						(69%)	(21%)	(18%)	(32%)	
7	23.8	444	0	180[c]	4.76	2.83	0.96	1.21	0.85	
						(59%)	(20%)	(25%)	(18%)	
8	23.8	444	358	180[c]	4.52	2.77	0.95	0.81	0.90	
						(61%)	(21%)	(18%)	(20%)	
9	24.1	447	0	300[c]	7.23	3.94	1.56	1.69	1.24	
						(55%)	(22%)	(23%)	(17%)	
10	24.1	447	706	300[c]	7.23	3.94	1.50	1.59	1.46	
						(55%)	(21%)	(22%)	(20%)	

[a] Observed concentrations in units of mTorr, with no corrections of any kind applied to data. [b] Irradiation time, analysis performed immediately after irradiation. [c] Irradiation time, analysis performed after reaction mixture sat in dark for 10 min to allow complete decomposition of CF_3OH into COF_2. [d] Values in parentheses are molar yields relative to HFC-134a loss. [e] Not available.

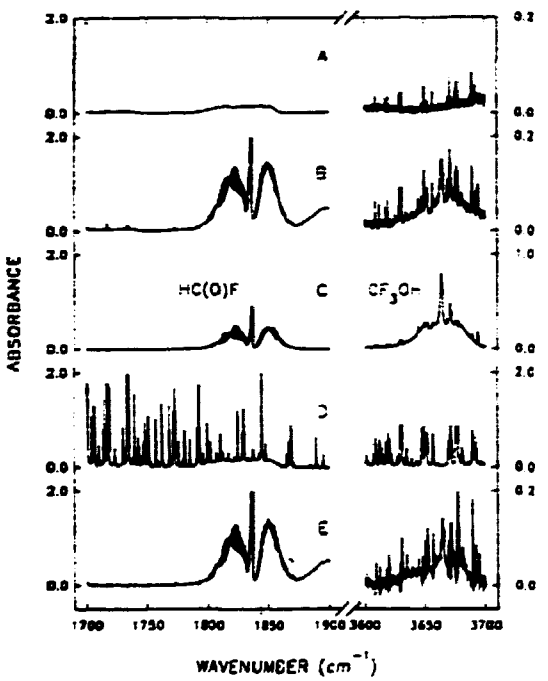

Figure 1. Spectra taken before (A) and after (B) 240-s irradiation of a mixture of 1.04 Torr of HFC-134a and 296 mTorr of Cl_2, in 700 Torr of air diluent. Comparison with reference spectra of HC(O)F and CF_3OH given in panel 1C shows the formation of these products. Spectra D and E were acquired before and after 240-s irradiation of a mixture of 1.03 Torr of HFC-134a, 296 mTorr of Cl_2, and 460 mTorr of H_2O. The H_2O features in panel E have been subtracted for clarity.

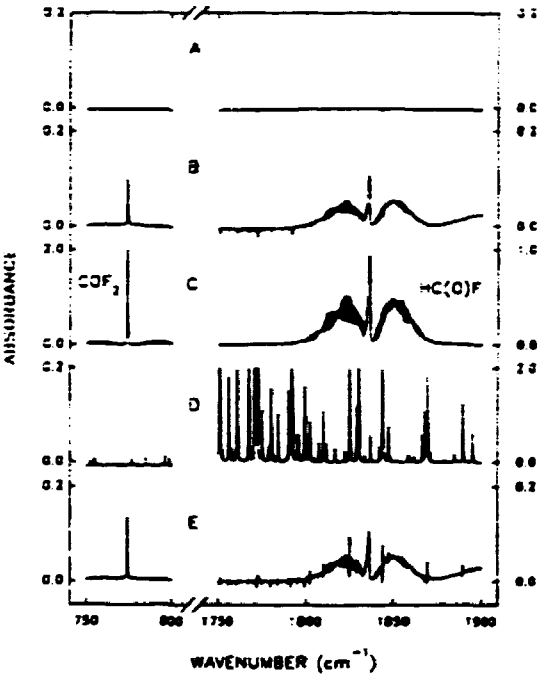

Figure 2. Spectra taken before (A) and after (B) 180-s irradiation of a mixture of 9.9 mTorr of HFC-134a and 438 mTorr of Cl_2, in 700 Torr of air diluent. Comparison with reference spectra of HC(O)F and COF_2 given in panel 1C shows the formation of these products. Spectra D and E were acquired before and after 180-s irradiation of a mixture of 10.1 mTorr of HFC-134a, 444 mTorr of Cl_2, and 916 mTorr of H_2O. The H_2O features in panel E have been subtracted for clarity.

for 10 min in the dark. As discussed above, CF_3OH rapidly decomposes into COF_2 in the reaction chamber. The detection limit of COF_2 was 0.02 mTorr. Reported product yields in Table III for experiment nos. 3–10 were measured after all dark chemistry had ceased (after 10 min). In all cases, within the experimental uncertainties, the yields of HC(O)F and CF_3COF were unaffected by the presence of H_2O. In contrast, the yield of COF_2 increased significantly with increased $[H_2O]$. Conversely, the measured $CF_3O_2CF_3$ yield decreased with increased $[H_2O]$. This observation is consistent with a competition between reactions 3 and 12 for the available CF_3O radicals.

To illustrate these observations, Figure 2A,B shows spectra acquired before and after irradiation of a mixture of 9.9 mTorr of HFC-134a and 438 mTorr of Cl_2 in 700 Torr of air (experiment no. 3). Figure 2D,E shows spectra taken before and after irradiation of the reaction mixture used in experiment no. 6. Experiment no. 6 was essentially a repeat of no. 3 but with 916 mTorr of H_2O added. For clarity H_2O features in 2E have been subtracted. Comparison of Figures 2B,E with reference spectra of COF_2 and HC(O)F (given in panel 2C) shows that these species are products and that the yield of COF_2 is significantly larger in the presence of H_2O.

The ratio of the COF_2 yield in the presence of H_2O to that observed in the absence of H_2O is plotted as a function of the concentration ratio $[H_2O]/[HFC\text{-}134a]$ in Figure 3. The solid line is a linear least squares fit forced through a y-axis intercept of unity. Assuming that (i) COF_2 is formed solely from the decomposition of CF_3OH, (ii) reactions 3 and 11 are the only

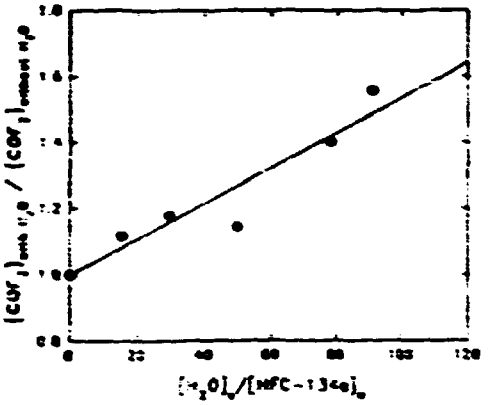

Figure 3. Ratio of COF_2 yield observed in the presence of H_2O to that observed in the absence of H_2O versus $[H_2O]_0/[HFC\text{-}134a]_0$; see text for details.

TABLE IV: Reaction Mechanism

reaction	k(296 ± 2 K)[a]
$Cl_2 \rightarrow 2Cl$	
$Cl + CF_3CFH_2 \rightarrow HCl + CF_3CFH$	1.4×10^{-13}
$CF_3CFH + O_2 \rightarrow CF_3CFHO_2$	2×10^{-12}
$CF_3CFHO_2 + CF_3CFHO_2 \rightarrow 2CF_3CFHO + O_2$	6×10^{-12}
$CF_3CFHO_2 + CF_3CFHO_2 \rightarrow CF_3COF + CF_3CFHOH + O_2$	1×10^{-12}
$CF_3CFHO_2 + CF_3O_2 \rightarrow CF_3CFHO + CF_3O + O_2$	8×10^{-12}
$CF_3CFHO \rightarrow CF_3 + HC(O)F$	2×10^{6}
$CF_3CFHO + O_2 \rightarrow CF_3COF + HO_2$	9×10^{-16}
$CF_3 + O_2 \rightarrow CF_3O_2$	8.5×10^{-12}
$CF_3O_2 + CF_3O_2 \rightarrow CF_3O + CF_3O + O_2$	1.8×10^{-12}
$CF_3O + CF_3O_2 \rightarrow CF_3O_2CF_3$	2.5×10^{-11}
$CF_3O + CF_3CFHO_2 \rightarrow CF_3CFHO_2CF_3$	1.8×10^{-11}
$CF_3CFHO_2CF_3 \rightarrow CF_3CFHO_2 + CF_3O$	5.0×10^{-3} [b,c]
$\rightarrow CF_3CFHO + CF_3O_2$	5.0×10^{-3} [b,c]
$CF_3O + CF_3CFH_2 \rightarrow CF_3CFH + CF_3OH$	4.5×10^{-16}
$CF_3OH \rightarrow CF_2O + HF$	1×10^{-3} [b,d]
$Cl + HC(O)F \rightarrow HCl + FCO$	2.0×10^{-15}

[a] Units of cm^3 molecule^{-1} s^{-1}. [b] Units of s^{-1}. [c] Assumed equal to rate of CF_3OH decomposition. [d] Measured in this work.

sources of CF_3OH, and (iii) formation of CF_3OH is a relatively minor fate of CF_3O radicals (i.e., there are CF_3O radicals available which can be diverted by reaction with H_2O to give CF_3OH), then the following expression holds:

$$Y(COF_2)_{H_2O}/Y(COF_2) = 1 + (k_3/k_{11})([H_2O]/[HFC\text{-}134a])$$

$Y(COF_2)_{H_2O}$ is the molar yield of COF_2 observed when H_2O is present, $Y(COF_2)$ is the corresponding yield when H_2O is absent, and k_3/k_{11} is the ratio of the rate constants for reactions 3 and 11. Linear least-squares analysis of the data in Figure 3 gives $k_3/k_{11} = (5.4 \pm 1.3) \times 10^{-3}$. The quoted error represents 2 standard deviations.

Discussion of Experimental Results

The observed product yields given in Table III can be compared to those expected based upon recent studies of the Cl atom initiated oxidation of HFC-134a in our laboratory.[16] The Acuchem chemical kinetic modeling program[28] together with the mechanism in Table IV (taken from ref 16) was used to calculate the expected product yields. In experiment no. 1 we could not quantify the loss of HFC-134a, so absolute yields for the HC(O)F, CF_3COF, $CF_3O_2CF_3$, COF_2, and CF_3OH are unknown. However, we can compare the observed yields on a relative basis. Relative to HC(O)F, the yields of CF_3COF, $CF_3O_2CF_3$, COF_2, and CF_3OH after 240 s of irradiation were 29%, 27%, 27%, and 12% respectively. Simulation of experiment no. 1 using the chemical mechanism given in Table IV predicts yields of 28%, 31%, 20%, and 13% for these species, reasonably consistent with the experimental observations. The results from experiment nos. 1 and 2 were indistinguishable, and hence the latter can also be adequately simulated using the mechanism in Table IV.

In contrast, for nos. 3, 7, and 9 the mechanism in Table IV greatly underpredicts the COF_2 yield. For example, under the experimental conditions of no. 3 the predicted HC(O)F, CF_3COF, $CF_3O_2CF_3$, and COF_2 yields are 70%, 20%, 31%, and 1% compared to the observed yields of 61%, 22%, 25%, and 21%, respectively. The mechanism in Table IV has only one process that forms CF_3OH and hence COF_2—namely reaction of CF_3O with HFC-134a. Clearly, for the experimental conditions of experiment no. 3, additional reactions that form either CF_3OH, or COF_2, or both, are missing from the mechanism in Table IV. As discussed previously,[16] in addition to HFC-134a, other hydrogen-containing species are present with which CF_3O radicals can react. Examples include, HC(O)F, HO_2 radicals (formed from the reaction of CF_3CFHO radicals with O_2), H_2O_2 (formed by the self-reaction of HO_2 radicals), CF_3OOH (formed by the reaction of CF_3O_2 with HO_2), and CF_3CFHOH (a product of reaction 7b). These, and other, possibilities were considered and shown to be of minor importance in our previous investigation of the source of CF_3OH following irradiation of HFC-134a/Cl_2/air mixtures with initial concentrations of HFC-134a of approximately 1 Torr. However, such reactions may be important in experiments employing lower HFC-134a concentrations.

To provide insight into the possible impact of reactions of CF_3O with hydrogen containing species other than HFC-134a, reactions 13–16 were added to the chemical mechanism with $k_{13} = 1.1 \times 10^{-10}$, $k_{14} = 1.7 \times 10^{-12}$, $k_{15} = 4.1 \times 10^{-13}$, and $k_{16} = 3.0 \times 10^{-12}$ cm^3 molecule^{-1} s^{-1}. Kinetic data were taken from ref 29. As noted previously,[16] the reactivity of CF_3O radicals towards hydrocarbons is comparable to that of OH radicals. Reactions 13 and 14 were assumed to proceed at the same rate as the corresponding OH radical reactions. For experiment no. 3, the inclusion of reactions 13–16 does not change the predicted yields for HC(O)F and CF_3COF. However, the yields of $CF_3O_2CF_3$ and COF_2 change to 25% and 17%, respectively. These yields are consistent with those experimentally observed. Inclusion of reactions 13–16 in a simulation of experiment no. 1 gives predicted yields of CF_3COF, $CF_3O_2CF_3$, COF_2, and CF_3OH relative to HC(O)F (28%, 24%, 29%, and 18%, respectively) that are close to those experimentally observed. The agreement between the predicted yields based upon the mechanism which includes reactions 13–16 suggests but does not prove that these reactions are important. Uncertainties remain in our understanding of the mechanism(s) by which COF_2 is formed in experiments employing low HFC-134a concentrations.

$$CF_3O + HO_2 \rightarrow CF_3OH + O_2 \quad (13)$$

$$CF_3O + H_2O_2 \rightarrow CF_3OH + HO_2 \quad (14)$$

$$Cl + H_2O_2 \rightarrow HCl + HO_2 \quad (15)$$

$$HO_2 + HO_2 \rightarrow H_2O_2 + O_2 \quad (16)$$

The purpose of the present work is to search for evidence for reaction 3, not to study the reaction mechanism of the Cl atom initiated oxidation of HFC-134a. Modeling of the product yields was not pursued further. While imperfect, the chemical mechanism given in Table IV, with reactions 13–16 added, provides insight into the complex chemistry occurring. As seen from Table III, the addition of H_2O to reaction mixtures containing low initial HFC-134a concentrations leads to an increase in the yield of COF_2 and a decrease in that of $CF_3O_2CF_3$. In contrast, the observed yields of HC(O)F and CF_3COF were unchanged. The presence of H_2O perturbs the chemistry associated with CF_3O

and/or CF_3O_2 radicals. Two possibilities exist:

$$CF_3O + H_2O \rightarrow CF_3OH + OH \quad (3)$$

$$CF_3O_2 + H_2O \rightarrow CF_3OOH + OH \quad (17)$$

with the products, CF_3OH or CF_3OOH, decomposing to give COF_2.

To check on the behavior of CF_3OOH in the chamber an experiment was performed using the UV irradiation of a mixture of 315 mTorr of Cl_2, 17 mTorr of CF_3I, and 4.5 Torr of H_2 in 700 Torr air. Following irradiation, CF_3OOH was identified as a major product by virtue of its characteristic IR absorptions at 1246, 1382, and 3572 cm^{-1}.[30,31] On standing in the dark for 10 min there was no observable decay of CF_3OOH (<5%). There was also no observable decay when CF_3OOH was left to stand in the dark for 5 min with 275 mTorr of H_2O added to the reaction mixture. We conclude that reaction 17 does not contribute to the increased COF_2 yield observed in experiment nos. 3–10 when H_2O is added.

The possible reaction of CF_3O and CF_3O_2 radicals with species on the reaction chamber walls needs consideration. Using the mechanism consisting of Table IV plus reactions 13–16 the lifetimes of CF_3O and CF_3O_2 radicals in the chamber with respect to gas phase reactions are calculated to be <100 and <600 ms respectively. These lifetimes preclude significant interaction with the chamber walls.

Finally, we need to consider the possibility that the trioxide, $CF_3O_3CHFCF_3$, which is a short-lived product observed during the simulated atmospheric oxidation of HFC-134a,[16] may react with H_2O to form either CF_3OH or COF_2. $CF_3O_3CHFCF_3$ decomposes into either CF_3O_2 and CF_3CHFO, or CF_3O and CF_3CFHO_2 radicals.[16] Reaction with H_2O may compete with decomposition. However, such a competition would not be affected by the HFC-134a concentration used. Hence, if reaction of $CF_3O_3CFHFCF_3$ with H_2O was important then increased CF_3OH and/or COF_2 yields would be expected in experiments using both high and low initial HFC-134a concentrations. This is inconsistent with the experimental observations (for example, compare experiment nos. 2 and 4 in Table III) suggesting that reaction of $CF_3O_3CFHFCF_3$ with H_2O is not a complication in the present work.

We believe that the most likely explanation for the observed increase of COF_2 product on addition of H_2O is the gas-phase reaction of CF_3O radicals with H_2O. To derive a value for k_3, we need to construct a chemical mechanism which accurately predicts the product yields observed in the absence of H_2O. Then we need to add reaction 3 to the model and optimize k_3 to reproduce the experimentally observed product yields in the presence of H_2O. Unfortunately, as discussed above, the mechanism by which COF_2 is formed in experiments using low HFC-134a concentrations is not completely understood. Thus, it is difficult to estimate the rate constant k_3. However, we note that because of the presence of sources of CF_3OH, and thereby COF_2 other than reaction 11, the rate constant ratio k_3/k_{11} derived from the data in Figure 3 is a lower limit. Hence, $k_3/k_{11} > (5.4 \pm 1.3) \times 10^{-3}$, using $k_{11} = (1.1 \pm 0.7) \times 10^{-15}$ then gives $k_3 > 2 \times 10^{-18}$ cm^3 $molecule^{-1}$ s^{-1}.

Computational Results and Discussion

That reaction 3 should proceed spontaneously in the gas phase is interesting for two reasons: first, the reaction has important implications for the atmospheric chemistry of CF_3O radicals; second, it implies a remarkably strong O–H bond in CF_3O-H, far stronger than that observed for any other alcohol. The O–H bond in water is among the strongest single bonds known (119.2 kcal/mol).[32] By comparison, the O–H bond dissociation energy in methanol, which is typical of most all alcohols, is 104.4 kcal/mol.[33a] For reaction 3 to occur spontaneously, as the experimental results suggest, the O–H bond in trifluoromethanol must be comparable in strength to that in water, or 15 kcal/mol stronger than for a typical alcohol. Such a result is quite surprising. The anomalous behavior of trifluoromethyl compounds has been noted previously, both in the unusually large O–O bond strength in bis(trifluoromethyl) peroxide[34] and the unusual stability of the bis(trifluoromethyl) trioxide. Trifluoromethanol appears to present yet another example of this curious behavior.

TABLE V: Computationally Determined Heats of Hydrogen Exchange along with Available Experimental Heats of Reaction, from Bond Energy Measurements (All Energies in kcal/mol)

	ΔH_{calc}^{298}	ΔH_{exp}^{298}
$CF_3O + H_2O \rightarrow CF_3OH + OH$	−1.7	
$CF_3O + CH_4 \rightarrow CF_3OH + CH_3$	−14.3	
$CF_3O + H_2 \rightarrow CF_3OH + H$	−15.2	
$CH_3O + H_2O \rightarrow CH_3OH + OH$	11.7	14.6
$CH_3O + CH_4 \rightarrow CH_3OH + CH_3$	−0.9	0.4
$CH_3O + H_2 \rightarrow CH_3OH + H$	−1.8	−0.2

Clearly, an accurate value for the CF_3O–H bond strength is needed, both to establish the thermodynamic feasibility of reaction 3 and to compare with water and other alcohols. Unfortunately, its direct evaluation either experimentally or computationally is quite difficult. In particular, direct calculation of bond scission energies is notoriously inaccurate because of the overriding importance of correlation in describing the electron pairing process.[25] However, computational methods can be used to evaluate to a reasonable level of accuracy the energies of reactions in which the total number of unpaired electrons is conserved (isogyric reactions), and in particular to obtain useful energetic trends among reactions of a similar type. To this end, we have calculated the heat of reaction of CF_3O with water, methane, and hydrogen. Additionally, the heats of the corresponding CH_3O reactions were calculated for comparison with the available experimental results.

Table II contains the raw energy data for all the molecules studied. The energies were obtained by single point calculations at the MP4/6-311+G(d,p) level using fully optimized MP2/6-31G(d,p) geometries. This basis set and degree of correlation were chosen as a compromise between the desired level of accuracy and computational expense, based on our own work and earlier calculations comparing various levels of correlation and extended triple-split-valence bases.[35] Even these relatively extensive (and expensive) calculations are not sufficient to obtain accurate absolute molecular energies, but we expect them to provide reasonably accurate (±3 kcal/mol) energy differences for the isogyric reactions. The MP2 vibrational frequencies were used to obtain zero point and thermal corrections to 298.15 K, and Table II also includes these values.

Table V contains the calculated heats of reaction of the methoxy radical with three hydrogen donors, obtained from the thermally corrected total energies in Table II. The table also contains experimental values for the three methoxy reactions, calculated from the X–H bond dissociation energies using the following equation:[33]

$$\Delta H^{298.15} = D^\circ_{298.15}(CH_3O\text{–}H) - D^\circ_{298.15}(X\text{–}H)$$

A comparison of the experimental and theoretical results should help establish the accuracy of the computational method. The experimental bond energies are reportedly accurate to ±1 kcal/mol. Thus, we can expect the experimental results in Table V to be accurate to within ±2 kcal/mol. Given this level of uncertainty, the agreement between experimental and computed results is very good. As expected from the experimental data, the reaction of methoxy radical with water is a strongly endothermic process. In contrast, the reactions of methoxy radical with methane and hydrogen are nearly thermoneutral processes, reflecting the similarity of the CH_3O–H, H–H, and CH_3–H bond

strengths. The computational results systematically underestimate the experimental results by 1–3 kcal/mol, or slightly greater than the experimental uncertainty, which probably results from inadequacies in our basis set. However, the computational results have adequate accuracy to address the thermodynamics of reaction 3.

Table V also contains the calculated heats of reaction of the CF_3O radical with the three hydrogen donors. The energies are shifted downward 13.4 kcal/mol relative to the methoxy results. This shift reflects a corresponding increase in the computed O–H bond strength from methanol to trifluoromethanol. In contrast to the CH_3O results, the CF_3O reactions with the hydrogen molecule and methane are predicted to be strongly exothermic processes. Consistent with these results, we have previously observed the reaction of CF_3O radicals with methane in our chamber.[16]

The 13.4 kcal/mol shift from the methoxy to trifluoromethoxy case is just enough to make the reaction with water exothermic. We calculate the heat of this reaction to −1.7 kcal/mol. Lower levels of theory, including the MP2/6-31G(d,p) calculations and the MP2 and MP3/6-311+G(d,p) results, give slightly (0–2 kcal/mol) more negative values. Given the likely level of error, and in particular the systematic error observed in the methoxy results, we cannot definitely conclude from the calculations that the reaction is exothermic or spontaneous. However, we can say with confidence that the reaction is close to thermoneutrality and that unlike the reaction of typical alkoxy radicals with water, the abstraction of a hydrogen atom from water by trifluoromethoxy radical is energetically feasible.

While our calculations by themselves do not provide a good estimate of the O–H bond energy in trifluoromethanol, we can combine the heats of reaction in Table V with the experimental bond energies of hydrogen, methane, or water, to obtain an "experimentally corrected" value. Using this approach yields an O–H bond energy of 119–121 kcal/mol, depending on the reaction used. A safe estimate, based on our results, is 120 ± 3 kcal/mol. As already noted, this value is comparable to or greater than the bond energy of water and is roughly 15 kcal/mol greater than that typically observed for an alcohol. Thus, the bond is among the strongest single bonds known.

Implications for Atmospheric Chemistry

In the present work we present computational results which show that the reaction of CF_3O radicals with H_2O is thermodynamically feasible, and experimental results which suggest this reaction has a rate constant that lies in the range $4 \times 10^{-16} > k_3 > 2 \times 10^{-18}$ cm^3 molecule^{-1} s^{-1} at 296 K.

At present, the atmospheric loss mechanism for CF_3O radicals is believed to be reaction with NO and hydrocarbons. Bevilacqua et al.[14] and Zellner[36] both report rate constants of approximately 2×10^{-11} cm^3 molecule^{-1} s^{-1} for reaction with NO, while Saathoff and Zellner[37] have measured $k(CF_3O+CH_4) = 2.2 \times 10^{-14}$ cm^3 molecule^{-1} s^{-1}. Reasonable estimates for the global tropospheric concentrations of NO, CH_4, and H_2O are 2.5×10^8 (10 ppt), 5×10^{13} (2 ppm), and 3×10^{17} cm^{-3} (50% relative humidity). Using $k_3 = (0.2–40) \times 10^{-17}$ cm^3 molecule^{-1} s^{-1} then leads to atmospheric lifetimes of CF_3O radicals (at room temperature) with respect to reaction with NO, CH_4, and H_2O of 200, 0.9, and 0.01–1.7 s, respectively. It appears that reaction 3 may play a significant role in the atmospheric chemistry of CF_3O radicals, and hence, in the atmospheric degradation of CFC replacements such as HFC-134a. Further study is required to define k_3 more precisely and to provide kinetic data for the reactions of CF_3O radicals with organic species and H_2O as a function of temperature.

Note Added in Proof. It has recently come to our attention that Dixon at the du Pont Chemical Co. has calculated a CF_3O–H bond strength of 118.5 kcal mol^{-1}. The result obtained by Dixon is in good agreement with our calculations.

Acknowledgment. We thank Ernie Tuazon (University of California, Riverside) for useful discussions concerning the IR spectrum of CF_3OH, Geoff Tyndall (National Center for Atmospheric Research) for discussions regarding k_3, and David Dixon (du Pont) for discussions regarding the CF_3O–H bond strength.

References and Notes

(1) Farman, J. D.; Gardiner, B. G., Shanklin, J. D. *Nature* **1985**, *315*, 207.

(2) Solomon, S. *Nature* **1990**, *347*, 6291 and references therein.

(3) World Meteorological Organization Global Ozone Research and Monitoring Project, Report No. 20; Scientific Assessment of Stratospheric Ozone, 1989; Vol. 1.

(4) World Meteorological Organization Global Ozone Research and Monitoring Project, Report No. 20; Scientific Assessment of Stratospheric Ozone, 1989; Vol. 2.

(5) Wallington, T. J.; Nielsen, O. *J. Chem. Phys. Lett.* **1991**, *187*, 33.

(6) Wallington, T. J.; Hurley, M. D.; Ball, J. C.; Kaiser, E. W., *Environ. Sci. Technol.* **1992**, *26*, 1318.

(7) Edney, E. O.; Driscoll, D. J. *Int. J. Chem. Kinet.* **1992**, *24*, 1067.

(8) Tuazon, E. C.; Atkinson, R. *J. Atmos. Chem.*, in press.

(9) Sehested, J.; Ellermann, T.; Nielsen, O. J.; Wallington, T. J.; Hurley, M. D. *Int. J. Chem. Kinet.*, in press.

(10) Nielsen, O. J.; Ellermann, T. Sehested, J.; Bartkiewicz, E.; Wallington, T. J.; Hurley, M. D. *Int. J. Chem. Kinet.* **1992**, *24*, 1009.

(11) Wallington, T. J.; Dagaut, P.; Kurylo, M. J. *Chem. Rev.* **1992**, *92*, 667.

(12) Lightfoot, P. D.; Cox, R. A.; Crowley, J. N.; Destriau, M.; Hayman, G. D.; Jenkin, M. E.; Moortgat, G. K.; Zabel, F. *Atmos. Environ.* **1992**, *26*, 1805.

(13) Chen, J.; Zhu, T.; Niki, H. *J. Phys. Chem.* **1992**, *96*, 6115.

(14) Bevilacqua, T. J.; Hanson, D. R.; Howard, C. J. *J. Phys. Chem.*, in press.

(15) Chen, J.; Zhu, T.; Niki, H.; Mains, G. J. *Geophys. Res. Lett.* **1992**, *19*, 2215.

(16) Sehested, J.; Wallington, T. J. *Environ. Sci. Technol.* **1993**, *27*, 146.

(17) Wallington, T. J.; Gierczak, C. A.; Ball, J. C.; Japar, S. M. *Int. J. Chem. Kinet.* **1989**, *21*, 1077.

(18) Morgan, H. W.; Staats, P. A.; Goldstein, J. H. *J. Chem. Phys.* **1956**, *25*, 337.

(19) Wallington, T. J.; Sehested, J.; Dearth, M. A.; Hurley, M. D. *J. Photochem. Photobiol., A: Chem.* **1993**, *70*, 5.

(20) Gaussian 88; Frisch, M. J.; Head-Gordon, M., Schlegel, H. B.; Raghavachari, K.; Binkley, J. S.; Gonzalez, C.; Defrees, D. J.; Fox, D. J.; Whiteside, R. A.; Seeger, R.; Melius, C. F.; Baker, J.; Martin, R.; Kahn, L. R.; Stewart, J. J. P.; Fluder, W. M.; Topiol, S.; Pople, J. A. Gaussian, Inc.: Pittsburgh, PA, 1988.

(21) DeFrees, D. J.; Levi, B. A.; Pollack, S. K.; Hehre, W. J.; Binkley, J. S.; Pople, J. A. *J. Am. Chem. Soc.* **1979**, *101*, 4085.

(22) Francisco, J. S. *Spectrochim. Acta* **1984**, *40A*, 923.

(23) Li, Z.; Francisco, J. S. *Chem. Phys. Lett.* **1991**, *186*, 333, 343.

(24) Curtiss, L. A.; Kock, L. D.; Pople, J. A. *J. Chem. Phys.* **1991**, *95*, 4040.

(25) Hehre, W. J.; Radom, L.; Schleyer, P. v. R.; Pople, J. A. *Ab Initio Molecular Orbital Theory*; Wiley: New York, 1986.

(26) Del Bene, J. E.; Mettee, H. D.; Frisch, M. J.; Luke, B. T.; Pople, J. A. *J. Phys. Chem.* **1983**, *87*, 3279.

(27) Lewis, G. N.; Randall, M. *Thermodynamics*; revised by Pitzer, K. S., Brewer, L., McGraw-Hill: New York, 1961.

(28) Braun, W.; Herron, J. T.; Kahaner, D. K. *Int. J. Chem. Kinet.* **1988**, *20*, 51.

(29) DeMore, W. B.; Sander, S. P.; Golden, D. M.; Hampson, R. F.; Kurylo, M. J.; Howard, C. J.; Ravishankara, A. R.; Kolb, C. E.; Molina, M. J. JPL Publication 92-20, 1992.

(30) Talbot, R. L. *J. Org. Chem.* **1968**, *33*, 2097.

(31) Bernstein, P. A.; Hohorst, F. A.; DesMarteau, D. D. *J. Am. Chem. Soc.* **1971**, *93*, 3882.

(32) Chase, M. W.; Davies, C. A.; Downey, J. R.; Frurip, D. J.; McDonald, R. A.; Syverud, A. N. *JANAF Thermochemical Tables*, 3rd ed.; *J. Phys. Chem. Ref. Data* **1985**, *14*, Suppl. 1.

(33) (a) McMillen, D. F., Golden, D. M. *Annu. Rev. Phys. Chem.* **1982**, *33*, 493. (b) Baldwin, R. R.; Drewery, G. R.; Walker, R. W. *J. Chem. Soc., Faraday Trans. 1* **1984**, *80*, 2827.

(34) Descamps, B.; Forst, W. *J. Phys. Chem.* **1976**, *80*, 933.

(35) Pople, J. A.; Luke, B. T.; Frisch, M. J.; Binkley, J. S. *J. Phys. Chem.* **1985**, *89*, 2198.

(36) Zellner, R., private communication, 1993.

(37) Saathoff, H.; Zellner, R. *Chem. Phys. Lett.* **1993**, *206*, 349.

Atmospheric Chemistry of Hydrofluorocarbon 134a. Fate of the Alkoxy Radical CF_3O

Jens Sehested

Section for Chemical Reactivity, Environmental Science and Technology Department, Risø National Laboratory, DK-4000 Roskilde, Denmark

Timothy J. Wallington*

Research Staff, SRL-3083, Ford Motor Company, P.O. Box 2053, Dearborn, Michigan 48121-2053

■ The atmospheric chemistry of the alkoxy radical CF_3O produced in the photooxidation of hydrofluorocarbon (HFC) 134a has been investigated using Fourier transform infrared spectroscopy. CF_3O radicals are shown to react with methane and CF_3CFH_2 to give CF_3OH. CF_3OH decomposes to give COF_2 and HF. The rate constant for the reaction $CF_3O + CF_3CFH_2$ (HFC-134a) → $CF_3OH + CF_3CFH$ was determined to be $k_{19} = (1.1 \pm 0.7) \times 10^{-15}$ cm^3 molecule^{-1} s^{-1} at 297 K. The implications of our results for the atmospheric chemistry of CF_3O radicals and HFC-134a are discussed.

Introduction

Recognition of the adverse effect of chlorofluorocarbon (CFC) release into the atmosphere has led to an international effort to replace CFCs with environmentally acceptable alternatives (*1–3*). Hydrofluorocarbon 134a (1,1,1,2-tetrafluoroethane) is a viable substitute for CFC-12 in automotive air-conditioning systems. Prior to large-scale industrial use of HFC-134a, the environmental consequences of its release into the atmosphere should be considered. To define the environmental impact of HFC-134a release, the atmospheric photooxidation products of HFC-134a need to be determined.

The main atmospheric loss mechanism for HFC-134a is reaction with the OH radical, reaction 1. Studies of the

$$CF_3CFH_2 + OH \rightarrow CF_3CFH + H_2O \qquad (1)$$

HFC-134a

kinetics of this reaction (*4*) have shown that the atmospheric lifetime of HFC-134a is approximately 15 years. The alkyl radical formed in reaction 1 reacts rapidly (within 1 μs under tropospheric conditions) with molecular oxygen to give the peroxy radical CF_3CFHO_2 (reaction 2).

$$CF_3CFH + O_2 + M \rightarrow CF_3CFHO_2 + M \qquad (2)$$

Studies in our laboratories have shown that reaction with

 0013-936X/93/0927-0146$04.00/0

Table I. Observed Product Yields[a,b] Following the Irradiation of HFC-134a/Cl_2 Mixtures in 700 Torr Air

expt	$[HFC\text{-}134a]_0$	$[Cl_2]_0$	t_{UV} (s)	Δ[HFC-134a]	Δ[HC(O)F]	Δ[CF_3COF]	Δ[$CF_3O_3CF_3$]	Δ[CF_2O]
1	1625	207	300	na[c]	73.8	22.8	19.4	37.3
2	1452	194	60	na	15	4.2	2.66	8.0
3	100	95	300	9.0	6.21	1.8	1.94	1.47
					(69%)[d]	(20%)	(22%)	(16%)
4	100.3	1065	240	30	19.1	6.9	6.78	3.7
					(64%)	(23%)	(23%)	(12%)
5	94.3	231 (F_2)	300	8.5	5.41	1.98	1.45	1.4
					(64%)	(23%)	(17%)	(16%)
6[e]	95.6	101	300	8.6	7.5	0.6	2.4	1.8
					(87%)	(7%)	(28%)	(21%)

[a] Observed concentrations in units of milliTorr; no corrections of any kind applied to data. [b] Product analyses were performed after dark chemistry ceased. [c] Not applicable. [d] Values in parentheses are molar yields. [e] Experiment performed using 2.5 Torr O_2 in 700 Torr total pressure N_2.

NO is a significant atmospheric sink for CF_3CFHO_2 radicals and that the products of this reaction are CF_3CFHO radicals and NO_2 (5).

$$CF_3CFHO_2 + NO \rightarrow CF_3CFHO + NO_2 \quad (3)$$

CF_3CFHO radicals formed in reaction 3 either decompose to give CF_3 radicals and HC(O)F or react with O_2 to give CF_3COF. In the atmosphere, approximately 70% of the CF_3CFHO radicals formed from the photooxidation of HFC-134a decompose, while 30% react with O_2 (6).

$$CF_3CFHO + O_2 \rightarrow CF_3COF + HO_2 \quad (4)$$

$$CF_3CFHO \rightarrow CF_3 + HC(O)F \quad (5)$$

CF_3 radicals formed in reaction 5 react with O_2 to give CF_3O_2 radicals, which in turn react rapidly with NO to form CF_3O radicals (4, 7, 8):

$$CF_3 + O_2 + M \rightarrow CF_3O_2 + M \quad (6)$$

$$CF_3O_2 + NO \rightarrow CF_3O + NO_2 \quad (7)$$

The atmospheric fate of CF_3O radicals is uncertain. It is generally assumed that CF_3O radicals are converted into COF_2 in the atmosphere (9), although the exact mechanism for this conversion is unclear. In a previous study of the simulated atmospheric chemistry of HFC-134a, we observed the formation of COF_2 when reaction mixtures were left to age in the dark (6). However, we were unable to identify the mechanism by which this product was formed. As part of a collaborative research program between Ford and Risø National Laboratory to determine the environmental impact of CFC replacements, we have revisited the mechanism by which COF_2 is formed in the simulated atmospheric oxidation of HFC-134a. Results are reported herein.

Experimental Section

The experimental setup used for the present work has been described previously (10) and is only briefly discussed here. The apparatus consists of a Mattson Instruments Inc. Sirius 100 FT-IR spectrometer interfaced to a 140-L, 2-m-long evacuable pyrex chamber. White-type multiple-reflection optics were mounted in the reaction chamber to provide a total path length of 28 m for the IR analysis beam. The spectrometer was operated at a resolution of 0.25 cm^{-1}. Infrared spectra were derived from 128 coadded interferograms. Experiments were performed at 297 K and a total pressure of 700 Torr.

CF_3 radicals were generated by two different methods: chlorine- or fluorine-initiated oxidation of HFC-134a or photolysis of CF_3NO. For the chlorine- or fluorine-initiated experiments, the following concentration ranges were used: HFC-134a, 94–1625 mTorr; Cl_2, 95–1065 mTorr, or F_2, 231 mTorr; O_2, 2.5–150 Torr, with N_2 added as appropriate to maintain a total pressure of 700 Torr. Chlorine or fluorine atoms were generated by the photolysis of the corresponding molecular halogen using the output of 24 UV fluorescent lamps (GTE F40BLB).

$$Cl_2/F_2 + h\nu\ (\lambda > 300\ nm) \rightarrow 2Cl/F \quad (8)$$

For experiments using CF_3NO, photolysis was achieved using visible light from 12 fluorescent lamps (GTE F40CW):

$$CF_3NO + h\nu\ (\lambda > 400\ nm) \rightarrow CF_3 + NO \quad (9)$$

Initial concentrations used were as follows: CF_3NO, 14–110 mTorr; CH_4, 0–1300 mTorr.

Products were quantified by fitting reference spectra of the pure compounds to the observed product spectra using integrated absorption features. Reference spectra were obtained by expanding known volumes of the reference material into the long-path-length cell. Systematic uncertainties associated with quantitative analyses using these reference spectra are estimated to be <10%. The procedure was as follows: HFC-134a or CF_3NO was first quantified and subtracted from the product spectra using characteristic absorption features over the wavelength regions 800–1500 or 1100–1700 cm^{-1}. HC(O)F, COF_2, CF_3COF, and $CF_3O_3CF_3$ were then identified and quantified using features over the following wavelength ranges: 1700–1900, 700–900 and 1800–2000, 700–800 and 1800–2000, and 700–900 cm^{-1}, respectively.

HFC-134a, Cl_2, CF_3NO, CF_3COF, and COF_2 were purchased from commercial vendors at purities of ≥99%. HC(O)F was prepared from the reaction of benzoyl chloride with dry formic acid and anhydrous potassium fluoride (11). $CF_3O_3CF_3$ was prepared by the UV irradiation of CF_3H–F_2–O_2–He mixtures (12). Ultrapure synthetic air or mixtures of ultrapure N_2 and O_2 were used as diluents.

Results

Following the irradiation of mixtures of HFC-134a and Cl_2 in air, the observed carbon-containing products were CF_3COF, HC(O)F, COF_2, and $CF_3O_3CF_3$. Yields of these species observed in the present work are reported in Table I together with the initial conditions pertinent to each experiment. The concentrations of CF_3COF, HC(O)F, COF_2, and $CF_3O_3CF_3$ increased when reaction mixtures were left to age in the dark. Reported values in Table I are yields measured after all dark chemistry had ceased. A majority of experiments were performed using Cl atom initiated oxidation of HFC-134a. One experiment was performed using F atom initiation. As seen in Table I, indistinguishable results were obtained with F and Cl atom initiation. In experiments 1 and 2 (Table I), the initial

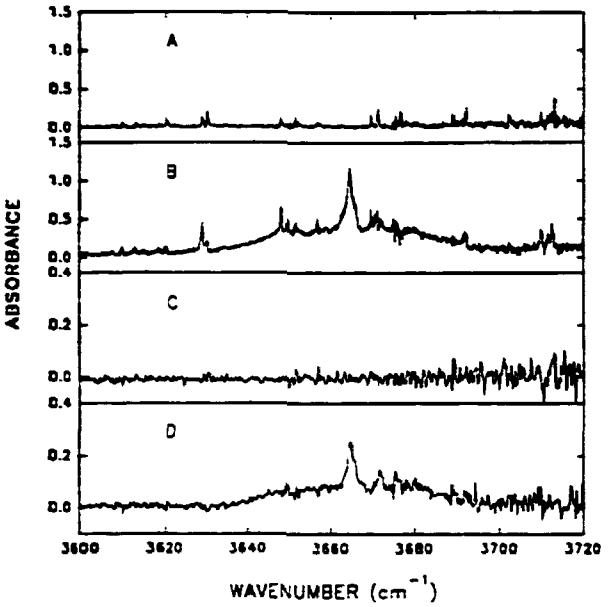

Figure 1. Spectra taken before (A) and 25 min after (B) 300 s of UV irradiation of a mixture of 1625 mTorr HFC-134a and 207 mTorr Cl_2. Spectra C and D were acquired before and after irradiation of a mixture of 109.4 mTorr CF_3NO and 1.3 Torr CH_4. Both experiments were conducted in 700 Torr total pressure of air diluent.

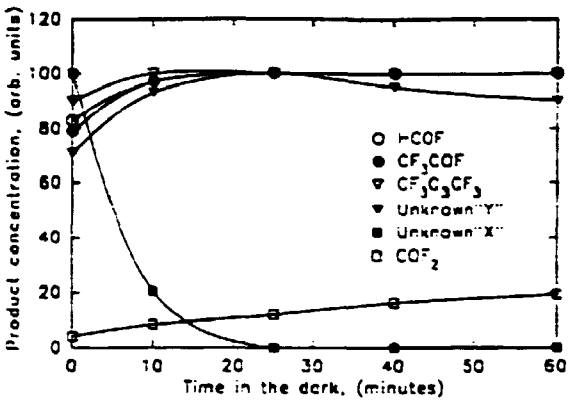

Figure 2. Observed behavior of HC(O)F, CF_3COF, $CF_3O_3CF_3$, COF_2, unknown X, and unknown Y when the reaction mixture from experiment 1 (see Table I) was left to age in the dark. Yields of HC(O)F, CF_3COF, $CF_3O_3CF_3$, and Y are normalized to the concentration observed after standing in the dark for 25 min. The yield of X is normalized to the concentration of this species immediately following the illumination period. The yield of COF_2 is normalized to its final concentration after the reaction mixture was left to stand in the dark for 24 h. The solid lines are cubic spline fits to aid visual inspection of the data trends.

HFC-134a concentrations were greater than 1 Torr. With such high concentrations, the IR absorption features attributable to HFC-134a were saturated; consequentially, we are unable to quantify the loss of HFC-134a in these experiments. The average of the observed HC(O)F and CF_3COF yields in experiments 3–5 are 66 and 21%, respectively (yields are expressed in terms of moles of product formed per mole of HFC-134a consumed). Chlorine and fluorine atoms do not react with CF_3COF. However, they do react with HC(O)F, so we must correct the observed yield of HC(O)F for reaction with Cl or F atoms to derive the true product yield of this species. The rate constant for reaction of HC(O)F with Cl atoms is k[Cl+HC(O)F] = 2.0×10^{-15} cm^3 molecule^{-1} s^{-1} (*6*). The rate constant for reaction of HC(O)F with F atoms is k[F+HC(O)F] = 2.3×10^{-12} cm^3 molecule^{-1} s^{-1} (*13*). Rate constants for reaction of Cl and F atoms with HFC-134a are k(Cl+HFC-134a) = 1.4×10^{-15} cm^3 molecule^{-1} s^{-1} (*14*) and k(F+HFC-134a) = 1.4×10^{-12} cm^3 molecule^{-1} s^{-1} (*15*). These kinetic data can be used to correct for secondary loss of HC(O)F in experiments 3–5 by reaction with Cl or F atoms. The corrected HC(O)F yields in experiments 3–5 are 73, 78, and 69%, respectively. The average of the corrected HC(O)F yields from these experiments is then 73%.

Results from the present work are in agreement with yields of 73 and 21% for HC(O)F and CF_3COF from the Cl atom initiated oxidation of HFC-134a in 700 Torr air previously reported by our laboratory (*6*).

In addition to CF_3COF, HC(O)F, COF_2, $CF_3O_3CF_3$, and HCl, unknown product features were observed at 756, 894, and 3664 cm^{-1}. Figure 1 shows the infrared spectrum in the region 3600–3720 cm^{-1} before (A) and 25 min after (B) a 5-min irradiation of 1625 mTorr HFC-134a and 207 mTorr Cl_2 in air. Figure 1B clearly shows the formation of a product which absorbs at 3664 cm^{-1}. The unknown product features at 756, 894, and 3664 cm^{-1} decayed when reaction mixtures were left to age in the dark. The two absorptions at 756 and 894 cm^{-1} decayed at the same rate with a half-life at 4–5 min. The absorption feature at 3664 cm^{-1} decayed more slowly with a life time of 1–5 h. It seems reasonable to assign the absorption features at 756 and 894 cm^{-1} to one product species that we refer to as "X" and that at 3664 cm^{-1} to another product we label "Y".

HC(O)F, CF_3COF, $CF_3O_3CF_3$, and COF_2 all increased in concentration when reaction mixtures were left to age in the dark. The time scale over which HC(O)F, CF_3COF, and $CF_3O_3CF_3$ increased was, within our experimental uncertainties, indistinguishable from that of the decay of the unknown X. This behavior is illustrated in Figure 2. In Figure 2 we have plotted the observed temporal behavior of HC(O)F, CF_3COF, $CF_3O_3CF_3$, COF_2, and the two unknown products. For ease of comparison, HC(O)F, CF_3COF, and $CF_3O_3CF_3$ have been normalized to the concentrations observed after 25 min of aging in the dark. The unknown X is normalized to its concentration immediately following photolysis. COF_2 is normalized to its final concentration observed after standing in the dark for 24 h. As seen from Figure 2, in addition to HC(O)F, CF_3COF, and $CF_3O_3CF_3$, the unknown Y initially increases upon aging in the dark. However, in contrast to HC(O)F, CF_3COF, and $CF_3O_3CF_3$, the unknown Y decays at times longer than 25 min.

The chemistry occurring in the reaction chamber during the first 25 min of aging in the dark is clearly complex. The unknown X decays in the dark to form directly, or indirectly, HC(O)F, CF_3COF, $CF_3O_3CF_3$, Y, and possibly COF_2.

At longer times in the dark the chemistry is less complex. After 25 min of aging in the dark, only Y is observed to decay and only COF_2 is observed to form. In Figure 3 we plot the decay of Y and the formation of COF_2 when the reaction mixture from Figure 2 was left to stand for 24 h in the dark. The first data point in Figure 3 corresponds to 25 min of aging; X has disappeared at this time. The solid curves in Figure 3 are first-order decay and rise fits to the unknown Y and COF_2 data, respectively. As seen from Figure 3, the decay of Y and the formation of COF_2 both follow first-order kinetics. The first-order decay rate for the absorption feature at 3664 cm^{-1} is 291 ± 14 min; the first-order rise time for COF_2 is 282 ± 28 min. Quoted errors are 2 standard deviations from the least squares fits. The identical kinetics observed for the decay of the absorption feature at 3664 cm^{-1} and the formation of COF_2 shows that COF_2 is a product of the decomposition of the unidentified species Y.

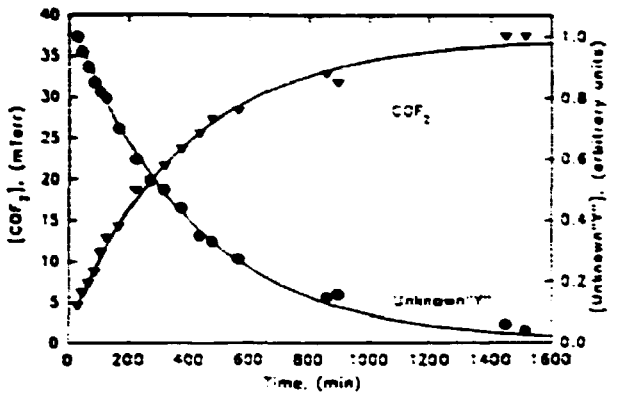

Figure 3. Observed behavior of unknown Y and COF_2 when the reaction mixture from experiment 1 (see Table I) was left to age in the dark. Solid lines are fits of first-order kinetics to the data.

At times longer than 25 min in the dark, no other features were observed to change apart from COF_2 and the absorption feature at 3664 cm^{-1}. Possible other decomposition products of compound Y either do not absorb or only absorb weakly in the infrared between 650 and 1000, 1500 and 2950, and 3050 and 3800 cm^{-1}. The frequency intervals 1000–1500 and 2950–3050 cm^{-1} were optically black due to absorption of HFC-134a; any changes in absorption in these regions went undetected in our experiments.

We believe that Y is CF_3OH. Reasons for this assignment are as follows. The product Y has an IR absorption feature at 3664 cm^{-1}. This frequency is characteristic of an O–H stretching mode and shows the presence of an OH group in the molecule. The unknown is either an alcohol or a hydroperoxide. In the simulated atmospheric photooxidation of HFC-134a, possible alcohol and hydroperoxide products are CF_3OH, CF_3OOH, CF_3CFHOH, or $CF_3CFHOOH$. Hydroperoxides are formed by the reaction of HO_2 and peroxy radicals. The only source of HO_2 radicals in our experiments is the reaction of molecular oxygen with CF_3CFHO radicals, reaction 4. We can minimize HO_2 radical production, and hence hydroperoxide formation, by reducing the oxygen concentration in our experiments. An experiment was performed using initial conditions of 1.7 Torr HFC-134a, 0.2 Torr Cl_2, and 2.5 Torr O_2 with N_2 added to give a total pressure of 700 Torr. Under these conditions using the rate constant ratio $k_4/k_5 = 1.58 \times 10^{-25} \exp(3600/T)$ cm^3 $molecule^{-1}$ (6) (3.2×10^{-20} cm^3 $molecule^{-1}$ at 297 K), we calculate that <0.5% of the CF_3CFHO radicals produced during the oxidation of HFC-134a will react with O_2; thus HO_2 formation will be negligible. In this low-O_2 experiment, the unknown product which absorbs at 3664 cm^{-1} was observed with a yield that was actually larger than observed in experiments in air diluent. Clearly, the unknown is not a hydroperoxide.

We are left with two possibilities: CF_3OH and CF_3CFHOH. Infrared spectral data are available in the literature for CF_3OH (*16*) but not for CF_3CFHOH. Klöter and Seppelt (*16*) reported an O–H stretching frequency of 3675 cm^{-1} for gas phase CF_3OH at −78 °C. The unknown Y has an IR O–H stretching frequency of 3664 cm^{-1} at room temperature. A priori it is not expected that decreasing the temperature from room temperature to −78 °C would shift the O–H stretching frequency by as much as 11 cm^{-1}. The literature spectral data for CF_3OH are then not consistent with our unknown. This result is surprising, as it is difficult to explain how CF_3CFHOH decomposes to give COF_2 without forming other products that would be detected by our IR analytical system. The expected decomposition products of CF_3CFHOH are HF and CF_3CHO.

$$CF_3CFHOH \rightarrow CF_3CHO + HF \quad (10)$$

In view of this unexpected result, experiments were performed to generate CF_3OH in the chamber to provide an in-situ calibration using a chemical system which could not produce CF_3CFHOH. Howard (*17*) has reported that CF_3O radicals react readily with methane, giving CF_3OH:

$$CF_3O + CH_4 \rightarrow CF_3OH + CH_3 \quad (11)$$

We used the photolysis of CF_3NO in air, in the presence of CH_4, to generate CF_3OH. The mechanism by which CF_3OH is formed is

$$CF_3NO + h\nu \rightarrow CF_3 + NO \quad (9)$$

$$CF_3 + O_2 + M \rightarrow CF_3O_2 + M \quad (6)$$

$$CF_3O_2 + NO \rightarrow CF_3O + NO_2 \quad (7)$$

$$CF_3O + CH_4 \rightarrow CF_3OH + CH_3 \quad (11)$$

Prior to the addition of methane, control experiments were performed where CF_3NO was photolyzed in air to check for any interfering product absorptions in the region 3500–3700 cm^{-1}; none were observed. Panels C and D in Figure 1 are spectra in the region 3500–3700 cm^{-1} of a mixture of 109.4 mTorr CF_3NO with 1.3 Torr CH_4 in 700 Torr air taken before (C) and after (D) 20-min irradiation. We ascribe the IR feature at 3664 cm^{-1} formed in the irradiation of CF_3NO–CH_4–air mixtures to CF_3OH. As seen from Figure 1, the IR feature at 3664 cm^{-1} is the same in both the CF_3NO–CH_4 and the HFC-134a–Cl_2 experiments. We conclude that the unknown Y is CF_3OH. The origin of the discrepancy between our measured O–H stretching frequency of 3664 cm^{-1} for CF_3OH and that of 3675 cm^{-1} reported previously (*16*) is unknown.

By analogy to our recent study of the decomposition of mono- and dichloromethanol (*18*), we expect trifluoromethanol to decompose to give COF_2 and HF.

$$CF_3OH \rightarrow COF_2 + HF \quad (12)$$

HF absorbs in the infrared at frequencies above 3800 cm^{-1} and is thus not detected by our spectrometer. The half-life of CF_3OH in our reaction chamber increased from 1 to 5 h during the course of our experiments, presumably reflecting conditioning of the chamber walls for this species. The longest half-life we observed (5 h) may still have a significant heterogeneous component. This lifetime then serves as a lower limit for the atmospheric lifetime of CF_3OH with respect to thermal decomposition into COF_2 and HF.

If we assume that CF_3OH decomposes stoichiometrically into COF_2 and HF, we can calibrate our CF_3OH spectrum by equating it with the observed formation of COF_2. The spectrum shown in Figure 1B was taken 25 min after irradiation of a mixture of 1625 mTorr HFC-134a and 207 mTorr Cl_2 in air. When this mixture was allowed to sit in the chamber in the dark for 24 h, the CF_3OH decayed to 3% of the initial concentration and 32.8 mTorr COF_2 was formed (see Figure 3). Equating 97% of the spectrum in Figure 1B with 32.8 mTorr, we can then derive an absorption cross section of $\sigma_{3664cm^{-1}}(CF_3OH) = 9 \times 10^{-19}$ cm^2 $molecule^{-1}$.

Having established the identity of the unknown Y as CF_3OH, we now return to unknown X. Unknown X decomposes to form directly, or indirectly, HC(O)F, CF_2O, $CF_2O_2CF_2$, and CF_3OH. We believe that the unknown X is the trioxide $CF_3CFHO_2CF_2$, formed by the reaction

$$CF_3CFHO_2 + CF_2O \rightarrow CF_3CFHO_2CF_2 \quad (13)$$

Decomposition of $CF_3CFHO_2CF_2$ probably proceeds via two channels:

$$CF_3CFHO_2CF_3 \rightarrow CF_3O + CF_3CFHO_2 \quad (14)$$

$$\rightarrow CF_3O_2 + CF_3CFHO \quad (15)$$

There are three reasons for this assignment. First, CF_3O is known to form stable trioxides with CF_3O_2 (*12*) and $CF_3CF_2O_2$ (*19*). CF_3CFHO_2 and CF_3O radicals are known to be present during the degradation of HFC-134a. It therefore seems likely that CF_3O radicals will combine with CF_3CFHO_2 to give a trioxide. Second, the decomposition products [HC(O)F, CF_3COF, $CF_3O_3CF_3$, and CF_3OH] show that the unknown X fragments to give either (a) CF_3CFHO_2 radicals, (b) CF_3CFHO radicals, or (c) radicals that attack HFC-134a to form CF_3CFH radicals. The decomposition of $CF_3CFHO_2CF_3$ will form CF_3CFHO_2 or CF_3CFHO radicals, or both, while CF_3O radicals will be formed which can abstract a hydrogen atoms from HFC-134a. Third, the absorption features at 756 and 894 cm^{-1} are similar in both frequency and shape to those of $CF_3O_3CF_3$ at 773 and 897 cm^{-1} (*12*). The absorption features of $CF_3O_3CF_3$ at 773 and 897 cm^{-1} are symmetric and asymmetric O–O–O stretching modes, respectively (*20*). Substitution of a CF_3O group by the heavier CF_3CFHO group would be expected to lower the frequencies of both modes, with the symmetric O–O–O stretch lowered most. We observe that the probable symmetric O–O–O stretch is lowered by 16 cm^{-1} and the probable asymmetric O–O–O stretch is lowered by 3 cm^{-1}.

Discussion

There are two possible sources of CF_3OH in our study of the simulated atmospheric oxidation of HFC-134a. Either CF_3OH is formed by reaction of CF_3O_2 radicals with other peroxy radicals or it is formed by reaction of CF_3O radicals with hydrogen-containing species. There are two peroxy radicals which could react with CF_3O_2 to give CF_3OH: HO_2 and CF_3CFHO_2.

$$CF_3O + HO_2 \rightarrow CF_3OH + O_2 \quad (16)$$

$$CF_3O_2 + CF_3CFHO_2 \rightarrow CF_3OH + CF_3COF + O_2 \quad (17)$$

Our experimental results at low O_2 concentration (see experiment 6 in Table I) suggest that reactions 16 and 17 are not major sources of CF_3OH in our system. With an O_2 partial pressure of 2.5 Torr, HO_2 radical formation is negligible, and yet CF_3OH is observed in a yield which is larger than that observed in air diluent. Clearly, reaction 16 is of negligible importance. The COF_2 (and hence CF_3OH) yield in our experiment at low $[O_2]$ is 3 times that of the CF_3COF. If reaction 17 was the main source of CF_3OH, we would expect comparable yields of COF_2 and CF_3COF. Clearly, reaction 17 is not the main source of CF_3OH, although it could be responsible for the formation of up to 33% of the observed COF_2.

Hydrogen-containing species that CF_3O radicals could react with to give CF_3OH include HFC-134a, HC(O)F, CF_3CFHOH, and HCl. In light of the insensitivity of the CF_3OH yield toward the O_2 partial pressure noted above, we do not consider reaction of CF_3O with H_2O_2 or other hydroperoxides. As seen in Table I, the observed COF_2 yield was unchanged when F atom initiation was employed instead of Cl atom initiation. Thus, reaction of CF_3O radicals with HCl is not significant in our work.

In our chemical system there is only one source of the alcohol CF_3CFHOH, reaction 18b:

$$CF_3CFHO_2 + CF_3CFHO_2 \rightarrow CF_3CFHO + CF_3CFHO + O_2 \quad (18a)$$

$$CF_3CFHO_2 + CF_3CFHO_2 \rightarrow CF_3COF + CF_3CFHOH + O_2 \quad (18b)$$

Our measured CF_3COF yield at low oxygen partial pressure provides an upper limit of 8% for the yield of CF_3CFHOH in our system. As seen in Table I, this yield is significantly below that of CF_3OH (determined by the yield of COF_2 when mixtures were left in the dark). There is insufficient CF_3CFHOH present in the chamber to account for the observed formation of COF_2.

If reaction of CF_3O with HC(O)F is significant in the present experiments, then the HC(O)F yields would be expected to decrease as the consumption of HFC-134a increases. No such trend is apparent from Table I. In experiments 3 and 4 (Table I), the consumption of HFC-134a differs by a factor of 3 while the yield of HC(O)F is essentially unchanged.

The most likely explanation for the CF_3OH product in our simulated atmospheric oxidation of HFC-134a is reaction of CF_3O radicals with HFC-134a.

$$CF_3O + CF_3CFH_2 \rightarrow CF_3OH + CF_3CFH \quad (19)$$

Evidence for the importance of reaction 19 can be seen in Table I. The only known source of HC(O)F in our experiments is reaction 5. For every HC(O)F molecule produced, a CF_3 radical is formed. The yield of HC(O)F then provides a measure of the total formation of CF_3 radicals. The yield of COF_2 observed when all dark chemistry has ceased (up to 24 h after initiation of the experiment) provides a measure of the production of CF_3OH. The product ratio $[COF_2]/[HC(O)F]$ is then a measure of the efficiency by which CF_3 radicals are converted into CF_3OH. As seen in Table I, the product ratio $[COF_2]/[HC(O)F]$ is insensitive to changes in $[Cl_2]_0$ by a factor of 10, HFC-134a consumption by a factor of 3, and use of F atom instead of Cl atom initiation. However, the $[COF_2]/[HC(O)F]$ ratio increases when the initial concentration of HFC-134a is increased. With $[HFC\text{-}134a]_0 \approx 0.1$ Torr, $[COF_2]/[HC(O)F] = 0.19–0.26$; with $[HFC\text{-}134a]_0 \approx 1.5$ Torr, $[COF_2]/[HC(O)F] = 0.51–0.53$. This is explained by the competition between reactions 19 and 20 for the available CF_3O radicals.

$$CF_3O + CF_3O_2 \rightarrow CF_3O_3CF_3 \quad (20)$$

To provide an estimate for the rate constant of reaction 19 we have modeled the system using the Acuchem program (*21*) with the chemical mechanism given in Table II. Kinetic data in Table II were taken from the literature and recent studies in our laboratories (*6*, *22–24*). Two parameters were varied to provide a fit to the experimental data: k_{13} and k_{19}. As shown in Figure 4, the chemical mechanism given in Table II [with values of $k(CF_3O+HFC\text{-}134a) = 4.5 \times 10^{-16}$ cm^3 $molecule^{-1}$ s^{-1} and $k(CF_3O+CF_3CFHO_2) = 1.8 \times 10^{-11}$ cm^3 $molecule^{-1}$ s^{-1}] provides a reasonable fit to our experimental results. Values of k_{13} and k_{19} needed to fit our data are sensitive to the chosen rate constant for the reaction of CF_3O with CF_3O_2. The value of $k(CF_3O+CF_3O_2) = 2.5 \times 10^{-11}$ cm^3 $molecule^{-1}$ s^{-1} that we have used is a lower limit and is based upon our observed 100% product yield of the trioxide $CF_3O_3CF_3$ following the self-reaction of CF_3O_2 radicals (*22*). If we allow $k(CF_3O+CF_3O_2)$ to increase to 1.0×10^{-10} cm^3 $molecule^{-1}$ s^{-1}, we need to employ values of $k(CF_3O+HFC\text{-}134a) = 1.8 \times 10^{-15}$ cm^3 $molecule^{-1}$ s^{-1} and $k(CF_3O+CF_3CFHO_2) = 7.0 \times 10^{-11}$ cm^3 $molecule^{-1}$ s^{-1} to fit our observed product yields. We choose to report the average of the values of k_{13} and k_{19} obtained when $k(CF_3O+CF_3O_2)$ was varied between its lower and likely upper limit together with error limits which encompass both extremes. Hence, $k(CF_3O+HFC\text{-}134a) = (1.1 \pm 0.7) \times 10^{-15}$ cm^3 $molecule^{-1}$ s^{-1} and $k(CF_3O + CF_3CFHO_2) = (4.4 \pm 2.6) \times 10^{-11}$ cm^3 $molecule^{-1}$ s^{-1}.

The purpose of the present study is not to define the kinetics of reactions 13 and 19; rather it is to understand

Table II. Reaction Mechanism

reaction	k (297 ± 5 K)[a]	ref
$Cl_2 \rightarrow 2Cl$		
$Cl + CF_3CFH_2 \rightarrow HCl + CF_3CFH$	1.4×10^{-13}	14
$CF_3CFH + O_2 \rightarrow CF_3CFHO_2$	2×10^{-12}	*c*
$CF_3CFHO_2 + CF_3CFHO_2 \rightarrow 2CF_3CFHO + O_2$	6×10^{-12}	24
$CF_3CFHO_2 + CF_3CFHO_2 \rightarrow CF_3COF + CF_3CFHOH + O_2$	1×10^{-12}	24
$CF_3CFHO_2 + CF_3O_2 \rightarrow CF_3CFHO + CF_3O + O_2$	8×10^{-12}	24
$CF_3CFHO \rightarrow CF_3 + HC(O)F$	2×10^{4}	24
$CF_3CFHO + O_2 \rightarrow CF_3COF + HO_2$	9×10^{-16}	24
$CF_3 + O_2 \rightarrow CF_3O_2$	8.5×10^{-12}	4
$CF_3O_2 + CF_3O_2 \rightarrow CF_3O + CF_3O + O_2$	1.8×10^{-12}	22
$CF_3O + CF_3O_2 \rightarrow CF_3O_3CF_3$	2.5×10^{-11}	22, 23
$CF_3O + CF_3CFHO_2 \rightarrow CF_3CFHO_3CF_3$	1.8×10^{-11}	*d*
$CF_3CFHO_3CF_3 \rightarrow CF_3CFHO_2 + CF_3O$	2.0×10^{-3} [b]	*d*
$CF_3CFHO_3CF_3 \rightarrow CF_3CFHO + CF_3O_2$	2.0×10^{-3} [b]	*d*
$CF_3O + CF_3CFH_2 \rightarrow CF_3CFH + CF_3OH$	4.5×10^{-16}	*d*
$CF_3OH \rightarrow CF_2O + HF$	4×10^{-5} [b]	*d*
$Cl + HC(O)F \rightarrow HCl + FCO$	2.0×10^{-15}	6

[a] Units of cm^3 molecule^{-1} s^{-1}. [b] Units of s^{-1}. [c] Estimated. [d] This work.

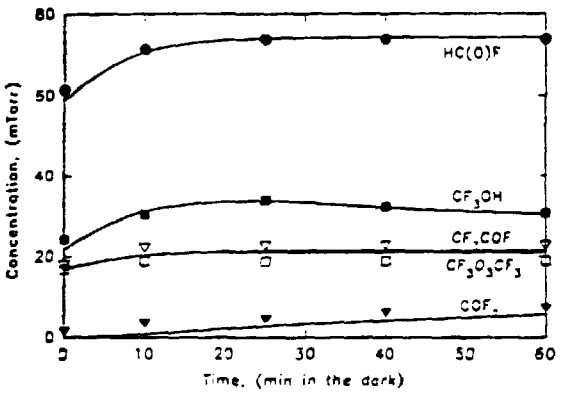

Figure 4. Comparison of predicted product yields from the chemical mechanism given in Table III (solid lines) with experimentally observed yields (symbols) for experiment 1.

the mechanism by which COF_2 is formed in the simulated atmospheric oxidation of HFC-134a. We have shown that reaction of CF_3O radicals with HFC-134a is important, that CF_3OH is a product of this reaction, and that CF_3OH decomposes to give COF_2. In the atmosphere, the concentration of HFC-134a is many orders of magnitude less than used in laboratory studies of its atmospheric chemistry. Reaction 19 will not be important in the atmosphere. Nevertheless, our study of reaction 19 taken together with the recent work of Howard (*17*) has important implications for the atmospheric chemistry of CF_3O radicals.

Implications for Atmospheric Chemistry

The rate constant for reaction 19 reported here, $k_{19} = (1.1 \pm 0.7) \times 10^{-15}$ cm^3 molecule^{-1} s^{-1}, is approximately 4 times slower than reaction of OH radicals with HFC-134a [k(OH+HFC-134a) = 4.8×10^{-15} cm^3 molecule^{-1} s^{-1} (*4*)]. Howard has reported rate constants for the reactions of CF_3O radicals with CH_4 and i-C_4H_{10} which are comparable (within a factor of 2) to those observed for OH radical attack (*17*). If the kinetics of reaction of CF_3O radicals with other organic species are within 1 order of magnitude of that of OH radicals, then reaction of CF_3O radicals with organic compounds will be an important, if not dominant, atmospheric fate of CF_3O radicals. As shown for HFC-134a here, and as expected for other saturated organic species, these reactions proceed via a hydrogen abstraction mechanism to give CF_3OH.

In the atmosphere, trifluoromethanol will either decompose (homogeneously and/or heterogeneously), photolyze, react with OH radicals, or be incorporated into water droplets. The observed decay of CF_3OH in our chamber places a lower limit on the atmospheric lifetime with respect to decomposition of 5 h. By analogy to other alcohols (*25*), the absorption of UV by CF_3OH is expected to occur at wavelengths below 200 nm. Photolysis will then only occur above the ozone layer (>50 km). Transport to such high altitudes is slow, so that photolysis is not expected to be a significant atmospheric fate of CF_3OH.

By virtue of the strong O–H bond [109 kcal/mol (*23*)], the reaction of CF_3OH with OH radicals is expected to be slow. We can estimate the atmospheric lifetime of CF_3OH with respect to OH attack by considering the atmospheric lifetime of CH_4 which is determined by OH attack. The C–H bond strength in methane is 104 kcal/mol, and each C–H bond is expected to be more reactive than the O–H bond in CF_3OH. Since the atmospheric lifetime of methane is approximately 10 years, the lifetime of CF_3OH with respect to OH radical attack will probably be at least 40 years.

In contrast to photolysis and reaction with OH, incorporation of CF_3OH into water is rapid (*9*). Following absorption into cloudwater or seawater, CF_3OH will decompose to give HF and CO_2 (*9*). Either decomposition (reaction 12) or rain-out will dominate removal of CF_3OH from the atmosphere. The exact removal mechanism is unimportant as the decomposition product from reaction 12, COF_2, is removed by rain-out and decomposes in water to give CO_2 and HF (*9*).

To conclude, it appears that reaction with hydrocarbons is an important atmospheric removal process for CF_3O radicals. As shown here for HFC-134a and CH_4, this reaction produces CF_3OH. Trifluoromethanol is expected to either directly or indirectly (via COF_2) be incorporated into water droplets and decompose to CO_2 and HF. Concentrations of HF in rainwater resulting from the release of HFCs will be low. For example, HFC-134a is a replacement for CFC-12. In 1986 the global production of CFC-12 was 4.0×10^8 kg. If HFC-134a replaces CFC-12 on an equal mass basis and all the HFC-134a is released without recovery, the emission to the atmosphere would be 4.0×10^8 kg or 3.9×10^9 mol/year. At steady state, assuming each F atom in HFC-134a is converted into HF, 1.6×10^{10} mol of HF would be formed in the atmosphere annually. The annual global rainfall is 4.9×10^{17} L (*26*). Thus, rainwater might be expected to contain 3.3×10^{-6} M (0.6 ppb) HF. This additional fluoride burden is not expected to have any direct effect on plant systems (*9*). For comparison, ~1 ppm fluoride level is currently added to drinking water in most U.S. cities.

Acknowledgments

We thank Roscoe Carter and Steve Japar (both of Ford Motor Co.), Carl Howard (NOAA), Ole John Nielsen (Risø National Laboratory, Roskilde, Denmark), and Dave Rowley (Cambridge University, England) for helpful discussions.

Literature Cited

(1) Farman, J. D.; Gardiner, B. G.; Shanklin, J. D. *Nature* **1985**, *315*, 207.
(2) Solomon, S. *Nature* **1990**, *347*, 6291, and references therein.
(3) World Meteorological Organization Global Ozone Research and Monitoring Project. *Scientific Assessment of Stratospheric Ozone*; Report No. 20; 1989; Vol. 1.
(4) DeMore, W. B.; Sander, S. P.; Golden, D. M.; Molina, M. J.; Hampson, R. F.; Kurylo, M. J.; Howard, C. J.; Ravish-

ankara, A. R. *JPL Publ.* **1990**, *No. 90-1*.
(5) Wallington, T. J.; Nielsen, O. J. *Chem. Phys. Lett.* **1991**, *187*, 33.
(6) Wallington, T. J.; Hurley, M. D.; Ball, J. C.; Kaiser, E. W. Environ. Sci. Technol. **1992**, *26*, 1318.
(7) Wallington, T. J.; Dagaut, P.; Kurylo, M. J. *Chem. Rev.* **1992**, *92*, 667.
(8) Lightfoot, P. D.; Cox, R. A.; Crowley, J. N.; Destriau, M.; Hayman, G. D.; Jenkin, M. E.; Moortgat, G. K.; Zabel, F. *Atmos. Environ.* **1992**, *26*, 1805.
(9) World Meteorological Organization Global Ozone Research and Monitoring Project. *Scientific Assessment of Stratospheric Ozone*; Report No. 20; 1989; Vol. 2.
(10) Wallington, T. J.; Gierczak, C. A.; Ball, J. C.; Japar, S. M. *Int. J. Chem. Kinet.* **1989**, *21*, 1077.
(11) Morgan, H. W.; Staats, P. A.; Goldstein, J. H. *J. Chem. Phys.* **1956**, *25*, 337.
(12) Wallington, T. J.; Sehested, J.; Dearth, M. A.; Hurley, M. D. *J. Photochem. Photobiol., A*, in press.
(13) Francisco, J. S.; Zhao, Y. *J. Chem. Phys.* **1990**, *93*, 276.
(14) Wallington, T. J.; Hurley, M. D. *Chem. Phys. Lett.* **1992**, *189*, 437.
(15) Wallington, T. J.; Hurley, M. D.; Shi, J.; Maricq, M. M.; Sehested, J.; Nielsen, O. J.; Ellermann, T. *Int. J. Chem. Kinet.*, submitted for publication.
(16) Klöter, G.; Seppelt, K. *J. Am. Chem. Soc.* **1979**, *101*, 347.
(17) Howard, C. J. *Abstracts of Papers*, 203rd National Meeting of the American Chemical Society, San Francisco, CA, April 1992; American Chemical Society: Washington, DC, 1992; PHYS 101.
(18) Tyndall, G. S.; Wallington, T. J.; Hurley, M. D.; Schneider, W. F. *J. Phys. Chem.*, in press.
(19) Patai, S. *The Chemistry of Functional Groups: Peroxides*; John Wiley: New York, 1983, p 496.
(20) Hirschmann, R. P.; Fox, W. B.; Anderson, L. R. *Spectrochim. Acta* **1969**, *25*, 811.
(21) Braun, W.; Herron, J. T.; Kahaner, D. K. *Int. J. Chem. Kinet.* **1988**, *20*, 51.
(22) Nielsen, O. J.; Ellermann, T.; Sehested, J.; Bartkiewicz, E.; Wallington, T. J.; Hurley, M. D. *Int. J. Chem. Kinet.* **1992**, *24*, 1009.
(23) Batt, L.; Walsh, R. *Int. J. Chem. Kinet.* **1982**, *14*, 933.
(24) Maricq, M.; Szente, J. *J. Phys. Chem.*, submitted for publication.
(25) Calvert, J. G.; Pitts, J. N., Jr. *Photochemistry*; John Wiley: New York, 1966.
(26) Erchel, E. *World Water Balance*; Elsevier: New York, 1975.

Received for review June 11, 1992. Revised manuscript received September 10, 1992. Accepted September 21, 1992.

Volume 206, number 1,2,3,4 CHEMICAL PHYSICS LETTERS 30 April 1993

Absolute rate constants for the reaction of CF_3O_2 and CF_3O radicals with NO at 295 K

Jens Sehested and Ole John Nielsen

Chemical Reactivity Section, Environmental Science and Technology Department, Riso National Laboratory, DK-4000 Roskilde, Denmark

Received 2 February 1993

Using a pulse radiolysis UV absorption technique and subsequent simulations of experimental NO_2 and FNO absorption transients, rate constants for reaction between CF_3O and CF_3O_2 radicals with NO were determined. $CF_3O_2+NO\rightarrow CF_3O+NO_2$ (3). $CF_3O+NO\rightarrow CF_2O+FNO$ (5). k_3 was derived to be $(1.68\pm0.26)\times10^{-11}$ cm^3 molecule^{-1} s^{-1}, and $k_5=(5.2\pm2.7)\times10^{-11}$ cm^3 molecule^{-1} s^{-1}. Results are discussed in the context of the atmospheric chemistry of halocarbons.

1. Introduction

Recognition of the adverse environmental effect of chlorofluorocarbons (CFC) release into the atmosphere has led to an international agreement to phase out CFCs by the end of 1995. Efforts have been made to find environmentally acceptable alternatives. Among these alternatives are hydrofluorocarbons (HFCs). Prior to large-scale industrial use the environmental impact of HFCs must be investigated. HFCs, when released to the atmosphere, will react with OH to form alkyl radicals which will, in turn, react with O_2 to form peroxy radicals [1]. In the case of CF_3H (HFC-23),

$$CF_3H+OH\rightarrow CF_3+H_2O\,, \qquad (1)$$

$$CF_3+O_2+M\rightarrow CF_3O_2+M\,. \qquad (2)$$

An important reaction of CF_3O_2 in the atmosphere is reaction with NO. The reaction of CF_3O_2 with NO is known to give predominantly, if not solely, NO_2 and CF_3O [2,3],

$$CF_3O_2+NO\rightarrow CF_3O+NO_2\,. \qquad (3)$$

The alkoxy radical CF_3O is of considerable interest because it is formed as a product from the atmospheric degradation of at least three different HFCs: CF_3H (HFC-23) [4], CF_3CF_2H (HFC-125) [5], and CF_3CFH_2 (HFC-134a) [6]. The atmospheric oxidation of other HFCs containing CF_3 groups will probably also produce CF_3O radicals.

The atmospheric fate of CF_3O radicals is uncertain [1]. It has been shown recently, that CF_3O radicals react with hydrogen-containing species [6–9] by hydrogen abstraction,

$$CF_3O+RH\rightarrow CF_3OH+R\,. \qquad (4)$$

The fate of CF_3OH in the atmosphere is either decomposition to CF_2O and HF or reaction with water droplets to HF and CO_2.

CF_3O radicals have also been shown to react fast with NO to form CF_2O and FNO [7,9,10],

$$CF_3O+NO\rightarrow CF_2O+FNO\,. \qquad (5)$$

Bevilaqua et al. [7] and Zellner et al. [9] report the rate constant k_5 to be $(2\pm1)\times10^{-11}$ and $(2.5\pm0.4)\times10^{-11}$ cm^3 molecule^{-1} s^{-1}, respectively.

The main objective of this study is to determine k_5. Since the CF_3O radical cannot be detected by UV absorption in our system, we had to derive k_5 indirectly. This is done by fitting FNO UV absorption transients using the chemical mechanism shown in table 1. The rate of formation of FNO in our kinetic system is rather insensitive to other rate constants than k_3 and k_5. We have therefore determined k_3 by simulations of NO_2 absorption transients. Values for both k_3 and k_5 are reported in this work.

Table 1
Reaction mechanism

Reaction	Rate constant (cm^3 $molecule^{-1}$ s^{-1})	Ref.
$F+CF_3H \rightarrow CF_3+HF$	1.3×10^{-13}	[4,11,12]
$F+O_2+M \rightarrow FO_2+M$	2.0×10^{-13}	[13]
$F+NO+M \rightarrow FNO+M$	6.0×10^{-12}	[14]
$CF_3+O_2+M \rightarrow CF_3O_2+M$	8.5×10^{-12}	[15]
$CF_3+NO+M \rightarrow CF_3NO+M$	1.8×10^{-11}	[16]
$CF_3+NO_2+M \rightarrow$ products	2.5×10^{-11}	[17,18]
$CF_3O_2+NO \rightarrow CF_3O+NO_2$	see text	
$CF_3O_2+NO_2 \rightarrow CF_3O_2NO_2$	8.0×10^{-12}	[3]
$CF_3O_2+CF_3O_2 \rightarrow CF_3O+CF_3O+O_2$	1.8×10^{-12}	[4,11]
$CF_3O+NO_2 \rightarrow CF_3ONO_2$	9.0×10^{-12}	[9]
$CF_3O+CF_3O_2 \rightarrow CF_3O_3CF_3$	2.5×10^{-11}	[4]
$CF_3O+CF_3O \rightarrow CF_3O_2CF_3$	2.5×10^{-11}	[4]
$CF_3O+NO \rightarrow CF_2O+FNO$	see text	

2. Experimental

The experimental technique used for this work has been described in detail previously [14,19] and will only be briefly described here.

Radicals were produced in a one liter stainless-steel reaction cell upon a 30 ns irradiation by 2 MeV electrons from a Febetron 705B field emission accelerator. The irradiation dose was varied by inserting stainless-steel attenuators between the cell and the Febetron. A chromel/alumel thermocouple measured the temperature inside the reaction cell close to the center. All experiments were performed at 295 ± 2 K.

The gas mixture was analyzed using UV–VIS light from a pulsed xenon lamp. This light beam was reflected eleven times in the gas cell by internal White-type optics giving a total optical path length of 120 cm. The analyzing light was passed into a McPherson 1 m grating monochromator operated at spectral resolution of 0.8 nm and was detected by a Hamamatsu photomultiplier coupled to a Biomation digitizer. Data handling and storage were done on a PDP11 computer.

The gas mixtures always contained SF_6 in great excess. F atoms are produced upon irradiation of SF_6 with high-energy electrons [14],

$$SF_6+2\ \text{MeV}\ e^- \rightarrow F+\text{products}. \qquad (6)$$

The yield of F atoms was determined by irradiation of gas mixtures of 5 mbar CH_4, 35 mbar O_2, and 960 mbar SF_6. CH_3O_2 radicals formed in this system were detected at 240 nm. The absorbance at 240 nm was measured as a function of the dose. The absorbance was proportional to the dose up to 53% of maximum dose. A linear regression analysis of the absorption data up to this dose gave a slope of 0.237 ± 0.010. Using the reported absorption cross section for CH_3O_2 at 240 nm, 4.42×10^{-18} cm^2 $molecule^{-1}$ [2], an initial fluorine atom concentration at full dose of $(3.23\pm0.35)\times10^{15}$ molecules cm^{-3} was found for irradiation of 1000 mbar SF_6. The reported uncertainty in the fluorine atom yield contains uncertainties in the recorded absorption at 240 nm and 10% uncertainty in $\sigma_{CH_3O_2}$. The initial F atom yield used in the simulations was calculated from the dose and the fluorine atom yield at full dose reported above.

CF_3O radicals were generated by pulse radiolysis of mixtures of $CF_3H/O_2/NO/SF_6$. The subsequent reactions are shown in table 1 and are discussed below.

Reagents and concentrations used were: SF_6, 889–894.5 mbar, supplied by Gerling and Holz at a stated purity of 99.9%; NO(>99.8%), 0.3–1.0 mbar, received from Messer Griesheim; Ultra high-purity O_2, 5–10 mbar, obtained from L'Air Liquide; CF_3H(>99.3%), 100 mbar, delivered by Fluorochem Ltd. All reagents were used as received.

3. Results

3.1. Determination of k_3 and k_5

The two rate constants k_3 and k_5 are derived from kinetic simulations of experimentally obtained absorbance transients at 400 and 310.5 nm, respectively. NO_2 transients, detected at 400 nm, were simulated by the kinetic model in table 1 to derive k_3. The uncertainty was found by varying k_3 until the simulated transients were outside the noise level on the experimental transients, see fig. 1. Some extra uncertainty has to be added, because the value of k_3 is derived from a complex kinetic model with uncertainties in the rate constants for each reaction.

Determination of k_5 is sensitive to the value used for k_3. It is important that the model is able accurately to predict the NO_2 concentration as a function of time, since the CF_3O radicals are formed simultaneously with NO_2. As seen in fig. 1 our model could reproduce the NO_2 transients very well. We simulated the FNO transients obtained at 310.5 nm by variation of k_5. An example is shown in fig. 2. Again the uncertainty was determined by the noise level, and again some extra uncertainty had to be added, because the value for k_5 is derived from a complex kinetic model with uncertainties in the rate constants for each reaction.

In the following we first discuss the parameters used in the kinetic model shown in table 1. Then we examine the origin of the absorption at 310.5 and 400 nm, and derive values for k_3 and k_5.

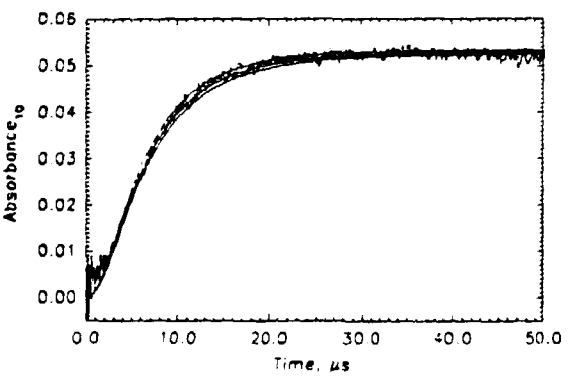

Fig. 1. Transient absorption at 400 nm following pulse radiolysis of a mixture of 100 mbar CF_3H, 10 mbar O_2, 0.5 mbar NO, and 889.5 mbar SF_6. Single pulse, full dose, no signal averaging. The three solid lines are simulations using the chemical reaction mechanism in table 1. See text.

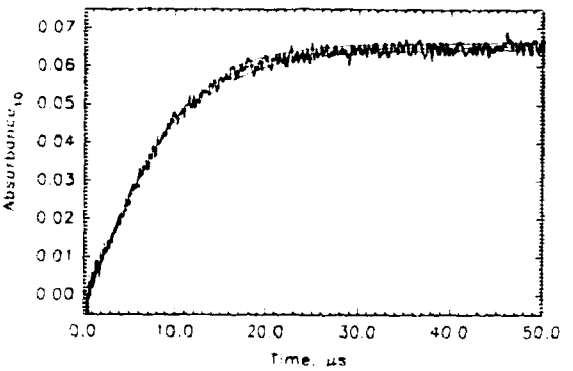

Fig. 2. Transient absorption at 310.5 nm following pulse radiolysis of a mixture of 100 mbar CF_3H, 10 mbar O_2, 0.5 mbar NO, and 889.5 mbar SF_6. Single pulse, full dose, no signal averaging. The three solid lines are simulations using the chemical reaction mechanism in table 1. See text.

3.2. Kinetic model

To derive the two rate constants k_3 and k_5 the kinetic model displayed in table 1 was used to fit the experimental data. All rate constants are taken from the literature apart from k_3 and k_5. We have assumed that the reaction between CF_3O_2 and NO gives a 100% yield of CF_3O and NO_2. Our results show that the NO_2 yield from reaction (1) is indistinguishable from full yield, which is in agreement with literature data [2,3]. In addition we have assumed that the reaction between CF_3O and NO only gives CF_2O and FNO as products and not CF_3ONO. This is consistent with our experimental results showing fast formation of FNO and the reported 100% yield of FNO and CF_2O reported by Chen et al. [10]. However, we cannot exclude a small yield (<10%) of CF_3ONO. There is also considerable controversy about the product distribution of the reaction between CF_3 and NO_2 [7,17], but since only a small amount of CF_3 radicals are removed by this reaction (<0.2%), we have chosen not to specify the products.

Generally, the rate constants and the reaction products for the most important reactions in the kinetic model in table 1 are well known. The main loss mechanisms in the model for the experimental con-

ditions used in this work are the reaction between F and O_2 (< 12%), F and NO (< 29%), and CF_3 and NO (< 14%). All three rate constants are well known and so are the products. The only potential problem is formation of FO_2, because this species could react with NO to form FNO and O_2. Therefore we varied the O_2 concentration by a factor of 2; no effect on k_3 or k_5 was observed. This indicates that FO_2 formation does not have significant influence on the formation of NO_2 and FNO in our system.

3.3. Transient absorption and absorbing species

Two species were detected in the present work: NO_2 at 400 nm and FNO at 310.5 nm. The absorption cross section used for NO_2 at 400 nm was 6.0×10^{-19} cm^2 molecule^{-1} [15]. To check that the absorption obtained at 400 nm following pulse radiolysis of $CF_3H/O_2/NO/SF_6$ mixtures was due to NO_2, an absorption transient was recorded at 450 nm ($\sigma_{450nm}(NO_2)=4.3\times10^{-19}$ cm^2 molecule^{-1} [15]). This transient was identical with the 400 nm transient within the noise level when absorptions were scaled to each other according to the ratio between the absorption cross section at the two wavelengths. To make sure that FNO did not absorb at 400 nm, a mixture of NO and SF_6 was radiolyzed. FNO is formed in this chemical system by the following reactions [20]:

$$SF_6 + 2\ \text{MeV}\ e^- \rightarrow F + \text{products}, \quad (6)$$

$$F + NO + M \rightarrow FNO + M. \quad (7)$$

The absorbance at 400 nm following pulse radiolysis of 1 mbar NO and 999 mbar SF_6 was less than 0.002 indicating that the absorbance of FNO at 400 nm is negligible.

As an additional check of the system, mixtures of SF_6, SF_6/CF_3H, $SF_6/O_2/CF_3H$, and $SF_6/CF_3H/NO$ were radiolyzed. The maximum absorbance at 400 nm was in all cases less than 0.003. Comparable checks were performed, detecting the absorbance in the 4 different chemical systems at 310.5 nm. Also at this wavelength the absorbances that could not be accounted for by initial formation of FNO were found to be negligible (< 0.002).

The absorption cross section of FNO at 310.5 nm is $(4.7\pm0.3)\times10^{-19}$ cm^2 molecule^{-1} [20]. In the $SF_6/CF_3H/NO/O_2$ system NO_2 absorbs at this wavelength. The absorption cross section is 1.87×10^{-19} cm^2 molecule^{-1} [15]. Therefore approximately 25%–30% of the absorbance at 310.5 nm is due to NO_2. To establish that the main absorption in the $SF_6/NO/CF_3H/O_2$ at 310.5 nm was indeed FNO, SF_6/NO and $SF_6/NO/CF_3H/O_2$ mixtures were radiolyzed and transients were recorded at 317 nm. The absorbance in the first system showed that the absorption cross section of FNO at 317 nm is ⅓ of that at 310.5 nm. Pulse radiolysis of 0.5 mbar NO, 10 mbar O_2, 100 mbar CF_3H and 889.5 mbar SF_6, and 52% of full dose gave a maximum absorbance of 0.035 at 310.5 nm and 0.019 at 317 nm. When absorption due to NO_2 is subtracted, absorption due to FNO is 0.025 and 0.08 at 310.5 and 317 nm, respectively. This is in excellent agreement with σ_{317nm}

Table 2
Experimental conditions and results

Dose frac. of max dose	$[CF_3H]$ mbar	$[O_2]$ mbar	[NO] mbar	$[SF_6]$ mbar	$k(CF_3O_2+NO)$ cm^3 molecule^{-1} s^{-1}	$k(CF_3O+NO)$ cm^3 molecule^{-1} s^{-1}
0.53	100	10	0.5	889.5	$(1.70\pm0.15)\times10^{-11}$	$(5.0\pm2.0)\times10^{-11}$
1.00	100	10	0.5	889.5	$(1.70\pm0.15)\times10^{-11}$	$(5.0\pm2.0)\times10^{-11}$
0.32	100	10	0.5	889.5	$(1.65\pm0.25)\times10^{-11}$	$(6.0\pm3.0)\times10^{-11}$
0.53	100	5	0.5	894.5	$(1.65\pm0.15)\times10^{-11}$	$(5.0\pm2.5)\times10^{-11}$
0.53	100	10	0.3	889.7	$(1.80\pm0.20)\times10^{-11}$	$(6.0\pm3.0)\times10^{-11}$
0.53	100	10	0.75	889.25	$(1.65\pm0.15)\times10^{-11}$	$(5.0\pm2.0)\times10^{-11}$
0.53	100	10	1.00	889.0	$(1.60\pm0.15)\times10^{-11}$	$(4.5\pm2.0)\times10^{-11}$
				ave.	$(1.68\pm0.18)\times10^{-11}$	$(5.2\pm2.4)\times10^{-11}$

$(FNO)/\sigma_{310\ nm}(FNO) = l$, indicating that FNO is indeed formed in this system.

3.4. $CF_3O_2 + NO$

To determine the rate constant for the reaction between CF_3O_2 and NO, we have performed seven different experiments in which dose, $[NO]$, and $[O_2]$ have been varied. The experimental conditions and results are shown in table 2. The results are obtained as the best fit of the simulated transient, using the chemical reaction mechanism in table 1 with k_3 set at 5.0×10^{-11} cm^3 molecule^{-1} s^{-1}, to the experimental NO_2 transients. Fig. 1 shows a measured absorption transient obtained at 400 nm following pulse radiolysis of 0.5 mbar NO, 10 mbar O_2, 100 mbar CF_3H, and 889.5 mbar SF_6. Fig. 1 also contains three simulations of the absorption transient using the chemical mechanism in table 1, with $k_3 = 1.6$, 1.7, and 1.85×10^{-11} cm^3 molecules^{-1} s^{-1}, respectively. As shown in the figure both the simulated transients using $k_3 = 1.6\times10^{-11}$ cm^3 molecules^{-1} s^{-1} and $k_3 = 1.85\times10^{-11}$ cm^3 molecules^{-1} s^{-1} fall outside the noise level in the data. In this way we have obtained an uncertainty in k_3; we choose to report $k_3 = (1.70\pm0.15)\times10^{-11}$ cm^3 molecule^{-1} s^{-1}. The other values obtained for k_3 shown in table 2 were obtained in a similar way. Using the average of the k_3 values in table 2 and conventional propagation of error we obtain $k_3 = (1.68\pm0.18)\times10^{-11}$ cm^3 molecule^{-1} s^{-1}. We choose to add an extra 5% uncertainty because the result is derived from a complex kinetic mechanism. The reported value is therefore $k_3 = (1.68\pm0.26)\times10^{-11}$ cm^3 molecule^{-1} s^{-1}. This value is in excellent agreement with the values from two previous investigations, $(1.78\pm0.36)\times10^{-11}$ [21] and $(1.45\pm0.2)\times10^{-11}$ cm^3 molecule^{-1} s^{-1} [22].

3.5. $CF_3O + NO$

The rate constant for the reaction of CF_3O with NO was derived by simulation of experimental absorption transients, in this case FNO transients recorded at 310.5 nm. Seven experimental transients were fitted using the chemical reaction mechanism in table 1. An example of an absorption transient is shown in fig. 2. The transient displayed in fig. 2 is recorded at the same conditions as the transient in fig. 1: $[SF_6] = 889.5$ mbar, $[NO] = 0.5$ mbar, $[O_2] = 10$ mbar, $[CF_3H] = 100$ mbar and full dose. Included in fig. 2 are three simulations using $k_5 = 3$, 5, and 7×10^{-11} cm^3 molecule^{-1} s^{-1}. In all three simulations $k_3 = 1.7\times10^{-11}$ cm^3 molecule^{-1} s^{-1} was used. It is seen from fig. 2 that the simulated transient is not consistent with the experimentally obtained transient for $k_5 = 3\times10^{-11}$ or 7×10^{-11} cm^3 molecule^{-1} s^{-1}. Therefore we choose to report $k_5 = (5\pm2)\times10^{-11}$ cm^3 molecule^{-1} s^{-1}. k_5 values are determined from the six other FNO transients in a similar way. The results are given in table 2. Using the average and conventional propagation of error calculations we get $(5.2\pm2.4)\times10^{-11}$ cm^3 molecule^{-1} s^{-1}. By adding an extra 5% uncertainty because the result is derived from a complex mechanism we arrive at $(5.2\pm2.7)\times10^{-11}$ cm^3 molecule^{-1} s^{-1}.

The absorbance transient in fig. 2 was also simulated using $k_3 = 1.6$ and 1.85×10^{-11} cm^3 molecule^{-1} s^{-1}. When $k_3 = 1.6\times10^{-11}$ cm^3 molecule^{-1} s^{-1} was used a k_5 of $(5\text{–}7)\times10^{-11}$ cm^3 molecule^{-1} s^{-1} fitted the absorbance transient in fig. 2 well. However, an important difference from using $k_3 = 1.7\times10^{-11}$ cm^3 molecule^{-1} s^{-1} was that the model became insensitive to increase in k_5. When $k_3 = 1.85\times10^{-11}$ cm^3 molecule^{-1} s^{-1} was used, $k_5 = (4\pm1)\times10^{-11}$ cm^3 molecule^{-1} s^{-1} gave the optimal fit of the model calculated transient to the experimental transient. It is important to note that using $k_5 = 3\times10^{-11}$ cm^3 molecule^{-1} s^{-1} gave too slow formation of FNO.

4. Discussion

Two potential complications may interfere with the measurements above: (1) CF_3H might be radiolyzed directly, possibly producing CF_2H radicals. (2) The small amount of NO_2 formed before radiolysis by addition of O_2 to NO might interfere with the measurements:

$$2NO + O_2 + M \rightarrow 2NO_2 + M . \quad (8)$$

The first complication might introduce up to 10% change in the radical distribution. Because of the low concentration ratio between CF_3H and SF_6 and the fact that SF_6 is an efficient electron scavenger, we

estimate this contribution to be less than 5%.

The NO_2 formed by reaction (8) prior to radiolysis, could be estimated by the change in the baseline of the detection before and after the mixture was introduced into the reaction cell. The NO_2 concentration was estimated to be a few percent of the NO concentration. Using an initial NO_2 concentration of a few percent in a simulation of a NO_2 and a FNO transient did not alter the absorption transient significantly. It is therefore likely that the initial NO_2 concentration is insignificant.

The rate constant obtained for reaction between CF_3O and NO, $k_5 = (5.2 \pm 2.7) \times 10^{-11}$ cm^3 molecule^{-1} s^{-1}, is 2–3 times larger than the values reported by Bevilaqua et al. [7], $k_5 = (2 \pm 1) \times 10^{-11}$ cm^3 molecule^{-1} s^{-1} and by Zellner [9] $k_5 = (2.5 \pm 0.4) \times 10^{-11}$ cm^3 molecule^{-1} s^{-1}. Even though one of the previously reported values for k_5 is within our reported error limits and the uncertainty of the other value overlaps our uncertainty it should be noted that none of our experimental transients could be fitted with $k_5 = 3 \times 10^{-11}$ cm^3 molecule^{-1} s^{-1}. The reason for this discrepancy is unknown. We recommend further investigations of the reaction between CF_3O and NO.

Atmospheric implications. CF_3H (HFC-23), CF_3CF_2H (HFC-125), CF_3CFH_2 (HFC-134a) and probably also other HFCs containing CF_3 groups will, upon release to the atmosphere, produce CF_3O radicals [4–6]. This radical will either react with NO to produce FNO and CF_2O or abstract hydrogen from hydrogen-containing species [6]. The importance of CF_3O radicals reaction with NO in the atmosphere can be estimated using the background concentration of NO, ≈ 10 pptv [1], and hydrocarbons, $[C_2H_6] = 1.3$–4.5 ppbv and $[C_3H_8] = 1.1$–2.0 ppbv [23,24], together with the relative rates between the reactions of CF_3O with NO, C_2H_6, C_3H_8, as done by Chen et al. [8]. From this data it seems reasonable to assume that reaction between CF_3O and NO is less important than CF_3O hydrogen abstraction reaction on a global scale. However, the reaction between CF_3O and NO might be more important than the CF_3O reaction with hydrocarbons in areas with high NO concentrations.

Acknowledgement

Thanks are due to Dr. Thomas Bevilaqua and Professor Carlton Howard (NOAA) for providing their data prior to publication, and to Dr. Knud Sehested (Risø) and Dr. Timothy J. Wallington (Ford Motor Co.) for helpful discussions. JS would like to thank the Danish Research Academy for a research scholarship, and OJN would like to thank the Commission of the European Communities for financial support.

References

[1] Alternative Fluorocarbon Environmental Acceptability Study, W.M.O. Global Ozone Research and Monitoring Project, Report No. 20: Scientific assessment of stratospheric ozone, Vol. 2 (1989).
[2] T.J. Wallington, P. Dagaut and M.J. Kurylo, Chem. Rev. 92 (1992) 667.
[3] P.D. Lightfoot, R.A. Cox, J.N. Crowly, M. Destriau, G.D. Hayman, M.E. Jenkin, G.K. Moortgat and F. Zabel, Atmos. Environ. 26A (1992) 1805.
[4] O.J. Nielsen, T. Ellerman, J. Sehested, E. Bartkiewicz, T.J. Wallington and M.D. Hurley, Intern. J. Chem. Kinetics 24 (1992) 1009.
[5] J. Sehested, T. Ellerman, O.J. Nielsen, T.J. Wallington and M.D. Hurley, to be published.
[6] J. Sehested and T.J. Wallington, Environ. Sci. Technol. 27 (1993) 146.
[7] T.J. Bevilaqua, D.R. Hanson and C.J. Howard, J. Phys. Chem., in press.
[8] J. Chen, T. Zhu, H. Niki and G.J. Mains, Geophys. Res. Letters 19 (1992) 2215.
[9] R. Zellner (1993), private communication.
[10] J. Chen, T. Zhu and H. Niki, J. Phys. Chem. 96 (1992) 6115.
[11] M.M. Mariq and J.J. Szente, J. Phys. Chem. 96 (1992) 4925.
[12] T.J. Wallington, M.D. Hurley, J. Shi, M.M. Maricq, J. Sehested, O.J. Nielsen and T. Ellermann, to be published.
[13] T. Ellermann, J. Sehested, O.J. Nielsen, T.J. Wallington and P. Pagsberg, to be published.
[14] T. Ellermann, Risø National Laboratory Report Risø-M-2932 (1991).
[15] W.B. DeMore, S.P. Sander, D.M. Golden, M.J. Molina, R.F. Hampson, M.J. Kurylo, C.J. Howard and A.R. Ravishankara, JPL Publication 90-1 (1990).
[16] A.B. Vatkin and A.K. Petrov, Spectrochim. Acta 46 (1990) 603.
[17] J. Francisco and Z. Li, Chem. Phys. Letters 168 (1989) 528.
[18] K. Sugawara, T. Nakanaga, H. Takeo and C. Matsumura, J. Phys. Chem. 93 (1989) 1894.

[19] O.J. Nielsen, Risø National Laboratory Report Risø-R-480 (1984).
[20] T. Ellermann, unpublished results.
[21] I.C. Ryan and K.R. Ryan, Chem. Phys. Letters 92 (1982) 236.
[22] A.M. Dognon, F. Caralp and R. Lesclaux, J. Chim. Phys. 82 (1985) 349.
[23] H.B. Singh and P.B. Maker, Gaseous pollutants: characterization and cycling, ed. J.O. Nriagu (Wiley, New York, 1992).
[24] T. Jobson, H. Wu, H. Niki and L.A. Barrie, J. Geophys. Res., submitted for publication.

Volume 213, number 5,6 CHEMICAL PHYSICS LETTERS 15 October 1993

Upper limits for the rate constants of the reactions of CF_3O_2 and CF_3O radicals with ozone at 295 K

Ole John Nielsen and Jens Sehested

Chemical Reactivity Section, Environmental Science and Technology Department, Riso National Laboratory, DK-4000 Roskilde, Denmark

Received 8 August 1993; in final form 17 August 1993

Using the pulse radiolysis UV absorption technique and subsequent simulations of experimental absorption transients at 254 and 276 nm, upper limits of the rate constants for the reactions of CF_3O_2 and CF_3O radicals with ozone were determined at 295 K, $CF_3O_2+O_3\rightarrow CF_3O+2O_2$ (4), $CF_3O+O_3\rightarrow CF_3O_2+O_2$ (5). The upper limits were derived as $k_4<0.5\times10^{-14}$ cm^3 molecule^{-1} s^{-1}, and $k_5<1\times10^{-13}$ cm^3 molecule^{-1} s^{-1}. Results are discussed in the context of the atmospheric chemistry and ozone depletion by hydrofluorocarbons.

1. Introduction

Recognition of the adverse environmental effect of release into the atmosphere of chlorofluorocarbons (CFC) has led to an international agreement to stop the production of CFCs by the end of 1995. Efforts have been made to find acceptable environmental alternatives. Among these alternatives are hydrofluorocarbons (HFCs). Prior to large scale industrial use, the environmental impact of HFCs must be investigated. HFCs, when released into the atmosphere, will react with OH to form alkyl radicals which in turn will react with O_2 to form peroxy radicals [1]. In the case of CF_3H (HFC-23) [2],

$$CF_3H+OH\rightarrow CF_3+H_2O, \quad (1)$$

$$CF_3+O_2+M\rightarrow CF_3O_2+M. \quad (2)$$

CF_3O radicals can then be formed in the atmosphere from CF_3O_2 radicals by reaction with NO,

$$CF_3O_2+NO\rightarrow CF_3O+NO_2. \quad (3)$$

The atmospheric oxidation of other HFCs, like HFC-134a (CF_3CFH_2) and HFC-125 (CF_3CF_2H) containing a CF_3 group, is also known to produce CF_3O_2 radicals [3,4]. Because HFC-134a is a potential substitute for CFCs in cooling systems, substantial production of this compound is likely to occur before the year 2000. Consequently, investigation of the fate of HFC-134a, CF_3O_2 and CF_3O in the atmosphere has been the subject of a substantial international research effort.

Recently, attention has been drawn to the behavior of CF_3O_2 and CF_3O in the stratosphere [5]. It is well known that 5%–10% of the HFC-134a released into the atmosphere will react with OH in the stratosphere [5], and initiate a series of reactions leading to CF_3O_2 and CF_3O.

In the stratosphere, CF_3O_2 and CF_3O may be involved in a catalytic destruction of ozone as is the case for Cl, Br, OH, etc.,

$$CF_3O_2+O_3\rightarrow CF_3O+2O_2, \quad (4)$$

$$CF_3O+O_3\rightarrow CF_3O_2+O_2. \quad (5)$$

A value for the rate constant for reaction (5), $k_5=1\times10^{-12}$ cm^3 molecule^{-1} s^{-1} has been reported recently by Biggs et al. [6]. In their study, k_5 was determined in an indirect way and further investigations of these reactions are needed.

The main objective of this work was to determine k_4 and k_5. This is done by measuring ozone concentration in a stainless steel cell as a function of time by UV absorption spectroscopy in the presence of CF_3O_2 and CF_3O radicals. The observed absorption transients at 254 and 276 nm could be fitted by a

chemical model, which did not include reactions (4) and (5). By including these reactions and varying their rate constants, upper limits for k_4 and k_5 could be established. The implications for the atmospheric chemistry of HFCs containing CF_3 groups are discussed.

2. Experimental

The experimental technique applied in this work has been described in detail elsewhere [7,8] and will only be briefly described here.

Radicals were produced in a one liter stainless steel reaction cell upon a 30 ns irradiation by 2 MeV electrons from a Febetron 705B field emission accelerator. A chromel/alumel thermocouple measured the temperature inside the reaction cell close to the center. All experiments were performed at 295 ± 2 K.

The produced radicals were monitored using UV light from a pulsed xenon lamp. A 4 ms light pulse had stable intensity to less than 0.001 in absorbance units. The light beam from the xenon lamp was reflected 3 times in the gas cell by internal White-type optics giving a total optical path length of 40 cm. The analyzing light was passed into a McPherson 1 m grating monochromator operated at spectral resolution of 0.8 nm and was detected by a Hamamatsu photomultiplier coupled to a Biomation digitizer. Data handling and storage were done using a PDP11 computer.

The gas mixtures always contained SF_6 in great excess. F atoms are produced upon irradiation of SF_6 with high-energy electrons [8],

$$SF_6 + 2\ \text{MeV}\ e^- \rightarrow F + \text{products}. \quad (6)$$

The yield of F atoms was determined by irradiation of gas mixtures of 1 mbar CH_4 and 1000 mbar SF_6. CH_3 radicals formed in this system were detected at 216.4 nm. The absorbance at 216.4 nm was measured as a function of the dose. The absorbance was measured up to 32% of the maximum dose and was found to be proportional to the dose. A linear regression analysis of the absorption data gave a slope of 2.15 ± 0.16. Using the reported absorption cross section for CH_3 at 216.4 nm, 4.12×10^{-17} cm^2 molecule^{-1} [9], an initial fluorine atom concentration of $(3.0 \pm 0.4) \times 10^{15}$ molecule cm^{-3} was found for irradiation of 1000 mbar SF_6 at full dose. The reported uncertainty in the fluorine atom yield includes uncertainties in the recorded absorption and 10% uncertainty in σ_{CH_3}.

CF_3O_2 radicals were generated by pulse radiolysis of $CF_3H/O_2/O_3/SF_6$ mixtures. The subsequent reactions determining the fate of CF_3O_2 and CF_3O radicals are shown in table 1 and are discussed below.

Table 1
Reaction mechanism

Number	Reaction	Rate constant (cm^3 molecule^{-1} s^{-1})	Ref.
(7)	$F + CF_3H \rightarrow CF_3 + HF$	1.3×10^{-13}	[2,10]
(8)	$F + O_2 + M \rightarrow FO_2 + M$	2.0×10^{-13}	[11]
(9)	$F + O_3 \rightarrow FO + O_2$	1.0×10^{-11}	this work
(10)	$F + CF_3 + M \rightarrow CF_4 + M$	1.4×10^{-11}	[12]
(2)	$CF_3 + O_2 + M \rightarrow CF_3O_2 + M$	8.5×10^{-12}	[13]
(11)	$CF_3 + O_3 \rightarrow CF_3O + O_2$	9.3×10^{-12}	[14]
(12)	$CF_3 + CF_3O_2 \rightarrow CF_3O + CF_3O$	1.3×10^{-11}	[12]
(13)	$CF_3 + CF_3 + M \rightarrow C_2F_6 + M$	2.5×10^{-11}	[15]
(14)	$FO + FO \rightarrow 2F + O_2$	1.5×10^{-11}	[13]
(15)	$FO_2 + FO_2 \rightarrow$ products	1.7×10^{-17}	[16]
(16)	$FO_2 + M \rightarrow F + O_2 + M$	810 s^{-1}	[16]
(17)	$CF_3O_2 + CF_3O_2 \rightarrow CF_3O + CF_3O + O_2$	1.8×10^{-12}	[2,12]
(18)	$CF_3O_2 + CF_3O \rightarrow CF_3OOOCF_3$	1.0×10^{-10}	see text
(19)	$CF_3O + CF_3O \rightarrow CF_3OOCF_3$	2.1×10^{-11}	[17]
(4)	$CF_3O_2 + O_3 \rightarrow CF_3O_2 + 2O_2$	varied	this work
(5)	$CF_3O + O_3 \rightarrow CF_3O_2 + O_2$	varied	this work

Reagents and concentrations used were: SF_6, 780–890 mbar, supplied by Gerling and Holz at a stated purity of 99.9%; ultra-high-purity O_2, 10–20 mbar, obtained from L'Air Liquide; CF_3H (>99.3%), 100–200 mbar, delivered by Fluorochem Ltd. Ozone was produced by flowing O_2 through a conventional discharge ozonizer. The O_2 was purified before entering the ozonizer by flowing through silicagel and the ozone/oxygen mixture was purified for trace amounts of NO, NO_2, N_2O_5, and HNO_3 by flowing it through silicagel cooled to -80°C and used directly without further purification. Up to 1.6% ozone in oxygen could be produced in this way.

Ozone concentrations were determined by measurements of the absorption at 254 or 276 nm in the irradiation cell before and after filling with other gasses. No change in the absorption could be detected when the cell was filled with any other gas than ozone. The ozone absorption cross sections used for quantifying ozone were 1.15×10^{-17} cm^2 at 254 nm and 5.42×10^{-18} cm^2 at 276 nm [13]. Ozone concentrations used were in the range $(0.7–7.7)\times10^{15}$ molecule cm^{-3}.

3. Results

Ozone kinetics were monitored at 254 or 276 nm in the presence of CF_3O_2 and CF_3O radicals and the observed absorption transients were compared to model calculations. Three examples of experimental and modelled transients with increasing initial ozone concentration are shown in fig. 1. As seen from fig. 1, transients obtained in this work could be fitted quite nicely with the chemical mechanism displayed in table 1 without including reactions (4) and (5). Consequently, only upper limits for k_4 and k_5 could be determined. k_4 or k_5 were varied until the simulated transients differed from the experimental transients by approximately the experimental noise level. This is illustrated in fig. 2.

In the following we first discuss the kinetic model. Then we derive $k_9(F+O_3)$ from the behavior of the transients in the time range 0–10 μs, and show that FO_2 formed in our system does not react with ozone on the experimental time scales used in this work. Finally we derive upper limits for k_4 and k_5.

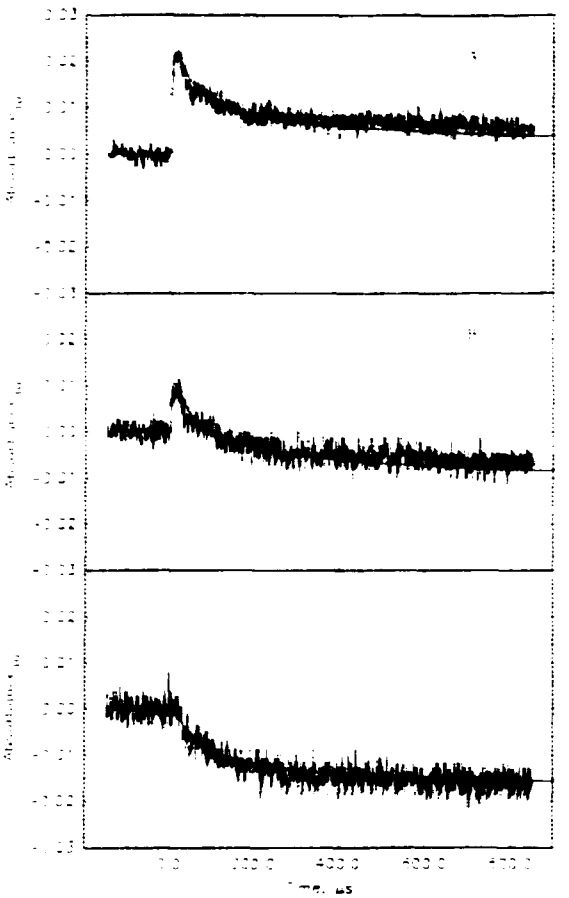

Fig. 1. Three transient absorptions at 254 nm following pulse radiolysis of a mixture of mixtures of 100 mbar CF_3H, 10 mbar O_2, 890 mbar SF_6 and 0, 0.74, 1.35×10^{15} cm^{-3} O_3, respectively. Single pulse, full dose, no signal averaging, and path length equal to 40 cm. The solid lines are simulations using the chemical reaction mechanism in table 1 with k_4 and k_5 equal to zero.

3.1. The kinetic model

To derive upper limits for the two rate constants k_4 and k_5, the reactions displayed in table 1 were used in the kinetic model to fit the experimental data. All rate constants are taken from the literature apart from k_4, k_5, k_9, and k_{18}. $k_9(F+O_3)$ is determined in this work, $k_9=1.0\times10^{-11}$ cm^3 molecule^{-1} s^{-1}. This is in agreement with the literature value of 1.3×10^{-11} cm^3 molecule^{-1} s^{-1} [13] and a new determination by Maricq and Szente [18] of 1.0×10^{-11} cm^3 molecule^{-1} s^{-1}. k_{18} is an important rate constant in the

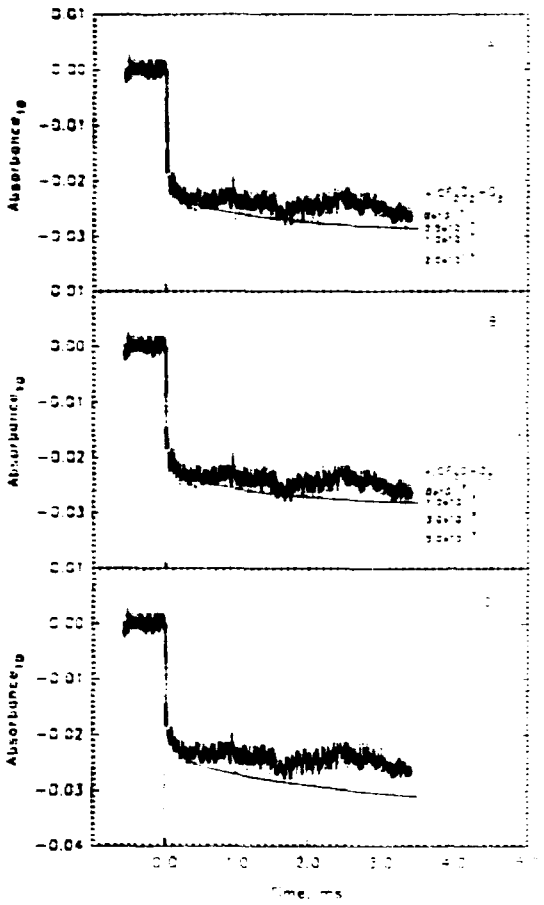

Fig. 2. Transient absorptions at 276 nm following pulse radiolysis of 200 mbar CF_3H, 20 mbar O_2, 7.6×10^{15} cm^{-3} O_3, and 780 mbar SF_6. Single pulse, full dose, no signal averaging. The four solid lines in (A) are simulations using k_4 equal to 0, 0.5, 1, and 2×10^{-14} cm^3 molecule^{-1} s^{-1}. In the four simulations in fig. (B) k_5 was equal to 0, 1, 3, and 5×10^{-13} cm^3 molecule^{-1} s^{-1}.

reaction system because the upper limits derived for k_4 and k_5 depend strongly on this value. Unfortunately, only a lower limit for $k(CF_3O_2+CF_3O)$ is reported in the literature [2]. Therefore we choose a high rate for this reaction in order to avoid underestimating the upper limits for k_4 and k_5. Some uncertainty exists concerning the product distribution of reaction (11). Biggs et al. [6] report CF_3O and O_2 while Howard and co-workers [19] observe the formation of CF_2O following reaction (11). Both studies were carried out at 1–2 Torr total pressure. In the following we show that the reaction of CF_3 with O_3 is only a minor fate of the CF_3 radicals under our experimental conditions. Therefore we do not need to be concerned about the product distribution of this reaction. k_{16} had to be calculated from the work of Pagsberg et al. [16]. They report the equilibrium constant $K_{eq}=k_8/k_{16}$ for the equilibrium between F atoms, O_2 and FO_2 to be 2.38×10^{-16} cm^3 molecule^{-1} at 293 K. Using $k_8=2.0\times10^{-13}$ cm^3 molecule^{-1} s^{-1} we derive $k_{16}=810$ s^{-1} at 1000 mbar total pressure of SF_6.

Generally, the rate constants and the reaction products for the most important reactions in the kinetic model in table 1 are well known. The main loss mechanisms for F and CF_3 in our system are

$$F+O_2+M\rightarrow FO_2+M, \quad (8)$$

$$F+O_3\rightarrow FO+O_2, \quad (9)$$

$$F+CF_3+M\rightarrow CF_4+M, \quad (10)$$

$$CF_3+O_2+M\rightarrow CF_3O_2+M, \quad (2)$$

$$CF_3+O_3\rightarrow CF_3O+O_2, \quad (11)$$

$$CF_3+CF_3O_2\rightarrow CF_3O+CF_3O, \quad (12)$$

$$CF_3+CF_3+M\rightarrow C_2F_6+M, \quad (13)$$

giving rise to the following losses of F and CF_3: <13% for reaction (8), <8.5% for reaction (9), <0.6% for reaction (10), <1.2% for reaction (11), <0.4% for reaction (12) and <0.2% for reaction (13).

Potential problems from products of these reactions include FO_2 from reaction (8) and FO from reaction (9). FO is formed in up to 8.5% yield under our experimental conditions. It could react with O_3 as suggested by Starrico and Schumacher [20] and Wagner and Zetzsch [21]. This would result in degradation of ozone in our reaction cell, leading to higher upper limits of k_4 and k_5. As the experimental transients are fitted well without including a reaction between FO and ozone, we did not include this reaction in our chemical mechanism.

The up to 13% yield of FO_2 could complicate the system, by reaction with ozone and other radical species. We show that the reaction between FO_2 and ozone is not significant on the time scale of these experiments. FO_2 radicals could also react with other radical species in the reaction mixture even though FO_2 radicals are fairly unreactive towards other species. One reaction which might take place could be the reaction between CF_3O and FO_2, with the prod-

ucts being either CF_3OF and O_2 or CF_3OOOF. Since neither CF_3OF nor CF_3OOOF are observed in the product study of the self-reaction of CF_3O_2 radicals [2], it is unlikely that this reaction is significant in this investigation.

The other reactions listed above ((10)–(13)) only consume small fractions of the initial F atoms, so we consider their reaction products to be of only minor importance in this work.

Before the kinetic model could be used to simulate the experimentally obtained absorption transients, absorption cross sections for O_3, CF_3O_2 and FO_2 at 254 and 276 nm have to be established from the literature. The following cross sections are used: at 254 nm: $\sigma(O_3)=1.15\times10^{-17}$ cm^2 [13], $\sigma(CF_3O_2)=5.3\times10^{-19}$ cm^2 and $\sigma(FO_2)=6.3\times10^{-19}$ cm^2; at 276 nm: $\sigma(O_3)=5.42\times10^{-17}$ cm^2 [13], $\sigma(CF_3O_2)=8\times10^{-20}$ cm^2 and $\sigma(FO_2)=1.8\times10^{-19}$ cm^2 [12]. $\sigma(FO_2)$ at 254 nm is the average of the absorption cross sections reported by Maricq and Szente [12] and Ellermann et al. [11]. $\sigma(CF_3O_2)$ is the average of the values reported by Maricq and Szente [12] and Nielsen et al. [2].

3.2. Determination of $k(F+O_3)$ and discussion of the importance of $k(FO_2+O_3)$

The absorption predicted by the kinetic model at short time scales (first 10 μs) was sensitive to the rate constant of reaction (9) below,

$$F+O_3\rightarrow FO+O_2\,. \qquad (9)$$

This is because ozone has very strong absorptions at 254 and 276 nm. Consequently, small amounts of ozone removed by reaction (9) can be observed as a significant drop in the absorption at short time scale. The value of k_9 reported in the literature is 1.3×10^{-11} cm^3 molecule^{-1} s^{-1} [13]. This rate constant overpredicts the initial ozone loss, thus a small correction must be made. When $k_9=1.0\times10^{-11}$ cm^3 molecule^{-1} s^{-1} was used the initial absorption of all experimental transients could be fitted well. Consequently, this number was used throughout the present study. Our value is well within the uncertainty of the previously reported value. The authors of one of the accompanying papers [18] were only able to fit their data using a value of k_9 identical to the one determined in this work.

As an additional check on this result and to address whether FO_2 could react with ozone, mixtures of 50 mbar O_2, $(0.71–1.54)\times10^{15}$ cm^{-3} O_3, and 950 mbar SF_6 were radiolysed. The transient absorption was measured at 254 nm. The major fate of F atoms in this system was the reaction with O_2 to form FO_2, but a small fraction of the F atoms also reacted with O_3. The ozone loss predicted by the kinetic model did not fit the transients at short time scales (10 μs), as the ozone loss predicted by the model was too high using $k_9=1.3\times10^{-11}$ cm^3 molecule^{-1} s^{-1}. However, using $k_9=1.0\times10^{-11}$ cm^3 molecule^{-1} s^{-1}, model calculations fit the experimental transients well at short time scales. Since this value agrees with the determination of k_9 above it gives us confidence in this rate constant. At longer time scales, 1 ms, the absorbance was stable, indicating that FO_2 does not react with ozone on this time scale. It should be noted that if FO_2 reacted with O_3 the result would be an increase in the upper limit for k_4 and k_5.

3.3. Determination of upper limits of k_4 and k_5

In order to determine upper limits of k_4 and k_5 simulations of experimental transients were used. k_4 or k_5 were varied until the simulated transients differed from the experimental transients by approximately the experimental noise level. An example of this approach is seen in fig. 2A, where the chemical model in table 1 with $k_4=0$, 0.5, 1, 2×10^{-14} cm^3 molecule^{-1} s^{-1} and $k_5=0$ was used. The simulations show that when using $k_4=0.5\times10^{-14}$ cm^3 molecule^{-1} s^{-1} we are well outside the noise level of the experimental transients. We therefore chose to report the upper limit for k_4 determined from this experiment to be $k_4<0.5\times10^{-14}$ cm^3 molecule^{-1} s^{-1}.

The upper limit for k_5 was determined in a similar way. In fig. 2B a simulation of the experimental transient absorption using the chemical mechanism in table 1 is shown, $k_4=0$ and $k_5=0$, 1, 3, 5×10^{-13} cm^3 molecule^{-1} s^{-1}. In fig. 2B it is seen that the simulation using $k_5=1\times10^{-13}$ cm^3 molecule^{-1} s^{-1} is well outside the noise level of the transient and we therefore chose to report this value as the upper limit of k_5 determined by this experiment.

In fig. 2C the effect of setting both $k_4\neq0$ and $k_5\neq0$ has been shown. The simulation using $k_4=0.5\times10^{-14}$ cm^3 molecule^{-1} s^{-1} and $k_5=1\times10^{-13}$

Table 2
Experimental conditions and results

Experiment No.	t [a] (ms)	$[CF_3H]$ (mbar)	$[O_2]$ (mbar)	$[O_3]$ (10^{15} cm^{-3})	$[SF_6]$ (mbar)	$k(CF_3O_2+O_3)$ (cm^3 molecule^{-1} s^{-1})	$k(CF_3O+O_3)$ (cm^3 molecule^{-1} s^{-1})
1 [b]	1	100	10	2.55	890	$<0.9\times10^{-14}$	$<2\times10^{-13}$
2 [b]	1	100	10	1.35	890	$<2\times10^{-14}$	$<3\times10^{-13}$
3 [b]	1	100	10	2.12	890	$<1\times10^{-14}$	$<3\times10^{-13}$
4 [b]	1	200	20	5.17	780	$<1\times10^{-14}$	$<2\times10^{-13}$
5 [b]	1	100	10	0.74	890	$<2\times10^{-14}$	$<6\times10^{-13}$
6 [c]	1	200	20	4.99	780	$<0.9\times10^{-14}$	$<2\times10^{-13}$
7 [c]	4	100	10	3.50	890	$<0.6\times10^{-14}$	$<1.5\times10^{-13}$
8 [c]	4	200	20	7.70	780	$<0.5\times10^{-14}$	$<1\times10^{-13}$

[a] Measurement time.
[b] Transient recorded at 254 nm.
[c] Transient recorded at 276 nm.

cm^3 molecule^{-1} s^{-1} gives an additive ozone destroying effect as compared to keeping either k_4 or k_5 different from zero.

Eight determinations of k_4 and k_5 are listed in table 2. O_2 and CF_3H concentrations have been varied by a factor of two, ozone by a factor of ten, time scale by a factor of four and two different wavelengths were used for the determination of the upper limits of k_4 and k_5. As seen from table 2, experiments with high ozone concentration and long time scale were most sensitive to k_4 and k_5 and the lowest upper limits were derived at these experiments. The best fit of the experimental transient is obtained for $k_4=k_5=0$ suggesting that the upper limits could very well be even lower.

4. Discussion

The magnitude of the upper limits for k_4 and k_5 agrees with other measured rate constants of reactions of ozone with different oxy and peroxy radicals. The rate constants for the reactions of HO_2, OH, CH_3O, and CH_3O_2 with ozone are all low: 2×10^{-15} cm^3 molecule^{-1} s^{-1} [13], 6.8×10^{-14} cm^3 molecule^{-1} s^{-1} [13], $<2\times10^{-15}$ cm^3 molecule^{-1} s^{-1} [22], and $<3\times10^{-17}$ cm^3 molecule^{-1} s^{-1} [13].

Our upper limit for k_5 reported here is in disagreement with the value reported by Biggs et al. [6] of $k_5=1\times10^{-12}$ cm^3 molecule^{-1} s^{-1}. Their value was derived from a complicated chemical system involving the reaction of CF_3 radicals with O_3 as the source of CF_3O, see eq. (11).

Howard and co-workers [19] have investigated this reaction using a flow tube coupled to a mass spectrometer allowing them to monitor the products of the reaction. They recognize one of the products of reaction (11) to be CF_2O. Both the experiments by Biggs et al. [6] and the experiments by Howard et al. [19] were carried out at 1–2 Torr total pressure. Since F atoms are known to react fast with ozone (reaction (9)) the determined rate constant for the reaction of CF_3O with ozone might be influenced by F atoms formed by reaction of CF_3 radicals with ozone. This may explain why the value of k_5 reported by Biggs et al. [6] is higher than our upper limit for k_5.

However, our upper limit for k_5 is in good agreement with the upper limits $k(CF_3O+O_3)<3\times10^{-14}$ cm^3 molecule^{-1} s^{-1} [23] and $k(CF_3O+O_3)<5\times10^{-14}$ cm^3 molecule^{-1} s^{-1} [18] reported in two other Letters following this Letter.

4.1. Atmospheric implications

CF_3H (HFC-23), CF_3CF_2H (HFC-125), CF_3CFH_2 (HFC-134a) and probably also other HFCs containing CF_3 groups will, upon release to the atmosphere, form CF_3O_x radicals [2–4], which will also be present in the stratosphere. Recently it has been suggested that CF_3O_x radicals destroy ozone in a catalytic cycle, involving reactions (4) and (5). Upper limits for k_4 and k_5 are essential for model

calculations of the ozone depletion efficiency of CF_3O_x radicals in the stratosphere. Model calculation is beyond the scope of this work, but in the following an overview of the involved reactions will be given.

The rate constants known for CF_3O_x reactions of stratospheric interest are listed in table 3. Most of the rate constants have been determined at room temperature only. Changing the temperature from 295 to 220 K will slow down the bimolecular reactions listed in table 3. However, for an order-of-magnitude calculation the room temperature rate constants will be sufficient. The key reactions in the possible cyclic stratospheric ozone destruction can be divided into three groups: the chain initiating step, formation of CF_3O_x from HFCs containing CF_3 groups; the chain propagating steps, CF_3O_x reactions with ozone; and the terminating steps, CF_3O reaction with NO and CH_4. In addition holding processes and "zero" ozone destruction cycles are also important. An example of a holding process is the reaction of CF_3O_2 with NO_2 producing a reservoir species, $CF_3O_2NO_2$. This reaction decreases the amount of CF_3O_x radicals available for ozone destruction. A prominent "zero" ozone destruction cycle consists of the reaction of CF_3O with ozone followed by reaction of CF_3O_2 with NO and NO_2 photolysis. The O atoms from the NO_2 photolysis react with O_2 to give ozone. Hence, no net ozone destruction results from this cycle.

The products of reaction of CF_3O_x with ozone are not known, but the reaction could produce the species shown in table 3. The product distribution of the reaction of CF_3O radicals with NO is very important since it is one of the main chain termination reactions known at the moment. The products of the reaction of CF_3O with NO have been determined at room temperature. At stratospheric temperatures the product could be CF_3ONO. This species could photolyze to reform CF_3O_x radicals and thereby not terminate the chain process. The products of this reaction at low temperatures should be one of the major targets for future investigations.

Other potential loss processes for CF_3O_x in the stratosphere include the reaction of CF_3O with NO_2 and hydrocarbons. The products of the NO_2 reaction have not been determined, and one reaction channel could give FNO_2 and CF_2O by analogy to the NO reaction. However, the most likely reaction product is CF_3ONO_2. The reaction of CF_3O radicals with hydrocarbons is also important in the stratosphere. This reaction is known to produce CF_3OH and alkyl radicals. CF_3OH will presumably be stable in the stratosphere, since a lower limit of 5 h lifetime has been observed at room temperature [3]. By analogy with CH_3OH, it is unlikely that CF_3OH will photolyze.

Table 3
Summary of CF_3O_x reactions

Reaction	Rate constant (295 K) (cm^3 $molecule^{-1}$ s^{-1})	
$CF_3O_2+O_3 \rightarrow CF_3O+2O_2$	$<0.5\times10^{-14}$	this work
$CF_3O_2+NO_2+M \rightarrow CF_3O_2NO_2+M$	3.8×10^{-12} [a,b]	[24]
$CF_3O_2NO_2+M \rightarrow CF_3O_2+NO_2+M$	1.5×10^{-10} [a,c]	[24]
$CF_3O_2+NO \rightarrow CF_3O+NO_2$	2.3×10^{-11} [a]	[24]
$CF_3O+O_3 \rightarrow CF_3O_2+O_2$	$<1\times10^{-13}$	this work
$CF_3O+O_3 \rightarrow CF_3O_2+O_2$	1×10^{-12}	[6]
$CF_3O+O_3 \rightarrow CF_3O_2+O_2$	$<6\times10^{-14}$	[23]
$CF_3O+O_3 \rightarrow CF_3O_2+O_2$	$<5\times10^{-14}$	[18]
$CF_3O+NO \rightarrow CF_2O+FNO$	2.5×10^{-11}	[25-27]
$CF_3O+NO_2+M \rightarrow CF_3ONO_2+M$	9×10^{-12}	[26]
$CF_3O+CO \rightarrow$ products	4.4×10^{-14}	[25]
$CF_3O+CH_4 \rightarrow CF_3OH+CH_3$	2.2×10^{-14}	[28]

[a] $T=220$ K.
[b] $P=10$ mbar.
[c] Unit: s^{-1}.

and attack by OH will be insignificant due to the strong O–H bond in CF_3OH [29]. Deposition of CF_3OH on particles in the stratosphere will presumably give CF_2O and HF as products.

In fig. 3 the estimated lifetimes of CF_3O_x with respect to the trace species in the stratosphere are displayed as a function of altitude. The trace gas concentrations are noon values taken from Brasseur and Solomon [30]. For the reactions of CF_3O_x with ozone, upper limits of $k_4 < 0.5\times10^{-14}$ cm^3 molecule^{-1} s^{-1} and k_5 from the following Letters [18,23], $k_5 < 5\times10^{-14}$ cm^3 molecule^{-1} s^{-1}, have been used in the calculations. It can be seen from fig. 3 that the reaction of CF_3O_x radicals with ozone is still the main reaction channel for these radicals in the stratosphere.

It is interesting to consider the model work by Ko and Sze [31] in the light of the upper limits of k_4 and k_5. By model calculations and using $k_4 = 3\times10^{-15}$ cm^3 molecule^{-1} s^{-1}, $k_5 = 2\times10^{-11}$ cm^3 molecule^{-1} s^{-1}, and assuming the rate constant and the products of the reaction of CF_3O and NO at 298 K to be valid at 220 K, Ko and Sze [31] estimate an ODP for HFC-134a of the order of 10^{-2}. It seems reasonable to assume that the ODP of HFC-134a is approximately proportional to k_5, since chain length of the ozone depleting cycle is approximately proportional to k_5. Then, by comparing the upper limit for k_5 determined in this work with the model work of Ko and Sze [31], we arrive at an ODP for HFC-134a which is around two orders of magnitude less, which is 3–4 orders of magnitude less than the ODPs of CFCs and two orders of magnitude less than ODPs of hydrochlorofluorocarbons (HCFCs).

It should be emphasized that the calculation above is very approximate and that several assumptions had to be made e.g., using room temperature rate constants, and assuming reaction products between reaction of CF_3O radicals and NO at stratospheric temperatures. However, this work together with the two papers following immediately after this one suggest that the ODP of HFCs due to a CF_3O_x cycle is negligible.

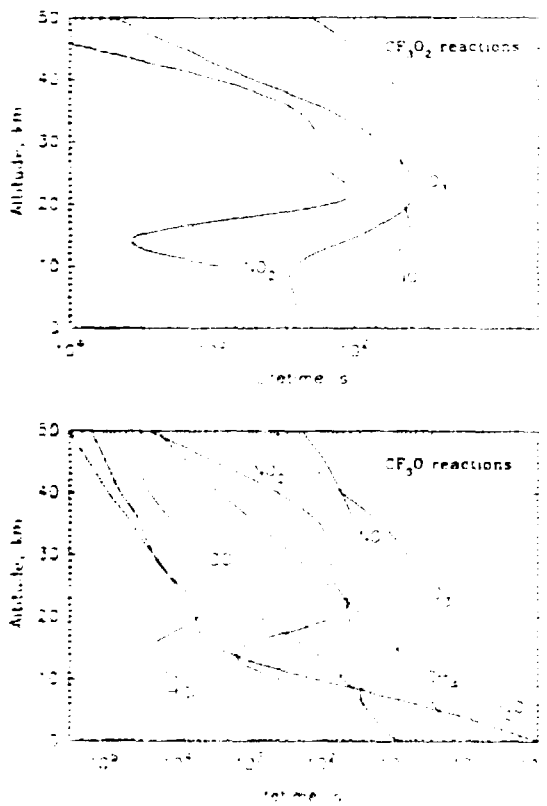

Fig. 3. Lifetimes of CF_3O_2 (A) and CF_3O (B) with respect to reactions with trace species in the stratosphere. Noon concentrations are taken from Brasseur and Solomon [30]. For k_4 and k_5, 0.5×10^{-14} cm^3 molecule^{-1} s^{-1} and 5×10^{-14} cm^3 molecule^{-1} s^{-1} were used.

Acknowledgement

JS would like to thank the Danish Research Academy for a research scholarship, and we thank AFEAS for financial support. The authors also wish to thank Dr. Knud Sehested (Risø), Dr. Malcolm Ko and Dr. Dak Sze (AER Inc.); and Dr. Timothy J. Wallington and Dr. Matti M. Maricq (Ford Motor Company) for valuable discussions during the work and for making their results available to us prior to publication. Finally we would like to thank AFEAS for financial support under contract CTR 93-45/P93-120.

References

[1] Alternative Fluorocarbon Environmental Acceptability Study, World Meteorological Organisation Global Ozone Research and Monitoring Project, Report No. 20, Scientific assessment of stratospheric ozone, Vol. 2 (1989).

[2] O.J. Nielsen, T. Ellermann, J. Sehested, E. Bartkiewicz, T.J. Wallington and M.D. Hurley, Intern. J. Chem. Kinetics 24 (1992) 1009.
[3] J. Sehested and T.J. Wallington, Environ. Sci. Technol. 27 (1993) 146.
[4] J. Sehested, T. Ellermann, O.J. Nielsen, T.J. Wallington and M.D. Hurley, Intern. J. Chem. Kinetics, 25(1993) 701.
[5] Presentations and discussions at the STEP-HALOCSIDE/Alternative Fluorocarbon Environmental Acceptability Study Workshop in Dublin, March 23–25 (1993).
[6] P. Biggs, C.E. Canosa-Mas, D.E. Shallcross, R.P. Wayne, C. Kelly and H.W. Sidebottom, Proceedings of the STEP-HALOCSIDE/Alternative Fluorocarbon Environmental Acceptability Study Workshop, March 23–25 (1993) Dublin.
[7] O.J. Nielsen, Risø National Laboratory Report Risø-R-480 (1984).
[8] T. Ellermann, Risø National Laboratory Report Risø-M-2932 (1991).
[9] T. Macpherson, M.J. Pilling and M.J.C. Smith, J. Chem. Phys. 89 (1985) 2268.
[10] T.J. Wallington, M.D. Hurley, J. Shi, M.M. Maricq, J. Sehested, O.J. Nielsen and T. Ellermann, Intern. J. Chem. Kinetics, 25 (1993) 651.
[11] T. Ellermann, J. Sehested, O.J. Nielsen, T.J. Wallington and P. Pagsberg, Chem. Phys. Letters, submitted for publication.
[12] M.M. Maricq and J.J. Szente, J. Phys. Chem. 96 (1992) 4925.
[13] W.B. DeMore, S.P. Sander, D.M. Golden, M.J. Molina, R.F. Hampson, M.J. Kurylo, C.J. Howard and A.R. Ravishankara, JPL Publication 90-1 (1990).
[14] M.J. Rossi, J.R. Barker and D.M. Golden, J. Chem. Phys. 71 (1979) 3722.
[15] G.A. Skorobogatov, O.N. Slesar and N.D. Torbin, J. Chimya 4 (1988) 30.
[16] P. Pagsberg, E. Ratajcak, A. Sillesen and J. Jodkowski, Chem. Phys. Letters 141 (1987) 88.
[17] L. Batt and J.J. Walsh, Intern. J. Chem. Kinetics 14 (1982) 933.
[18] M.M. Maricq and J.J. Szente, Chem. Phys. Letters 213 (1993) 449.
[19] T.J. Bevilacqua, D.R. Hanson, N.R. Jensen and C.J. Howard, STEP-HALOCSIDE/Alternative Fluorocarbon Environmental Acceptability Study Workshop in Dublin, March 23–25 (1993).
[20] E.H. Starrico and H.J. Schumacher, Z. Physik. Chem. 31(1962) 385.
[21] H.G. Wagner and C. Zetzsch, Ber. Bunsenges. Phys. Chem. 76 (1972) 526.
[22] R. Simonaitis and J. Heicklen, J. Phys. Chem. 79 (1975) 298.
[23] T.J. Wallington, M.D. Hurley and W.F. Schneider, Chem. Phys. Letters 213 (1993) 442.
[24] P.D. Lightfoot, R.A. Cox, J.N. Crowley, M. Destriau, G. Hayman, M.E. Jenkin, G.K. Moortgat and F. Zabel, Atmos. Environ. 26 (1992) 1805.
[25] R. Zellner, private communication.
[26] J. Sehested and O.J. Nielsen, Chem. Phys. Letters 206 (1993) 369.
[27] T.J. Bevilacqua, D.R. Hanson and C.J. Howard, J. Phys. Chem. 97 (1993) 3750.
[28] H. Saathoff and R. Zellner, Chem. Phys. Letters 206 (1993) 349.
[29] T.J. Wallington, M.D. Hurley, W.F. Schneider, J. Sehested and O.J. Nielsen, J. Phys. Chem. 97 (1993) 7606.
[30] G. Brasseur and S. Solomon, in: Aeronomy of the middle atmosphere (Reidel, Dordrecht, 1986).
[31] M. Ko and D. Sze, private communication (1993).

Spectrokinetic Study of SF_5 and SF_5O_2 Radicals and the Reaction of SF_5O_2 with NO

JENS SEHESTED, THOMAS ELLERMANN,* and OLE JOHN NIELSEN†
Chemical Reactivity Section, Environmental Science and Technology Department, Risø National Laboratory, DK-4000 Roskilde, Denmark

TIMOTHY J. WALLINGTON†
Ford Research Laboratory, SRL-3083, Ford Motor Company, Dearborn, P.O. Box 2053, Michigan 48121-2053

Abstract

UV spectra of SF_5 and SF_5O_2 radicals in the gas phase at 295 K have been quantified using a pulse radiolysis UV absorption technique. The absorption spectrum of SF_5 was quantified from 220 to 240 nm. The absorption cross section at 220 nm was $(5.5 \pm 1.7) \times 10^{-19}$ cm^2. When SF_5 was produced in the presence of O_2 an equilibrium between SF_5, O_2, and SF_5O_2 was established. The rate constant for the reaction of SF_5 radicals with O_2 was $(8 \pm 2) \times 10^{-13}$ cm^3 molecule^{-1} s^{-1}. The decomposition rate constant for SF_5O_2 was $(1.0 \pm 0.5) \times 10^5$ s^{-1}, giving an equilibrium constant of $K_{eq} = [SF_5O_2]/[SF_5][O_2] = (8.0 \pm 4.5) \times 10^{-18}$ cm^3 molecule^{-1}. The SF_5-O_2 bond strength is (13.7 ± 2.0) kcal mol^{-1}. The SF_5O_2 spectrum was broad with no fine structure and similar to the UV spectra of alkyl peroxy radicals. The absorption cross section at 230 nm was found to $(3.7 \pm 0.9) \times 10^{-18}$ cm^2. The rate constant of the reaction of SF_5O_2 with NO was measured to $(1.1 \pm 0.3) \times 10^{-11}$ cm^3 molecule^{-1} s^{-1} by monitoring the kinetics of NO_2 formation at 400 nm. The rate constant for the reaction of F atoms with SF_4 was measured by two relative methods to be $(1.3 \pm 0.3) \times 10^{-11}$ cm^3 molecule^{-1} s^{-1}. © 1994 John Wiley & Sons, Inc.

Introduction

Alkyl peroxy radicals play a central role as reaction intermediates in the atmospheric oxidation of all volatile organic compounds. Recognition of the importance of peroxy radicals has led to the development of a substantial spectroscopic and kinetic data base for alkyl-, haloalkyl-, acyl-, oxygen substituted-, and unsaturated peroxy radicals [1,2]. In contrast there is relatively little available information concerning noncarbon centered peroxy radicals.

Recently, Turnipseed et al. [3] have presented evidence for an equilibrium between CH_3S, O_2, and CH_3SO_2, with an equilibrium constant of approximately 7×10^{-20} cm^3 molecule^{-1} s^{-1} at room temperature. We report here a study of the equilibrium between SF_5, O_2, and SF_5O_2. Pulse radiolysis with time resolved UV absorption spectroscopy was employed to determine the UV absorption spectrum of the SF_5O_2 radical, the equilibrium constant between SF_5, O_2, and SF_5O_2, and the rate constant for the reaction of SF_5O_2 with NO to form NO_2 and SF_5O. The results are discussed

* Present address: National Environmental Research Institute, Department of Emission and Air Pollution, Frederiksborgvej 399, DK-4000 Roskilde, Denmark.
† To whom correspondence should be addressed.

International Journal of Chemical Kinetics, Vol. 26, 615–629 (1994)

CCC 0538-8066/94/060615-15

in the context of the literature data of sulfur fluoride radicals and the atmospheric chemistry of SF_6 and sulfur radicals.

Experimental

Pulse radiolysis was used to initiate reactions while transient UV absorption was employed to study the UV absorption spectra and the kinetics of SF_5 and SF_5O_2 radicals. The experimental setup has been described in detail elsewhere [4,5,6] and will only be briefly discussed here.

The analyzing light, provided by a pulsed 150 W Xenon lamp, was reflected in the reaction cell three to eleven times by internal White type optics to give total optical path-lengths of 40, 80, and 120 cm. The light beam was detected by a 1 m McPherson grating monochromator operated at a spectral resolution of 0.8 nm, linked to a Hamamatsu R928 photomultiplier and a Biomation 8100 transient digitizer. A PDP11 computer controlled the data handling and storage of the data. All transients used in this work are single pulse transients, no signal averaging was used.

Reagents used were: SF_6, 880–1000 mbar, delivered by Gerling and Holz (>99.97%); Ultra high purity O_2, 0–80 mbar, supplied by L'Air Liquide; CH_4, 10 mbar, received from Gerling and Holz (>99%); SF_4, 0.25–40 mbar, obtained from Fluorochem (>99%); NO, 0.3–5 mbar, delivered by Messer Griesheim (>99.8%).

The reactions were initiated by radiolysis of chemical mixtures in a 1 liter stainless steel cell containing gas mixtures with SF_6 in great excess. A 30 ns pulse of 2 MeV electrons from a 705B Febetron accelerator was used to produce F atoms:

(1) $$SF_6 + 2\ \text{MeV}\ e^- \longrightarrow F + \text{products}$$

The irradiation dose, given relative to full dose herein, was varied by inserting stainless steel attenuators into the electron beam.

The fluorine atom yield, required for quantification of UV absorption spectra, was established by converting F atoms into CH_3O_2 radicals via the following reactions:

(2) $$F + CH_4 \longrightarrow CH_3 + HF$$

(3) $$CH_3 + O_2 + M \longrightarrow CH_3O_2 + M$$

The CH_3O_2 yield was determined by measurements of the maximum absorption at 260 nm using 80 cm path length following radiolysis of mixtures of 10 mbar CH_4, 40 mbar O_2, and 950 mbar SF_6 at various doses. The maximum absorption at 260 nm was proportional to the dose up to a dose of 0.219 times that of full dose. At higher doses, the observed maximum absorption fell below a linear extrapolation of the low dose absorptions. This is due to radical-radical reactions, which become significant at high doses. Linear least squares analysis of a plot of the maximum transient absorption versus fraction of the maximum dose for the low dose data gave a slope of 0.307 ± 0.016. Before the yield of F atoms could be calculated, a small correction for the formation of FO_2 radicals was made:

(4) $$F + O_2 + M \longrightarrow FO_2 + M$$

Using $k_4 = 1.9 \times 10^{-13}$ cm^3 molecule^{-1} s^{-1} [7], $k_3 = 6.8 \times 10^{-11}$ cm^3 molecule^{-1} s^{-1} [8] and the initial concentrations of CH_4 and O_2. Yields of FO_2 and CH_3O_2 relative to the initial F atom concentration were determined to be 1.1% and 98.9%, respectively. Combining this with the absorption cross sections $\sigma_{260\,nm}$ (CH_3O_2) = 3.18×10^{-18} cm^2 [1] and $\sigma_{260\,nm}$ (FO_2) = 3.2×10^{-19} cm^2 [9], and the absorption measured at

260 nm we obtain a fluorine atom yield of $(2.95 \pm 0.33) \times 10^{15}$ molecules cm^{-3} at full dose. The uncertainty in the fluorine atom yield was calculated by normal error propagation of a 10% uncertainty in $\sigma(CH_3O_2)$ and the uncertainty in the maximum absorption.

The uncertainties reported in this article are 2 standard deviations unless otherwise stated. Normal statistical error propagation is used to calculate combined uncertainties.

Results

Radiolysis of gas mixtures of 5 mbar of SF_4 and 1000 mbar SF_6 leads to production of SF_5 radicals by the following reactions [10,11]:

(1) $$SF_6 + 2MeV\ e^- \longrightarrow F + products$$

(5) $$F + SF_4 + M \longrightarrow SF_5 + M$$

When mixtures of 40 mbar O_2, 20 mbar SF_4 and 940 mbar SF_6 were radiolyzed a transient absorption was observed between 215 nm and 270 nm. The experimental transient observed at 230 nm is shown in Figure 1(D). This absorption was assigned to the peroxy radical SF_5O_2.

(6a,-6a) $$SF_5 + O_2 + M \rightleftharpoons SF_5O_2 + M$$

In the following we will first determine k_5 by two independent relative methods. Second, the UV spectrum of the SF_5 radical and an upper limit of the self reaction rate constant of the SF_5 radical will be determined. Third, $\sigma(SF_5O_2)$, k_{6a}, and k_{-6a} will be determined from simulations of experimental transients. Finally, the rate constant for the reaction of SF_5O_2 with NO will be derived.

F + SF_4

A relative approach was used to measure the reactivity of F atoms towards SF_4. In this method a reference compound whose reactivity towards F atoms is known was added to the reaction mixture to compete with SF_4 for the available F atoms. In the present study NO and O_2 were employed as reference compounds. By measuring the fraction of F atoms which react with SF_4 as a function of the concentration ratio [SF_4]/[reference] the rate constant ratio $k(F + SF_4)/k(F + reference)$ can be deduced.

Radiolysis of mixtures of NO and SF_6 generates FNO by the following two reactions [12]:

(1) $$SF_6 + 2\ MeV\ e^- \longrightarrow F + Products$$

(7) $$F + NO + M \longrightarrow FNO + M$$

FNO radicals absorb at 310.5 nm [13]. Mixtures of 970–995 mbar SF_6, 5 mbar NO, and 0–25 mbar SF_4 were radiolyzed using a 0.527 dose and a 120 cm optical path length, and the absorbance at 310.5 nm was measured. This absorbance is plotted as a function of [SF_4]/[NO] in Figure 2. For low [SF_4]/[NO] the absorbance approaches that of FNO in the pure SF_6/NO system where all F atoms are scavenged by NO. For high [SF_4]/[NO] the absorbance approaches an absorbance of 0.01. In this case most of the F atoms react with SF_4 to give SF_5 by reaction (5). SF_5 radicals do not absorb at 310.5 nm. The absorbance at high [SF_4]/[NO] ratios must therefore be due

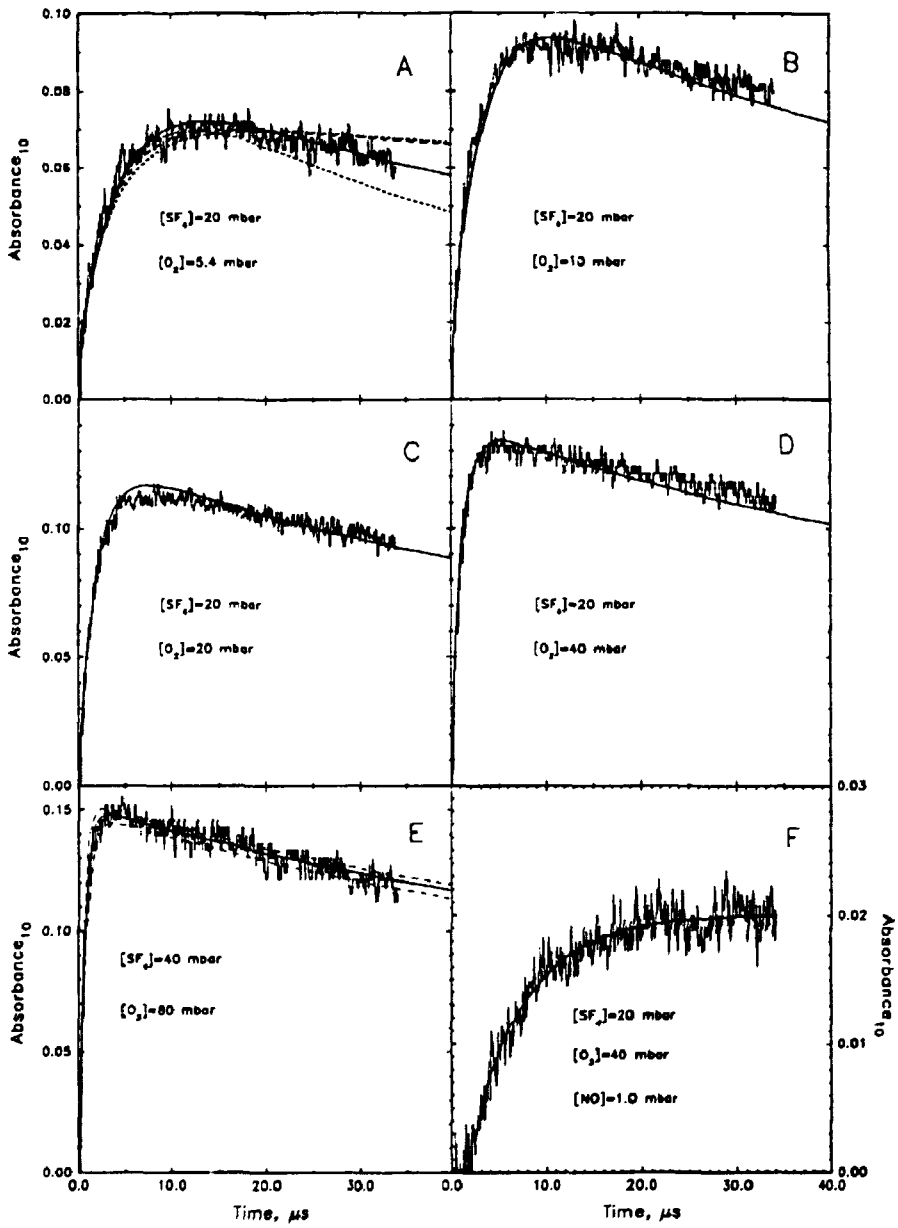

Figure 1. UV absorption transients at 230 and 400 nm following pulse radiolysis of mixtures of 20 mbar SF_6: (A) 5.4; (B) 10; (C) 20; (D) 40; and (E) 80, mbar O_2; and SF_6 up to 1000 mbar with dose 0.416 and pathlength 80 cm. Solid lines are simulations using the model in Table I. The dashed lines are simulations using other kinetic parameters. See text. (F) NO_2 formation measured at 400 nm. The solid line is a first-order fit to the experimental data.

to something else. Since NO is known to react rapidly with most radicals we suggest a reaction between SF_5 and NO which may proceed through two channels:

(8a) $$SF_5 + NO + M \longrightarrow SF_5NO + M$$

(8b) $$SF_5 + NO \longrightarrow SF_4 + FNO$$

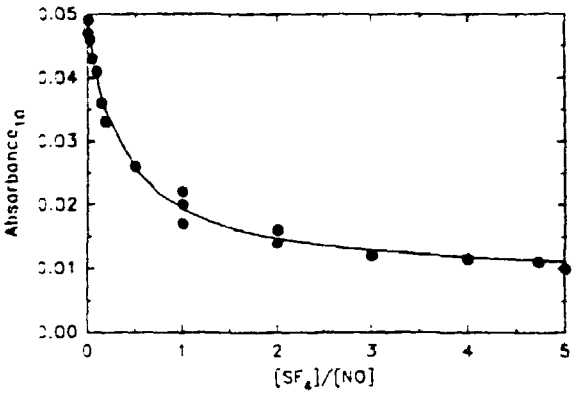

Figure 2. Maximum transient absorptions at 310.5 nm following pulse radiolysis of 5 mbar NO, 0–25 mbar SF_4, and 970–995 mbar SF_6. Dose 0.527 and path-length 120 cm were employed. The solid line is a fit to the data. See text.

Since the absorbance at high $[SF_4]/[NO]$ ratios is approximately 20% of the absorbance in the pure SF_6/NO system we can put an upper limit on channel (8b) of 20%. However, the importance of this reaction channel may be lower, since SF_5NO may absorb at 310.5 nm.

It seems reasonable to assume that under our experimental conditions all SF_5 radicals are scavenged by NO in reaction (8). With this assumption the data in Figure 2 can be fitted using the expression:

$$\text{(I)} \qquad A_{max} = (A_{FNO} + A_{SF5NO}\{k_5[SF_4]/k_7[NO]\})/\{1 + k_5[SF_4]/k_7[NO]\}$$

where A_{max} is the observed maximum transient absorption, A_{FNO} is the maximum transient absorption of FNO if all F atoms are converted into this species, and A_{SF5NO} is the absorption if all F atoms are converted into SF_5NO. As mentioned earlier A_{SF5NO} in eq. (I) might be due to absorption from FNO if reaction (8) gives 20% FNO and SF_5NO does not absorb at this wavelength. However, the validity of the fit is independent of the origin of the absorption at high $[SF_4]/[NO]$ ratios. The parameters A_{FNO}, A_{SF5NO}, and k_5/k_7 were fitted simultaneously and gave a best fit for $A_{FNO} = 0.0488 \pm 0.0014$, $A_{SF5NO} = 0.0083 \pm 0.0021$, and $k_5/k_7 = 2.68 \pm 0.66$. The fit is shown in Figure 2 as a solid line.

To obtain an absolute value of k_5, k_7 has to be determined. k_7 may be calculated by fitting the rise of FNO absorption at 310.5 nm following radiolysis of SF_6/NO to a first-order expression. The first-order rate constants obtained are plotted as a function of [NO] in Figure 3. From the slope we calculate a rate constant of $k_7 = (4.8 \pm 0.2) \times 10^{-12}$ cm^3 molecule^{-1} s^{-1} in agreement with a previous determination of $(5.5 \pm 0.7) \times 10^{-12}$ cm^3 molecule^{-1} s^{-1} [13]. With $k_7 = (4.8 \pm 0.2) \times 10^{-12}$ cm^3 molecule^{-1} s^{-1} and $k_5/k_7 = 2.68 \pm 0.66$ we arrive at a value for the rate constant for the reaction of F atoms with SF_4 of $(1.3 \pm 0.3) \times 10^{-11}$ cm^3 molecule^{-1} s^{-1}.

k_5 was also determined relative to k_4. The experimental conditions were: $[SF_6]$ = 937–950 mbar, $[O_2]$ = 50 mbar, $[SF_4]$ = 0–13 mbar, dose = 0.416, and pathlength = 80 cm. Maximum transient absorption data at 230 nm are plotted in Figure 4. With no SF_4 in the reaction mixture all F atoms are converted into FO_2 radicals. When $[SF_4]$ is increased the maximum transient absorbance drops until it reaches a level of approximately 0.105. This absorbance is due to SF_5O_2. Further increase of $[SF_4]$

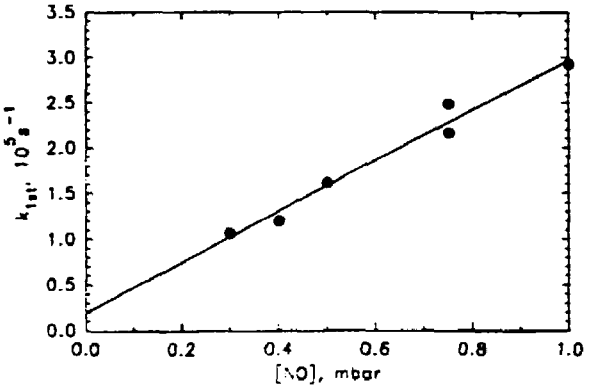

Figure 3. FNO formation rates plotted as a function of [NO].

had no discernible effect on the maximum absorbance. By analogy with the data in Figure 2 the data in Figure 4 can be fitted using the following expression:

$$\text{(II)} \qquad A_{max} = (A_{FO2} + A_{SF5O2}\{k_5[SF_4]/k_4[O_2]\})/\{1 + k_5[SF_4]/k_4[O_2]\}$$

Three parameters were varied in the fit: A_{FO2}, A_{SF5O2}, and k_5/k_4. The best fit was obtained for the parameters $A_{FO2} = 0.180 \pm 0.003$, $A_{SF5O2} = 0.102 \pm 0.003$, and $k_5/k_4 = 61.5 \pm 11.4$. See Figure 4. From $k_4 = (1.9 \pm 0.3) \times 10^{-13}$ cm^3 molecule^{-1} s^{-1} [7] we obtain $k_5 = (1.3 \pm 0.3) \times 10^{-11}$ cm^3 molecule^{-1} s^{-1}, which is identical to the value found above.

UV Spectrum of SF_5

To map out the SF_5 spectrum experiments were performed to measure the maximum absorption between 220 nm and 310 nm following the pulsed irradiation of 5 mbar SF_4 and 995 mbar SF_6. The absorbance was small. Only for wavelengths shorter than or equal to 240 nm were the absorbencies greater than 0.02 (full dose

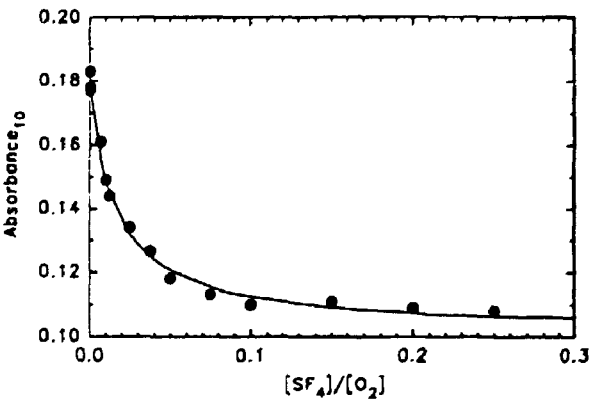

Figure 4. Maximum transient absorptions at 230 nm following pulse radiolysis of mixtures of 50 mbar O_2, 0–13 mbar SF_4, and 937–950 mbar SF_6. Dose 0.416 and pathlength 80 cm were employed. The solid line is a fit to the data. See text.

was used). The absorbencies at 240 nm, 230 nm, and 220 nm were 0.022, 0.033, and 0.056, respectively. Fitting the rise of the absorption transients recorded at 240, 230 and 220 nm gave rate constants of $(0.55 - 2.0) \times 10^{-11}$ cm^3 molecule^{-1} s^{-1} for the reaction of F atoms with SF_4; consistent with $k_5 = 1.3 \times 10^{-11}$ cm^3 molecule^{-1} s^{-1} derived above.

Before absorption cross sections could be calculated from the recorded absorbencies, potential complications had to be evaluated. Two possible complications which might interfere with the measurements are; (i) the reaction of F atoms with SF_5 radicals and (ii) the self reaction of SF_5 radicals.

(9) $$F + SF_5 + M \longrightarrow SF_6 + M$$

(10) $$SF_5 + SF_5 + M \longrightarrow S_2F_{10} + M$$

Ryan and Plumb [10] estimate k_9 to be close to 9×10^{-12} cm^3 molecule^{-1} s^{-1}, and Tsang and Herron [14] find $k_9 = 1 \times 10^{-11}$ cm^3 molecule^{-1} s^{-1}, which both represent high pressure limits. These values are close to that of the reaction between F atoms and SF_4. Therefore SF_5 and SF_4 will compete for the F atoms. However, the initial F atom concentration and hence the maximum possible SF_5 concentration is about 50 times less than $[SF_4]_0$. Reaction (9) will therefore consume less than 2% of the F atoms in our system. This is negligible compared with the experimental uncertainty.

The self reaction of SF_5 radicals is very slow. The observed half life of the SF_5 radicals in our system is > 1 ms when $[SF_5] = 3 \times 10^{15}$ molecules cm^{-3}. This implies that $k_{10} < 2.3 \times 10^{-13}$ cm^3 molecule^{-1} s^{-1}, which makes reaction (10) negligible as a complication in measuring the maximum absorbance of the SF_5 radical in the system. The upper limit for k_{10} determined above is a factor of 5 less than the high pressure limit for reaction (10) of 9×10^{-13} cm^3 molecule^{-1} s^{-1} reported by Herron [15]. The reason for this discrepancy is unclear. However, it should be noted that the literature value was derived from pyrolysis experiments and a complicated kinetic mechanism.

From the absorbances of the SF_5 radical, 0.056 at 220 nm, 0.033 at 230 nm and 0.022 at 240 nm and the F atom yield at full dose, $(2.95 \pm 0.033) \times 10^{15}$ molecules cm^{-3}, we calculate $\sigma(SF_5) = 55$, 32, and 21×10^{-20} cm^2 at 220, 230, and 240 nm, respectively. We estimate the uncertainty of these absorption cross sections to be less than 30%.

$$SF_5 + O_2 \rightleftharpoons SF_5O_2$$

When mixtures of SF_6, SF_4, and O_2 were radiolyzed the maximum transient absorption between 215 and 270 nm was substantially greater than that observed in the absence of O_2. Examples of transient absorptions can be seen in Figure 1. The maximum transient absorption increased as increasing amounts of oxygen were added to the reaction mixture. Figure 5 displays the transient absorbance as a function of initial oxygen concentration using a dose of 0.416. The absorbencies in the figure are corrected for FO_2 formed directly from reaction of F atoms with O_2, using the rate constant for the reaction of F atoms with O_2, 1.9×10^{-13} cm^3 molecule^{-1} s^{-1} [7], and an absorption cross section of FO_2 at 230 nm of 5.08×10^{-18} cm^2 [7]. Corrections were less than 6.4%.

Two reactions may explain the increased absorbance when O_2 is present.

(6a) $$SF_5 + O_2 + M \longrightarrow SF_5O_2 + M$$

(6b) $$SF_5 + O_2 \longrightarrow SF_4 + FO_2$$

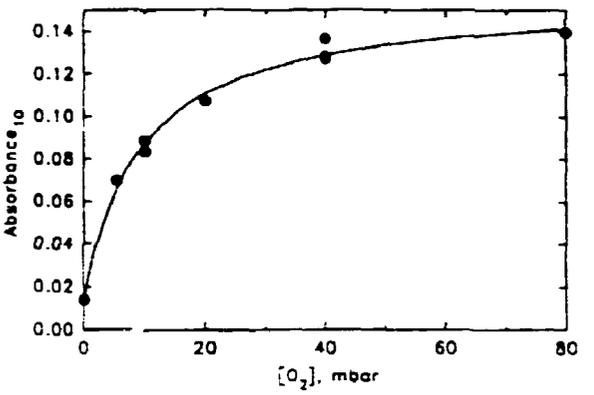

Figure 5. Maximum transient absorptions at 230 nm following pulse radiolysis of a mixture of 0.0–80 mbar O_2, 20–40 mbar SF_4, and 880–975 mbar SF_6. Dose 0.416 and pathlength 80 cm were employed. The solid line is a fit to the data. See text.

Czarnowski and Schumacher [16] have studied the products resulting from the thermal decomposition of $SF_5O_3SF_5$ with and without the addition of up to 450 mbar O_2. Using IR spectroscopy the only sulfur containing products detected were SF_5OSF_5 and $SF_5O_2SF_5$. No SF_4 was observed. Under the experimental conditions employed by Czarnowski and Schumacher there was a substantial concentration of SF_5 radicals. The absence of any SF_4 product shows that reaction (6b) proceeds slowly, if at all, at ambient temperature. This conclusion is in agreement with three pieces of experimental evidence from the present work: First, the observed decay of the transient absorption is much too fast to be ascribed to FO_2. Second, the observed UV spectrum of the unknown species is distinct from that of FO_2. Third, we will show later that the unknown species reacts with NO to form NO_2. The reaction of FO_2 radicals with NO to give NO_2 is endothermic by 6.3 kcal mol^{-1} [17]. It therefore seems reasonable to conclude that SF_5O_2 is formed by the reaction of SF_5 and O_2 and that SF_5O_2 radicals are responsible for the UV absorption seen in Figure (1(A)–1(E)).

From Figure 5 it is evident that the maximum absorbance increases with increasing $[O_2]$. This behavior can be due to unwanted secondary radical-radical reactions and/or an equilibrium between SF_5, O_2 and SF_5O_2:

(6a,-6a) $$SF_5 + O_2 + M \rightleftharpoons SF_5O_2 + M$$

To establish whether secondary chemistry can explain the drop in absorbance at lower O_2 concentrations we need to carefully evaluate possible secondary radical-radical reactions. Such reactions potentially include:

(9) $$F + SF_5 + M \longrightarrow SF_6 + M$$

(10) $$SF_5 + SF_5 + M \longrightarrow S_2F_{10} + M$$

(11) $$F + SF_5O_2 \longrightarrow \text{products}$$

(12) $$SF_5 + SF_5O_2 + M \longrightarrow SF_5O_2SF_5 + M$$

(13) $$SF_5O_2 + SF_5O_2 \longrightarrow \text{products}$$

Reactions (9) and (10) have been discussed previously and rate constant values of 1×10^{-11} cm^3 $molecule^{-1}$ s^{-1} and 2.3×10^{-13} cm^3 $molecule^{-1}$ s^{-1} will be used in the modelling. With the SF_4 pressures used in this work, reaction (11) is negligible

because F atoms are removed rapidly by reaction with SF_4. Reaction (12) is of importance in the system, especially at low $[O_2]$. Czarnowski and Schumacher [22] identified the product, $SF_5O_2SF_5$, and estimated the rate constant of reaction (12), 3×10^{-12} cm^3 molecule^{-1} s^{-1}, from the product distribution of the thermal decomposition of $SF_5O_3SF_5$. There is no available kinetic data for reaction (13). From the observed rate of decay of the UV absorption attributed to SF_5O_2 radicals in the present work using 40 mbar O_2, 20 mbar of SF_4 and 920 mbar of SF_6, we derive an observed rate constant of $k_{13obs} = 2.9 \times 10^{-12}$ cm^3 molecule^{-1} s^{-1}. Reaction (13) is too slow to influence the formation kinetics of SF_5O_2. The overall kinetic model used to simulate the formation kinetics of SF_5O_2 is given in Table I. The model includes, two unknown rate constants, k_{6a} and k_{-6a}. The literature value of k_{12} is only a crude estimate.

The dependence of the maximum transient absorption on the O_2 concentration seen in Figure 5 can be modelled using the kinetic scheme in Table I. By assuming that $k_{6a} = 0$ and varying k_{6a} and k_{12} the data can be fit with $k_{6a} = 10^{-12}$ and $k_{12} = 1.2 \times 10^{-10}$ cm^3 molecule^{-1} s^{-1}. Even though the model predicts the maximum absorbances in Figure 5 well, the model can not predict the formation and the decay rate of SF_5O_2 at low oxygen concentrations. In Figure 1A the upper short dash line is a simulation of the SF_5O_2 transient at $[O_2]_0 = 5.4$ mbar. As seen from the figure both the rise and the decay of the simulated curve are too slow compared with the experimental data. In addition it seems unlikely that reaction (12) which is a reaction between large molecules is diffusion controlled. Therefore we conclude that it is necessary to include the thermal decomposition of SF_5O_2 in the kinetic model to reproduce the experimentally observed transients.

If the equilibrium between SF_5, O_2, and SF_5O_2 should explain the rise in the maximum transient absorbance in Figure 5 alone, and assuming for the moment that secondary radical-radical reactions were negligible in the system, the data in Figure 5 could be fitted using an analytical expression:

$$A = A_{SF5} + A_{SF5O2}\{K_{eq}[O_2]/(1 + K_{eq}[O_2])\} \quad \text{(III)}$$

where A is the maximum transient absorbance, A_{SF5} and A_{SF5O2} are the absorbances if all F atoms were converted into either SF_5 or SF_5O_2 radicals. $[O_2]$ is the oxygen concentration and K_{eq} is the equilibrium constant between SF_5, O_2, and SF_5O_2:

TABLE I. Chemical mechanism.

No.	Reaction	$10^{12}k_1$(cm^3 molecule^{-1} s^{-1})	Ref.
5	$F + SF_4 + M \rightarrow SF_5 + M$	13	This work
4	$F + O_2 + M \rightarrow FO_2 + M$	0.19	[7]
9	$F + SF_5 + M \rightarrow SF_6 + M$	10	[10,14]
10	$SF_5 + SF_5 \rightarrow$ Products	0.23	This work[a]
13	$SF_5O_2 + SF_5O_2 \rightarrow$ Products	2.9	See text
12	$SF_5 + SF_5O_2 + M \rightarrow SF_5O_2SF_5 + M$	20	This work[b]
6a	$SF_5 + O_2 + M \rightarrow SF_5O_2 + M$	0.8	This work[b]
-6a	$SF_5O_2 + M \rightarrow SF_5 + O_2 + M$	10^5	This work[b]

[a] Upper limit.
[b] From modelling.
[c] Unit: s^{-1}

(IV) $$K_{eq} = [SF_5O_2]/[SF_5][O_2]$$

A three parameter fit was performed varying A_{SF5}, A_{SF5O2}, and K_{eq}.

Even if secondary chemistry, such as reactions (9–13), is important the absorbance at high $[O_2]$ should not be influenced. However, as $[O_2]$ is decreased the importance of secondary chemistry will increase and lead to a decrease in the absorbance. The consequence of secondary chemistry will be a decrease of the maximum transient absorbance for low oxygen concentrations while the maximum transient absorbance at high $[O_2]$ will be unaffected. Therefore the value of K_{eq} derived from a fit of eq. (III) to the data in Figure 5 will be lower limit for the "true" K_{eq}. The curve fitted to the experimental data can be seen in the figure as a solid line. The best fit was obtained using $K_{eq} = (4.3 \pm 1.1) \times 10^{-18}$ cm^3 molecule^{-1}, $A_{SF5O2} = 0.1561 \pm 0.0078$, and $A_{SF5} = 0.0146 \pm 0.0082$.

To determine the "true" K_{eq}, k_{6a}, and k_{-6a}, detailed modelling of the experimental absorbance transients was carried out. The following initial values were used for the simulations: $\sigma(SF_5)_{230\,nm} = 3.2 \times 10^{-19}$ cm^2, $\sigma(SF_5O_2)_{230\,nm} = 3.7 \times 10^{-18}$ cm^2, $k_{12} = 3 \times 10^{-12}$ cm^3 molecule^{-1} s^{-1} and $K_{eq} = 4.3 \times 10^{-18}$ cm^3 molecule^{-1}. k_{6a} was determined by fitting the transient predicted by the model to the experimental transient in Figure 1(E). The initial concentrations used for this transient were: $[O_2] = 80$ mbar, $[SF_4] = 40$ mbar, and $[SF_6] = 880$ mbar. At this high oxygen concentration both secondary chemistry and influence of the equilibrium between SF_5 and O_2 is negligible. Hence, the fit is insensitive to k_{12} and k_{-6a}. The value obtained for k_{6a} was 8×10^{-13} cm^3 molecule^{-1} s^{-1} and the simulation is shown as a solid line in Figure 1(E). The dashed lines in the figure are results of simulations using $k_{6a} = 6 \times 10^{-13}$ and $k_{6a} = 10 \times 10^{-13}$ cm^3 molecule^{-1} s^{-1}. $k_{6a} = 8 \times 10^{-13}$ cm^3 molecule^{-1} s^{-1} was kept constant in the simulations described below.

Using $k_{6a} = 8 \times 10^{-13}$ cm^3 molecule^{-1} s^{-1} and $K_{eq} = 4.3 \times 10^{-18}$ cm^3 molecule^{-1} an upper limit for k_{-6a} was determined to be 1.86×10^5 s^{-1}. An example of a simulated transient at low $[O_2]$ using the rate constants above is shown in Figure 1(A) by a long dash line. It is evident from the figure that both the simulated formation and the decay of SF_5O_2 radicals are too slow at low oxygen concentrations. The fit of the data was improved by decreasing k_{-6a} and increasing k_{12} until $k_{-6a} = 10^5$ s^{-1} and $k_{12} = 2.0 \times 10^{-11}$ cm^3 molecule^{-1} s^{-1}. A simulation using these values is shown in Figure 1(A) by the solid line. If k_{12} was increased and k_{-6a} decreased further the decay kinetics were too fast at low $[O_2]$ (see the lower short dash line in Fig. 1(A). In Figure 1(A)–1(E) the experimental transients are shown together with the model simulations (solid lines) using $k_{6a} = 8 \times 10^{-13}$ cm^3 molecule^{-1} s^{-1}, $k_{-6a} = 10^5$ s^{-1}, and $k_{12} = 2.0 \times 10^{-11}$ cm^3 molecule^{-1} s^{-1}.

As a check of our chemical model, the observed and the modelled maximum transient absorptions at 230 nm as a function of dose are compared in Figure 6. The experimental condition was $[SF_4] = 20$ mbar, $[O_2] = 40$ mbar, $[SF_6] = 940$ mbar and pathlength 80 cm. The agreement between the observed data and the modelled results supports the results from the simulations of the transients in Figure 1.

k_{-6a} and k_{12} were derived from simulations of experimental transients using a complex chemical model. We estimate the uncertainty on these values to be of the order of 50%. We believe, that the uncertainty of k_{6a} and $\sigma(SF_5O_2)$ are less than 25%. k_{6a} was virtually determined from the rise time of SF_5O_2 alone at high O_2 concentration, and therefore has less uncertainty. $\sigma(SF_5O_2)$ could not be varied by 15% and still give a good fit of the data. Since the uncertainty in the F atom yield is of the order of 10% we choose to report an uncertainty for $\sigma(SF_5O_2)$ of 25%.

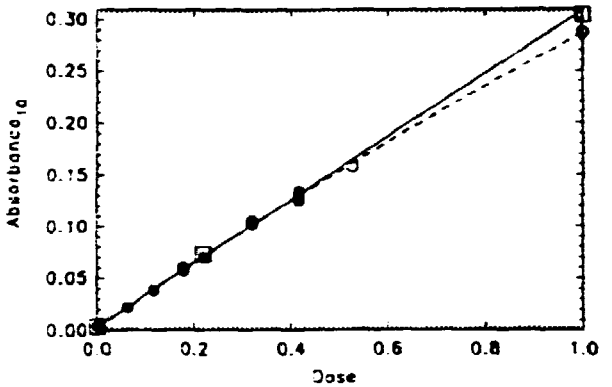

Figure 6. Maximum transient absorptions as a function of dose at 230 nm following pulse radiolysis of a mixture of 40 mbar O_2, 20 mbar SF_4, and 940 mbar SF_6. A path-length of 80 cm were employed. Circles are experimental points and squares are results of simulations using the model in Table I. The dash lines are a second-order fit to the experimental data to help the inspection of the data.

UV Spectrum of SF_5O_2

To map out the spectrum of SF_5O_2 we have measured the maximum transient absorption following pulse radiolysis, dose = 0.416, of mixtures of $[SF_4]$ = 20 mbar, $[O_2]$ = 40 mbar, $[SF_6]$ = 940 mbar between 215 nm and 270 nm. After a small correction (< 7%) for FO_2 the absorbances were scaled to the absorption cross section at 230 nm. The absorption cross sections are listed in Table II and the spectrum is shown in Figure 7. The broad and featureless UV spectrum of SF_5O_2 is similar to conventional peroxy spectra.

SF_5O_2 + NO → SF_5O + NO_2

The kinetics of the reaction between SF_5O_2 and NO were studied by monitoring the rate of increase in the absorption at 400 nm (attributed to the formation of NO_2) following the radiolysis of mixtures of 0.3–1.0 mbar NO, 20 mbar SF_4, 40 mbar O_2, and 920 mbar SF_6. This method has been used extensively in our laboratory to study the reaction of RO_2 and NO and is discussed in detail elsewhere [18–20]. Figure 1(F) shows the result from a radiolysis experiment with [NO] = 1.0 mbar. The smooth line

TABLE II. UV absorption cross sections of SF_5 and SF_5O_2 radicals.

Wavelength (nm)	$10^{20}\sigma_{SF_5}$ (cm^2 molecule^{-1})	$10^{20}\sigma_{SF_5O_2}$ (cm^2 molecule^{-1})
215	-	550
220	55	469
225	-	434
230	32	370
235	-	311
240	21	235
250	-	126
260	-	65
270	-	36

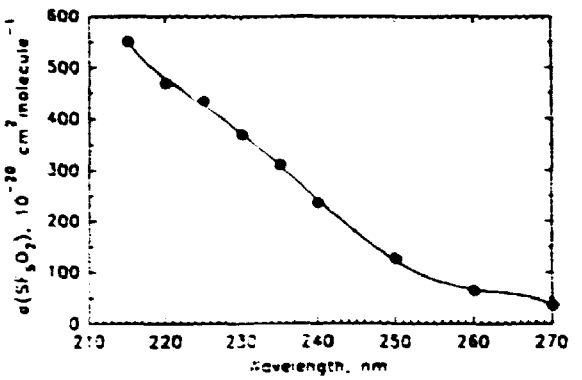

Figure 7. The UV spectrum of the SF_5O_2 radical.

in Figure 1(F) is a first-order fit of the data from 3 μs after the pulse. In all cases, the rise in the absorption at 400 nm followed first-order kinetics. Control experiments were performed in which $SF_6/SF_4/O_2$, SF_6/O_2, or just SF_6 were radiolyzed; no change in absorption at 400 nm was observed. It seems reasonable to conclude that NO_2 is the species responsible for the absorption change following radiolysis of $SF_6/SF_4/O_2/NO$ mixtures.

The first-order rate constants obtained by fitting NO_2 absorption transients with a first-order expression are plotted as a function of [NO] in Figure 8. The solid line in the figure is a linear regression. The slope gives $k(SF_5O_2 + NO) = (1.1 \pm 0.2) \times 10^{-11}$ cm^3 molecule^{-1} s^{-1} and an intercept at $(2 \pm 3) \times 10^4$ s^{-1}. Quoted errors are two standard deviations and represents precision only.

As discussed previously [19,20] there are two potential complications that need to be considered when the rise of NO_2 product is used to derive kinetic data for the reaction of peroxy radicals (RO_2) with NO. These complications are (i) the need to separate the time-scale of RO_2 radical formation from that of their subsequent reaction with NO and (ii) possible loss of NO_2 product via reaction with the alkoxy radical product (RO).

With regard to the first consideration, in the presence of 40 mbar of O_2 the half-life of the decay of SF_5 radicals with respect to conversion into SF_5O_2 radicals is

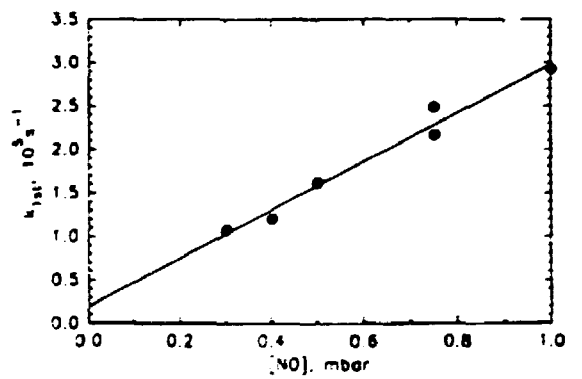

Figure 8. The first-order formation rate constants for the formation of NO_2 plotted as a function of [NO]. The solid line is a linear least squares fit of the data. The slope is $(1.1 \pm 0.2) \times 10^{-11}$ cm^3 molecule^{-1} s^{-1} and the intercept is $(0.2 \pm 0.3) \times 10^5$ s^{-1}.

0.9 μs. The NO_2 formation transients were fit from 3 μs after the radiolysis pulse at which time the formation of SF_5O_2 was essentially complete. With regard to the second complication, as discussed by Sehested et al. [19] consumption of NO_2 via reaction with SF_5O should manifest itself as a significant intercept in a plot of k_{1st} vs. [NO]. Within the experimental uncertainties, no such effect is evident in Figure 8. We conclude that the value of $k(SF_5O_2 + NO) = (1.1 \pm 0.2) \times 10^{-11}$ cm^3 molecule^{-1} s^{-1} derived from the data in Figure 8 is not significantly impacted by secondary reactions. Potential systematic errors are estimated to add an additional 10% uncertainty range. Hence, we arrive at $k(SF_5O_2 + NO) = (1.1 \pm 0.3) \times 10^{-11}$ cm^3 molecule^{-1} s^{-1}.

Discussion

Several of the rate constants measured in this work have been reported previously. The reaction between F atoms and SF_4 has been investigated by Ryan and Plumb [10] in 1–10 mbar of He. They found $k_5 = (0.9 - 3.0) \times 10^{-12}$ cm^3 molecule^{-1} s^{-1} at low pressures and estimated the high pressure limit to be of the order of 5×10^{-12} cm^3 molecule^{-1} s^{-1}. RRKM calculations in the same article indicated that the high pressure limit for reaction (5) was 10^{-11} cm^3 molecule^{-1} s^{-1}, which is in good agreement with the value of $(1.3 \pm 0.3) \times 10^{-11}$ cm^3 molecule^{-1} s^{-1} reported in this work.

We estimate that the rate constant for the self reaction of SF_5 radicals is less than 2.3×10^{-13} cm^3 molecule^{-1} s^{-1}. An earlier determination of 9×10^{-13} cm^3 molecule^{-1} s^{-1} in nonpolar solvents is the only other direct study of this rate constant [21]. Czarnowski and Schumacher [22] have estimated that k_{10} is less than 2×10^{-14} cm^3 molecule^{-1} s^{-1} in the gas phase. Our value is consistent with the estimate of Czarnowski and Schumacher but inconsistent with the work of Tait and Howard [21]. The origin of this discrepancy is uncertain but may be due to differences between gas and liquid phase reactions. Further study of this rate constant is needed since it is of some commercial interest due to the use of SF_6 in transformation stations and the possible production of SF_5 and S_2F_{10} in these systems.

Johnson et al. [23] report that SF_5 absorbs strongly below 400 nm in methanol with an absorption maximum at 300 nm. This absorption band is also expected to be prominent in the gas phase. However, the weak absorption below 240 nm is the only absorption of SF_5 below 310 nm detected in the present work. The reason why SF_5 absorbs strongly at 300 nm in methanol while it does not in the gas phase is unknown.

Formation of SF_5O_2 from SF_5 and O_2 and the decomposition of SF_5O_2 at 298 K have been measured as a part of this work. The rate constant for the reaction of SF_5 radicals with O_2 is $(8 \pm 2) \times 10^{-13}$ cm^3 molecule^{-1} s^{-1}. Czarnowski and Schumacher [22] based on a product study of pyrolysis of $SF_5O_3SF_5$ have estimated $k_{6a} = 3.3 \times 10^{-12}$ cm^3 molecule^{-1} s^{-1} at 283 K. Considering the uncertainties inherent in the estimation of k_{6a} by Czarnowski and Schumacher [22] their estimated value is consistent with our measurements. In addition k_{6a} has been measured before by Plumb and Ryan [24] who reported an upper limit of 5×10^{-16} cm^3 molecule^{-1} s^{-1}. The low value of k_{6a} found by Plumb and Ryan can be explained by this work. Using the equilibrium constant of 8×10^{-18} cm^3 molecule^{-1} derived here and the oxygen concentration of 3.14×10^{15} molecules cm^{-3} employed by Plumb and Ryan, we can calculate that equilibrium is reached in their system when $[SF_5O_2]$ is 2.5% of $[SF_5]$. This explains why Plumb and Ryan did not observe any SF_5O_2.

The decomposition rate of SF_5O_2 derived from this work is 10^5 s^{-1}. To our knowledge the only literature value for k_7 is a value calculated from a model by Czarnowski and Schumacher [22] of 2150 s^{-1} at 283 K and a total pressure of 50–100 torr. This is 50 times lower than the value derived in this work. The reason for this difference is unclear at present. While it is expected that the rate of SF_5O_2 decomposition should decrease at lower temperatures a 50 fold change in the decomposition rates at 295 and 283 K is unexpectedly large.

By combining the equilibrium constant for reaction (1), $K_{eq} = (8.0 \pm 4.5) \times 10^{-17}$ cm^3 $molecule^{-1}$ (197 ± 111 atm^{-1}) measured in the present work with the thermodynamical relationship $\Delta G = -RT \ln(K_p)$ a value of $\Delta G = -(3.0 \pm 0.4)$ kcal mol^{-1} can be derived. It seems reasonable to assume that the entropy change in the association reaction of SF_5 radicals with O_2 will be similar to that for the analogous association reactions CH_3, C_2H_5, C_3H_7, $HOCH_2$, and CH_3S radicals which all lie in the range (31–41) cal mol^{-1} K^{-1} [2,3]. Using $\Delta G = \Delta H - T\Delta S$, a bond strength of ($13.7 \pm 2.0$) kcal mol^{-1} is calculated for the $SF_5—O_2$ bond. This is in good agreement with the value found by Czarnowski and Schumacher [16] of 12–15 kcal mol^{-1}. The $SF_5—O_2$ bond strength measured here is comparable to, although slightly stronger than, the $CH_3S—O_2$ bond which is ≈11 kcal mol^{-1} [3]. It is interesting to note that the strength of the S—O bond appears to be only weakly influenced by the substituents on the sulfur atom. As noted by Turnipseed et al. [3], although bond strengths of the order of 10–15 kcal mol^{-1} imply rapid decomposition of the sulfur centered peroxy radical, because of the abundance of O_2 in the atmosphere, it is possible that a substantial fraction of the sulfur centered radical pool would exist in the form of peroxy radicals in the atmosphere. The atmospheric chemistry of weakly bound sulfur centered peroxy radicals has yet to be investigated.

The reaction of SF_5O_2 with NO is very similar to the reaction of alkyl peroxy radicals with NO. Both the rate constants and the products are similar. This is also the case for the UV absorption spectra.

Finally, the results from the present work need to be placed into perspective in terms of the atmospheric chemistry of SF_6. The Earth's atmosphere contains a few pptv of SF_6 [25]. The atmospheric fate of SF_6 has been the subject of two recent publications [25,26]. The degradation of SF_6 is very slow. Estimates of the atmospheric lifetime of SF_6 range from 3 to 25 thousand years [25,26]. The major loss of SF_6 is believed to be via reaction with free electrons in the mesosphere to produce SF_6^- ions. SF_6^- ions may then undergo either electron-photodetachment to regenerate SF_6 or react with positively charged ions leading to ejection of one or more F atoms from the SF_6 group [27]. At the present time the products of such neutralization reactions are unknown and it is not possible to assess the role played by SF_5 and SF_5O_2 radicals in the atmosphere.

Acknowledgment

JS would like to thank the Danish Research Academy for a research scholarship and OJN would like to thank the Commission of the European Communities for financial support. We would like to thank Robert A. Morris for discussions regarding the fate of SF_6 in the atmosphere and Bill Schneider for discussions regarding the entropy change in reaction (6). Finally, we would like to thank Steve Japar (Ford) for helpful comments.

Bibliography

[1] T.J. Wallington, P. Dagaut, and M.J. Kurylo, *Chem. Rev.*, **92**, 667 (1992).
[2] P.D. Lightfoot, R.A. Cox, J.N. Crowley, M. Destriau, G.D. Hayman, M.E. Jenkin, G.K. Moortgat, and F. Zabel, *Atmos. Environ.*, **26A**, 1805 (1992).
[3] A.A. Turnipseed, S.B. Barone, and A.R. Ravishankara, *J. Phys. Chem.*, **96**, 7502 (1992).
[4] K.B. Hansen, R. Wilbrandt, and P. Pagsberg, *Rev. Sci. Instrum.*, **50**, 1532 (1979).
[5] O.J. Nielsen, Riso-R-480, Riso National Laboratory, Roskilde, Denmark, 1984.
[6] T. Ellermann, Riso-M-2932, Riso National Laboratory, Roskilde, Denmark, 1991.
[7] T. Ellermann, O.J. Nielsen, P. Pagsberg, J. Sehested, and T.J. Wallington, *Chem. Phys. Lett.*, **218**, 287 (1994).
[8] T.J. Wallington, M.D. Hurley, J. Shi, M.M. Maricq, J. Sehested, O.J. Nielsen, and T. Ellermann, *Int. J. Chem. Kinet.*, **25**, 651 (1993).
[9] M.M. Maricq and J.J. Szente, *J. Phys. Chem.*, **96**, 4925 (1992).
[10] K.R. Ryan and I.C. Plumb, *Plasma Chem. Plasma Process.*, **8**, 281 (1988).
[11] W. Tsang and J.T. Herron, *J. Chem. Phys.*, **96**, 4272 (1992).
[12] T. Ellermann, unpublished results.
[13] T.J. Wallington, T. Ellermann, O.J. Nielsen, and J. Sehested, *J. Phys. Chem.*, **98**, 2346 (1994).
[14] W. Tsang and T. John, *J. Chem. Phys.*, **96**, 4272 (1992).
[15] J.T. Herron, *Int. J. Chem. Kinet.*, **19**, 129 (1987).
[16] J. Czarnowski and H.J. Schumacher, *Int. J. Chem. Kinet.*, **11**, 613 (1979).
[17] W.B. DeMore, S.P. Sander, D.M. Golden, R.F. Hampson, M.J. Kurylo, C.J. Howard, A.R. Ravishankara, C.E. Kolb, and M.J. Molina, JPL 92-20, Pasadena, California, 1992.
[18] T.J. Wallington and O.J. Nielsen, *Chem. Phys. Lett.*, **187**, 33 (1991).
[19] J. Sehested, O.J. Nielsen, and T.J. Wallington, *Chem. Phys. Lett.*, **213**, 457 (1993).
[20] T.J. Wallington, T. Ellermann, and O.J. Nielsen, *J. Phys. Chem.*, **97**, 8442 (1993).
[21] J.C. Tait and J.A. Howard, *Can. J. Chem.*, **53**, 2361 (1985).
[22] J. Czarnowski and H.J. Schumacher, *Int. J. Chem. Kinet.*, **11**, 1089 (1979).
[23] D.W. Johnson and G.A. Salmon, *J. Chem. Soc. Faraday Trans. 1*, **73**, 2031 (1977).
[24] I.C. Plumb and K.R. Ryan, *Plasma Chem. Plasma Process.*, **6**, 247 (1986).
[25] M.K.W. Ko, N.D. Sze, W. Wang, G. Shia, A. Goldman, F.J. Murcray, D.G. Murcray, and C.P. Rinsland, *J. Geophys. Res.*, **98**, 10499 (1993).
[26] A.R. Ravishankara, S. Solomon, A.A. Turnipseed, and R.F. Warren, *Science*, **295**, 194 (1993).
[27] R.A. Morris, private communication, 1993.

Received November 4, 1993
Accepted January 20, 1994

Reprinted from The Journal of Physical Chemistry, 1994, 98.

Atmospheric Chemistry of CF_3CO_x Radicals: Fate of CF_3CO Radicals, the UV Absorption Spectrum of $CF_3C(O)O_2$ Radicals, and Kinetics of the Reaction $CF_3C(O)O_2 + NO \rightarrow CF_3C(O)O + NO_2$

Timothy J. Wallington* and Michael D. Hurley

Research Staff, SRL-E3083, Ford Motor Company, Dearborn, Michigan 48121-2053

Ole J. Nielsen* and Jens Sehested

Section for Chemical Reactivity, Environmental Science and Technology Department, Risø National Laboratory, DK-4000 Roskilde, Denmark

*Received: February 16, 1994; In Final Form: March 28, 1994**

The atmospheric fate of CF_3CO radicals has been studied using a pulse radiolysis technique to provide kinetic data and FTIR-smog chamber system to provide product data. In 1 atm of SF_6 at 296 ± 2 K, CF_3CO radicals decompose to give CF_3 radicals and CO with a rate of $(1.2 \pm 0.8) \times 10^5$ s^{-1} and react with O_2 to form $CF_3C(O)O_2$ radicals with a rate constant of $(7.3 \pm 1.1) \times 10^{-13}$ cm^3 molecule^{-1} s^{-1}. In 1 atm of N_2 at 296 ± 2 K, the rate constant ratio $k(CF_3CO + O_2 \rightarrow CF_3C(O)O_2)/k(CF_3CO \rightarrow CF_3 + CO) = (7.4 \pm 0.6) \times 10^{-18}$ cm^3 molecule^{-1}. Reaction with O_2 accounts for 99.5% of the loss of CF_3CO radicals in the atmosphere. The ultraviolet absorption spectrum of $CF_3C(O)O_2$ radicals has been studied over the wavelength range 220–300 nm, and at 230 nm, $\sigma_{CF_3C(O)O_2} = (3.78 \pm 0.43) \times 10^{-18}$ cm^2 molecule^{-1}. Monitoring the rate of NO_2 formation at 400 nm allowed a lower limit of $k_4 > 9.9 \times 10^{-12}$ cm^3 molecule^{-1} s^{-1} to be derived for the rate constant of the reaction of $CF_3C(O)O_2$ radicals with NO. Reaction of $CF_3C(O)O_2$ radicals with NO produces the alkoxy radical $CF_3C(O)O$, which undergoes C–C bond scission rapidly with a rate greater than 6×10^6 s^{-1}. Results are discussed with respect to the atmospheric chemistry of CF_3CO_x radicals. As part of the present work, a rate constant $k_6 = (2.3 \pm 0.4) \times 10^{-11}$ cm^3 molecule^{-1} s^{-1} was determined for the reaction of F atoms with CF_3CHO.

Introduction

By international agreement, industrial production of chlorofluorocarbons (CFCs) will be phased out. CFC replacements are being sought. Hydrofluorocarbons (HFCs) and hydrochlorofluorocarbons (HCFCs) are two classes of potential CFC substitutes. Prior to the large scale industrial use of these compounds, it is important to establish the environmental impact of their release. HCFCs and HFCs of the general type $CF_3CH_yX_{2-y}$ (X = F, Cl) can degrade by a variety of different pathways in the atmosphere to produce CF_3CO radicals. For example, the atmospheric oxidation of HFC-134a (CF_3CFH_2) produces $CF_3C(O)F$.[1,2] The oxidation of HFC-143a (CF_3CH_3) produces CF_3CHO.[3] In the upper stratosphere, photolysis of $CF_3C(O)F$ could produce CF_3CO radicals. Reaction of OH radicals with CF_3CHO produces CF_3CO radicals. Once formed, CF_3CO radicals are expected to either decompose to give CF_3 radicals and CO or add O_2 to give $CF_3C(O)O_2$ radicals. Assessment of the environmental impact of the release of compounds having the general formula CF_3CX_3 (X = H, F, Cl) requires information concerning the atmospheric chemistry of CF_3CO_x radicals (x = 1–3).

As part of a joint program between our two laboratories to survey the atmospheric chemistry of HFCs and HCFCs,[4-9] we have used pulse radiolysis and long path length Fourier transform infrared techniques to provide kinetic and mechanistic data concerning reactions 1–4. Results are reported herein.

$$CF_3CO + M \rightarrow CF_3 + CO + M \quad (1)$$

$$CF_3CO + O_2 + M \rightarrow CF_3C(O)O_2 + M \quad (2)$$

$$CF_3C(O)O + M \rightarrow CF_3 + CO_2 + M \quad (3)$$

$$CF_3C(O)O_2 + NO \rightarrow CF_3C(O)O + NO_2 \quad (4)$$

Experimental Section

Two different experimental systems were used. Both have been described in detail in previous publications[10,11] and will only be discussed briefly here.

Pulse Radiolysis System. $CF_3C(O)O_2$ radicals were generated by the radiolysis of $SF_6/O_2/CF_3CHO$ gas mixtures in a 1-L stainless steel reactor with a 30-ns pulse of 2-MeV electrons from a Febetron 705B field emission accelerator. SF_6 was always in great excess and was used to generate fluorine atoms:

$$SF_6 + 2\ MeV\ e^- \rightarrow F + products \quad (5)$$

$$F + CF_3CHO \rightarrow CF_3CO + HF \quad (6)$$

$$CF_3CO + O_2 + M \rightarrow CF_3C(O)O_2 + M \quad (2)$$

Four sets of experiments were performed using the pulse radiolysis system. First, the rate of the appearance of ultraviolet absorption attributed to CF_3CO radicals following the radiolysis of SF_6/CF_3CHO mixtures was measured as a function of the initial concentration of CF_3CHO to determine k_6. Second, O_2 was added to the reaction mixtures, and the rate of increase in ultraviolet absorption attributed to $CF_3C(O)O_2$ and CF_3O_2 radicals was measured as a function of the O_2 concentration to determine k_1 and k_2. Third, initial conditions were selected to ensure that the majority of CF_3CO radicals react with O_2, and the UV spectrum of $CF_3C(O)O_2$ radicals was recorded. Fourth, NO was added to the reaction mixtures, and the rate of NO_2

* Authors to whom correspondence may be addressed.
* Abstract published in *Advance ACS Abstracts*, May 1, 1994.

0022-3654/94/2098-5686$04.50/0

formation following the radiolysis pulse was monitored to provide information about the kinetics of reactions 3 and 4.

To monitor the transient UV absorption, the output of a pulsed 150-W Xenon arc lamp was multipassed through the reaction cell using internal White cell optics (80- or 120-cm path length). A McPherson grating monochromator, Hamamatsu R 955 photomultiplier and Biomation 8100 waveform digitizer were used to detect and record the light intensity at the desired wavelength. The spectral resolution used was 0.8 nm. Reagent concentrations used were SF_6, 945–995 mbar, O_2, 0–50 mbar, NO, 0–1.0 mbar, and CF_3CHO, 0–5 mbar. All experiments were performed at 296 K. Ultrahigh purity O_2 was supplied by L'Air Liquide. SF_6 (99.97%) was supplied by Gerling and Holz. NO (99.8%) was obtained from Messer Griesheim. CF_3CHO was synthesized by the dropwise addition of trifluoroacetaldehyde methyl hemiacetal to a H_2SO_4/P_2O_5 slurry. IR analysis did not reveal any observable impurities. All other reagents were used as received.

FTIR-Smog Chamber System. The FTIR system was interfaced to a 140-L Pyrex reactor. Radicals were generated by the UV irradiation of mixtures of CF_3CHO (14–28 mTorr), Cl_2 (100–120 mTorr), NO (0–40 mTorr), and O_2 (0–40 Torr) at 80–700 Torr total pressure of N_2 diluent at 296 K using 22 blacklamps (760 Torr = 1013 mbar). The loss of CF_3CHO and the formation of products were monitored by FTIR spectroscopy using an analyzing path length of 25 m and a resolution of 0.25 cm^{-1}. Infrared spectra were derived from 32 coadded spectra. Reference spectra were acquired by expanding known volumes of reference materials into the reactor. The IR spectrum of CF_3CHO was consistent with that reported by Shechter and Conrad.[12] The IR feature of CF_3CHO at 1305 cm^{-1} is broad and essentially devoid of structure at the spectral resolution (0.25 cm^{-1}) used in this work. The IR absorption cross section at 1305 cm^{-1} was $(4.9 \pm 0.3) \times 10^{-19}$ cm^2 molecule^{-1}. This feature was a convenient reference point to calibrate the CF_3CHO concentrations used in the FTIR experiments. N_2 and O_2 (both 99.999%) and Cl_2 (99.999%) were obtained from Airco. NO and Cl_2 (both research purity) were obtained from Matheson. All reagents were used as received.

Pulse Radiolysis Results

Study of F + CF_3CHO. Following the pulse radiolysis of a mixture of 990 mbar of SF_6 and 1–5 mbar of CF_3CHO, a small (absorbance of 0.08 ± 0.01 using full dose) transient UV absorption was observed at 230 nm. No absorption was observed when either 5 mbar of CF_3CHO or 990 mbar of SF_6 were radiolyzed separately. We ascribe the absorption observed upon radiolysis of SF_6/CF_3CHO mixtures to the formation of CF_3CO radicals via reaction 6. The increase in absorption displayed first-order kinetics. Figure 1 shows a plot of the observed pseudo-first-order rate of appearance of the absorption ascribed to CF_3CO radicals as a function of the concentration of CF_3CHO. The solid line is a linear least-squares fit. The y-axis intercept, $(2.1 \pm 2.6) \times 10^4$ s^{-1}, is not statistically significant. The slope gives $k_6 = (2.3 \pm 0.4) \times 10^{-11}$ cm^3 molecule^{-1} s^{-1}. This result is in good agreement with a recent determination of $k_6 = (2.7 \pm 0.1) \times 10^{-11}$ cm^3 molecule^{-1} s^{-1} using a relative rate technique.[13] Unless otherwise specified, all errors in the present manuscript are 2 standard deviations.

$$F + CF_3CHO \rightarrow CF_3CO + HF \qquad (6)$$

Study of $CF_3CO + O_2 + M \rightarrow CF_3C(O)O_2 + M$ and $CF_3CO + M \rightarrow CF_3 + CO + M$. To investigate the kinetics of reactions 1 and 2, O_2 was added to the reaction mixtures. Following the radiolysis of $SF_6/CF_3CHO/O_2$ mixtures, the observed transient absorption was substantially greater (by a factor of 4 at 230 nm) than that observed in the absence of O_2. We conclude that

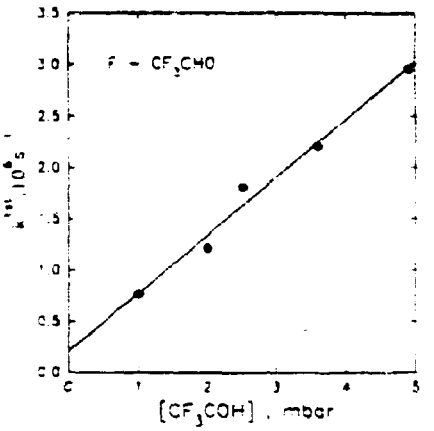

Figure 1. Plot of the first-order appearance of absorption attributed to CF_3CO radicals following radiolysis of SF_6/CF_3CHO mixtures (k^{1st} versus [CF_3CHO]). The line is a linear regression to the data.

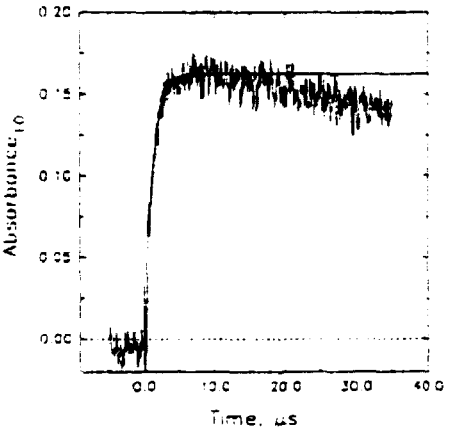

Figure 2. Transient absorption at 230 nm observed following pulsed radiolysis of a mixture of 5 mbar of CF_3CHO, 40 mbar of O_2, and 955 mbar of SF_6. The solid line is a first-order rise fit which gives $k^{1st} = 9.23 \times 10^5$ s^{-1}.

$CF_3C(O)O_2$ radicals absorb more strongly than CF_3CO radicals over the wavelength region of interest (220–300 nm). Figure 2 shows the transient absorption observed at 230 nm for the first 40 μs following the radiolysis of a mixture of 5 mbar of CF_3CHO, 40 mbar of O_2, and 955 mbar of SF_6 (0.527 dose, 80-cm UV analysis path length). The solid line is a first-order fit using the expression $Abs(t) = (A_{inf} - C)[1 - \exp(-k^{1st}t)] + C$, where $Abs(t)$ is the absorbance as a function of time, A_{inf} is the absorbance at infinite time, k^{1st} is the pseudo-first-order appearance rate of absorption, and C is the extrapolated absorbance at $t = 0$. For the data shown in Figure 2, $k^{1st} = 9.23 \times 10^5$ s^{-1}. In all cases, the rise in absorption followed first-order kinetics. Control experiments were performed in which CF_3CHO/O_2 mixtures or just SF_6 were radiolyzed; no transient absorption was observed.

A relevant question at this point is "What radical(s) cause the transient absorption shown in Figure 2?". There are several possibilities; CF_3CO, FO_2, $CF_3C(O)O_2$, and CF_3O_2 (produced following reaction 1). As previously noted, the absorption due to CF_3CO radicals is small at 230 nm and does not explain the absorption seen in Figure 2. The rate constant for the reaction of F atoms with O_2 (1.9×10^{-13} cm^3 molecule^{-1} s^{-1})[14] is 121 times less than that for the reaction of F atoms with CF_3CHO (2.3×10^{-11} cm^3 molecule^{-1} s^{-1}, this work). The concentration ratio $[O_2]/[CF_3CHO]$ used in the experiment shown in Figure 2 was 8. Hence, 6.2% of the F atoms react with O_2 to give FO_2 radicals. For the experiment shown in Figure 2, the radiolysis dose was 0.527 and the SF_6 pressure was 955 mbar. The initial F atom concentration is linearly proportional to the radiolysis dose and SF_6 pressure. The F atom yield at full radiolysis dose and 1000 mbar of SF_6 was 2.77×10^{15} cm^{-3}. The initial F atom con-

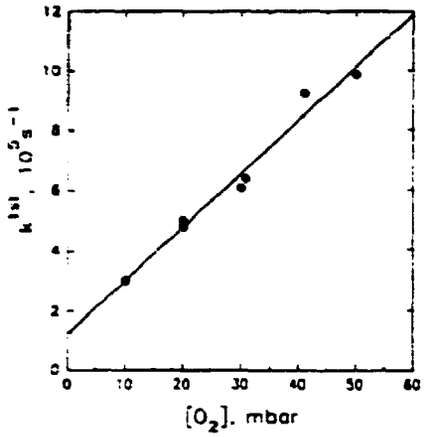

Figure 3. Plot of the first-order appearance of absorption attributed to $CF_3C(O)O_2$ and CF_3O_2 radicals following radiolysis of $SF_6/CF_3CHO/O_2$ mixtures (k^{1st} versus [O_2]). The line is a linear regression to the data. The intercept provides a value of k_1, and the slope gives k_2.

centration in the experiment shown in Figure 2 was ($0.527 \times 2.77 \times 10^{13} \times 0.955$) = 1.39×10^{13} cm^{-3}; hence the FO_2 concentration was 8.6×10^{13} cm^{-3}. At 230 nm, $\sigma(FO_2) = 5.48 \times 10^{-18}$ cm^2 molecule^{-1} [14] and the absorbance expected from FO_2 radicals will then be 0.016, which is a factor of 10 less than observed in Figure 2. The transient absorption shown in Figure 2 must then arise from either $CF_3C(O)O_2$ or CF_3O_2, or both.

For the purpose of studying the kinetics of reactions 1 and 2, it is irrelevant as to whether the absorption is due to either $CF_3C(O)O_2$ or CF_3O_2 radicals, or both. The rationale for this statement is as follows. Assume that reactions 6 and 7 proceed rapidly on the time scale of the present experiments (0–40 μs).

$$CF_3CO + M \rightarrow CF_3 + CO + M \quad (1)$$

$$CF_3CO + O_2 + M \rightarrow CF_3C(O)O_2 + M \quad (2)$$

$$F + CF_3CHO \rightarrow CF_3CO + HF \quad (6)$$

$$CF_3 + O_2 + M \rightarrow CF_3O_2 + M \quad (7)$$

Then, $d[CF_3CO]/dt = -(k_1 + k_2[O_2])[CF_3CO]$, $d[CF_3C(O)O_2]/dt = k_2[O_2][CF_3CO]$, and $d[CF_3O_2]/dt = k_1[CF_3CO]$. If $k_{all} = (k_1 + k_2[O_2])$, then $[CF_3CO](t) = [CF_3CO]_{t_0} \exp(-k_{all}t)$, $[CF_3C(O)O_2](t) = (k_2[O_2][CF_3CO]_{t_0}/k_{all})(1 - \exp(-k_{all}t))$, and $[CF_3O_2](t) = (k_1[CF_3CO]_{t_0}/k_{all})(1 - \exp(-k_{all}t))$. The important point to note is that both $CF_3C(O)O_2$ and CF_3O_2 are formed with a rate constant $k_{all} = (k_1 + k_2[O_2])$. Hence, regardless of whether the absorption is due to $CF_3C(O)O_2$ or CF_3O_2 or both, the first-order rate constant for the appearance of UV absorption is k_{all}. If k_{all} is measured as a function of [O_2], then a plot of k_{all} versus [O_2] will give a slope of k_2 and an intercept of k_1. Such a plot is shown in Figure 3. The intercept gives $k_1 = (1.2 \pm 0.8) \times 10^5$ s^{-1} and the slope gives $k_2 = (7.3 \pm 1.1) \times 10^{-13}$ cm^3 molecule^{-1} s^{-1} at 1000 mbar total pressure of SF_6 diluent and 296 ± 2 K.

At this point, it is germane to consider the validity of the two assumptions made above, namely that reactions 6 and 7 proceed rapidly on the present experimental time scales. Using $k_6 = 2.3 \times 10^{-11}$ cm^3 molecule^{-1} s^{-1} (this work) gives the lifetime of F atoms in the presence of 5 mbar of CF_3CHO as 0.35 μs. On the basis of the work of Caralp et al.,[15] reaction 7 should be close to the high-pressure limit of $k_7 = 8.5 \times 10^{-12}$ cm^3 molecule^{-1} s^{-1} [16] at 1000 mbar of SF_6. At the lowest [O_2] of 10 mbar, the lifetime of CF_3 radicals with respect to reaction 7 is 0.5 μs. The time scale of the experimental observations was 3–11 μs. It appears that both assumptions made above are justified.

Study of the UV Absorption Spectrum of $CF_3C(O)O_2$ Radicals. After the absolute rates for reactions 1 and 2 have been established, experimental conditions can be chosen to maximize the production of $CF_3C(O)O_2$ radicals and minimize fragmentation of CF_3CO radicals into CF_3 and CO. Clearly, to study the UV spectrum of $CF_3C(O)O_2$ radicals, it is desirable to work under conditions of high [O_2]. However, there is a limit to the amount of O_2 that is desirable, as with increasing [O_2], reaction 8 competes with reaction 6 for the available F atoms.

$$F + O_2 + M \rightarrow FO_2 + M \quad (8)$$

To investigate the UV spectrum of $CF_3C(O)O_2$ radicals, the experimental conditions used were 5 mbar of CF_3CHO, 40 mbar of O_2, and 955 mbar of SF_6. Measurement of the absolute absorption spectrum of the $CF_3C(O)O_2$ radical requires calibration of the initial F atom concentration. The yield of F atoms was established by monitoring the transient absorption at 260 nm due to methylperoxy radicals produced by radiolysis of $SF_6/CH_4/O_2$ mixtures as described previously.[17] In the present series of experiments, based upon a value of 3.18×10^{-18} cm^2 molecule^{-1} for $\sigma(CH_3O_2)$ at 260 nm,[18] the yield of F atoms at 1000 mbar of SF_6 was $(2.77 \pm 0.30) \times 10^{15}$ cm^{-3} at full irradiation dose. The quoted error on the F atom calibration includes both statistical (2 standard deviations) and potential systematic errors associated with a 10% uncertainty in $\sigma(CH_3O_2)$. Errors are propagated using conventional error analysis methods.

Following the pulsed radiolysis of mixtures of 5 mbar of CF_3CHO, 40 mbar of O_2, and 955 mbar of SF_6, a rapid increase (complete within 5 μs) in UV absorption in the region 220–300 nm was observed, followed by a slower decay. Control experiments were performed in which 1000 mbar of SF_6 or 5 mbar of CF_3CHO were radiolyzed. As mentioned in the previous section dealing with the kinetics of reaction 6, no significant absorption (<0.02 absorbance units) was observed upon radiolysis of SF_6 or CF_3CHO. As discussed above, the reaction of CF_3CO radicals with O_2 proceeds with a rate constant of $k_2 = (7.3 \pm 1.1) \times 10^{-13}$ cm^3 molecule^{-1} s^{-1} at 1000 mbar total pressure of SF_6 diluent. In the presence of 40 mbar of O_2, the lifetime of CF_3CO radicals with respect to reaction with O_2 is then 1.4 μs. Consistent with this calculation, the transient absorption observed on radiolysis of $SF_6/CF_3CHO/O_2$ mixtures reached a maximum in 5 μs.

To measure the absorption spectrum of $CF_3C(O)O_2$ radicals, it is necessary to consider potential secondary reactions that could interfere with the conversion of F atoms into $CF_3C(O)O_2$ radicals. Potential complications include (i) competition for the available F atoms by reaction with molecular oxygen,

$$F + O_2 + M \rightarrow FO_2 + M \quad (8)$$

and (ii) unwanted radical–radical reactions such as

$$F + CF_3CO \rightarrow \text{products} \quad (9)$$

$$F + CF_3C(O)O_2 \rightarrow \text{products} \quad (10)$$

$$CF_3CO + CF_3C(O)O_2 \rightarrow CF_3C(O)O + CF_3C(O)O \quad (11)$$

To minimize complications caused by FO_2 radicals, experiments were performed using [CF_3CHO] = 5 mbar and [O_2] = 40 mbar. Using rate constants for reactions 6 and 8 measured in our laboratory ($k_6 = 2.3 \times 10^{-11}$ cm^3 molecule^{-1} s^{-1} (see previous section), $k_8 = 1.9 \times 10^{-13}$ cm^3 molecule^{-1} s^{-1} [16]), we calculate that 6.2% percent of the F atoms are converted into FO_2 and 93.8% percent into CF_3CO radicals. Using the rate constant ratio $k_2/k_1 = 6 \times 10^{-18}$ cm^3 molecule^{-1} (see previous section), it can be calculated that, in the presence of 40 mbar of O_2, 86% of the CF_3CO radicals produced in reaction 6 are converted into $CF_3C(O)O_2$ and 14% decompose to give CF_3 radicals and CO. CF_3 radicals will be rapidly converted into CF_3O_2 radicals. Corrections for the presence of 6.2% of FO_2 and (0.938)(0.14)(100) = 13.1% of CF_3O_2 radicals were calculated using the expression of

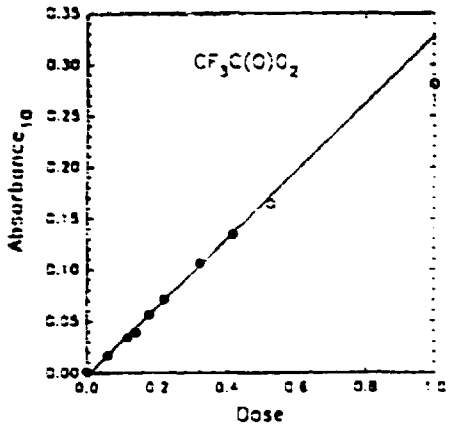

Figure 4. Maximum transient absorption at 230 nm following the pulsed radiolysis of mixtures of 5 mbar CF_3CHO, 40 mbar of O_2, and 955 mbar SF_6 as a function of the radiolysis dose. The solid line is a linear regression to the data (full- and half-dose experiments excepted). The dotted line is a second-order regression fit to the entire data set to aid in visual inspection of the data trend.

TABLE 1: Measured UV Absorption Cross Sections

wavelength (nm)	σ (10^{20} cm^2 molecule^{-1}) $CF_3C(O)O_2$
220	501
230	378
240	257
250	185
260	133
270	78
280	45
290	16

$\sigma(CF_3C(O)O_2) = (\sigma(\text{Observed}) - ((0.062)\sigma(FO_2) + (0.131) \times \sigma(CF_3O_2))/0.807$. Values for $\sigma(CF_3O_2)$ and $\sigma(FO_2)$ were taken from the literature.[7,14]

As mentioned above, it is necessary to ensure that radical–radical reactions 9–11 do not complicate the data analysis. There are no literature data concerning the kinetics of reactions 9–11; hence we cannot calculate their importance. To check for these unwanted radical–radical reactions, the transient absorption at 230 nm was measured with the radiolysis dose varied by over 1 order of magnitude. The UV path length was 80 cm. Figure 4 shows the observed maximum of the transient absorption at 230 nm as a function of the dose. As seen from Figure 4, the maximum absorption is linear with the radiolysis dose up to a dose of 0.40 of maximum. At maximum dose (and possibly at half dose) the maximum transient absorption falls below that expected from a linear extrapolation of the low-dose results. We ascribe the curvature in Figure 4 to the importance of secondary radical–radical reactions 9–11 at high initial F atom concentrations.

The solid line drawn through the data in Figure 4 is a linear least-squares fit (maximum- and half-dose data expected). The slope is 0.331 ± 0.013 (errors are 2 standard deviations). From this value and three additional pieces of information, (i) the yield of F atoms of $(2.77 \pm 0.30) \times 10^{15}$ molecules cm^{-3} (full dose and $[SF_6] = 1000$ mbar), (ii) the conversion of F atoms into 80.7% $CF_3C(O)O_2$, 6.2% FO_2, and 13.1% CF_3O_2 radicals, and (iii) the absorption cross sections for FO_2 and CF_3O_2 at 230 nm ($\sigma = 5.48 \times 10^{-18}$ [14] and 2.06×10^{-18} cm^2 molecule^{-1},[7] respectively), we derive $\sigma(CF_3C(O)O_2)$ at 230 nm = $(3.78 \pm 0.43) \times 10^{-18}$ cm^2 molecule^{-1}. The quoted error includes statistical uncertainties from the linear regression of the data in Figure 4 and the potential systematic uncertainties associated with the calibration of the initial F atom yield. Errors have been propagated using standard error analysis.

To map out the spectrum of the $CF_3C(O)O_2$ radical, experiments were performed to measure the initial absorption between 220 and 300 nm following the pulsed irradiation of $SF_6/CF_3CHO/O_2$ mixtures. The initial absorptions were scaled to that at 230 nm and then corrected for FO_2 and CF_3O_2 to obtain absolute absorption cross sections. Absorption cross sections are given in Table 1 and shown in Figure 5.

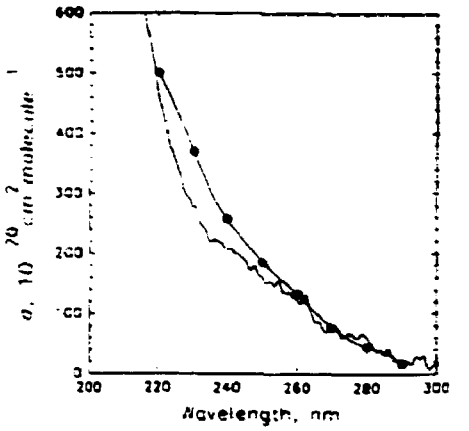

Figure 5. Absorption cross section data for $CF_3C(O)O_2$ radicals measured in this work (●). The solid line is the spectrum recorded by Maricq and Szente.[19]

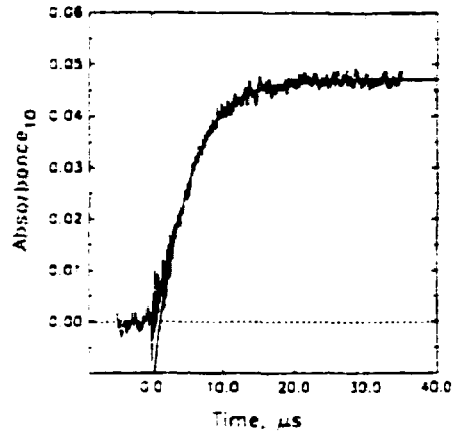

Figure 6. Transient absorption at 400 nm observed following pulsed radiolysis of a mixture of 0.6 mbar of NO, 5 mbar of CF_3CHO, 40 mbar of O_2, and 955 mbar of SF_6. The solid line is a first-order rise fit which gives $k^{1st} = 2.24 \times 10^5$ s^{-1}.

The absorption spectrum of $CF_3C(O)O_2$ measured in the present work is compared to that recorded by Maricq and Szente[19] using a flash photolysis technique in Figure 5. With the exception of the data point at 230 nm, the absorption cross sections from both studies are indistinguishable within the experimental uncertainties. For reasons which are unclear, the value of $\sigma(CF_3C(O)O_2)$ measured at 230 nm in the present work is 35% larger than that observed by Maricq and Szente.[19]

Kinetic Data for the Reaction $CF_3C(O)O_2 + NO \rightarrow CF_3C(O)O + NO_2$. The kinetics of reaction 4 were studied by monitoring the rate of increase in absorption at 400 nm (attributed to the formation of NO_2) following the radiolysis (dose 0.41 times that of maximum) of mixtures of 0.31–1.00 mbar of NO, 5 mbar of CF_3CHO, 40 mbar of O_2, and 940 mbar of SF_6. This method of measuring the kinetics of the reaction of peroxy radicals with NO has been used extensively in our laboratory and is discussed in detail elsewhere.[4,20,21,25] Figure 6 shows the results from a mixture with [NO] = 0.6 mbar. The UV pathlength was 120 cm. The smooth curve in Figure 6 is a first-order fit using the expression $\text{Abs}(t) = (A_{inf} - C)[1 - \exp(-k^{1st}t)] + C$, where Abs($t$) is the absorbance as a function of time, A_{inf} is the absorbance at infinite time, k^{1st} is the pseudo-first-order appearance rate of NO_2, and C is the extrapolated absorbance at $t = 0$.

Control experiments were performed in which SF_6/CF_3CHO, $SF_6/CF_3CHO/O_2$, SF_6/O_2, or just SF_6 were radiolyzed; no change

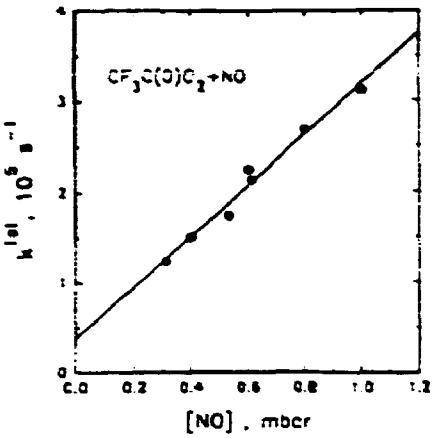

Figure 7. Plot of k^{1st} versus [NO]. The solid line is a linear regression to the experimental data. The dotted line is the behavior predicted using the chemical mechanism in Table 2; see text for details.

in absorption at 400 nm was observed. It seems reasonable to conclude that NO_2 is the species responsible for the absorption change following radiolysis of $SF_6/CF_3CHO/O_2/NO$ mixtures. In the presence of 40 mbar of O_2, the lifetime of CF_3CO radicals with respect to conversion into $CF_3C(O)O_2$ radicals is 1.4 μs. The transient absorption at 400 nm was fitted from 3 μs after the pulse. This delay was used to ensure adequate separation of the time scale for $CF_3C(O)O_2$ radical formation from that of the subsequent reaction with NO.

For the data shown in Figure 6, $k^{1st} = 2.24 \times 10^5$ s^{-1}. As seen from Figure 7, the pseudo-first-order rate constant, k^{1st}, increased linearly with [NO]. Linear least-squares analysis gives $k_4 = (1.14 \pm 0.15) \times 10^{-11}$ cm^3 molecule^{-1} s^{-1}. The y-axis intercept in Figure 7 is $(3.9 \pm 2.4) \times 10^4$ s^{-1} and is statistically significant.

The increase in absorbance at 400 nm can be combined with the literature values of σ_{NO_2} (400nm) = 6.0×10^{-19} cm^2 molecule^{-1} [16] to calculate the yield of NO_2. The yield of NO_2 in the seven experiments performed, expressed as moles of NO_2 produced per mole of $CF_3C(O)O_2$ radicals consumed, was 174 ± 30%, suggesting that the majority of reaction 4 proceeds to give NO_2 and, by implication, $CF_3C(O)O$ radicals. In this calculation, allowance was made for loss of F atoms via reaction with O_2 and NO using $k_6 = 1.9 \times 10^{-13}$ cm^3 molecule^{-1} s^{-1} [14] and $k(F + NO \rightarrow FNO) = 5.5 \times 10^{-12}$ cm^3 molecule^{-1} s^{-1} [25] and for the fact that 14% of the CF_3CO radicals formed in the system decompose via reaction 1 (see discussion in the previous two sections).

The fact that the NO_2 yield exceeds 100% shows that the alkoxy radical $CF_3C(O)O$ formed in reaction 4 rapidly decomposes to give CF_3 radicals which add O_2 to form CF_3O_2 radicals which then react with NO to give more NO_2. The presence of additional processes forming NO_2 subsequent to reaction 4 increases the time taken for the NO_2 to reach a maximum. Hence, the rate constant derived from the data in Figure 7, $k_4 = (1.14 \pm 0.15) \times 10^{-11}$ cm^3 molecule^{-1} s^{-1}, is actually a lower limit. Thus, we report $k_4 > 9.9 \times 10^{-12}$ cm^3 molecule^{-1} s^{-1}.

As seen in Figure 6, the NO_2 concentration reaches a limiting value 15 μs after the radiolysis pulse. Thereafter, the NO_2 concentration is unchanged. This behavior places an upper limit of 15 μs for the lifetime of $CF_3C(O)O$ radicals with respect to decomposition via reaction 10; hence $k_{12} > 6 \times 10^4$ s^{-1}.

$$CF_3C(O)O + M \rightarrow CF_3 + CO_2 + M \qquad (12)$$

To provide insight into the origin of the positive intercept in the plot of k^{1st} versus [NO] shown in Figure 7, the chemical system was modeled using the Acuchem program[22] with the chemical mechanism given in Table 2. Kinetic data were taken from the literature.[14,16,18,23,24-26] The modeling exercise was an

TABLE 2: Chemical Mechanism Used To Model the NO_2 Formation Traces

reaction	rate constant[a]	ref
$F + CF_3CHO \rightarrow CF_3CO + HF$	2.3×10^{-11}	this work
$F + O_2 + M \rightarrow FO_2 + M$	1.9×10^{-13}	14
$F + NO \rightarrow FNO$	5.5×10^{-12}	25
$CF_3CO + O_2 + M \rightarrow CF_3C(O)O_2 + M$	7.3×10^{-13}	this work
$CF_3CO + M \rightarrow CF_3 + CO + M$	1.2×10^5	this work
$CF_3C(O)O_2 + NO \rightarrow CF_3C(O)O + NO_2$	$1.0\text{–}2.5 \times 10^{-11}$	see text
$CF_3C(O)O_2 + NO_2 \rightarrow CF_3C(O)O_2NO_2$	6.6×10^{-12}	26
$CF_3C(O)O + M \rightarrow CF_3 + CO_2$	$0.01\text{–}1.0 \times 10^{8}$[b]	see text
$CF_3 + O_2 + M \rightarrow CF_3O_2$	8.5×10^{-12}	16
$CF_3O_2 + NO \rightarrow CF_3O + NO_2$	1.8×10^{-11}	18
$CF_3O_2 + NO_2 + M \rightarrow CF_3O_2NO_2 + M$	6.0×10^{-12}	18
$CF_3O + NO \rightarrow COF_2 + FNO$	5.2×10^{-11}	24
$CF_3O + NO_2 + M \rightarrow CF_3ONO_2$	1.5×10^{-11}	23

[a] Units of cm^3 molecule^{-1} s^{-1}. [b] Units of s^{-1}.

iterative process consisting of three steps. First, the mechanism in Table 2 was used to simulate the formation of NO_2. Second, a regression analysis was used to fit a first-order rise to the NO_2 formation. The resulting pseudo rate constant was then compared to that expected from the product $k_4[NO]_0$. Third, values of k_4 and k_{12} were then varied and the sequence repeated.

Several insights were provided by the modeling exercise. First, consistent with the experimental observations, the simulated NO_2 formation trace was well fit by first-order kinetics even though NO_2 is produced by the reaction of both $CF_3C(O)O_2$ and CF_3O_2 radicals with NO. Second, the pseudo-first-order NO_2 rise time was in all cases slower than the product $k_4[NO]_0$. Third, the NO_2 yields (expressed relative to the formation of $CF_3C(O)O_2$ radicals) were consistent with the experimental observation of 173 ± 30%. Fourth, the pseudo-first-order rate constant for the formation of NO_2 was dependent on the values of both k_4 and k_{12} used in the model. k_4 obviously determines the rate of NO_2 production from $CF_3C(O)O_2$ directly. k_{12} determines the rate at which CF_3 and hence CF_3O_2 radicals are formed and, hence, determines the subsequent NO_2 formation. If values of k_{12} are chosen such that the time scale for $CF_3C(O)O$ radical decomposition is comparable to that of the experimental time scale (μs), then plots of the simulated k^{1st} values versus [NO] gave positive intercepts. As an example, the dotted line in Figure 7 shows the behavior predicted using $k_4 = 2.5 \times 10^{-11}$ cm^3 molecule^{-1} s^{-1} and $k_{12} = 1.5 \times 10^6$ s^{-1}. The intercept, 2×10^4 s^{-1}, is indistinguishable from the value of $(3.9 \pm 2.4) \times 10^4$ s^{-1} observed experimentally. It seems likely that the cause of the positive intercept observed in Figure 7 is that decomposition of $CF_3C(O)O$ radicals occurs on a time scale which is comparable to that of the experimental observations.

While it is pleasing that the chemical mechanism in Table 2 reproduces the experimentally observed NO_2 formation profiles, the derivation of a precise value of k_4 is clearly complex. In view of the complexities in the present system, we choose to quote a lower limit of $k_4 > 9.9 \times 10^{-12}$ cm^3 molecule^{-1} s^{-1}. The kinetics and products of the reaction of $CF_3C(O)O_2$ radicals with NO measured in the present work are consistent with the available literature data base for the reaction of halogenated peroxy radicals with NO.[20]

FTIR Results

Study of the Rate Constant Ratio k_2/k_1. In a set of experiments designed to complement those described above, the rate constant ratio k_2/k_1 was determined using an FTIR-smog chamber system. In these experiments, $Cl_2/CF_3CHO/O_2$ mixtures in 80–700 Torr of N_2 diluent with, and without, added NO were irradiated using UV blacklamps. The loss of CF_3CHO and the formation of products were monitored by FTIR spectroscopy.

Following the irradiation of $CF_3CHO/Cl_2/O_2/N_2$ mixtures, five carbon-containing products were identified: $CF_3O_3CF_3$, CF_3-

OH, CO, CO_2, and COF_2. The observation of these products is consistent with the following reactions occurring in the chamber:

$$Cl + CF_3CHO \rightarrow CF_3CO + HCl \quad (13)$$

$$CF_3CO + M \rightarrow CF_3 + CO + M \quad (1)$$

$$CF_3CO + O_2 + M \rightarrow CF_3C(O)O_2 + M \quad (2)$$

$$CF_3 + O_2 + M \rightarrow CF_3O_2 + M \quad (7)$$

$$CF_3C(O)O_2 + CF_3C(O)O_2 \rightarrow CF_3C(O)O + CF_3C(O)O + O_2 \quad (14a)$$

$$CF_3C(O)O \rightarrow CF_3 + CO_2 \quad (12)$$

$$CF_3O_2 + RO_2\ (R = CF_3, CF_3CO) \rightarrow CF_3O + RO + O_2 \quad (15)$$

$$CF_3O + CF_3CHO \rightarrow CF_3OH + CF_3CO \quad (16)$$

$$CF_3O + CF_3O_2 + M \rightarrow CF_3OOOCF_3 \quad (17)$$

$$CF_3OH \rightarrow COF_2 + HF \quad (18)$$

In addition to the identified carbon-containing products, an unidentified product which we will label as "X" was observed with IR features at 762, 1053, 1298, and 1859 cm^{-1}. The unknown product X decayed rapidly with a lifetime of approximately 100 s when reaction mixtures were allowed to stand in the dark. The CF_3OH product also decayed when reaction mixtures were left to stand in the dark. The rate of decay of CF_3OH was substantially slower than that of the unknown X. CF_3OH decay giving COF_2 (and presumably HF) was first order with a rate in the range 2–3 $\times 10^{-4}$ s^{-1}. HF absorbs in the infrared at frequencies above 3800 cm^{-1} and is not detected by our spectrometer. The decay of CF_3OH in glass reaction chambers is well documented and probably heterogeneous in nature.[8,27] During the decay of the unknown X, the concentration of CF_3OH in the reaction chamber increased slightly while that of CF_3CHO decreased slightly. When X had decayed completely, there was no further loss of CF_3CHO. CF_3OH is a product of the reaction of CF_3O radicals with saturated organic compounds.[8,27] It seems reasonable to suppose that the unknown X is a compound that can decompose to generate CF_3O radicals which would then give CF_3OH via reaction 16.

There are several possibilities for X that need consideration: $CF_3C(O)OOC(O)CF_3$, $CF_3C(O)OOOCF_3$, and $CF_3C(O)OOCF_3$. These compounds could be formed in reaction 14b, 19, or 20

$$CF_3C(O)O_2 + CF_3C(O)O_2 \rightarrow CF_3(O)OOC(O)CF_3 + O_2 \quad (14b)$$

$$CF_3C(O)O_2 + CF_3O + M \rightarrow CF_3C(O)OOOCF_3 + M \quad (19)$$

$$CF_3C(O)O + CF_3O + M \rightarrow CF_3C(O)OOCF_3 + M \quad (20)$$

In the previous section a lower limit for the lifetime of $CF_3C(O)O$ of 15 μs with respect to dissociation via reaction 12 was derived. The radical–radical reaction (20) cannot compete with reaction 12 for $CF_3C(O)O$ radicals, and hence X cannot be $CF_3C(O)OOCF_3$. In previous studies of the products following the self-reaction of CF_3O_2, $CF_3CF_2O_2$, and CF_3CFHO_2 radicals, the trioxides formed by the association reaction of CF_3O with RO_2 radicals (R = CF_3,[7] CF_3CF_2,[28] CF_3CFH[2]) were important products. By analogy to these previous studies, it seems likely that "X" is the trioxide $CF_3C(O)OOOCF_3$. The 762-cm^{-1} IR

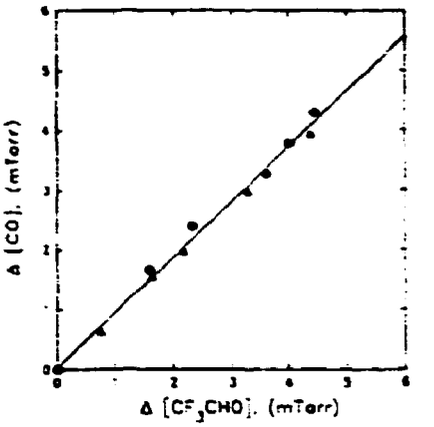

Figure 8. Plot of the observed yield of CO as a function of the loss of CF_3CHO following the irradiation of mixtures of 25–30 mTorr of CF_3CHO and 110–115 mTorr of Cl_2 at 700 Torr total pressure of N_2 with (▲) and without (●) the addition of 34 mTorr of NO.

feature displayed by the unknown X can be assigned to a symmetric O–O–O stretch. The peroxide $CF_3C(O)OOC(O)CF_3$ is not expected to have an IR feature at this frequency. The IR features displayed by X at 1053, 1298, and 1859 cm^{-1} are characteristic of C–C, C–F, and C=O stretches and are consistent with the identification of X as the trioxide $CF_3C(O)OOOCF_3$. The results presented above can be compared to an analogous study reported recently by Richer et al.,[29] who irradiated Cl_2/CF_3CHO mixtures in 720 Torr of air diluent. Observed products were COF_2, CF_3OH, CO_2, and an unknown which was believed to be $CF_3C(O)OOOCF_3$. Richer et al.[29] did not report any CF_3OOOCF_3 or CO products. The high oxygen partial pressure used by Richer et al. explains the absence of CO. There are two possible explanations for the absence of CF_3OOOCF_3. Either the initial CF_3CHO concentration was sufficiently high that CF_3O radicals were efficiently scavenged by reaction 16 or CF_3OOOCF_3 was produced but not identified. The initial conditions used by Richer et al.[29] are unclear, and it is not possible to distinguish between these two possibilities. Richer et al.[29] did not report absolute product yields, and so a quantitative comparison of the results form the present work and those of Richer et al.[29] is not possible.

The aim of the present FTIR experiments was to establish the relative importance of reactions 1 and 2 as fates for CF_3CO radicals in the atmosphere, and not to conduct an exhaustive study of the products following the self-reaction of $CF_3C(O)O_2$ radicals. To measure k_1/k_2, we need only to consider two products: CO and CO_2. For each CF_3CO radical that decomposes, one CO molecule is formed. For each CF_3CO radical that reacts with O_2, one CO_2 molecule is formed. This statement is true irrespective of the identity of the unknown X, so long as sufficient time is allowed for the X to decompose. In the FTIR experiments the reaction mixtures were analyzed after X had decomposed completely.

Assuming that reactions 1, 2, 7, 12, 13, 14a, 15–18, and –19

$$CF_3C(O)OOOCF_3 + M \rightarrow CF_3O + CF_3C(O)O_2 + M \quad (-19)$$

describe the chemistry occurring following the irradiation of $CF_3CHO/Cl_2/O_2/N_2$ mixtures and that CO and CO_2 are not lost in any process, then the sum of the molar yields of CO and CO_2 should be 100%. Experimentally, this was observed to be the case. The relative yields of CO and CO_2 were dependent upon the O_2 partial pressure present in the reaction chamber. As the O_2 concentration increased, the CO_2 yield increased at the expense of CO. Figures 8 and 9 show results from the extreme cases where $[O_2] \approx 0.0$ and 147 Torr. In 700 Torr of N_2 diluent with no added O_2, the CO yield was 93 ± 8%, and traces of CO_2 were

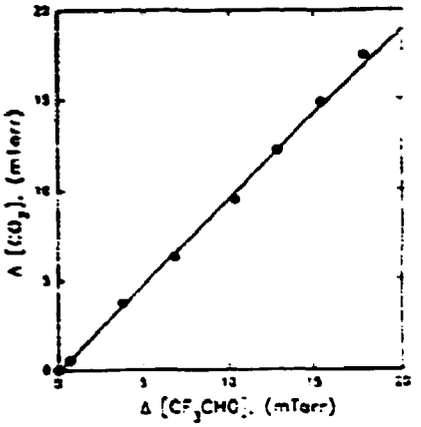

Figure 9. Plot of the observed yield of CO_2 as a function of the loss of CF_3CHO following the irradiation of a mixture of 29.5 mTorr of CF_3CHO and 112 mTorr of Cl_2 at 700 Torr total pressure of air.

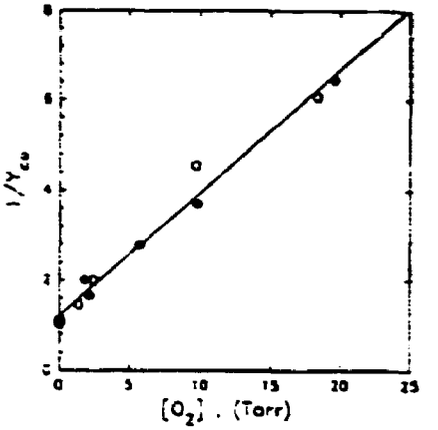

Figure 10. Plot of the reciprocal of the molar CO yield versus the partial pressure of O_2 following the irradiation of $CF_3CHO/Cl_2/O_2$ mixtures in 700 Torr total pressure of N_2 diluent. Open symbols were obtained in the absence of NO. Filled points were obtained with 25–30 mTorr of NO initially present in the reaction mixture.

observed corresponding to a yield of 6 ± 2%. In 700 Torr of air with $[O_2]$ = 147 Torr, the yield of CO_2 was 97 ± 4% with traces of CO observed corresponding to a yield of 5 ± 2%. With O_2 concentrations of 2–40 Torr, both CO and CO_2 were observed products. With the assumptions that (i) CO is produced only from the reaction 1, (ii) reactions 1 and 2 are the sole fate of CF_3CO radicals, and (iii) CO is not lost by any process, the following expression holds:

$$1/Y_{CO} = 1 + (k_2/k_1)[O_2] \qquad (I)$$

where Y_{CO} is the molar yield of CO, k_1 and k_2 are the rate constants for reactions 1 and 2, and $[O_2]$ is the concentration of O_2. Experiments were performed with the partial pressure of O_2 varied over the range 0–40 Torr at a constant total pressure of 700 Torr made up with N_2 diluent. Figure 10 shows a plot of $1/Y_{CO}$ versus $[O_2]$. The experimental data are clearly consistent with the functional form of expresson I.

As noted above, in the derivation of expression I it is assumed that there are no significant losses of CO in the chamber. There are three species present in the chamber that may react with CO: Cl atoms, CF_3O, and possibly CF_3O_2 radicals.

$$Cl + CO + M \rightarrow ClCO + M \qquad (21)$$

$$CF_3O + CO \rightarrow CF_3 + CO_2 \qquad (22)$$

$$CF_3O_2 + CO \rightarrow CF_3O + CO_2 \qquad (23)$$

The rate constant for reaction 21 (2.9×10^{-14} cm^3 molecule^{-1} s^{-1} at 700 Torr of N_2)[16] is 62 times slower than for the reaction of Cl atoms with CF_3CHO (1.8×10^{-12} cm^3 molecule^{-1} s^{-1}).[13] For the typical range of CF_3CHO conversions used in the present work (2–25%), loss of CO via reaction 21 is negligible.

Quantitative assessment of the role of reactions 22 and 23 is hampered by the sparsity of the kinetic data for CF_3O and CF_3O_2 radicals. To test for the importance of reactions 22 and 23, $CF_3CHO/Cl_2/O_2/N_2$ mixtures were irradiated in the presence of 20–40 mTorr of added NO. NO reacts rapidly with CF_3O and CF_3O_2 radicals, $k_{24} = (5.2 \pm 2.7) \times 10^{-11}$ [24] and $k_{25} = 1.8 \times 10^{-11}$ cm^3 molecule^{-1} s^{-1},[18] thereby removing any possible complications caused by reactions 22 and 23.

$$CF_3O + NO \rightarrow COF_2 + FNO \qquad (24)$$

$$CF_3O_2 + NO \rightarrow CF_3O + NO_2 \qquad (25)$$

As seen from Figure 10, there was no observable difference in results obtained with, and without, NO present in the reaction chamber, showing that reactions 22 and 23 are not a complication in the present work.

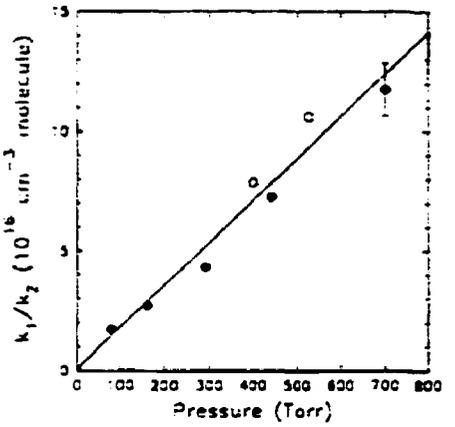

Figure 11. Plot of k_1/k_2 as a function of total pressure of N_2 diluent. Open symbols were obtained in the absence of NO. Filled points were obtained with 25–30 mTorr of NO initially present in the reaction mixture.

Linear least-squares analysis of the data in Figure 10 gives a slope = $k_2/k_1 = (7.4 \pm 0.6) \times 10^{-18}$ cm^3 molecule^{-1}, and an intercept = 1.3 ± 0.4. Quoted errors are 2 standard deviations. The value of $k_2/k_1 = (7.4 \pm 0.6) \times 10^{-18}$ cm^3 molecule^{-1} obtained at 700 Torr of N_2 diluent is consistent with that of $k_2/k_1 = (6.1 \pm 4.2) \times 10^{-18}$ cm^3 molecule^{-1} at 1000 mbar of SF_6 diluent obtained using the pulse radiolysis technique.

To investigate the effect of total pressure on the rate constant ratio k_2/k_1, experiments were performed at total pressures ranging from 80 to 700 Torr (N_2 used as diluent). The results are presented in Figure 11. The data point at 700 Torr was derived from the slope of the plot in Figure 10; the error bars represent the statistical uncertainty (2 standard deviations). All other data points in Figure 11 were derived from single determinations and hence have not been ascribed statistical uncertainties. It should be noted that the single-point determinations will be less certain than the value derived at 700 Torr from the composite data set shown in Figure 10. We estimate that the single-point determinations have a ±20% uncertainty.

From Figure 11 it can be seen that the rate constant ratio k_1/k_2 decreases as the total pressure is reduced. Another way to express this is to state that reaction 1 displays a greater pressure dependence than reaction 2. This finding is entirely consistent with the greater molecular complexity of the adduct in reaction 2. As seen from Figure 11, within the experimental uncertainties, there is no distinguishable difference between data acquired with and without NO. The rate constant ratio k_1/k_2 displays an

essentially linear dependence on total pressure over the range studied. The entire data set in Figure 11 have been arbitrarily fit using a linear least-squares regression to give $k_1/k_2 = (5.44 \pm 1.05) \times 10^{-3}$[M] molecule cm^{-3} where [M] is the third-body concentration in molecule cm^{-3}.

Implications for Atmospheric Chemistry. The results presented here substantially improve our understanding of the atmospheric chemistry of CF_3CO_x radicals. As demonstrated here, CF_3CO radicals undergo both decomposition to give CF_3 radicals and CO, and reaction with O_2 to give $CF_3C(O)O_2$ radicals.

$$CF_3CO + M \rightarrow CF_3 + CO + M \quad (1)$$

$$CF_3CO + O_2 + M \rightarrow CF_3C(O)O_2 + M \quad (2)$$

As shown herein, at 296 ± 2 K and 700 Torr total pressure of N_2 diluent, $k_2/k_1 = (7.4 \pm 0.6) \times 10^{-18}$ cm^3 molecule^{-1}. Reactions 1 and 2 are of equal importance at an O_2 partial pressure of 4 Torr. In the presence of 760 Torr of air (160 Torr O_2), 97% of CF_3CO radicals will react to give $CF_3C(O)O_2$ with 3% decomposing to CF_3 and CO. In the earth's atmosphere both temperature and pressure decrease with increasing altitude. It is important to consider the effect of changes in temperature and pressure upon the relative importance of reactions 1 and 2. A decrease in temperature will cause both reactions 1 and 2 to slow down. Reaction 1 is a unimolecular decomposition; the rate of reaction 1 is expected to decrease substantially as the temperature is lowered. In contrast, the rate of the bimolecular association reaction 2 is not expected to be strongly temperature dependent. Using the value of $k_1 = (1.2 \pm 0.8) \times 10^5$ s^{-1} measured in the presence of 1 atm of SF_6 diluent in the present work and assuming a typical A factor for this type of reaction of 10^{13} s^{-1} gives the activation energy for reaction 1 as 10.8 kcal mol^{-1}. This estimate is consistent with an earlier estimate of $E_a = 10.0$ kcal mol^{-1} by Amphlett and Whittle[30] and a recent calculation of $E_a = 11.4$ kcal mol^{-1} by Francisco[31] but is inconsistent with the value of $E_a = 19.8$ kcal mol^{-1} deduced by Kerr and Wright.[32] As noted by Francisco,[31] the value reported by Kerr and Wright may be in error due to large uncertainties in the assumed parameters used in the RRKM modeling of the experimental data. With $E_a = 10.8$ kcal mol^{-1}, the rate of reaction 1 is expected to drop by a factor of 1100 on moving from 296 to 215K (corresponding to an altitude of 20 km). In contrast, by analogy to the available data for the association reaction of CF_3 radicals with O_2, the rate of reaction 2 is not expected to decrease dramatically. Indeed, the high-pressure limiting rate constant for the association reaction between CF_3 radicals and O_2 actually increases by 40% over this temperature range.[16] At reduced temperature, reaction 2 is then expected to be strongly favored over reaction 1.

At high altitudes the total pressure is substantially less than that at sea level (at 20 km the total pressure is 50 mbar). The rates of both reactions 1 and 2 will decrease as the pressure is reduced. As expected on the basis of the numbers of degrees of freedom in the molecules and as demonstrated in the present work, reaction 1 is more sensitive to pressure than reaction 2. At reduced pressure, reaction 2 is then expected to be favored over reaction 1.

The effects of reduced temperatures and pressures with increasing altitude reinforce each other in favoring reaction 2 over reaction 1. To quantify the relative importance of reactions 1 and 2 in the atmospheric chemistry of CF_3CO radicals, a simple 1-D model was used with the following input and assumptions. First, temperature and pressure profiles were taken from the U.S. Standard Atmosphere[33] up to 20 km. Second, CF_3CO radicals were assumed to be generated throughout the atmosphere at a rate which was linearly proportional to the atmospheric density (pressure). Third, the activation energy of reaction 1 was taken to be 10.8 kcal mol^{-1}, and reaction 2 was assumed to be temperature independent. Fourth, a ratio of $k_2/k_1 = (7.4 \pm 0.6) \times 10^{-18}$ cm^3 molecule^{-1} at 700 Torr and 296 K was used. Finally, it was assumed that the rate constant ratio k_1/k_2 was linearly dependent on the total pressure. Under these assumptions it was calculated that 99.5% of CF_3CO radicals formed in the atmosphere are converted into $CF_3C(O)O_2$ radicals. For all practical purposes the exclusive atmospheric fate of CF_3CO radicals is reaction with O_2.

Using $k_2 = 7 \times 10^{-13}$ cm^3 molecule^{-1} s^{-1}, we calculate a lifetime of 0.3 μs for CF_3CO radicals with respect to conversion into $CF_3C(O)O_2$ in 760 Torr of air. It is shown here that $CF_3C(O)O_2$ radicals react rapidly with NO to give $CF_3C(O)O$ radicals and NO_2. Using $k_4 > 9.9 \times 10^{-12}$ cm^3 molecule^{-1} s^{-1} together with a background tropospheric NO level of 2.5×10^9 cm^{-3} gives the lifetime of $CF_3C(O)O_2$ with respect to reaction with NO as <7 min. Reaction with NO is likely to be a major fate of $CF_3C(O)O_2$ radicals. It has been shown in the present work that $CF_3C(O)O$ radicals decompose rapidly to give CF_3 radicals and CO_2. An upper limit of 15 μs has been established for the lifetime of the $CF_3C(O)O$ radical at 296 K. If we assume an A factor of 10^{13} s^{-1} for this unimolecular decomposition, then we can derive $E_a < 11.1$ kcal mol^{-1}. This result is consistent with the value of $E_a = 4.9$ kcal mol^{-1} calculated by Francisco.[31] With an upper limit of $E_a = 11.1$ kcal mol^{-1} for the activation energy for the unimolecular decomposition of $CF_3C(O)O$ radicals, the rate of decomposition at 215 K will be approximately 1200 times slower than at 296 K. From the upper limit of 15 μs measured here at 296 K, the lifetime of $CF_3C(O)O$ radicals with respect to decomposition at a typical stratospheric temperature of 215 K is estimated to be <0.02 s. In the atmosphere the sole fate of $CF_3C(O)O$ radicals will be decomposition to produce CF_3 radicals and CO_2.

Finally, the results from the present work need to be placed within the broader perspective of assessing the environmental impact of HFCs. As stated in the introduction, HFCs have been chosen as CFC replacements in certain applications. The choice of HFCs was motivated by a number of factors, not the least of which is the fact that HFCs do not contain chlorine and so have no ozone depletion potential associated with the well established chlorine catalytic cycles. The atmospheric oxidation of HFCs produces a number of interesting fluorinated oxy and peroxy radicals such as FCO, $FC(O)O_2$, $FC(O)O$, CF_3O_2, CF_3O, $CF_3C(O)$, $CF_3C(O)O_2$, and $CF_3C(O)O$ radicals. Recently, there has been speculation regarding the possible participation of these radicals in catalytic ozone destruction cycles. The present work serves to define the atmospheric chemistry of the CF_3CO_x family. We show here that CF_3CO radicals are converted rapidly into $CF_3C(O)O_2$ radicals which in turn react with NO to give $CF_3C(O)O$ radicals. Carbon–carbon bond scission in $CF_3C(O)O$ radicals rapidly converts CF_3CO_x radicals into CF_3Ox radicals. CF_3O_x radicals do not impact stratospheric ozone,[34-38] and therefore CF_3CO_x radicals will not impact stratospheric ozone. We have recently arrived at the same conclusion for FCO_x radicals.[25] The available data show that neither FCO_x, CF_3O_x, nor CF_3CO_x radicals present a threat to stratospheric ozone. Hence, the use of HFCs as replacement compounds for CFCs is not expected to impact stratospheric ozone.

Acknowledgment. We thank Steve Japar (Ford) for helpful discussions and Greg Khitrov and Joe Francisco (Wayne State University) for providing the CF_3CHO sample used at Ford. Financial support for the work at Risø was provided by the Commission of the European Communities and by AFEAS under Contract No. CTR93-45/P43-120.

References and Notes

(1) Wallington, T. J.; Nielsen, O. J. *Chem. Phys. Lett.* **1991**, *187*, 33.
(2) Wallington, T. J.; Hurley, M. D.; Ball, J. C.; Kaiser, E. W. *Environ. Sci. Tech.* **1992**, *26*, 1318.

(3) Nielsen, O. J.; Gamberg, E.; Sehested, J.; Wallington, T. J.; Hurley, M. D. *J. Phys. Chem.*, in press.
(4) Wallington, T. J.; Nielsen, O. J. *Chem. Phys. Lett.* **1991**, *187*, 33.
(5) Wallington, T. J.; Bull, J. C.; Nielsen, O. J.; Barthiewicz, E. *J. Phys. Chem.* **1992**, *96*, 1241.
(6) Nielsen, O. J.; Ellermann, T.; Barthiewicz, E.; Wallington, T. J.; Hurley, M. D. *Chem. Phys. Lett.* **1992**, *192*, 82.
(7) Nielsen, O. J.; Ellermann, T.; Sehested, J.; Barthiewicz, E.; Wallington, T. J.; Hurley, M. D. *Int. J. Chem. Kinet.* **1992**, *24*, 1009.
(8) Sehested, J.; Wallington, T. J. *Environ. Sci. Tech.* **1992**, *27*, 146.
(9) Nielsen, O. J.; Ellermann, T.; Sehested, J.; Wallington, T. J. *J. Phys. Chem.* **1992**, *96*, 10875.
(10) Nielsen, O. J. Risø-R-480, 1984.
(11) Wallington, T. J.; Japar, S. M. *J. Atmos. Chem.* **1989**, *9*, 399.
(12) Sherbacr, H.; Conrad, F. *J. Am. Chem. Soc.* **1950**, *72*, 3371.
(13) Wallington, T. J.; Hurley, M. D. *Int. J. Chem. Kinet.* **1993**, *25*, 819.
(14) Ellermann, T.; Sehested, J.; Nielsen, O. J.; Pagsberg, P.; Wallington, T. J. *Chem. Phys. Lett.* **1994**, *218*, 287.
(15) Caralp, F.; Lesclaux, R.; Dognon, A. M. *Chem. Phys. Lett.* **1986**, *129*, 433.
(16) DeMore, W. B.; Sander, S. P.; Golden, D. M.; Hampson, R. F.; Kurylo, M. J.; Howard, C. J.; Ravishankara, A. R.; Kolb, C. E.; Molina, M. J. Jet Propulsion Laboratory Publication 92-20, Pasadena, CA, 1992.
(17) Wallington, T. J.; Ellermann, T.; Nielsen, O. J. *J. Phys. Chem.* **1993**, *97*, 8442.
(18) Wallington, T. J.; Dagaut, P.; Kurylo, M. J. *Chem. Rev.* **1992**, *92*, 667.
(19) Marieq, M.; Szente, J. J. Private Communication, 1994.
(20) Sehested, J.; Nielsen, O. J.; Wallington, T. J. *Chem. Phys. Lett.* **1993**, *213*, 457.
(21) Sehested, J.; Nielsen, O. J.; Ellermann, T.; Wallington, T. J. *Int. J. Chem. Kinet.*, in press.
(22) Braun, W.; Herron, J. T.; Kahaner, D. K. *Int. J. Chem. Kinet.* **1988**, *20*, 51.
(23) Fockenberg, C.; Saathoff, H.; Zellner, R. Private communication.
(24) Sehested, J.; Nielsen, O. J. *Chem. Phys. Lett.* **1993**, *206*, 369.
(25) Wallington, T. J.; Ellermann, T.; Nielsen, O. J.; Sehested, J. *J. Phys. Chem.* **1994**, *98*, 2346.
(26) Wallington, T. J.; Nielsen, O. J.; Sehested, J. *Chem. Phys. Lett.*, in press.
(27) Chen, J.; Zhu, T.; Niki, H.; Mains, G. J. *Geophys. Res. Lett.* **1992**, *19*, 2215.
(28) Sehested, J.; Ellermann, T.; Nielsen, O. J.; Wallington, T. J.; Hurley, M. D. *Int. J. Chem. Kinet.* **1993**, *25*, 701.
(29) Richer, H. R.; Sodeau, J. R.; Burns, I. Proceedings of the STEP-HALOCIDE Workshop, University College, Dublin, Ireland, 1993.
(30) Amphlett, J. C.; Whittle, E. *Trans. Faraday Soc.* **1967**, *63*, 80.
(31) Francisco, J. S. *Chem. Phys. Lett.* **1992**, *191*, 7.
(32) Kerr, J. A.; Wright, J. P. *J. Chem. Soc., Faraday Trans 1* **1985**, *81*, 1471.
(33) U.S. Standard Atmosphere, 1976, NOAA, NASA, USAF, Washington, DC, 1976.
(34) Nielsen, O. J.; Sehested, J. *Chem. Phys. Lett.* **1993**, *213*, 433.
(35) Wallington, T. J.; Hurley, M. D.; Schneider, W. F. *Chem. Phys. Lett.* **1993**, *213*, 442.
(36) Marieq, M. M.; Szente, J. J. *Chem. Phys. Lett.* **1993**, *213*, 449.
(37) Fockenberg, Ch.; Saathoff, H.; Zellner, R. *Chem. Phys. Lett.* **1994**, *218*, 21.
(38) Ravishankara, A. R.; Turnipseed, A. A.; Jensen, N. R.; Barone, S.; Mills, M.; Howard, C. J.; Solomon, S. *Science* **1994**, *263*, 75.

ELSEVIER

26 August 1994

Chemical Physics Letters 226 (1994) 563–569

CHEMICAL PHYSICS LETTERS

Atmospheric chemistry of $CF_3C(O)O_2$ radicals. Kinetics of their reaction with NO_2 and kinetics of the thermal decomposition of the product $CF_3C(O)O_2NO_2$

Timothy J. Wallington [a,*], Jens Sehested [b], Ole J. Nielsen [b,*]

[a] *Research Staff, SRL-E3083, Ford Motor Company, Dearborn, MI 48121-2053, USA*

[b] *Section for Chemical Reactivity, Environmental Science and Technology Department, Riso National Laboratory, DK-4000 Roskilde, Denmark*

Received 21 March 1994; in final form 8 June 1994

Abstract

A pulse radiolysis technique has been used to measure a rate constant of $(6.6 \pm 1.3) \times 10^{-12}$ cm^3 molecule^{-1} s^{-1} for the association reaction between $CF_3C(O)O_2$ radicals and NO_2 at 295 K and one atmosphere total pressure of SF_6 diluent. A FTIR/smog chamber system was used to study the thermal decomposition $CF_3C(O)O_2NO_2$. The rate of decomposition of $CF_3C(O)O_2NO_2$ was independent of the total pressure of N_2 diluent over the range 100–700 Torr and was fit by the expression $k_{-1} = (1.9^{+2.6}_{-1.5}) \times 10^{16} \exp[(-14000 \pm 480)/T]$ s^{-1}. Implications for the atmospheric chemistry of CFC replacements are discussed.

1. Introduction

Industrial production of chlorofluorocarbons (CFCs) is being phased out and replacements are being sought. Hydrofluorocarbons (HFCs) and hydrochlorofluorocarbons (HCFCs) are two classes of potential CFC substitutes. Prior to their large scale use, it is important to establish the environmental impact of the release of HFCs and HCFCs. In discussions of the environmental impact of HFCs and HCFCs an important issue is the potential formation of long-lived oxidation products which may accumulate in the environment. The atmospheric oxidation of HFCs and HCFCs proceeds via the formation of peroxy radicals (RO_2). It is well recognized that peroxy radicals can react with NO_2 in the atmosphere to produce peroxy nitrates (RO_2NO_2). Alkyl peroxy nitrates ($R = CH_3$, C_2H_5, etc.) are relatively unstable and rapidly decompose to regenerate RO_2 radicals and NO_2. In contrast, carbonyl peroxy nitrates ($R = CH_3C(O)$, C_2H_5CO, etc.) are considerably more stable and can survive to be transported in the atmosphere over large distances (up to 1000 km) [1,2].

To place discussions of the environmental impact of HFCs and HCFCs on a firm scientific basis, data are required concerning the formation and persistence of halogenated acetyl peroxy nitrates. Unfortunately, with the exception of a recent study by Zabel et al. [3] no such data exist. As part of a joint program between our two laboratories to survey the atmospheric chemistry and, hence, the environmen-

* Corresponding author.

SSDI 0009-2614(94)00751-B

tal impact of HFCs and HCFCs [4–9] we have used pulse radiolysis and long pathlength Fourier transform infrared techniques to provide kinetic data for

$$CF_3C(O)O_2 + NO_2 + M \rightarrow CF_3C(O)ONO_2 + M . \quad (1)$$

$$CF_3C(O)O_2NO_2 + M \rightarrow CF_3C(O)O_2 + NO_2 + M . \quad (-1)$$

Results are reported herein.

2. Experimental

Two different experimental systems were used. Both have been described in detail previously [10–12] and will only be discussed briefly here.

2.1. Pulse radiolysis system

$CF_3C(O)O_2$ radicals were generated by the radiolysis of $SF_6/O_2/CF_3CHO$ gas mixtures in a one liter stainless steel reactor with a 30 ns pulse of 2 MeV electrons from a Febetron 705B field emission accelerator. SF_6 was always in great excess and was used to generate fluorine atoms.

$$SF_6 + 2\,MeV\ e^- \rightarrow F + products . \quad (2)$$

$$F + CF_3CHO \rightarrow CF_3CO + HF . \quad (3)$$

$$CF_3CO + O_2 + M \rightarrow CF_3C(O)O_2 + M . \quad (4)$$

In the present series of experiments the yield of F atoms at 1000 mbar of SF_6 was 2.77×10^{15} cm^{-3} at full irradiation dose [13]. The rate of reaction (1) was studied by monitoring the loss of NO_2 as deduced from its transient absorption at 400 nm. To monitor the transient UV absorption, the output of a pulsed 150 Watt Xenon arc lamp was multi-passed through the reaction cell using internal White cell optics (120 cm path length). A McPherson grating monochromator, Hamamatsu R 955 photomultiplier and Biomation 8100 waveform digitizer were used to detect and record the light intensity at the desired wavelength. The spectral resolution used was 0.8 nm. Reagent concentrations used were: SF_6, 960 mbar; O_2, 35 mbar; NO_2, 0.24–0.75 mbar; and CF_3CHO, 5 mbar. All experiments were performed at 296 ± 2 K. Ultra high purity O_2 was supplied by L'Air Liquide. SF_6 (99.97%) was supplied by Gerling and Holz. NO_2 (99.8%) was obtained from Messer Griesheim. CF_3CHO was synthesized by the dropwise addition of trifluoroacetaldehyde methyl hemiacetal to a H_2SO_4/P_2O_5 slurry. IR analysis did not reveal any observable impurities. All reagents were used as received.

2.2. FTIR-smog chamber system

The FTIR system was interfaced to a 140 ℓ pyrex reactor. $CF_3C(O)O_2NO_2$ was generated by the UV irradiation of mixtures of CF_3CHO, 20–30 mTorr; Cl_2, 100–150 mTorr; NO_2, 6–9 mTorr; O_2, 10 Torr; 100–700 Torr total pressure of N_2 diluent at 285–303 K (760 Torr = 1013 mbar). 'Blacklamps' which emit strongly in the region 300–400 nm were used to provide the UV radiation, reactions (1), (4) and

$$Cl_2 + h\nu \rightarrow 2Cl . \quad (5)$$

$$Cl + CF_3CHO \rightarrow CF_3CO + HCl . \quad (6)$$

The 140 ℓ pyrex reactor was not equipped with any temperature regulation equipment. Temperature regulation was achieved by altering the thermostat in the laboratory. The temperature of the laboratory was allowed to equilibrate overnight. Temperatures were measured using a mercury thermometer in contact with the pyrex reactor and were constant to within ± 0.2 K during each experiment. $CF_3C(O)O_2NO_2$ was monitored using the characteristic features at 1056 and 1170 cm^{-1}. An analyzing pathlength of 25 m and a resolution of 0.25 cm^{-1} was employed. Infrared spectra were derived from 32 co-added spectra.

Irradiation of the $CF_3CHO/Cl_2/O_2/NO_2$ mixtures was conducted in successive 10 s increments until all the NO_2 was consumed. Then a large excess of NO (50–80 mTorr) was added and the decay of $CF_3C(O)O_2NO_2$ monitored. The excess NO removes $CF_3C(O)O_2$ radicals via reaction (7), $k_7 > 9.9 \times 10^{-12}$ cm^3 molecule^{-1} s^{-1} [13], thereby precluding the reformation of $CF_3C(O)O_2NO_2$ via reaction (1).

$$CF_3C(O)O_2 + NO \rightarrow CF_3C(O)O + NO_2 . \quad (7)$$

CF_3CHO was synthesized by the dropwise addition of trifluoroacetaldehyde methyl hemiacetal to a

H_2SO_4/P_2O_5 slurry and was supplied by Greg Khitrov and Joe Francisco of Wayne State University. The IR spectrum of the CF_3CHO sample was consistent with that reported by Shechter and Conrad [14]. No impurities were detected. N_2 and O_2 (both 99.999%) and Cl_2 (99.999%) were obtained from Airco. NO_2 was prepared by reacting NO with a large excess of O_2. NO and Cl_2 (both research purity) were obtained from Matheson. All reagents were used as received.

3. Pulse radiolysis results; the rate constant k_1

Fig. 1 shows the transient absorption at 400 nm observed following the pulse radiolysis of a mixture of 960 mbar of SF_6, 5 mbar of CF_3CHO, 35 mbar of O_2, and 0.33 mbar of NO_2. The smooth solid line in Fig. 1 is a first-order fit to the transient. In all cases the observed decay of absorption was well fit by first-order kinetics. Of the species initially present in the reaction cell only NO_2 absorbs significantly at 400 nm. Control experiments were performed in which SF_6/CF_3CHO, $SF_6/CF_3CHO/O_2$, SF_6/O_2, or just SF_6 were radiolyzed; no change in absorption at 400 nm was observed. It seems reasonable to ascribe the change in absorption at 400 nm seen in Fig. 1 to the loss of NO_2 via reaction (1).

Pseudo-first-order NO_2 loss rates are plotted as a function of the initial NO_2 concentration in Fig. 2. As seen from Fig. 2, the pseudo-first-order rate constant, k^{1st}, increased linearly with $[NO_2]$. The initial F atom concentration employed in the present experiments (1.4×10^{-15} cm^{-3}) is a significant fraction (8%–24%) of that of the initial NO_2 concentration and deviations from pseudo-first-order kinetics may be expected. However, no such deviations were discernable within the experimental data scatter. Corrections have been applied to the $[NO_2]$ values given in Fig. 2 to account for the significant consumption of NO_2 during the reaction. Corrections were computed using the expression $[NO_2]_{corr}=[NO_2]_0-\frac{1}{2}[F]_0$. Corrections applied were in the range 4%–12%. Linear least-squares analysis of the data in Fig. 2 gives $k_1=(6.6\pm1.3)\times10^{-12}$ cm^3 molecule^{-1} s^{-1} (errors are 2 standard deviations). The y axis intercept in Fig. 2 is not statistically significant. There are two possible complications that need to be considered in the derivation of k_1 from the data shown in Figs. 1 and 2. First, there is the need to separate the time scale of $CF_3C(O)O_2$ radical formation from that of their subsequent reaction with NO_2. In the presence of 35 mbar of O_2 and one atmosphere total pressure of SF_6 diluent the lifetime of CF_3CO radicals with respect to conversion into $CF_3C(O)O_2$ radicals is 1.6 μs [13]. The NO_2 decay transients were fit from 3 μs after the radiolysis pulse so there is adequate separation of the time scales for $CF_3C(O)O_2$ radical formation and NO_2 decay. The second possible complication is the presence of unwanted secondary reactions leading to incomplete conversion of F atoms into $CF_3C(O)O_2$ radicals. Fluorine atoms are known to add to O_2 to give FO_2 radicals. Following the radiolysis pulse CF_3CHO and O_2 compete for the available F atoms, reaction (3) and

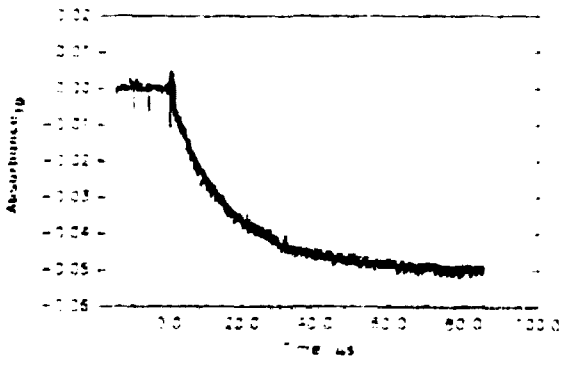

Fig. 1. Transient absorption at 400 nm observed following the pulse radiolysis of mixture of 960 mbar of SF_6, 5 mbar of CF_3CHO, 35 mbar of O_2, and 0.33 mbar of NO_2. The radiolysis dose was 53% of the maximum, the initial F atom concentration was $0.53\times2.77\times10^{15}\times0.96=1.41\times10^{15}$. The pathlength for the UV analysis light was 120 cm. The solid line is a first-order fit.

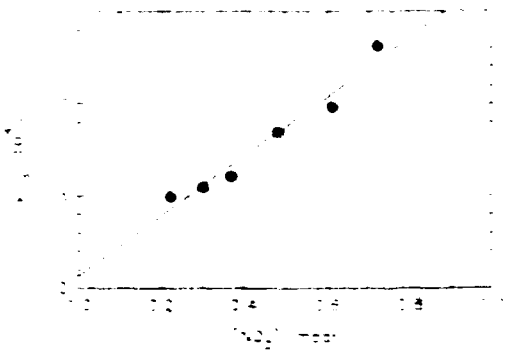

Fig. 2. Plot of k^{1st} versus $[NO_2]$. The line is a linear regression to the data.

$$F + O_2 + M \rightarrow FO_2 + M . \quad (8)$$

CF_3CO radicals formed in reaction (3) undergo both decomposition to give CF_3 radicals and CO and reaction with O_2 to give $CF_3C(O)O_2$ [13], reaction (4) and

$$CF_3CO \rightarrow CF_3 + CO . \quad (9)$$

Experiments were performed using $[CF_3CHO] = 5$ mbar and $[O_2] = 35$ mbar. Using rate constants for reactions (3) and (8) measured in our laboratory ($k_3 = 2.3 \times 10^{-11}$ cm^3 molecule^{-1} s^{-1} [13], $k_8 = 1.9 \times 10^{-13}$ cm^3 molecule^{-1} s^{-1} [15]), we calculate that 5.5% of the F atoms are converted into FO_2 and 94.5% into CF_3CO radicals. Using the rate constant ratio $k_4/k_9 = 6 \times 10^{-18}$ cm^3 molecule^{-1} measured in one atmosphere of SF_6 diluent [13] it can be calculated that in the presence of 35 mbar of O_2, 84% of the CF_3CO radicals produced in reaction (3) are converted into $CF_3C(O)O_2$ and 16% decompose to give CF_3 radicals and CO. CF_3 radicals will be rapidly converted into CF_3O_2 radicals. Hence, of the F atoms produced by the radiolysis pulse 5.5% are converted into FO_2 radicals, $0.945 \times 0.16 \times 100 = 15.1\%$ into CF_3O_2 radicals, and 79.4% into $CF_3C(O)O_2$.

FO_2 and CF_3O_2 radicals react with NO_2 with rate constants of 1.1×10^{-13} and 6.0×10^{-12} cm^3 molecule^{-1} s^{-1}, respectively [16,17]. The reactivity of CF_3O_2 radicals is indistinguishable from that of $CF_3C(O)O_2$ measured herein while FO_2 radicals react about 60 times more slowly. The presence of CF_3O_2 radicals will not interfere in the determination of k_1. Because the yield of FO_2 radicals is small (5.5%) their presence is not expected to significantly affect the measurement of k_1.

The decrease in absorbance at 400 nm can be combined with the literature value of σ_{NO_2} (400 nm:) = 6.0×10^{-19} cm^2 molecule^{-1} [18] to calculate the loss of NO_2. The loss of NO_2 in the six experiments given in Fig. 2, expressed as moles of NO_2 produced per mole of $CF_3C(O)O_2$ radicals consumed, was (114 ± 14)% consistent with the notion that the observed loss of absorption in Fig. 1 is caused by the loss of NO_2 via reaction (1). In this calculation allowance was made for loss of F atoms via reaction with O_2 using $k_8 = 1.9 \times 10^{-13}$ cm^3 molecule^{-1} s^{-1} [15].

Reaction (1) is an association reaction. At low pressures k_1 will display a dependence on the total pressure. By comparison with the existing data base [17], it is expected that reaction (1) will approach the high pressure limit at diluent pressures greater than 100 Torr of N_2. In one atmosphere of SF_6 diluent reaction (1) should be close to the high pressure limit. The value of k_1 measured in the present work is entirely consistent with the available literature data base for high pressure limiting rate constants for the reaction of peroxy radicals with NO_2 [17].

4. FTIR results: the rate constant k_{-1}

In a set of experiments designed to complement those described above, the rate of thermal decomposition of $CF_3C(O)O_2NO_2$ was studied using an FTIR-smog chamber system. In these experiments Cl_2/CF_3CHO/O_2/NO_2 mixtures in 700–700 Torr of N_2 diluent were irradiated using UV blacklamps. The formation of $CF_3C(O)O_2NO_2$ and loss of NO_2 were monitored using FTIR spectroscopy. When all the NO_2 had been consumed a large excess of NO was added and the slow decay of $CF_3C(O)O_2NO_2$ was monitored. The decay of $CF_3C(O)O_2NO_2$ followed first-order kinetics. Representative data are shown in Fig. 3. Linear least-squares analysis of the data in Fig. 3 together with other analogous plots give pseudo-

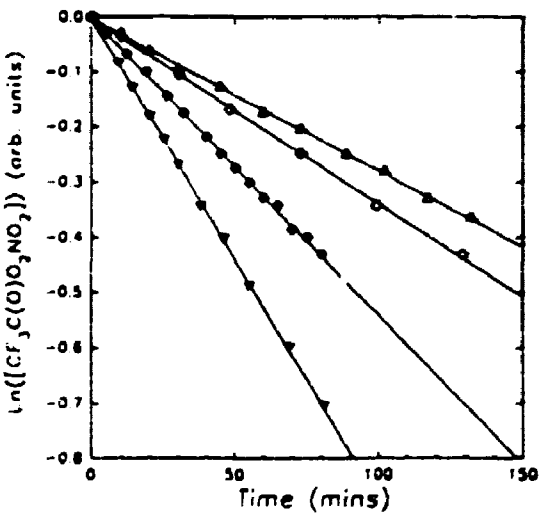

Fig. 3. Decay of $CF_3C(O)O_2NO_2$ versus time at (Δ) 296.1 K, (◇) 296.3 K, (●) 299.9 K, and (▼) 302.5 K.

first-order rate constants for the thermal decomposition of $CF_3C(O)O_2NO_2$. Results are listed in Table 1. An Arrhenius plot of the data from Table 1 is shown in Fig. 4. Experiments were performed at either 100 or 700 Torr total pressure (760 Torr = 1013 mbar). As seen from Fig. 4 there was no observable effect of total pressure, suggesting that reaction (−1) is at, or near, the high pressure limit at 100–700 Torr of N_2 diluent.

A potential complication in the present work is the formation of NO_2 from the thermal decomposition of $CF_3C(O)O_2NO_2$ via reaction (−1). The presence of NO_2 in the reaction chamber will lead to regeneration of $CF_3C(O)O_2NO_2$ via reaction (1). It can readily be shown that the observed rate of $CF_3C(O)O_2NO_2$ decay, k_{obs}, is related to the true rate of decay, k_{-1}, by the expression

Table 1
Measured values for k_{-1} in units of 10^{-4} s^{-1}

Temperature (K)	Total pressure (Torr) (nitrogen diluent)	k_{-1} (10^{-4} s^{-1})
303.1	100	1.72 ± 0.05 [a]
302.5	700	1.61 ± 0.04
299.9	700	0.981 ± 0.017
298.6	700	0.904 ± 0.038
296.3	700	0.626 ± 0.014
296.1	700	0.518 ± 0.016
284.8	700	0.112 ± 0.013

[a] Quoted errors are 2 standard deviations.

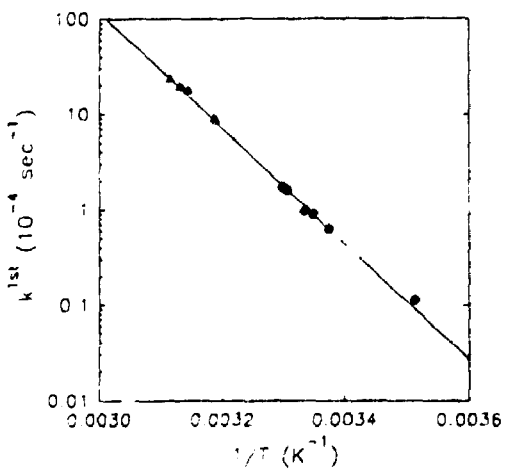

Fig. 4. Arrhenius plot for k_{-1}. Data from Zabel et al. [3] (▲) and the present work (●). The line is a linear regression to both sets of data.

$$k_{-1} = k_{obs}\{1 + (k_1[NO_2]/k_7[NO])\}.$$

The concentrations of NO and NO_2 in the chamber were monitored using their characteristic IR absorptions. Zabel et al. [3] have measured the ratio $k_1/k_7 = 0.64$ in one atmosphere of N_2 diluent. Using the rate constant k_1 measured as part of the present work and our previously reported lower limit of $k_7 > 9.9 \times 10^{-12}$ cm^3 molecule^{-1} s^{-1} [13] we derive $k_1/k_7 < 0.80$ in agreement with the result of Zabel et al. [3]. To correct our observed decay rates of $CF_3C(O)O_2NO_2$ for the effect of reaction (1) we have adopted a value of $k_1/k_7 = 0.64$. Corrections were in the range 9%–21% and have been applied to the data given in Fig. 4.

Zabel et al. [3] have also studied the kinetics of the thermal decomposition of $CF_3C(O)O_2NO_2$. As seen from Fig. 4, the results obtained by Zabel et al. [3] in 760 Torr of N_2 diluent are in excellent agreement with those from the present work. The line in Fig. 4 is a linear least-squares fit to the data from both studies and gives $k_{-1} = (1.9^{+7.6}_{-1.5}) \times 10^{16} \times \exp[(-14000 \pm 480)/T]$ s^{-1}. Quoted errors are 2 standard deviations. It should be noted that because the uncertainties in the A factor and activation energy are correlated the uncertainty in k_{-1} is not as great as might appear from the expression above. As the A factor increases so too must the activation energy. The expression $k_{-1} = 1.9 \times 10^{16} \times \exp[(-14000)/T]$ s^{-1} fits the experimental data to within 25% over the entire range studied. Reaction (1) is a radical association reaction and probably proceeds with little or no activation barrier. It then follows that the activation energy for reaction (−1) provides a measure of the $CF_3C(O)O_2$–NO_2 bond energy of 28 ± 1 kcal mol^{-1}. This value is indistinguishable from that in $CH_3C(O)O_2$–NO_2 (peroxy acetyl nitrate, PAN) of 27.0 ± 0.5 kcal mol^{-1} showing that the CF_3 group has little effect upon the RO_2–NO_2 bond strength.

Implications for atmospheric chemistry. The results presented here improve our understanding of the atmospheric chemistry of $CF_3C(O)O_2$ radicals. Using $k_1 = 6.6 \times 10^{-12}$ cm^3 molecule^{-1} s^{-1} together with an estimate for the background tropospheric concentration of NO_2 of 2.5×10^8 cm^{-3} [19], the lifetime of $CF_3C(O)O_2$ radicals with respect to reaction (1) is calculated to be 10 min. Other competing loss pro-

cesses for $CF_3C(O)O_2$ include reaction with NO, HO_2 radicals, and other peroxy radicals (RO_2). Concentrations of NO, NO_2, and RO_2 (represented by CH_3O_2) in the lower troposphere have been estimated by Atkinson [19] to be comparable at 2.5×10^8 cm^{-3}. The concentration of HO_2 is somewhat higher at approximately 10^9 cm^{-3} [19]. Using $k_7 > 9.9\times10^{-12}$ cm^3 $molecule^{-1}$ s^{-1} [13] gives a lifetime for $CF_3C(O)O_2$ with respect to reaction with NO of < 7 min. The reactivity of $CF_3C(O)O_2$ radicals towards HO_2 and RO_2 has not been studied. However, using the recommended kinetic data for the reactions of $CH_3C(O)O_2$ with HO_2 and CH_3O_2 (1.3×10^{-11} and 5.5×10^{-12} cm^3 $molecule^{-1}$ [17,20,21]) as a guide, gives lifetimes of 1.3 and 12 min for the reaction of $CF_3C(O)O_2$ radicals with HO_2 and RO_2 radicals, respectively. From the arguments above we conclude that the loss of $CF_3C(O)O_2$ radicals in the troposphere goes $\approx$ 70% via reaction with HO_2, 13% via reaction with NO, 10% via reaction with NO_2, and 7% via reaction with RO_2 radicals. The rate constant used for reaction with NO is a lower limit and hence the importance of the NO reaction is a lower limit. However, it is unlikely that the true value of k_7 lies more than a factor of 2 higher than the lower limit used in the above calculations so the importance of the reaction with NO is unlikely to be greater than about 25%.

While reaction with NO_2 is a minor fate of $CF_3C(O)O_2$ radicals the product, $CF_3C(O)O_2NO_2$ is of interest because of its thermal stability. Using the temperature profile of the US Standard Atmosphere [22] and the expression for k_{-1} derived in the present work, the lifetime of $CF_3C(O)O_2NO_2$ with respect to thermal decomposition can be calculated as a function of altitude. The result, shown in Fig. 5, dramatically illustrates the sensitivity of this compound to temperature, with its lifetime varying by 7 orders of magnitude from the earth's surface to an altitude of 12 km. As with other organic compounds two other loss mechanisms for $CF_3C(O)O_2NO_2$ need to be considered; reaction with OH radicals and photolysis. OH radicals are not expected to react with $CF_3C(O)O_2NO_2$. As discussed by Zabel et al. [3], the photolysis rate of $CF_3C(O)O_2NO_2$ is unknown but expected to be similar to that of $CH_3C(O)O_2NO_2$ which is $\approx$4–6 months [23]. The troposphere is a well mixed region. As seen from Fig. 5, below 2 km

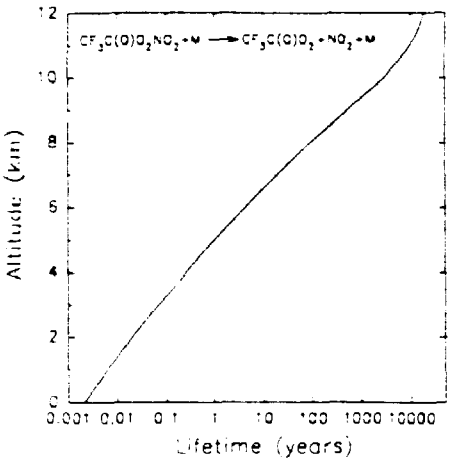

Fig. 5. Lifetime of $CF_3C(O)O_2NO_2$ with respect to thermal decomposition as a function of altitude in the US Standard Atmosphere.

the lifetime of $CF_3C(O)O_2NO_2$ with respect to thermal dissociation is short (< 7 days). The loss of $CF_3C(O)O_2NO_2$ will be dominated by thermal decomposition at low altitudes.

Acknowledgement

We thank Steve Japar (Ford) for helpful discussions. Financial support for the work at Risø was provided by the Commission of the European Communities and by AFEAS under contract No. CTR93-45/P43-120. Thanks are due to Greg Khitrov and Joe Francisco (both Wayne State University) for providing the CF_3CHO sample used in the experiments at Ford and to Friedhelm Zabel (University of Wuppertal, Germany) for communicating his results prior to publication.

References

[1] B.J. Finlayson-Pitts and J.N. Pitts Jr., Atmospheric chemistry: fundamentals and experimental techniques (Wiley, New York, 1986).
[2] R.P. Wayne, Chemistry of atmospheres, 2nd Ed. (Oxford Univ. Press, Oxford, 1991).
[3] F. Zabel, F. Kirchner and K.H. Becker, Intern. J. Chem. Kinetics, submitted for publication.
[4] T.J. Wallington and O.J. Nielsen, Chem. Phys. Letters 187 (1991) 33.

[5] T.J. Wallington, J.C. Ball, O.J. Nielsen and E. Bartkiewicz, J. Phys. Chem. 96 (1992) 1241.
[6] O.J. Nielsen, T. Ellermann, E. Bartkiewicz, T.J. Wallington and M.D. Hurley, Chem. Phys. Letters 192 (1992) 82.
[7] O.J. Nielsen, T. Ellermann, J. Sehested, E. Barkiewicz, T.J. Wallington and M.D. Hurley, Intern. J. Chem. Kinetics 24 (1992) 1009.
[8] J. Sehested and T.J. Wallington, Environ. Sci. Technol. 27 (1992) 146.
[9] O.J. Nielsen, T. Ellermann, J. Sehested and T.J. Wallington, J. Phys. Chem. 96 (1992) 10875.
[10] O.J. Nielsen, Risø-R-480 (1984).
[11] O.J. Nielsen, H.W. Sidebottom, L. Nelson, J.J. Treacy and D.J. O'Farrell, Intern. J. Chem. Kinetics 21 (1989) 1101.
[12] T.J. Wallington and S.M. Japar, J. Atmos. Chem. 9 (1989) 399.
[13] T.J. Wallington, M.D. Hurley, O.J. Nielsen and J. Sehested, J. Phys. Chem., submitted for publication.
[14] H. Shechter and F. Conrad, J. Am. Chem. Soc. 72 (1950) 3371.
[15] T. Ellermann, J. Sehested, O.J. Nielsen, P. Pagsberg and T.J. Wallington, Chem. Phys. Letters 218 (1994) 287.
[16] J. Sehested, K. Sehested, O.J. Nielsen and T.J. Wallington, J. Phys. Chem., in press.
[17] T.J. Wallington, P. Dagaut and M.J. Kurylo, Chem. Rev. 92 (1992) 667.
[18] W.B. DeMore, S.P. Sander, D.M. Golden, R.F. Hampson, M.J. Kurylo, C.J. Howard, A.R. Ravishankara, C.E. Kolb and M.J. Molina, Jet Propulsion Laboratory Publication 92-20, Pasadena, CA (1992).
[19] R. Atkinson, Alternative Fluorocarbon Environmental Acceptability Study, W.M.O. Global Ozone Research and Monitoring Project, Report No. 20; Scientific assessment of stratospheric ozone, Vol. 2 (1989) p. 167.
[20] G.K. Moortgat, B. Veyret and R. Lesclaux, Chem. Phys Letters 160 (1989) 443.
[21] G.K. Moortgat, B. Veyret and R. Lesclaux, J. Phys. Chem. 93 (1989) 2362.
[22] US Standard Atmosphere, 1976, NOAA, NASA, USAF, Washington (1976).
[23] G.I. Senum, Y.-N. Lee and J.S. Gaffney, J. Phys. Chem. 88 (1984) 1269.

List of Publications

1) Ole J. Nielsen, Thomas Ellermann, Jens Sehested, Elzbieta Bartkiewicz, Timothy J. Wallington, and Michael D. Hurley: "UV Absorption Spectra, Kinetics and Mechanisms of the Self Reaction of CF_3O_2 Radicals in the Gas Phase at 295 K", Int. J. Chem. Kinet. 24, 1009, 1992.

2) Ole J. Nielsen, Thomas Ellermann, Jens Sehested, and Timothy J. Wallington: "UV Absorption Spectrum, and Kinetics and Mechanism of the Self Reaction of $CHF_2CF_2O_2$ Radicals in the Gas Phase at 298 K", J. Phys. Chem. 96, 10875, 1992.

3) Timothy J. Wallington, Michael D. Hurley, Jichun Shi, Matti M. Maricq, Jens Sehested, Thomas Ellermann, and Ole J. Nielsen: "A Kinetic Study of the Reaction of Fluorine Atoms with CH_3F, CH_3Cl, CH_3Br, CF_2H_2, CO, CF_3H, CF_3CHCl_2, CF_3CH_2F, CHF_2CHF_2, CF_2ClCH_3, CHF_2CH_3, and CF_3CF_2H at (295±2) K", Int. J. Chem. Kinet. 25, 651, 1993.

4) Jens Sehested, Thomas Ellermann, Ole J. Nielsen, Timothy J. Wallington, and Michael D. Hurley: "UV Absorption Spectrum, and Kinetics and Mechanism of the Self Reaction of $CF_3CF_2O_2$ Radicals in the Gas Phase at 295 K", Int. J. Chem. Kinet. 25, 701, 1993.

5) Jens Sehested and Ole J. Nielsen: "Absolute Rate Constants for the Reactions of CF_3O_2 and CF_3O Radicals with NO at 295 K", Chem. Phys. Lett. 206, 369, 1993.

6) Timothy J. Wallington, Michael D. Hurley, William F. Schneider, Jens Sehested, and Ole J. Nielsen: "Atmospheric Chemistry of CF_3O: Reaction with H_2O". J. Phys. Chem. 97, 7606, 1993.

7) Jens Sehested, Ole J. Nielsen, and Timothy J. Wallington: "Absolute Rate Constants for the Reaction of NO with a Series of Peroxy Radicals in the Gas Phase at 298 K", Chem. Phys. Lett. 213, 457, 1993.

8) Thomas Ellermann, Jens Sehested, Ole J. Nielsen, Palle Pagsberg, and Timothy J. Wallington: "Reaction of F atoms with O_2 and UV Spectrum of FO_2 Radicals in the Gas Phase at 295 K", Chem. Phys. Lett., 218, 287, 1993.

9) Ole J. Nielsen and Jens Sehested: "Upper Limits for the Rate Constants of the Reactions of CF_3O_2 and CF_3O Radicals with Ozone at 295 K", Chem. Phys. Lett., 213, 433, 1993.

10) Jens Sehested and Timothy J. Wallington: "Atmospheric Chemistry of Hydrofluorocarbon 134a: Fate of the Alkoxy Radical CF_3O", Environ. Sci. Technol. 27, 146, 1993.

11) Timothy J. Wallington, Jens Sehested, Michael A. Dearth, and Michael D. Hurley: "Atmospheric Chemistry of CFC Replacement Compounds: Synthesis of bis(trifluoromethyl) trioxide and Anomalies in its Mass Spectral Analysis". J. Photochem. Photobiol. A: Chem. 70, 5, 1993.

12) Jens Sehested, Thomas Ellermann, and Ole J. Nielsen: "A Spectrokinetic Study of CH_2I and CH_2IO_2 Radicals", Int. J. Chem. Kinet., 26, 259, 1993.

13) Timothy J. Wallington, Michael D. Hurley, William F. Schneider, Jens Sehested, and Ole J. Nielsen: "Mechanistic Study of the Gas Phase Reaction of CF_2HO_2 with HO_2", Chem. Phys. Lett., 218, 34, 1994.

14) Timothy J. Wallington, Thomas Ellermann, Ole J. Nielsen, and Jens Sehested: "Atmospheric Chemistry of FCO_x Radicals: UV Spectra and Self Reaction Kinetics of FCO and $FC(O)O_2$, and Kinetics of some Reactions of FCO_x with O_2, O_3, and NO at 296 K", J. Phys. Chem., 98, 2346, 1994.

15) Jens Sehested, Thomas Ellermann, Ole J. Nielsen, and Timothy J. Wallington: "Spectrokinetic Study of SF_5 and SF_5O_2 Radicals and the Reaction of SF_5O_2 with NO", Int. J. Chem. Kinet., 26, 615, 1994.

16) William F. Schneider, Timothy J. Wallington, Michael D. Hurley, Jens Sehested, and Ole J. Nielsen: "Comment on the Thermochemistry of the CF_3O Radical and CF_3OH", J. Phys. Chem., 98, 2217, 1994

17) Jens Sehested: "A Spectrokinetic Study of CF_3CFCl and CF_3CFClO_2 Radicals and the Reaction of CF_3CFClO_2 with NO and NO_2 in the Gas Phase", Int. J. Chem. Kinet. 1994 in press.

18) Jens Sehested, Knud Sehested, Ole J. Nielsen, and Timothy J. Wallington: "Atmospheric Chemistry of FO_2 Radicals: Reaction with CH_4, O_3, NO, NO_2, and CO at 295K", J. Phys. Chem., 98, 6731, 1994.

19) Timothy J. Wallington, William F. Schneider, Douglas R. Worsnop, Ole John Nielsen, Jens Sehested, Warren Debruyn, and Jeffery A. Shorter: "Atmospheric Chemistry and Environmental Impact of CFC Replacements: HFCs and HCFCs", Env. Sci. tech., 28, 320, 1994.

20) Timothy J. Wallington, Michael D. Hurley, Ole J. Nielsen, and Jens Sehested: "Atmospheric Chemistry of CF_3CO_x Radicals: Fate of CF_3CO Radicals, the UV Spectrum of $CF_3C(O)O_2$ Radicals, and Kinetics of the Reaction $CF_3C(O)O_2 + NO \rightarrow CF_3C(O)O + NO_2$", J. Phys. Chem., 98, 5686, 1994.

21) Timothy J. Wallington, Ole J. Nielsen, and Jens Sehested: "Atmospheric Chemistry of CF_3CO_2 Radicals: Kinetics of the Reaction with NO_2 and Kinetics of the Thermal Decomposition of the Product $CF_3C(O)O_2NO_2$". Chem. Phys. Lett., 226, 563, 1994.

22) Ole J. Nielsen, Elisabeth Gamborg, Jens Sehested, Timothy J. Wallington, and Michael D. Hurley: "Atmospheric Chemistry of HFC.143a: Spectrokinetic Investigation of the $CF_3CH_2O_2$ Radical, Its Reactions with NO and NO_2, and Fate of CF_3CH_2O", J. Phys. Chem. in press 1994.

23) Timothy J. Wallington, Michael D. Hurley, James C. Ball, Thomas Ellermann, Ole J. Nielsen, and Jens Sehested: "Atmospheric Chemistry of HFC-152: UV Absorption Spectrum of CH_2FCHFO_2 Radicals, Kinetics of the Reaction $CH_2FCHFO_2 + NO \rightarrow CH_2FCHFO + NO_2$, and Fate of the Alkoxy Radical CH_2FCHFO", J. Phys. Chem., 98, 5435, 1994.

Bibliographic Data Sheet Risø-R-804(EN)

Title and author(s)

Atmospheric Chemistry of Hydrofluorocarbons and Hydrochlorofluorocarbons

Jens Sehested

ISBN	ISSN
87-550-2065-8	0106-2840

Dept. or group	Date
Environmental Science and Technology	March 1995

Groups own reg. number(s)	Project/contract no.(s)

Pages	Tables	Illustrations	References
207	11	23	106

Abstract (Max. 2000 characters)

Pulse radiolysis coupled with a time resolved UV absorption detection system and a FTIR spectrometer coupled to a 140 l reaction chamber was used to study the degradation of HCFCs and HFCs in the atmosphere. Reaction rates for a series of reactions of HFCs and HCFCs were investigated: F + RH, R + O_2 + M, RO_2 + NO, and RO_2 + NO_2 + M, together with UV absorption spectra of the halogenated alkyl (R) and halogenated alkyl peroxy radicals (RO_2). The products following the self reactions of RO_2 radicals for RO_2 = $CF_3CF_2O_2$, $CF_2HCF_2O_2$, $CF_3CH_2O_2$, CFH_2CFHO_2, CF_3O_2, and $CF_3C(O)O_2$ were investigated by the FTIR setup. The results show that the self reaction of halogenated peroxy radicals give the alkoxy radical, RO, as product. The atmospheric fate of these radicals were C-C bond cleavage for CF_3CF_2O, CHF_2CF_2O, CFH_2CHFO, and $CF_3C(O)O$; while CF_3CH_2O radicals react with O_2 to give CF_3CHO and HO_2. The reaction between CFH_2O_2 and HO_2 was shown to give 29±7% CH_2FCOOH and 71±11% HCOF as the carbon containing products. The following CF_3O reactions were studied: CF_3O+NO, $(5.2\pm2.7)\times10^{-11}$ cm^3 $molecule^{-1}$ s^{-1}; CF_3O+O_3, $< 10^{-13}$ cm^3 $molecule^{-1}$ s^{-1}; CF_3O+H_2O, $0.2\text{-}40\times10^{-17}$ cm^3 $molecule^{-1}$ s^{-1}. Reactions of FCO_x, x=1,2,3 and FO_x, x=0,1,2, were also studied: $k(FC(O)+NO)=(1.0\pm0.2)\times10^{-11}$ cm^3 $molecule^{-1}$ s^{-1}, $k(FC(O)O_2+NO)=(2.5\pm0.8)\times10^{-11}$ cm^3 $molecule^{-1}$ s^{-1}, $k(FC(O)O+NO)=(1.3\pm0.7)\times10^{-10}$ cm^3 $molecule^{-1}$ s^{-1}, $k(FC(O)O+O_3)<6\times10^{-14}$ cm^3 $molecule^{-1}$ s^{-1}, $k(FO_2+NO)=(1.47\pm0.08)\times10^{-12}$ cm^3 $molecule^{-1}$ s^{-1}, $k(FO_2+NO_2)=(1.05\pm0.15)\times10^{-13}$ cm^3 $molecule^{-1}$ s^{-1}, $k(FO_2+CO)<5.1\times10^{-16}$ cm^3 $molecule^{-1}$ s^{-1}, $k(FO_2+CH_4)<4.1\times10^{-15}$ cm^3 $molecule^{-1}$ s^{-1}, $k(FO_2+O_3)<3.4\times10^{-16}$ cm^3 $molecule^{-1}$ s^{-1}, and $k(FO+O_3)<1.2\times10^{-12}$ cm^3 $molecule^{-1}$ s^{-1}. The results from this work together with data available in the literature indicate that HFCs does not destroy stratospheric ozone.

Descriptors INIS/EDB

Alkoxy radicals, alkyl radicals, atmospheric chemistry, chlorinated aliphatic hydrocarbons, cleavage, fluorinated aliphatic hydrocarbons, infrared spectra, ozone, peroxy radicals, photolysis, pulse irradiation, radiolysis.

Available on request from Risø Library, Risø National Laboratory
(Risø Bibliotek, Forskningscenter Risø), P.O. Box 49,
DK-4000 Roskilde, Denmark
Telephone (+45) 46 77 46 77, ext. 4004/4005
Telex 43 116 · Telefax (+45) 46 75 56 27

RISØ

Objective

The objective of Risø's research is to provide industry and society with new potential in three main areas:

- *Energy technology and energy planning*
- *Environmental aspects of energy, industrial and plant production*
- *Materials and measuring techniques for industry*

As a special obligation Risø maintains and extends the knowledge required to advise the authorities on nuclear matters.

Research Profile

Risø's research is long-term and knowledge-oriented and directed toward areas where there are recognised needs for new solutions in Danish society. The programme areas are:

- *Combustion and gasification*
- *Wind energy*
- *Energy technologies for the future*
- *Energy planning*
- *Environmental aspects of energy and industrial production*
- *Environmental aspects of plant production*
- *Nuclear safety and radiation protection*
- *Materials with new physical and chemical properties*
- *Structural materials*
- *Optical measurement techniques and information processing*

Transfer of Knowledge

The results of Risø's research are transferred to industry and authorities through:

- *Research co-operation*
- *Co-operation in R&D consortia*
- *R&D clubs and exchange of researchers*
- *Centre for Advanced Technology*
- *Patenting and licencing activities*

To the scientific world through:

- *Publication activities*
- *Co-operation in national and international networks*
- *PhD- and Post Doc. education*

Risø-R-804(EN)
ISBN 87-550-2065-8
ISSN 0106-2840

Available on request from:
Department of Information Service
Risø National Laboratory
P.O. Box 49, DK-4000 Roskilde, Denmark
Phone +45 46 77 46 77, ext. 4004/4005
Telex 43116, Fax +45 46 75 56 27

Key Figures

Risø has a staff of just over 900, of which more than 300 are scientists and 80 are PhD and Post Doc. students. Risø's 1995 budget totals DKK 476m, of which 45% come from research programmes and commercial contracts, while the remainder is covered by government appropriations.